INVERSE VULCANISATION OF ELEMENTAL SULFUR FOR FUNCTIONAL MATERIALS

JESSICA A. SMITH

DATE: JULY 2020

Thesis submitted in accordance with the requirements of the University of Liverpool for the degree of Doctor of Philosophy

ABSTRACT

Synthetic polymers are the most extensively manufactured material on earth. The exponential increase in the production and application of synthetic polymers has led to growing concerns such as, depletion of fossil fuels. Due to this, there is a growing research interest in the development of sustainable, safe, biodegradable, and environmentally friendly plastics from renewable resources. Until recently, inorganic waste for functional renewable materials had been overlooked.

Sulfur is a highly abundant element and is also produced as a by-product of the petrochemicals industry. Over 70 million tonnes of sulfur is produced annually, with only a small fraction of this being used to produce commodity chemicals, such as sulfuric acid and fertilisers. This leaves huge unused stockpiles around the world, meaning sulfur is a cheap waste by-product.

However, until recently, it has not been conventionally used to produce functional materials because polymeric sulfur is unstable and decomposes back to crystalline sulfur (S_8). In 2013 Pyun and co-workers discovered inverse vulcanisation which allows polymeric sulfur to be stabilised by a small alkene crosslinker.

This work explores different inverse vulcanised sulfur polymers for functional materials and focuses on both discovering and improving the physical properties for different functions. The effect of crosslinker structure on the resultant polymer is assessed; the materials' mechanical properties are explored; the antibacterial activity of the materials is investigated, and catalyst/accelerators are explored to improve reaction conditions.

PRESENTATIONS, PUBLICATIONS, AND TRAVEL GRANTS

Publications:

1. Facile production of nanocomposites of carbon nanotubes and polycaprolactone with high aspect ratios with potential applications in drug delivery, E.Niezabitowsa, J.A.Smith, M.R.Prestly, R.Akhtar, F.W.von Aulock, Y.Lavallee, H.Ali-Boucetta and T.O.Mcdonald*, RSC advances, 2018, 8, 16444-16454.

2. High sulfur content polymers: the effect of crosslinker structure on inverse vulcanization, J.A. Smith, X.Wu, N.G.Berry, T.Hasell* Journal of Polymer Science Part A: Polymer chemistry, 2018, 56, 1777-1781.

3. Sulfur polymer composites as controlled-release fertilisers, M.Mann, J.E.Kruger, F.Andari, J.McErlean, J.R.Gascooke, J.A.Smith, M.J.H.Worthington, C.C.C.Mckinley, J.A.Campbell, D.A.Lewis, T.Hasell, M.V.Perkins, J.M.Chalker*, Organic & Biomolecular Chemistry, 2019, 17, 1929-1936.

4. Crosslinker copolymerization for Property Control in Inverse Vulcanization, J.A.Smith, S.J.Green, S.Petcher, D.J.Parker, B.Zhang, M.J.H.Worthington, X.Wu, C.A.Kelly, T.Baker, C.T.Gibson, J.A.Campbell, D.A.Lewis, M.J.jenkins, H.Willcock, J.M.Chalker*, T.Hasell*, Chemistry-A European journal, 2019, 25, 10433-10440.

5. Catalytic inverse vulcanization, Nature communications, X.Wu, J.A.Smith, S.Petcher, B.Zhang, D.J.Parker, J.M.Griffin, T.Hasell*, 2019, 10, 647.

6. Investigating the Antibacterial Properties of Inverse Vulcanized Sulfur Polymers, J.A.Smith, R.Mulhall, S.Goodman, G.Fleming, H.Allison, R.Raval*, T.Hasell*, ACS Omega, 2020, 5, 10, 5229-534.

7. Inverse Vulcanized Polymers with Shape Memory, Enhanced Mechanical Properties, and Vitrimer Behavior.Angewandte Chemie International Edition, P.Yan, W.Zhao, B.Zhang, L.Jiang, S.Petcher, J.A.Smith, D.J.Parker, A.I.Cooper, J.Lei, T.Hasell*, 2020.

Oral Presentations:

PhD symposium (University of Liverpool, 2020)

FunMat Materials Conference (Berlin 2019)

Seminar, Flinders University, Adelaide, SA.

Poster Presentations:

PhD symposium (University of Liverpool 2019)

Young Researchers Meeting (Edinburgh, 2017)-Macro Group UK

Travel Grants:

Royal Society International Exchange Grant

ACKNOWLEDGMENTS

Tom, thank you for the opportunity to do my PhD in your group. I am forever grateful for it. I feel working with you has made me a better scientist. You always give us just enough direction, with room for us to think and explore our own ideas. Thank you for encouraging me to go to Australia and experience a new lab, my experience is unforgettable. Thank you for being a supportive supervisor and encouraging me to step out of my comfort zones and grow. Thank you to all of the Hasell group past and present, there isn't one of you that I haven't learned something from. I wish everybody success.

To Jess, Becky, and Sophie, I don't even know where to start with you three. The unlimited coffees, the ups, and downs, the laughs and cries we have had. I can't thank you all enough. I don't even know how to. I am so grateful for friends like you, this will be you three soon, and I will be there cheering you on, just like you have for me. Every day we weren't sure what type of day each of us would have during these PhDs, but we did it!! Thank you for giving me a kick when needed and for the constant laughs, love, and support. I can't wait to make more memories with you all. I am very grateful to have friends like you that are more like family.

It wouldn't be right if I didn't thank the Department of Chemistry in some way. Debbie, John, and Sam in student support, you are all the backbone of our Department, and I don't know what anybody would do without you all. The times and laughs we have had; I will never forget. To all the cleaners, the workshop, and everyone who is the backbone of our department, thank you. You have all made my daily visits to the department cheery. I am grateful for all of our chats and everything you do for us all. And to Prof. Myers, thanks for all the fun and party organising and lifting everyone's spirits daily. There wouldn't be a department without you all.

I spent a lot of time teaching during my PhD. Gita, well haven't we all had a crazy rollercoaster on this demonstrating journey. Thank you for making us all laugh daily and equally, driving us all insane. I wouldn't change anything. Thanks to Prof. Mathias Brust, who I spent a lot of my demonstrating courses with. You made those hours entertaining, with your life stories and teachings.

I have too many people to thank in the Department. Anyone I have ever crossed path with I have learned something from, and I am very grateful.

To Holly, Vicky, and Tash. I think you've been more like therapists at times. I love that you and the girls above are more like sisters to me. On reflection, we have had so many laughs I can't even begin. I feel like Holly, you left me to do this PhD, but I have literally taken you on every journey with me. Thank you, Holly, Vicky, Tasha, Jess, Becky and Sophie, Rach and Verity. We are all like family to one another and have the best times. Thank you for listening to all my PhD moans and just being there for me every day. Let the good times continue girls!!!

To Will, wow. Can you believe it? We did it. These past 4 years have been tough for us both professionally and personally, but on reflection I would not change one tough time. 8 years growing up together in the Department of Chemistry, the belly laughs, the lessons we have learned, and we have faced things we would never have predicted. As my nan used to say, "when you make a plan god laughs', I think it is safe to say we have definitely learned this. We are now a unit, a team. After the things we have faced, I am no longer scared of anything because I know we are always there to lift one another. I can face anything together with you. Thank you for holding me up when I could no longer hold myself up. You really have been my scaffold. I cannot wait for the rest of our lives, you and me.

To my grandad, I am so privileged I get to live with you. I have seen you every day of my life, I can't imagine it any other way (although maybe I would change you being my personal alarm clock and waking me up at 5 am every day). Thank you so much for being the best dad/grandad a girl could ever wish for. Thank you for putting up with all my different emotions while writing this and the last four years. Money can buy a lot of things, but it can never buy a grandad like you. You've wiped every tear and gave me so many reasons to smile. This thesis and my achievements are as much yours as mine.

To my mum, I don't even know how to start thanking you. From day one, you always made learning fun for me. You nurtured my excitement for learning and my inquisitive nature. You encouraged me to keep asking why and to continue questioning everything even when it must have gotten a little annoying. You made me believe no matter who I was or where I was from, I could achieve anything with hard work, graft, and determination. I never needed parents or family with a university education to achieve anything. I got more. Unconditional love, support, and encouragement in everything I

ever did. You taught me how to pick myself up when times get hard and to get through the hard times with laughter and song. You showed me how education could open doors that you never had. Still, only encouraged me with the most important thing to you, always being my happiness. As I have grown older, I have realised how mums like you are rare. You've worked so hard your whole life to make sure I never did without, thank you for everything. In the last 4 months of writing this, I have loved having you with me every day, we have never had that before with you always working and me always working and studying. I know especially for you, not going to work at times because of the pandemic was tough, but we got through it together. I could write pages to you, but I know I don't need to, you know. This thesis, my education, and who I am today reflects how you as a mother has worked hard to keep me on the right path in life and just encouraged my love of learning from a young age. Sometimes with things going on, I have lost my love of learning at times, thank you for lifting me up and reminding me. Thank you for being my best friend (although at times I know you must have wanted to kill me). Writing this boxed in our house with you and my grandad during a global pandemic has been a rollercoaster at times, but I wouldn't have changed a second of it.

To my nan, John, Joan and Joseph, who left me during all of this. How lucky am I that I got to spend every day with you all and grandad? How lucky am I that I have so many people to thank and who are responsible for who I am today? You really all are and always will be life's greatest scientists to me. Thank you, although not present today, for leaving a part of you with me. Reminding me daily to never take life to seriously, and when bad things happen, it is only temporary. You all enstilled such a great sense of life and fun in me. You all moulded me into the strong woman I am today. Every day I spent with you all when I came home from school you all encouraged my love of learning in some way. Whether it be listening to WW2 stories or just all having unlimited time for me. I write this with a heavy heart. I wish you could be here to see this achievement as it belongs to you all as much as me. I am a product of you all. I would say I hope you are all proud of me, but I know you all are, with or without this thesis. This thesis is for all of you.

Time to close this book and open the next.

For my Joan

Although you don't remember me anymore, the only thing you have never forgotten is how to laugh. That is something I hope I never forget.

For my Mum

We won.

CONTENTS

ABBREVIATIONS

4VA	4-vinylaniline
AMR	Antimicrobial resistance
CDE	1, 4-cyclohexanedimethanol divinyl ether
cfu	Colony forming units
DCPD	Dicyclopentadiene
DFT	Density Functional Theory
DIB	1,3-diisopropenylbenzene
DSC	Differential Scanning Calorimetry
DVB	Divinylbenzene
E.coli	*Escherichia coli*
ECM	Extracellular matrix of polymers and polysaccharides
EDGMA	Ethylene glycol dimethacrylate
ENB	5-Ethylidene-2-norbornene
FTIR	Fourier Transformation Infrared
GBDA	glyoxal bis(diallylacetal)
GPC	Gel Permeation Chromatography
H_2S	Hydrogen sulfide
HDS	Hydrodesulfurisation
HRIP	High Refractive Index Polymers
IR	Infared
Li_2S	Lithium Sulfide
MMA	Methyl methacrylate
n	Refractive index
Na_2CO_3	Sodium Carbonate
NaCl	Sodium Chloride
NMI	N-methylimidazole
NMR	Nuclear Magnetic Resonance
ORMOCHALC	Organically modified chalcogenide polymer
PC	Polycarbonate
Poly(S-r-DIB)	poly(sulfur-random-1,3-diisopropenylbenzene)
Poly(s-r-TVSn)	Poly (sulfur-random-tetravinyltin (TVSn)
Poly(S-TABQ)	poly(S-tetra(allyloxy)-1,4-benxoquinone)
POSS	polyhedral oligomeric silsesquioxane
PS	Polystyrene
PXRD	Powder X-Ray Diffraction
ROP	Ring Opening Polymerisation

ROS	Reactive oxidative species
S.aureus	*Staphylococcus aureus*
S_8	Elemental sulfur
SCDLP	polyoxyethylene sorbitan monooleate
SDA	Sulfur diallyl disulfide
SEM	Scanning electron microscopy
STY	Styrene
T_c	Crystallisation temperature
T_g	Glass transition temperature
TGA	Thermogravimetric Analysis
TIB	1, 3, 5-triisopropenylbenzene
T_m	Melting transition temperature
TVTCSi	1,3,5,7-tetravinyltetramethylcyclotetrasiloxane
VNB	5-vinyldene-2-norbornene

CHAPTER 1

INTRODUCTION

Chapter 1: Introduction

1.1 The reasons for using elemental sulfur for functional materials

Sulfur, the tenth most abundant element in the universe has been used for many centuries as an antibacterial agent, in gun powder formulation, fabric bleaching and more recently vulcanisation for latex.[1,2,3] Today, sulfur is a waste by-product of the petroleum refining industry (purification of crude oil and gas reserves), where SO_2 is removed and converted, by hydrodesulfurisation, to S_8.[4] Over 70 million tonnes of sulfur is produced annually (Figure 1.1), with only a small fraction of this being used for the production of commodity chemicals such as sulfuric acid and fertilisers.[5,6] This leaves huge unused stockpiles of sulfur around the world, which is likely to increase over time due to strict regulations on reducing sulfur dioxide emissions within the petrochemical industry.[7] Although elemental sulfur is non-toxic, it is a flammable solid, therefore, producing functional materials and reducing these stockpiles around the world is prevalent.[8]

1.1.2 Why is sulfur removed in petroleum refining?

Over 82% of the world's energy comes from fossil fuel combustion, half of which is produced from petroleum refining.[7] Crude oil, a fossil fuel, is a complex mixture of liquid hydrocarbons, dissolved gases, water and salts.[9] It is currently the world's largest energy source with the major portions of crude oil being used for transportation

Figure 1.1 A stockpile of elemental sulfur produced by hydrodesulfurisation in petroleum refining. Approximately 70 million tons were produced in 2015. Image from ref 3.

fuels such as petrol, diesel and jet fuel.[7,10] One of the main properties that affect the value of crude oil is the sulfur content.[11]

Sulfur compounds (in particular H_2S) are one of the main causes of equipment failure in the petroleum refining process due to causing corrosion problems in pipeline, pumping and refining equipment, as well as deactivating some catalysts used in crude oil processing.[10] H_2S can contribute to general pitting corrosion and hydrogen attack (acid corrosion), causing cracks in pipelines and harmful gas leaks into the environment (Figure 1.2).[7] If sulfur compounds are left in transportation fuels this leads to the emission of sulfur dioxide.[7,12] When sulfur dioxide reacts with water in the atmosphere, both sulfates and acid rain are formed. This causes damage to buildings, reduces the efficacy of catalytic converters in cars, and changes pH levels in soil, which can lead to the destruction of forests and ecosystems.[13] Alongside this, sulfur emissions can also have adverse health effects on humans; respiratory illness, trigger asthma and aggravate heart disease.[7] Therefore, there is a huge drive both

Figure 1.2 Corrosion of steel pipelines by sulfur containing compounds in the petroleum refining process. Image from oil-naturalgas.com.

environmentally and economically to remove sulfur compounds from fuel. The most common industrial method for the removal of sulfur from fuels is hydrodesulfurisation. (HDS).

1.1.3 Hydrodesulfurisation (HDS)

Hydrodesulfurisation (HDS) is a high temperature, high-pressure catalytic process, which removes more than 70 million tonnes of sulfur per year.[5] The HDS process involves catalytic treatment with hydrogen to convert various sulfur compounds (mercaptans, sulfides, disulfides and thiophenes, Figure 1.3) to H_2S and sulfur free organic compounds.[7,14] Current implemented HDS techniques require severe conditions to operate (high temperature and high partial pressure of hydrogen).[15] Resulting H_2S is eventually converted to elemental sulfur by a modified version of the Claus process.[7]

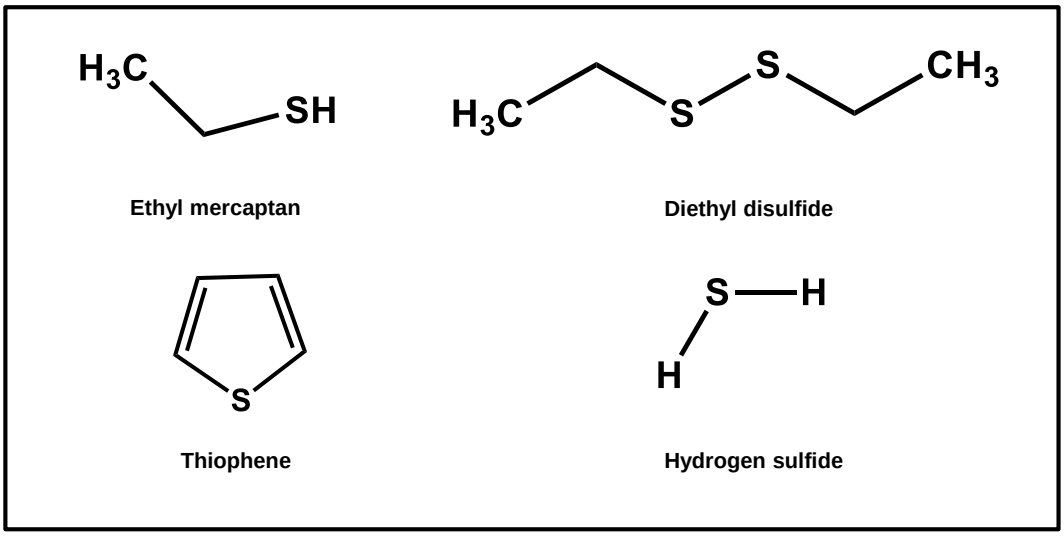

Figure 1.3 Examples of mercaptans, disulfides, thiophenes and sulfides.

The Claus process is a common technique used to treat gas streams containing above 50% H_2S.[16] The process involves the partial oxidation of hydrogen sulfide to sulfur dioxide and catalytically promotes the reaction of H_2S and SO_2 to produce elemental sulfur (eq.1 + eq.2).[16]

$$H_2S + \tfrac{3}{2}O_2 \rightarrow SO_2 + H_2O \quad (eq.1)$$

$$SO_2 + 2\,H_2S \rightarrow 3\,S + 2\,H_2O \quad (eq.2)$$

The conventional Claus process can achieve up to 98% sulfur recovery, with modifications of this process achieving 99.8% recovery to meet strict environmental regulations.[16] The strongest motivation for the reduction of sulfur in fuels is due to pressure from environmental regulations, which are continuously imposing strict limits for sulfur levels in transportation fuels.[10] With this said sulfur produced from this industry is set to increase. This makes sulfur an inexpensive waste product

(approx. 120 USD/ tonne)[1] that has the potential to be processed into functional materials such as, sustainable sulfur polymers.

1.1.4 Sustainable polymers from renewable resources

Synthetic polymers are ubiquitous and among the most extensively manufactured materials on earth.[17] As a global community, we rely heavily on plastics, with over 322 million tonnes of plastics produced in 2015 alone and this is set to rise.[1,18] The exponential increase in the production and application of synthetic polymers has led to growing concerns regarding, depletion of fossil resources and disposal of materials, which has resulted in the government altering policies.[19] Due to this, there is a growing research interest in the development of sustainable, safe, biodegradable, and environmentally friendly plastics from renewable resources. Since the 19th century, naturally occurring polymers have been used such as casein, natural rubber, starch, cellulose and chitin.[20] There has been a large focus on preparing sustainable polymers through chemical modification of these natural polymers, as well as the synthesising bio-based polymers through a two-step process from biomass (lignin, cellulose, starch, plant oils).[20] With the median ages of the entire world's population predicted to rise far into the future, fossil resources are predicted to carry on depleting. As a result, there is both a drive and a desire to produce renewable materials that are functional to conserve the earth's resources. Until recently, inorganic waste for functional, renewable materials has been somewhat overlooked.

1.2 Properties of elemental sulfur and the drawbacks of polymeric sulfur

There are approximately 30 characterised sulfur allotropes known that can be classified as both ambient pressure and high-pressure allotropes (dependent on preparation conditions).[21] The phase transitions and different allotropes of sulfur have been extensively discussed.[21] The thermodynamically favourable form of sulfur is orthorhombic sulfur (α-S_8). [21]

At temperatures less than 96 °C, S_8 exists as a yellow solid in its orthorhombic crystalline form (α-S_8) (Figure 1.4). [22,23,24] The α- S_8 form is then reported to transition to the monoclinic β-S_8 crystalline form, which is stable between 96 °C and 119 °C (melting point).23,24 S_8 then proceeds to melt into a clear yellow liquid phase (molten sulfur) between 120 °C- 124 °C (Figure 1.4). [23,24]

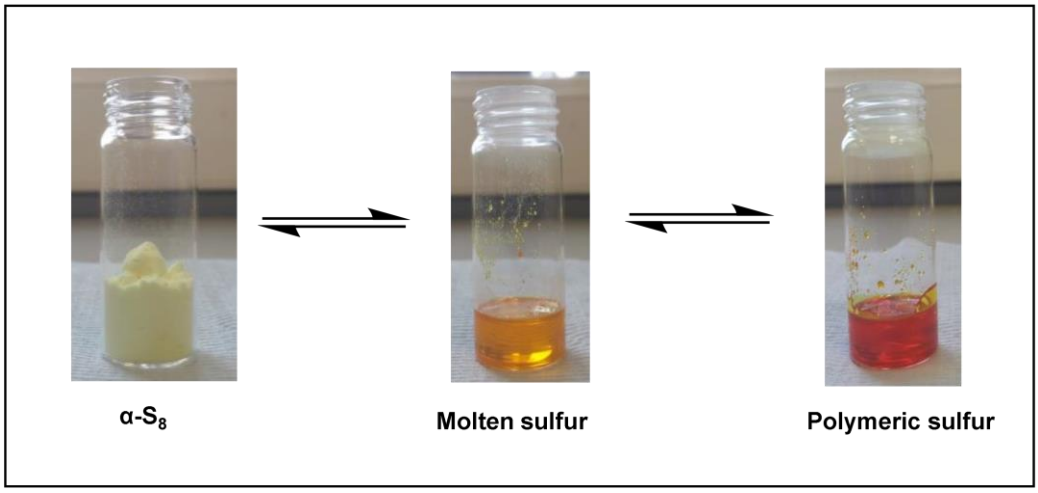

Figure 1.4 Left: Yellow orthorhombic (α) crystalline elemental sulfur (S_8). Middle: Molten sulfur that melts between ~120℃- 124℃. Right: Polymeric sulfur formed >159℃ (floor temperature) through a thermal initiated ring opening polymerisation (ROP).

At temperatures higher than 159 °C (floor temperature) a process known as equilibrium ring-opening polymerisation occurs (ROP) (Figure 1.5, part a).[1,5,25,21] S_8 rings will open above the floor temperature and S-S bond homolysis will provide thiyl radicals that can attack and open a ring of another molecule (Figure 1.5, part b).[1,24,21] Propagation then occurs with repeated S_8 ring opening and a growing polysulfide chain (Figure 1.5), eventually forming a viscous amorphous material, polymerising to a higher molecular weight polysulfide. One of the main challenges with using and preparing polymeric sulfur is that the reaction is reversible (Figure 1.5). This is due to the terminal thiyl radicals of the polysulfide causing depolymerisation back to S_8 or other allotropes of elemental sulfur. Backbiting, Figure 1.5, part c) is one suggested mechanism to how depolymerisation may occur to thermodynamically favourable S_8 orthorhombic form.[21] As a result, the polymeric sulfur generated from this thermal ROP has extremely poor mechanical properties and cannot be controlled or processed. In order to form a stable polymer made from mostly sulfur, the thiyl radicals must be quenched before depolymerisation.[1]

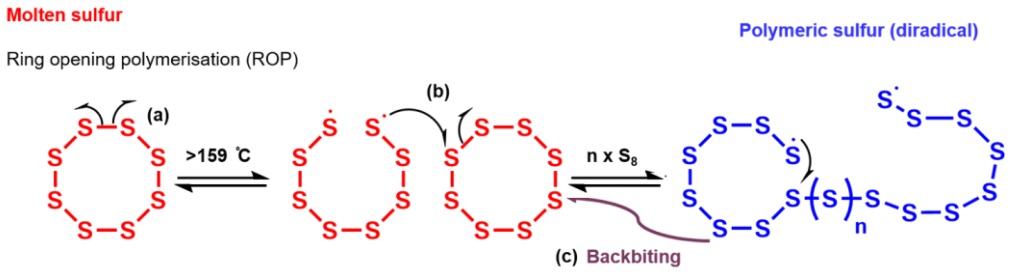

Figure 1.5. (a) Sulfur is heated above the floor temperature (>159 ℃). S-S bonds undergo homolysis and generate thiyl radicals. (b) The thiyl radicals can now react with another molecule of S_8 to form polymeric sulfur. (c) Without any way of quenching the thiyl radical (e.g. small diene molecule) they are unstable and depolymerise back to S_8. One way this can happen is through backbiting. Figure was adapted from ref 1.

Pyun and co-workers have shown that they can overcome issues associated with the depolymerisation of polymeric sulfur by trapping the thiyl radicals with small diene molecules, that can produce a polymer that is predominately prepared from elemental sulfur.[5] This process is known as inverse vulcanisation.[5]

1.3. Vulcanisation

In traditional vulcanisation, elemental sulfur is used in very small quantities to crosslink polyisoprene or other preformed elastic polymers (Figure 1.6). Vulcanisation is a necessary process to produce essential rubbery articles that our society needs such as car tyres.[26,27] By introducing crosslinks (a short chain of sulfur atoms, a single sulfur atom, an ionic cluster or a carbon-carbon bond) between polymer chains, this allows

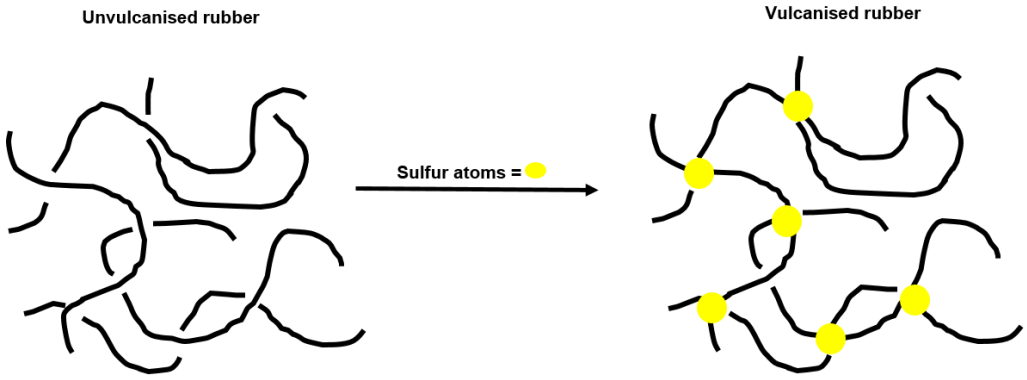

Figure 1.6 Network formation of vulcanised rubber by addition of short chain sulfur atoms. The sulfur crosslinks increase retractile force of rubber and decrease permanent deformation once the deforming force is removed.[26]

the retractile force on the material to increase and reduces permanent deformation after removing force.[26,27] This is a process that has been commercially available for decades with continuing efforts to improve and understand the mechanism.[27]

1.3.2 First discovery of inverse vulcanised sulfur polymers

In 2013, Pyun and co-workers discovered inverse vulcanisation, where a small diene molecule is used to quench thiyl radicals and produce stable branched sulfur polymers (Figure 1.7).[5] Through this process polymers containing between 50-80% sulfur by

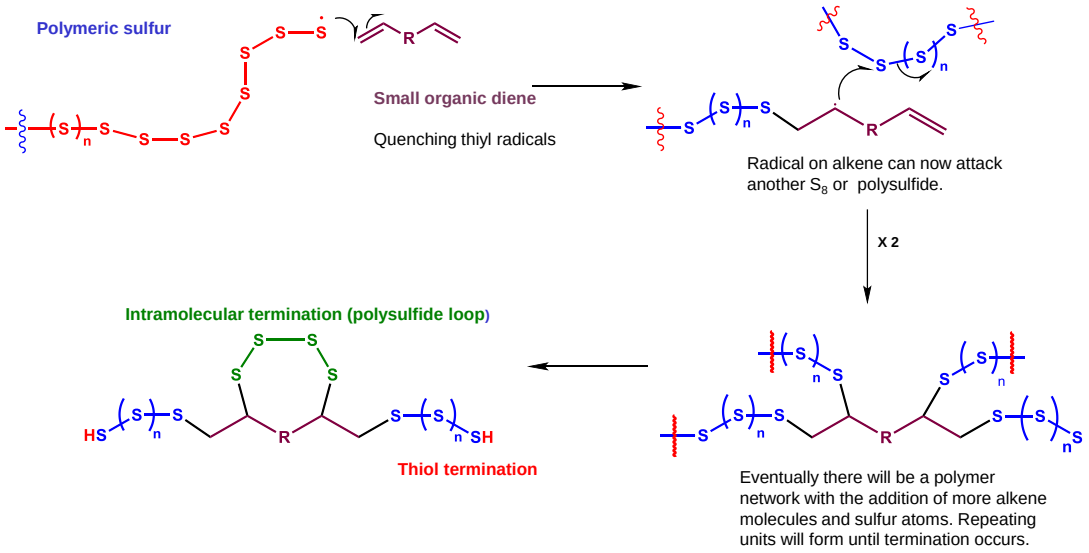

Figure 1.7. Small diene molecules can quench thiyl radicals. Without an organic alkene crosslinker polymeric sulfur can depolymerise by a backbiting mechanism (Figure 1.5c). Adding an alkene crosslinker, followed by radical termination can produce a stable inverse vulcanised sulfur polymer. There could be intramolecular termination forming a polysulfide loop. If H groups are available on the crosslinker, there may be hydrogen abstraction with conversion of thiyl groups to thiols (thiol termination).

mass can be prepared. Inverse vulcanisation requires no additional toxic solvents or initiators like traditional polymerisations (e.g. living polymerisations). The sulfur and alkene crosslinker are used as both the co-monomers and solvents in the reaction. As a result, the starting materials are incorporated into the product making the reaction atom efficient.

The first report of inverse vulcanisation by Pyun and co-workers was using a small organic molecule, 1,3-diisopropylbenzene (DIB) as a crosslinker (Figure 1.8a). Sulfur (50-90% sulfur by mass) was heated to 185 °C to initiate ring-opening polymerisation, DIB (10-50 wt.%) was then added subsequently, resulting in crosslinking and a red

glassy polymeric material that is referred to as poly(sulfur-random-1,3-diisopropenylbenzene) (poly (S-r-DIB)) (Figure 1.8b).[5] Pyun and co-workers have used the terminology 'random', as it is unclear unknown how many repeating units there are and where exactly crosslinking occurs. Due to this polymer having a sulfur backbone opposed to a carbon backbone, it has several interesting chemical and physical properties. Since 2013, poly(S-r-DIB) has been investigated for use as next

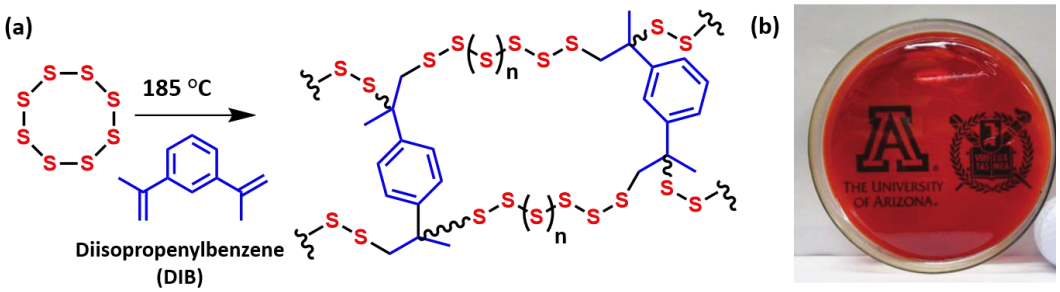

Figure 1.8 (a) Scheme showing reaction between sulfur and 1,3-diisopropylbenzene (DIB) to form a potentially hyperbranched inverse vulcanised poly(S-r-DIB). (b) Photograph of poly(S-r-DIB) at 70% sulfur by mass. The photograph shows a red glassy polymeric material. Image was reproduced by Pyun *et al.*[5]

generation cathode materials for lithium-sulfur batteries,[28] in thermal imaging and optical lenses - due to the high refractive index and the polymer absorbing in the IR region,[29,30] as well as in antimicrobial applications[31,32] (which will be discussed in length in Chapter 4). Since Pyun and co-worker's contribution in 2013, this has inspired further research into inverse vulcanisation with a variety of unsaturated crosslinkers reported.[1,3] Designing and understanding different inverse vulcanised sulfur polymers for different functions is the main theme in this thesis, with further applications being discussed in more detail. The exact mechanism of inverse vulcanisation remains unknown and still need extensive investigation.

1.3.3 Discussion of the potential mechanism

As discussed previously, conventional vulcanisation has been commercially available for decades.[27] Despite this, the mechanism is not completely understood as

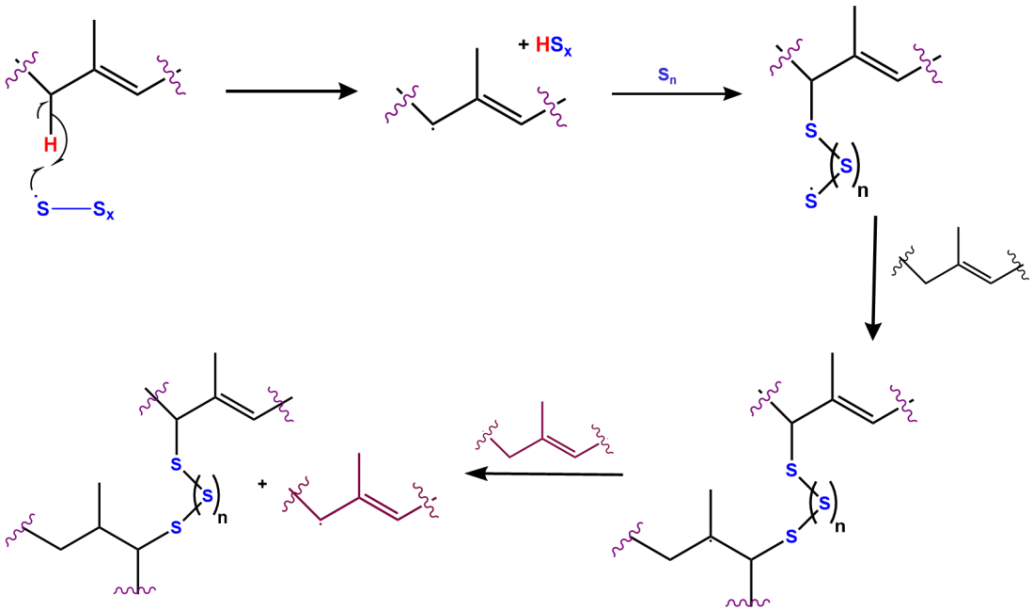

Figure 1.9 Reaction scheme of conventional vulcanisation. Crosslinking by proton substitution via hydrogen abstraction is the most likely mechanism.

it remains complex, difficult to characterise and a point of controversy.[33] The most agreed pathway in literature for conventional vulcanisation is hydrogen abstraction of the α hydrogen adjacent to the C=C (Figure 1.9).[33] This leads to crosslinking by proton substitution with sulfur atoms (Figure 1.9). Other mechanisms assumed are both free radical and ionic, this is due to sulfur being able to undergo homolytic and heterolytic fission (Figure 1.10). With the crosslinking process being complicated, there has been suggestions that the mechanism involves a combination of both radical and ionic species. [34]

Inverse vulcanisation is still a relatively new phenomenon and still needs extensive research into the potential mechanistic pathways. As discussed in previous sections, most of the existing discussion refers to bulk free radical copolymerisation of alkene

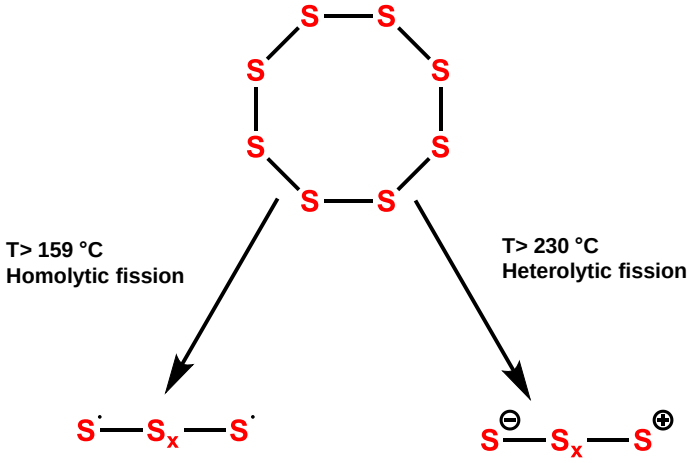

Figure 1.10 Cleavage of sulfur both homolytically (T>159 °C) and heterloytically (T> 230 °C).

co-monomers in molten sulfur.[1,5] Although free radical copolymerisation is the mechanism mostly discussed in the literature for inverse vulcanisation, hydrogen abstraction and H_2S evolution has also been reported.[35,36,37] Hydrogen abstraction most commonly occurs at higher reaction temperatures leading to unwanted side products.[25] Therefore, it is likely both radical addition to the double bond and hydrogen abstraction occur in both inverse vulcanisation and conventional vulcanisation reactions depending on reaction temperatures.

1.3.4 Controlling inverse vulcanisation for functional materials

Varying the feed ratio of sulfur to alkene crosslinker can control polymer structures formed. Controlling the sulfur rank (the number of sulfur atoms in between each crosslink) can result in a material that has different properties and is paramount in controlling the level of crystallinity in the polymer. It should be noted that some inverse vulcanised polymers are not always amorphous and have uncrosslinked free crystalline sulfur present.[38,39] Being able to control the sulfur rank would also be fundamental in this thesis, as the structure of inverse vulcanised sulfur polymers can affect its functions. However, for most of this research, there has been limited control of inverse vulcanisation due to the high temperatures used in the polymerisation (160-200 °C).[1] Thermal scission and recombination of the S-S bonds in the polysulfide

backbone due to reversibility of S-S bonds are likely to lead to random structures, which make it hard to control polymerisation and prepare a uniform polymer with a specific number of sulfur atoms in between each cross-link.[1] The high temperatures could also lead to hydrogen abstraction[40] or in the case of some polymerisations undesired by-products.[25,41,42] Whilst the research in this thesis was on-going there has been advancements in reducing the reaction temperatures of inverse vulcanisation.[33,43] Accelerators have now been employed in inverse vulcanisation reactions to lower reaction temperature (Chapter 5).[33,43] Although inverse vulcanisation is still in the early years of research, it is crucial to understand the process to design polymeric materials from sulfur for different applications.

1.4 Applications of inverse vulcanised sulfur polymers

The contributions of Pyun co-workers have resulted in inverse vulcanised sulfur polymers prepared with different alkene crosslinkers to obtain materials with completely different properties and functions.[44] The antimicrobial/antibacterial properties of these polymers will be discussed in Chapter 4 of this thesis (Figure 1.11).

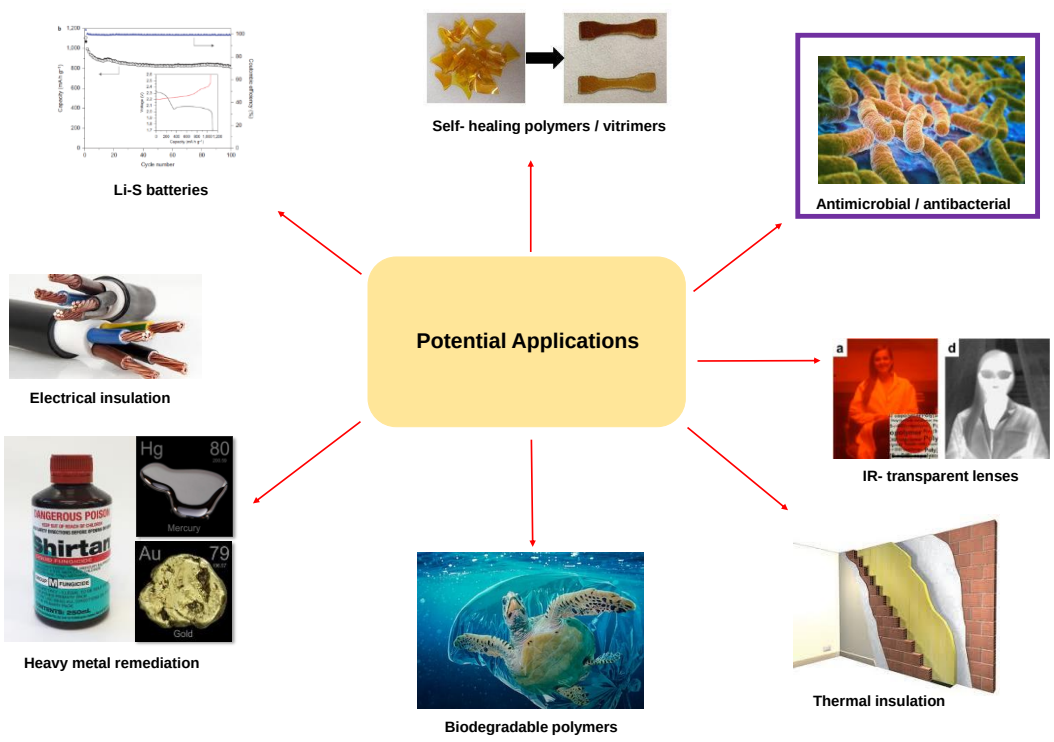

Figure 1.11 Mind map of different and potential applications of inverse vulcanised polymers. The antibacterial properties (highlighted in purple) of inverse vulcanised sulfur polymers will be discussed in Chapter 4 of this thesis.

1.4.1 Optical lenses

The development of polymeric materials for infrared (IR) optical applications has proven to be a challenge. One of the main challenges arises from designing systems that incorporate high refractive index (*n*) in the IR region.[5] Traditionally, polymers synthesised with greater than 1.50 refractive index in the visible region are considered high refractive index polymers (HRIPs). It is uncommon for organic polymers to exceed 1.70 in refractive index. Pyun and co-workers have shown that high sulfur content polymer, poly(S-r-DIB), has a high refractive index (*n*~1.8) and an IR region of transparency.[45] The high refractive index values of inverse vulcanised polymers are attributed to the abundance of sulfur present in these polymers.[45] The development of these polymers are crucial for applications in the military for thermal imaging (night vision lenses) and other optical applications.[29]

More recently, Boyd and co-workers reported the synthesis of organically modified chalcogenide (ORMOCHALC) polymer, poly (sulfur-random-tetravinyltin (TVSn)) (poly(S-r-TVSn)) (Figure 1.12).[46] This polymer is the first reported to contain an organometallic monomer and exhibited enhanced *n* and transmission in the IR region.[46] Although much more research is to be done in developing optical lenses of

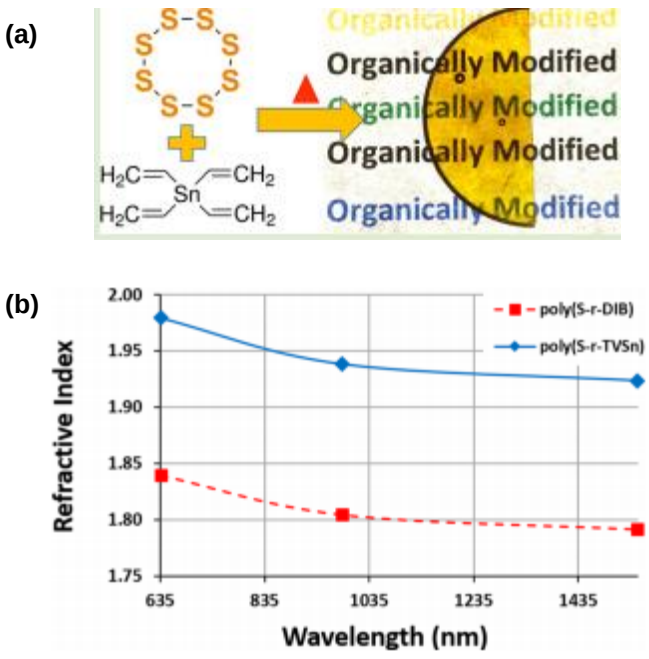

Figure 1.12 (a) S_8 ring with organometallic co monomer tetravinyltin (TVSn) to prepare an ORMOCHALC polymer for optical applications. (b) Comparison of refractive indices of both poly(S-r-TVSn) and poly(S-r-DIB), with poly(S-r-TVSn) having an enhanced refractive index. From ref 42.

inverse vulcanised sulfur polymers, the development of these materials for this

application is invaluable due to the low cost, quick processing and promising IR region transparency.

1.4.2 Thermal insulation

With the amount of fossil fuels depleting there must be development in thermal insulation materials. Alhassan and co-workers have presented porous sulfur foams employing divinylbenzene (DVB) as a crosslinker to produce potential thermal

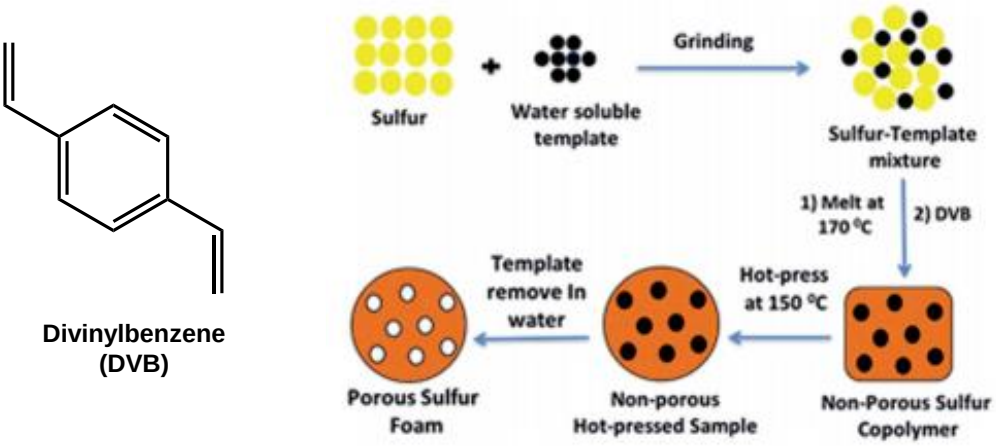

Figure 1.13 General method for the preparation of porous sulfur foams. From ref 43.

insulation materials (Figure 1.13).[47] Sodium chloride (NaCl), sodium carbonate (Na_2CO_3) and poly (sodium 4-styrenesulfonate) (PS) were all used as templates to prepare porous sulfur foams. The thermal conductivity of the proposed sulfur foam (0.032 W m^{-1} K^{-1}) was lower than that of pristine sulfur and close to commercially available insulators (0.035 – 0.16 W m^{-1} K^{-1}) [47,48] The development of inverse vulcanised sulfur polymers as thermal insulators is an understudied area with many potential future advancements to be made.

1.4.3 Self-healing polymers/ vitrimers

Whilst the recyclability and biodegradability of sulfur polymers is still in early stages, it is important to see if the polymers can be reprocessed. There are two types of polymers to consider here, thermoplastics and thermosets. Thermoplastics can often be reheated, remoulded and cooled without causing chemical changes, whereas a thermoset is a material that is strengthened when heated, but cannot be remoulded or heated after the original forming without changing the physical and chemical properties. In very recent years there has been a significant interest in a new class of crosslinked polymers, vitrimers.[49,50,51] Vitrimers are a class of polymers which are

derived from thermosetting polymers with reversible bonds and the ability to change their topology through thermoactivated bond exchange reactions. Recently, there have been some reports of inverse vulcanised sulfur polymers mimicking vitrimer behaviour,[49] exploiting the dynamic nature of S-S bonds to thermally reprocess sulfur polymers and heal surface scratches for IR optical applications,[30] and even fully reprocess sulfur polymers.[52]

1.4.4 Cathodes for Li-S batteries

Inverse vulcanised sulfur polymers have been investigated as potential active materials in cathode electrodes for Li-S batteries to improve performance. The very first example of using a high sulfur content polymer as a cathode material was poly(S-r-DIB).[5,28] Since then, there have been advances in this area with a range of different sulfur polymers being exploited for Li-S battery applications.[39,53,54,55,56,57] One of the main issues associated with Li-S batteries is a polysulfide shuttling effect, which causes polysulfide dissolution, and irreversible deposition of lithium sulfide charged products, which results in capacity loss.[58] The alkene monomers that are used to crosslink inverse vulcanised sulfur polymers have the potential to reduce the polysulfide shuttling effect by forming crosslinks with sulfur. However, many of the reported polymers that have been prepared by inverse vulcanisation still suffer this capacity loss during long-term cycling, due to polysulfide dissolution and the

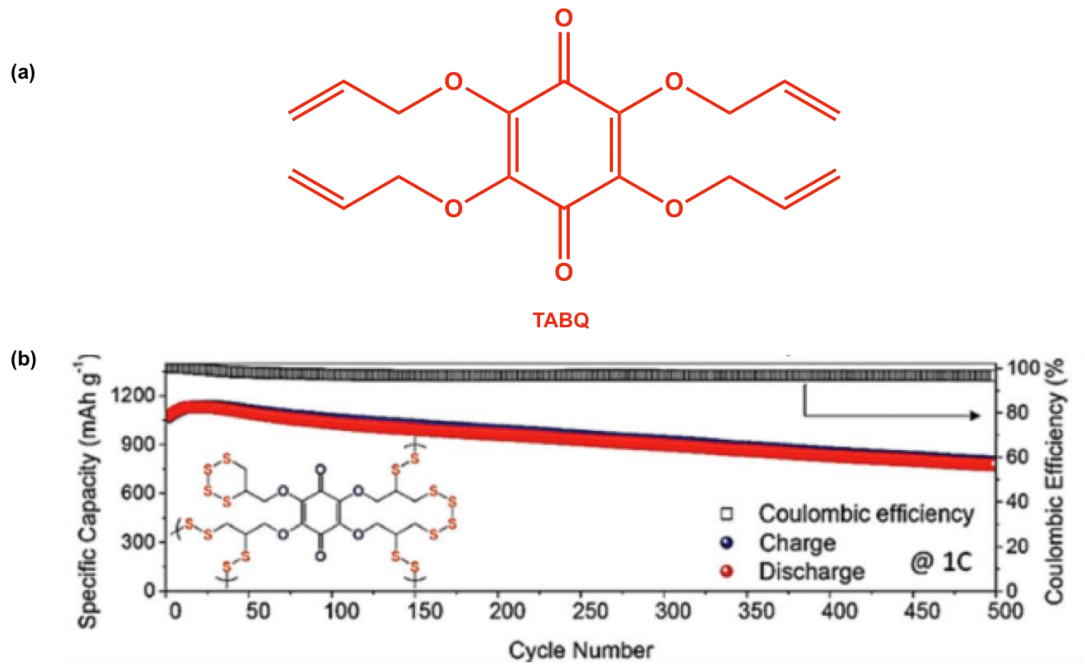

Figure 1.14 (a) Structure of tetra(allyloxy)-1,4-benzoquinone (TABQ). (b) Long life cycling with poly(S-TABQ) as an active cathode material in a lithium cell at 1C.

deposition of lithium sulfide products (e.g. Li_2S).[39,54,55,59] Many of the batteries prepared using inverse vulcanised sulfur polymers result in low cycling rates and a rapid capacity fade with increase cycling rates, although specific capacities reported are high.[39] Therefore, there is still scope for further development.

An exception to this is poly(S-tetra(allyloxy)-1,4-benxoquinone), poly(S-TABQ), which retained a high specific capacity of 833 mA h g^{-1} at a cycling of 10 C.[60] When this polymer was tested as an active cathode material, it exhibited excellent cycling capability suffering minimal capacity fade.[60] Figure 1.14b shows the long cycling of this material at 1C, there is a slight decrease in specific capacity, however, this is minimal in comparison to other reported inverse vulcanised materials acting as cathodes.

1.4.5 Heavy metal remediation/ environmental protection

With sulfur having a high affinity for mercury, the potential of these polymers for environmental protection and heavy metal remediation has been extensively studied. In particular, Chalker and Hasell *et al.* have investigated inverse vulcanisation with renewable alkene crosslinkers (Figure 1.15) and used the resultant materials to study

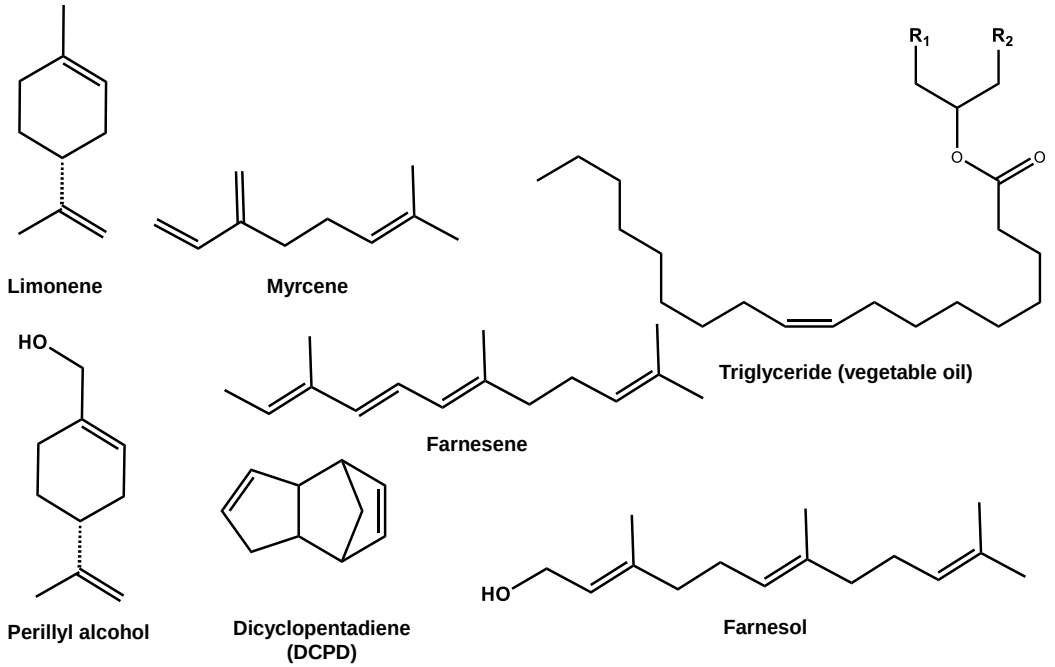

Figure 1.15 Renewable monomers used in inverse vulcanisation by both Chalker and Hasell *et al.*

heavy metal uptake.[25,61,62] The groups have employed salt templating methods and supercritical CO_2 foaming to induce porosity into these materials, in order to enhance metal and crude oil remediation.[44,61,63]

Chalker and co-workers were the first to report sulfur-limonene for the application of both palladium and mercury capture.[25] In later research, they then explored copolymers prepared from vegetable oils and demonstrated the use of these materials for metal uptake,[64] crude oil remediation[38] and slow-release fertilisers.[65] Following this, Hasell *et al.* prepared low-cost sulfur polymers with monomers dicyclopentadiene and renewable terpenes such as perillyl alcohol, myrcene, farnseol and farnesene (Figure 1.15).[61] Porosity was induced into these polymers to increase surface area and increase adsorption of mercury from aqueous mercury solutions.[44,63]

1.4.6 Biodegradable and recyclable sulfur polymers

As previously mentioned, synthetic polymers are among the most extensively manufactured materials on earth. Therefore, investigating the biodegradability of sulfur polymers is an avenue worth exploring. The mechanism of degradation is likely to be different depending on the percentage of sulfur in the material and the crosslinker used.[1] Chalker and co-workers highlight in their review that sulfur polymers may be degraded by long term exposure to sunlight or reductases found in living organisms, which is a result of the S-S bonds being susceptible to reduction and photolysis.[1] Although this is yet to be investigated, sulfur polymers could be designed in the future to potentially biodegrade at different lifetimes.

The biodegradability of the polymers could allow for an investigation into ways that these polymers could be recycled. S-S bonds are much weaker than C-C bonds, therefore there may be ways in which the polymers could be depolymerised back to their monomers or other precursors.[1] Investigating the biodegradability and recyclability of these materials is a necessary step to industrial scale-up and commercialisation.

1.4.7 Scale-up of sulfur polymers

With sulfur polymers showing very promising properties that can be applied to various functional applications, research must be conducted on the scale-up of high sulfur content polymers. Kilogram scale-up of these polymers has been already been reported.[28,38] However, scale-up has not been without its problems, with reports of the Trommsdorf-Norrish effect observed (Figure 1.16a) when attempting to prepare these sulfur polymers on a kilogram scale.[28] This effect is caused by an increase in viscosity

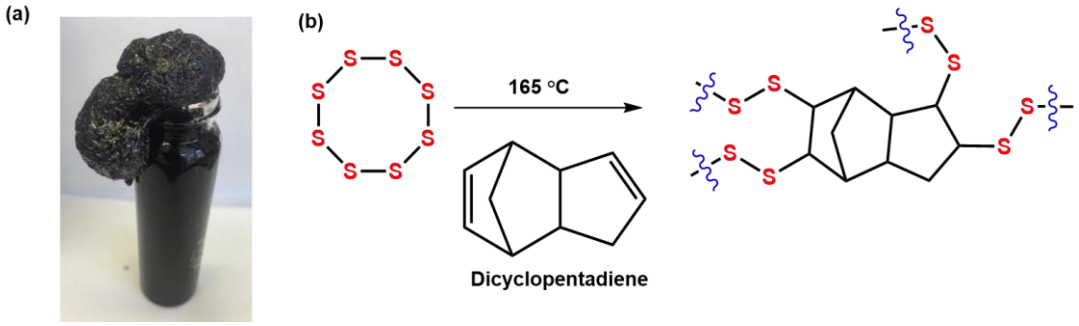

Figure 1.16 (a) Tromsdorff-Norish effect whilst reaction sulfur with dicylopentadiene. The effect is caused by increased viscosity during polymerisation causing the inhibition of termination steps, whilst initiation and propagation continue. (b) Reaction scheme showing sulfur reaction with dicyclopentadiene (DCPD).

during polymerisation, which in turn causes inhibition of termination steps whilst initiation and propagation continue.[66] This then leads to exothermic auto acceleration and a 'foaming' effect is observed (Figure 1.16a). Commercial applications of sulfur polymers may require upwards of hundreds of kilograms of polymer, the increase in viscosity during the reaction will make this a challenge. Therefore, there is a great need to develop a continuous process. There have been suggestions in the literature that a reactive extrusion process could provide large scale synthesis and could keep the Trommsdorf effect at bay.[1]

1.5 Thesis Overview

The first chapter of this thesis has described the principal aspects and development of inverse vulcanisation from the first discovery in 2013 by Pyun and co-workers.[5] Due to the unique properties these materials exhibit there are a lot of avenues still to explore and understand. More understanding of these materials will be crucial for future development. Whilst the research in this thesis has been ongoing there has been a growing interest in this field.

The main objective of the research presented in this thesis is to develop a range of inverse vulcanised sulfur polymers, to aid further understanding of these materials, and discover the limitations of the polymers prepared.

Attempts have been made to understand and to improve both the physical and chemical properties. The thesis is structured into the following chapters:

Chapter 2: **High sulfur content polymers: The effect of crosslinker structure on inverse vulcanisation**

This chapter will aim to discuss why seemingly similar crosslinkers result in polymers with radically different properties. The main three published polymers at the time of this research will be discussed, as well as a new system using 5-ethylidene-2-norbornene (ENB) as a crosslinker. This was the first crosslinker reported that could be stabilised up to 90% elemental sulfur by mass. Synthesis, spectroscopy, and modelling are combined to study the structure-property relationship of sulfur polymers.

Chapter 3: **Crosslinker copolymerisation for property control in inverse vulcanisation**

The third chapter will aim to discuss how the physical properties of sulfur polymers can be improved. Some crosslinkers were found to be unreactive with sulfur. This chapter will shed a light on how this was overcome with four new sulfur terpolymers reported. It will be discussed how two distinct alkene monomers could predictively tune glass transition, molecular weight, solubility, tune mechanical properties and colour.

Chapter 4: **Investigating the antibacterial properties of inverse vulcanised sulfur polymers**

The fourth chapter will discuss an under-researched area of sulfur polymers- the antibacterial properties. Two common bacteria species (*E.coli* & *S. Aureus*) were exposed to two structurally different inverse vulcanised sulfur polymers (sulfur-co-diisopropenylbenzene and sulfur-dicyclopentadiene), to study the antibacterial properties and investigate potential pathways to how antibacterial activity may occur.

Chapter 5: **Catalytic inverse vulcanisation**

The fifth chapter will discuss how the restricted choice of crosslinkers can be overcome by reducing reaction temperatures with catalysts. This catalytic method is effective for a wide range of crosslinkers, reduces both reaction temperature and time,

reduces H_2S production, increases yield, improves properties and allows crosslinkers that would otherwise be unreactive to be used.

Chapter 6: **Conclusions**

To conclude, the main results of this work will be summarised and their impact on the development of new inverse vulcanised sulfur polymers for functional materials will be outlined.

1.6 References

1 J. M. Chalker, Kucera.L.Renata and M. J. H. Worthington, *Green Chem.*, 2017, **00**, 1–6.

2 B. Seel, F, Muller, A, Krebs, *Sulfur in History: The role of sulfur in 'Black Powder', in Sulfur-Its Signficance for Chemistry, for the Geo-,Bio and Cosmophere and Technology*, Elservier, 5th edn., 1984.

3 Y. Zhang, R. S. Glass, K. Char and J. Pyun, *Polym. Chem.*, 2019, **10**, 4078–4105.

4 R. J. Angelici, *Acc. Chem. Res.*, 1988, **21**, 387–394.

5 W. J. Chung, J. J. Griebel, E. T. Kim, H. Yoon, A. G. Simmonds, H. J. Ji, P. T. Dirlam, R. S. Glass, J. J. Wie, N. a Nguyen, B. W. Guralnick, J. Park, A. Somogyi, P. Theato, M. E. Mackay, Y. Sung, K. Char, J. Pyun, Á. Somogyi, P. Theato, M. E. Mackay, Y. Sung, K. Char, J. Pyun, A. Somogyi, P. Theato, M. E. Mackay, Y. Sung, K. Char, J. Pyun, Á. Somogyi, P. Theato, M. E. Mackay, Y. Sung, K. Char and J. Pyun, *Nat. Chem.*, 2013, **5**, 518–524.

6 *Washingt. D.C Environ. Prot. Agency.*, 1991, 1–4.

7 V. C. Srivastava, 2012, **3**, *RSC. Adv* ,759–783.

8 J. A. Ober, *Concrete*, 2002, 202–298.

9 F. A. Duarte, P. D. A. Mello, C. A. Bizzi, M. A. G. Nunes, E. M. Moreira, M. S. Alencar, H. N. Motta, V. L. Dressler and É. M. M. Flores, *Fuel*, 2011, **90**, 2158–2164.

10 C. Song, *Catal. Today*, 2003, **86**, 211–263.

11 G. C. Laredo, C. R. López, R. E. Álvarez and J. L. Cano, *Fuel*, 2004, **83**, 1689–1695.

12 J. Ding, Y. Zhang and R. Wang, *New.J.Chem*, 2019, **43**, 7363–7370.

13 Y. Shiraishi, T. Hirai and I. Komasawa, *Energy Fuels*, 2004, **18**, 116–121.

14 Y. Shen, X. Liu and J. Jia, *RSC. Adv*, 2012, **2** ,8867–8882.

15 P. G. Moses, B. Hinnemann, H. Topsøe and J. K. Nørskov, *J. Catal.*, 2007, **248**, 188–203.

16 A. L. Kohl, R. B. Nielsen, Gas Purification, 5th Edition, 1997.

17 J. A. Smith, S. J. Green, S. Petcher, D. J. Parker, B. Zhang, M. J. H. Worthington, X. Wu, C. A. Kelly, T. Baker, C. T. Gibson, J. A. Campbell, D. A. Lewis, M. J. Jenkins, H. Willcock, J. M. Chalker and T. Hasell, *Chem. Eur.J.* ,2019, **25**, 10433–10440.

18 B. Worm, H. K. Lotze, I. Jubinville, C. Wilcox and J. Jambeck, *Annual review of environmental resources*, 2017, **42**, 1-26 .

19 R. C. Thompson, C. J. Moore, F. S. Saal and S. H. Swan, *Phil Trans R Soc Lond B Biol Sci.*,2010, **346**, 2153–2166.

20 G. Z. Papageorgiou, *Polymers*, 2018, **10**, 952.

21 B. Meyer, *Chem. Rev,* 1976, **3**, 376-388

22 R. Steudel and B. Eckert, *Elem. Sulfur Sulfur-Rich Compd. I*, 2003, 1–80.

23 E. Powell, H. Potter, *J.Am.Chem.Soc*,1935, **57**, 1316-1321.

24 D. A. Boyd, *Angew. Chemie - Int. Ed.*, 2016, **55**, 15486–15502.

25 M. P. Crockett, A. M. Evans, M. J. H. Worthington, I. S. Albuquerque, A. D. Slattery, C. T. Gibson, J. A. Campbell, D. A. Lewis, G. J. L. Bernardes and J. M. Chalker, *Angew. Chemie - Int. Ed.*, 2016, **55**, 1714–1718.

26 A.Y.Coran, *The science of rubber and Technology* (*Fourth Edition)*, 2013.

27 H. L. Fisher, *Ind. Eng. Chem.*, 1939, **31**, 1381–1389.

28 J. J. Griebel, G. Li, R. S. Glass, K. Char and J. Pyun, *J. Polym. Sci. Part A Polym. Chem.*, 2015, **53**, 173–177.

29 J. J. Griebel, N. A. Nguyen, S. Namnabat, L. E. Anderson, R. S. Glass, R. A. Norwood, M. E. Mackay, K. Char and J. Pyun, *ACS Macro Lett.*, 2015, **4**, 862–866.

30 T. S. Kleine, N. A. Nguyen, L. E. Anderson, S. Namnabat, E. A. LaVilla, S. A. Showghi, P. T. Dirlam, C. B. Arrington, M. S. Manchester, J. Schwiegerling, R. S. Glass, K. Char, R. A. Norwood, M. E. Mackay and J. Pyun, *ACS Macro Lett.*, 2016, **5**, 1152–1156.

31 Z. Deng, A. Hoefling, P. Théato and K. Lienkamp, *Macromol. Chem. physi*, 2018, **1700497**, 1–6.

32 J. A. Smith, R. Mulhall, S. Goodman, G. Fleming, H. Allison, R. Raval and T. Hasell, *ACS Omega*, 2020, **5**, 5229–5234.

33 Martin, J. M. & Smith, W. K. Handbook of Rubber Technology. Vol 1 (Satish Kumar Jain for CBS Publishers & Distributors, Delhi, 2007).

34 Q. Lian, Y. Li, K. Li, J. Cheng and J. Zhang, *Macromolecules*, 2017, **50**, 803–810.

35 M. Arslan, B. Kiskan and Y. Yagci, *Macromolecules*, 2015, **48**, 1329–1334.

36 J. A. Smith, X. Wu, N. G. Berry and T. Hasell, *J. Polym. Sci. Part A Polym. Chem.*, 2018, **56**, 1777–1781.

37 X. Wu, J. A. Smith, S. Petcher, B. Zhang, D. J. Parker, J. M. Griffin and T. Hasell, *Nat. Commun.*, 2019, **10**, 1–9.

38 M. J. H. Worthington, C. J. Shearer, L. J. Esdaile, J. A. Campbell, C. T. Gibson, S. K. Legg, Y. Yin, N. A. Lundquist, J. R. Gascooke, I. S. Albuquerque, J. G. Shapter, G. G. Andersson, D. A. Lewis, G. J. L. Bernardes and J. M. Chalker, *Chem.Eur.J*, 2018, **23**, 1–7.

39 A. Hoefling, Y. J. Lee and P. Theato, *Macrocol.Chem.Phys.*, 2016, **218**, 18–21.

40 M. Arslan, B. Kiskan and Y. Yagci, *Macromolecules*, 2016, **49**, 767–773.

41 M. A. Martin-Luengo, M. Yates, E. S. Rojo, D. Huerta Arribas, D. Aguilar and E. Ruiz Hitzky, *Appl. Catal. A Gen.*, 2010, **387**, 141–146.

42 S. A. Sanchez-Vazquez, T. D. Sheppard, J. R. G. Evans and H. C. Hailes, *RSC Adv.*, 2014, **4**, 61652–61655.

43 Y. Zhang, N. G. Pavlopoulos, T. S. Kleine, M. Karayilan, R. S. Glass, K. Char and J. Pyun, *J. Polym. Sci. Part A Polym. Chem.*, 2019, **57**, 7–12.

44 Y.Zhang, R.Glass, K.Chen and J.Pyun, *Polym.chem.*, 2019, **10**, 4078-4105.

45 J. J. Griebel, S. Namnabat, E. T. Kim, R. Himmelhuber, D. H. Moronta, W. J. Chung, A. G. Simmonds, K. J. Kim, J. Van Der Laan, N. A. Nguyen, E. L. Dereniak, M. E. MacKay, K. Char, R. S. Glass, R. A. Norwood and J. Pyun, *Adv. Mater.*, 2014, **26**, 3014–3018.

46 D. A. Boyd, V. Q. Nguyen, C. C. Mcclain, F. H. Kung, C. C. Baker, J. D. Myers, M. P. Hunt, W. Kim and J. S. Sanghera, *ACS Macro Lett.*, 2019, **8**, 113–116.

47 A. M. Abraham, S. V. Kumar and S. M. Alhassan, *Chem. Eng. J.*, 2018, **332**, 1–7.

48 V. S. Wadi, K. K. Jena, S. Z. Khawaja, V. M. Ranagraj and S. M. Alhassan, *RSC Adv.*, 2019, 4397–4403.

49 D. J. Parker, S. T. Chong and T. Hasell, 2018, *RSC.Adv*, **8**,27892–27899.

50 M. Capelot, M. M. Unterlass and L. Leibler, *ACS Macro Lett*, **1**, 2012, 1–4.

51 W. Denissen, J. M. Winne and F. E. Du Prez, *Chem. Sci.*, 2015, **7**, 30–38.

52 M. Arslan, B. Kiskan and Y. Yagci, *Macromolecules*, 2016, **49**, 767–773.

53 A. G. Simmonds, J. J. Griebel, J. Park, K. R. Kim, W. J. Chung, V. P. Oleshko, J. Kim, E. T. Kim, R. S. Glass, C. L. Soles, Y. Sung and K. Char, *ACS Macro Lett.*, 2014,**3**, 229-232.

54 Y. Zhang, J. J. Griebel, P. T. Dirlam, N. A. Nguyen, R. S. Glass, M. E. Mackay, K. Char and J. Pyun, *J.Polym.Sci.,Part A:Polym.Chem*, 2017, **55**,107–116.

55 F. Wu, S. Chen, V. Srot, Y. Huang, S. K. Sinha, P. A. van Aken, J. Maier and Y. Yu, *Adv. Mater.*, 2018, **30**, 1–8.

56 A. Hoefling, D. T. Nguyen, Y. J. Lee, S.-W. Song and P. Theato, *Mater. Chem. Front.*, 2017, **1**, 1818–1822.

57 P. T. Dirlam, A. G. Simmonds, T. S. Kleine, N. A. Nguyen, L. E. Anderson, A. O. Klever, A. Florian, P. J. Costanzo, P. Theato, M. E. Mackay, R. S. Glass, K. Char and J. Pyun, *RSC Adv.*, 2015, **5**, 24718–24722.

58 Y. X. Yin, S. Xin, Y. G. Guo and L. J. Wan, *Angew. Chemie - Int. Ed.*, 2013, **52**, 13186–13200.

59 I. Gomez, O. Leonet, J. A. Blazquez and D. Mecerreyes, *ChemSusChem*, 2016, **9**, 3419–3425.

60 H. Kang, H. Kim and M. J. Park, *Adv. Energy Mater.*, 2018, **8**, 1–9.

61 D. J. Parker, H. A. Jones, S. Petcher, L. Cervini, J. M. Griffin, R. Akhtar and T. Hasell, *J. Mater. Chem. A*, 2017, **5**, 11682–11692.

62 N. A. Lundquist, M. J. H. Worthington, N. Adamson, C. T. Gibson, M. R. Johnston, A. V. Ellis and J. M. Chalker, *RSC Adv.*, 2018, **8**, 1232–1236.

63 S. Petcher, D. J. Parker and T. Hasell, *Environ. Sci. Water Res. Technol.*, 2019, **5**, 2142–2149.

64 N. A. Lundquist, M. J. H. Worthington, N. Adamson, C. T. Gibson, M. R. Johnston, A. V. Ellis and J. M. Chalker, *RSC Adv.*, 2018, **8**, 1232–1236.

65 M. Mann, J. E. Kruger, F. Andari, J. McErlean, J. R. Gascooke, J. A. Smith, M. J. H. Worthington, C. C. C. McKinley, J. A. Campbell, D. A. Lewis, T. Hasell, M. V Perkins and J. M. Chalker, *Org. Biomol. Chem.*, 2019, **17**, 1929–1936.

66 D. J. Parker, H. A. Jones, S. Petcher, L. Cervini, J. M. Griffin, R. Akhtar and T. Hasell, *J. Mater. Chem. A*, 2017, **5**, 11682–11692.

CHAPTER 2

HIGH SULFUR CONTENT POLYMERS: THE EFFECT OF CROSSLINKER STRUCTURE

Chapter 2: High Sulfur Content Polymers: The Effect of Crosslinker Structure on Inverse Vulcanisation

2.1 Context

Section 2.2 is adapted from the paper "High Sulfur Content Polymers: The Effect of Crosslinker Structure on Inverse Vulcanisation", published in the Journal of Polymer Science Part A: Polymer Chemistry, 2018. Investigating high sulfur content polymers for many different applications is vital, as discussed in detail in Chapter 1. However, to optimise polymerisations, it is essential to understand how different crosslinkers and the percentage of sulfur can change the polymers' properties. Inverse vulcanised high sulfur content polymers have attracted much attention due to their low cost and diverse applications. Since Pyun and co-workers discovery of inverse vulcanised sulfur polymers,[1] there is now a wide range of polymers published.[2] Before this work, one aspect that had not been discussed in the literature is why structurally similar crosslinkers, in terms of molecular mass and degree of unsaturation, produce materials of dramatically different properties after reaction with sulfur e.g. viscous liquids to rubbery or glassy solids. There have been some suggestions and proposed mechanisms for inverse vulcanisation,[2,3,4] but in this chapter, we are assuming bulk free radical polymerisations. This research adds to the discussion about the reactivity of crosslinkers and presents new ways in how we can potentially screen crosslinkers before performing reactions. In this chapter, both computational and experimental data is presented to investigate the structure-property relationships of a series of related crosslinkers in inverse vulcanisation reactions.

2.1.2 Author contributions

Jessica. A. Smith conducted all experiments, wrote the manuscript, and prepared all figures with help and guidance from the other authors. Jessica. A. Smith presented to Prof. Neil. G. Berry the idea of using computational calculations. Prof. Neil. G. Berry taught Jessica. A. Smith how to conduct computational calculations and gave a lot of guidance and advice. Dr. Xiaofeng Wu advised on how to conduct gas capture experiments. Dr.Tom Hasell was the PI on this project and gave much advice and direction.

2.2. Introduction

2.1.1 Comparison of Crosslinkers

As mentioned in Chapter 1, it was Pyun and co-workers that initially reported poly (S-r-DIB).[1] DIB is relatively expensive as a crosslinker compared to sulfur, and since this discovery, there was a drive to use crosslinkers that are renewable and cost less. In 2016, Chalker *et al.* investigated the possibility of limonene as a crosslinker in inverse vulcanisation (Figure 2.1).[5] In comparison to DIB, limonene is cheaper, with the vast majority of limonene produced in the citrus industry (110-165 million lb/year).[5] Limonene has many advantages; being bio-derived, inexpensive, and renewable. However, the sulfur-limonene polymer formed was a low molecular weight

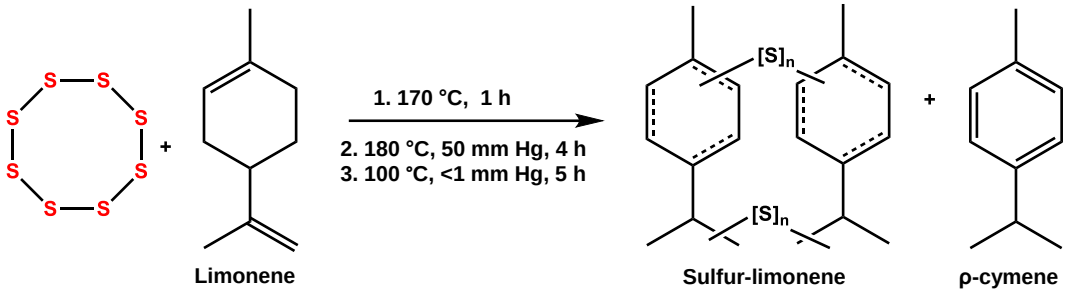

Figure 2.1 (a) Reaction between sulfur and limonene as reported by Chalker and co-workers. ρ-cymene was detected as a by-product.

polysulfide (Mw=242 $gmol^{-1}$), was not shape persistent (Figure 2.2) and only produced a stable polymer up to 50% sulfur by mass.[5]

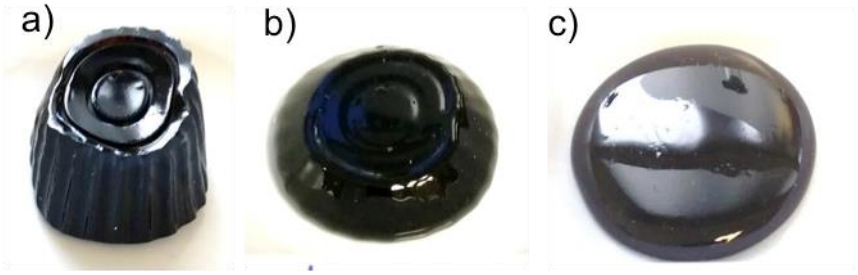

Figure 2.2 Photographs of sample of sulfur-limonene polysulfide (a) After removing from a mould (b) After 2 hours at room temperature (c) After 24 hours at room temperature.

Following this, dicyclopentadiene (DCPD) was used as a crosslinker to form sulfur-DCPD (S-DCPD) copolymer.[6] DCPD is a desirable material because it is abundant and inexpensive (as an industrial by-product from steam cracking naptha). However, this is not an entirely new phenomenon with research interest dating back to the 1970s, reports showing reactions with <50 wt.% sulfur reacting with DCPD.[7,8] Hasell *et al.* propose several different pathways for how sulfur could react with DCPD, with the reaction at both double bonds being most likely (Figure 2.3b).[6] At the time of this research, DCPD was one of the only inverse vulcanised sulfur polymers that formed a

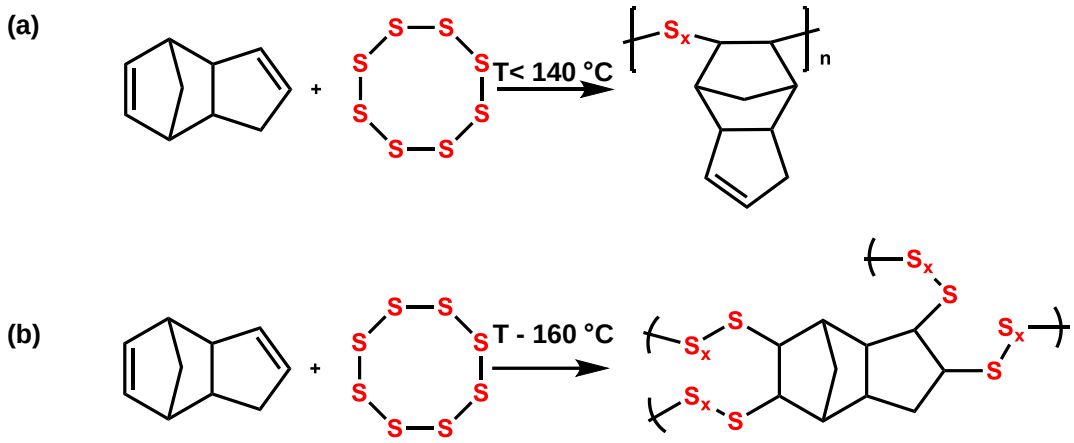

Figure 2.3 Different potential reactions of sulfur with DCPD leading to linear (a) or network (b) polymers.

highly crosslinked network and insoluble in most common organic solvents.

When DCPD and DIB are used to crosslink sulfur, amorphous polymers with up to 80% of sulfur by mass can be achieved. Sulfur-DCPD forms a highly crosslinked, insoluble network. It is assumed to be a hyperbranched network,[6] compared to sulfur-limonene, which is only stable up to a maximum of 50% sulfur by mass. In this chapter, we compare crosslinkers DCPD, DIB, and Limonene, with a new structurally similar alternative, 5-Ethylidene-2-norbornene (ENB) (Figure 2.4).

ENB was chosen as a potential crosslinker for comparison due to its structural similarities to DCPD, to gain a clearer insight into how inverse vulcanisation may be

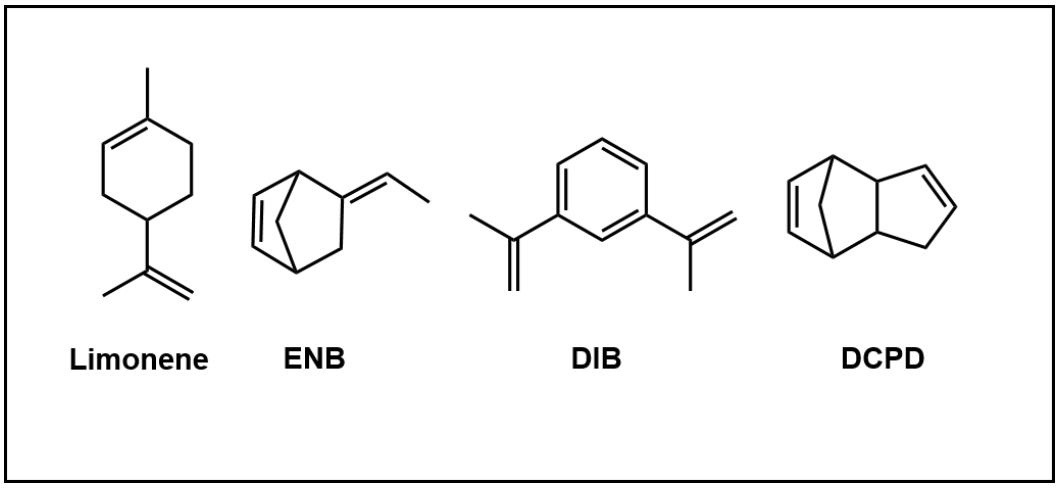

Figure 2.4 From left to right: Limonene, 5 Ethylidene-2-norbornene (ENB), 1, 3-diisopropenylbenzene (DIB) and dicyclopentadiene (DCPD).

controlled and occur. ENB, commonly used in the manufacturing of ethylene-propylene diene terpolymers (EPDM),[9] is inexpensive and can be readily sourced in bulk.

2.1.2 Fukui indices

The susceptibility of the double bond to reaction with sulfur radicals may determine the reaction temperature and rate, and the resultant molecular weight and degree of crosslinking. To aid understanding when comparing these crosslinkers, computational calculations known as Fukui indices were performed in this chapter to predict reactivity sites.

2.1.2 What are Fukui indices?

Fukui's Frontier Molecular Orbital Theory predicts the chemical reactivity of each atom in a molecule in a nucleophilic, electrophilic, or a radical sense. It is interpreted in terms of highest occupied molecular orbital (HOMO) and lowest unoccupied molecular orbital (LUMO) electron density.[10] Fukui indices themselves are reactivity descriptors to identify the most reactive sites for electrophilic, nucleophilic, and radical attack within a molecule. The larger the Fukui function, the more susceptible the double bond is to radical attack.[10]

$$Nucleophilic\ attack = q_N^A - q_{N+1}^A$$

$$Electrophilic\ attack = q_{N-1}^A - q_N^A$$

$$Radical\ attack = (\ q^{A}_{N-1}\ -\ q^{A}_{N+1}\ )/2$$

Equation 1: The definition of condensed Fukui functions where q^{A}_{N} is the partial charge of atom A in the molecule with N electrons. Where q^{A}_{N+1} and q^{A}_{N-1} are partial charges of atom A in the molecule with N+1 electrons and N-1 electrons, respectively.[10]

Calculating Fukui functions is a relatively simple computational calculation within the context of density functional theory (DFT). The mechanism for inverse vulcanisation is not yet certain and at the time of this research, the only mechanism assumed in literature was bulk free radical copolymerisation. Therefore, here we are assuming the S_8 ring undergoes homolytic fission and radicals are formed. The Fukui function is considered an indicator for radical activity as it describes the ability of an atom to accommodate an extra electron or to cope with the loss of an electron.[10] Fukui indices have been used previously to predict C-H radical functionalisation sites on fused arenes and there are continued efforts to improve errors associated with this calculation.[10] For this research, calculating Fukui indices gave new insights into how crosslinkers could potentially be screened before conducting experimental work.

2.3 Chapter Aims

1. Investigate 5 Ethylidene-2-norbonene (ENB) as a novel new crosslinker in inverse vulcanisation reactions.

2. Combine synthesis, spectroscopy and computational modelling to investigate structure-property relationships of the main previously published crosslinkers (DIB, DCPD, limonene) and the new S-ENB polymer.

3. Develop a way in which crosslinkers can be screened to potentially predict polymer structures before conducting experimental work.

2.4 Results and Discussion

In this study, "S-crosslinker" will be used henceforth to refer to a copolymer of sulfur and the stated crosslinker (or crosslinkers).

2.4.1 Synthesis and characterisation of S-ENB copolymers

Inverse vulcanised sulfur-ENB (S-ENB) copolymers were successfully prepared of ratios 50-90% elemental sulfur by mass (Figure 2.5, experimental procedure 2.6.2). This is a facile one-pot synthesis that does not require any solvents or initiators to encourage polymerisations. Elemental sulfur is heated until molten and ENB is directly added into the molten sulfur upon heating. What makes this reaction desirable is elemental sulfur acts as a solvent and monomer during this reaction with no need for an initiator, unlike traditional polymerisations (general experimental procedure 2.6.2).[14]

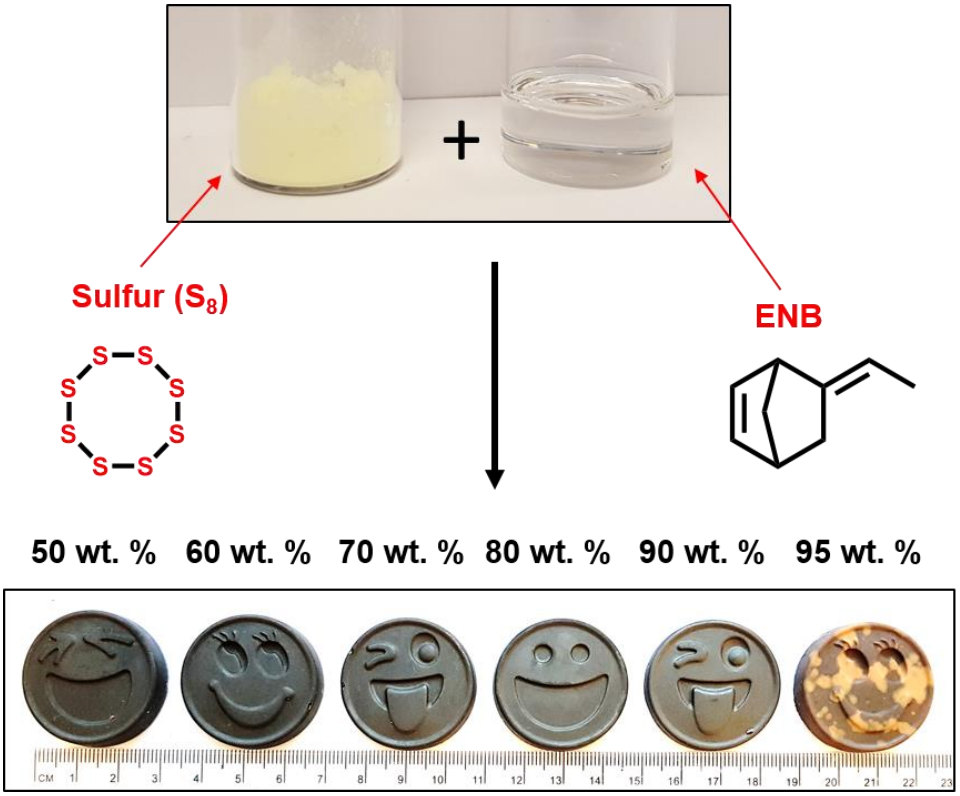

Figure 2.5. Top: elemental sulfur (left) and ENB crosslinker (right). Bottom: S-ENB polymers 50, 60, 70, 80 and 95% of elemental sulfur by mass. With the 95 wt. % ENB crosslinker photograph showing sulfur bloom (depolymerisation of sulfur back to S_8 crystals).

Before the reaction was successful, several experiments were conducted with varying conditions to optimise and understand the conditions of the S-ENB copolymerisation. Initially, a 12 mL vial (adapted general procedure 2.6.4) was used to carry out the reaction by inverse vulcanisation similar to other reported reaction conditions.[1,6] As the reaction proceeded the molten sulfur phase and ENB phase failed to mix. There was an increase in viscosity at the bottom of the two phases (molten sulfur phase); this

could indicate that either polymeric sulfur was beginning to form or oligomers. An increase in viscosity would be expected as the polymerisation proceeds; however, the

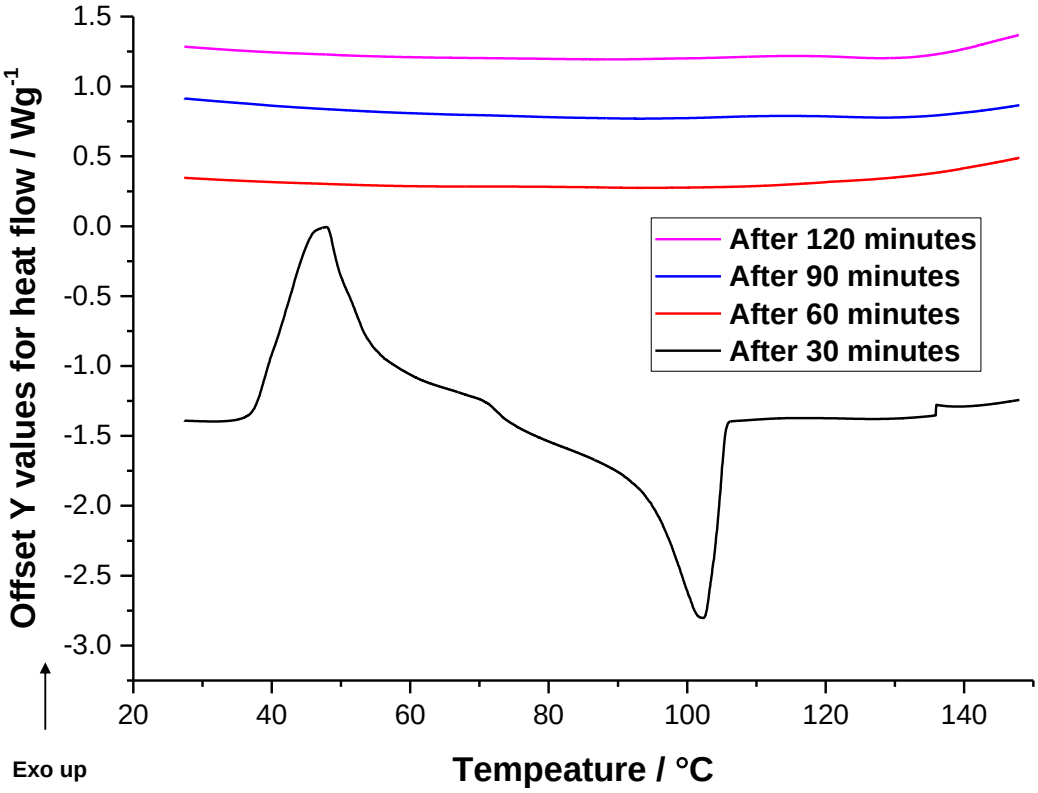

Figure 2.6 DSC thermogram for 50% elemental sulfur and 50% ENB by mass sample after 30, 60, 90- and 120 minute's reaction time. After 30 minutes reaction time a melting transition (T_m) for elemental sulfur is observed, suggesting this is not enough time for sulfur to be consumed.

separation in two phases was due to insufficient mixing. To overcome insufficient mixing, a sonicator and vortex were used to mix the two phases (molten sulfur and ENB). However, both of these methods were unsuccessful due to the rapid precipitation of elemental sulfur; therefore, no subsequent data was obtained for these samples. Eventually, insufficient mixing during the reaction was overcome by using a larger vial (40 mL) and a large cross stirrer bar (general experimental procedure 2.6.2). The reaction time of the polymerisation between sulfur and ENB was altered (30, 60, 90 and 120 minutes) for the 50% elemental sulfur by mass sample, without overnight curing, to observe when the sulfur was consumed. A reaction time of 30 minutes was not enough time for elemental sulfur to be react, as confirmed by the melting transition (T_m) at ~ 110 °C (Figure 2.6). From this, it could be concluded that a reaction temperature of 135 °C for 60 minutes before overnight curing was necessary to ensure the majority of sulfur was consumed.

The reaction temperature of S-ENB copolymerisation, in this work, is a lot lower than previously reported sulfur polymers at the time of this research.[1,5,6] The reaction was conducted at 135 °C, as the boiling point of the ENB crosslinker is 147.6 °C, therefore if conducted at higher temperatures, ENB would have likely evaporated and resulted in a less crosslinked polymer or no polymerisation. Although S-S homolysis is expected above the melting temperature of elemental sulfur, recent work on the rheology and self-healing properties of sulfur-containing polymers has suggested that homolysis of S-S occurs at temperatures lower than the melting transition temperatures of S_8 (110 °C and 119 °C), generating thiyl radicals which are below the reported floor temperature of S_8 (159 °C).[11] Other reactions have now been reported between molten sulfur with small organic crosslinkers significantly below the floor temperature of S_8.[12,13]

To identify whether the polymers prepared where amorphous, Powder-X-Ray Diffraction (PXRD) patterns where recorded (Figure 2.7). PXRD patterns for varying ratios (50- 90% sulfur by mass) of S-ENB show no evidence of crystalline sulfur

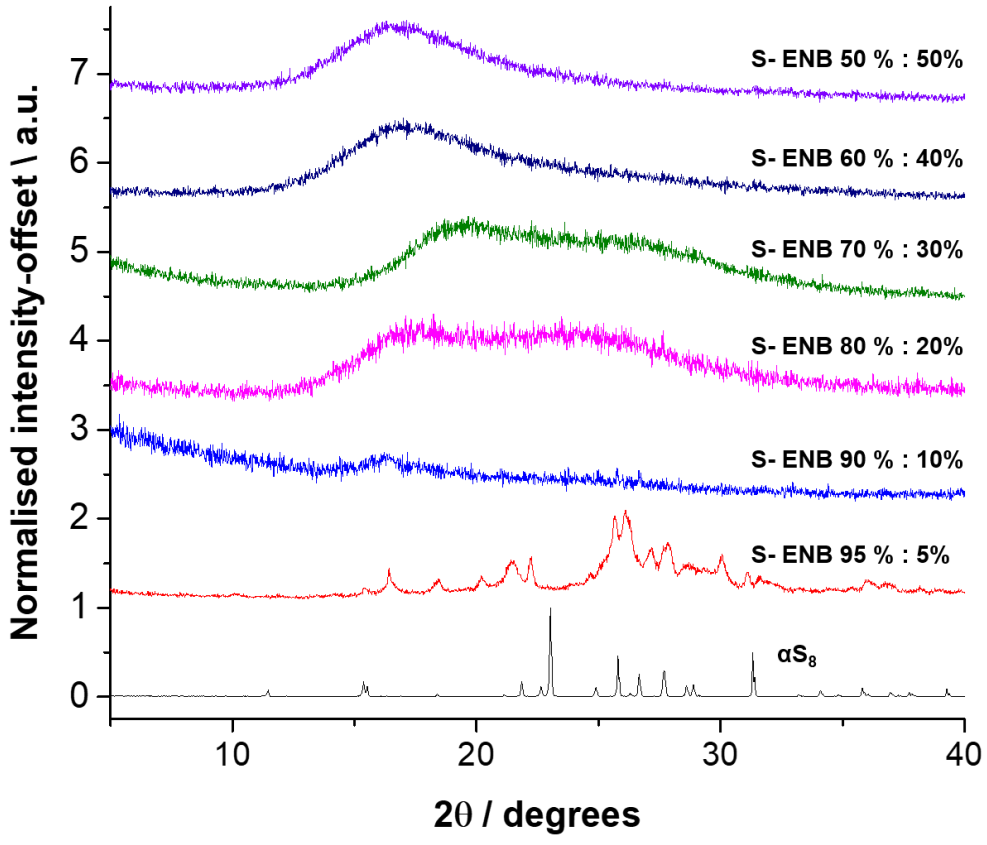

Figure 2.7 PXRD patterns of S-ENB and elemental sulfur, showing amorphous materials up to 90% sulfur by mass.

present, as there is no typical diffraction pattern for α-S_8 observed. This suggests that the S-ENB polymers are stable against depolymerisation of sulfur to S_8 after the reaction, even at ratios of up to 90% sulfur by mass. If polymers were not stable there would be evidence of S_8 crystals, and the polymer would not retain amorphous character. This level of stabilisation is remarkable in comparison with the majority of other inverse vulcanisation crosslinkers reported recently, with some of the best stabilising up to 80 wt. % sulfur,[1,6] but commonly 60 wt. %,[15] 50 wt. %[5] and even as low as 20 wt. %.[15] Of previously reported high sulfur content polymers, it is only sulfur-diallyl disulfide (SDA) that has proven to stabilise up to 90 wt. % of elemental sulfur in the form of a thin- film.[16] However, S-ENB provides a more readily sourced alternative to SDA, with comparable levels of sulfur stabilisation.

For an S-ENB copolymer that contains 95 wt.% of sulfur, we visibly see sulfur bloom (Figure 2.5), which is depolymerisation of sulfur back to S_8 crystals. This is further

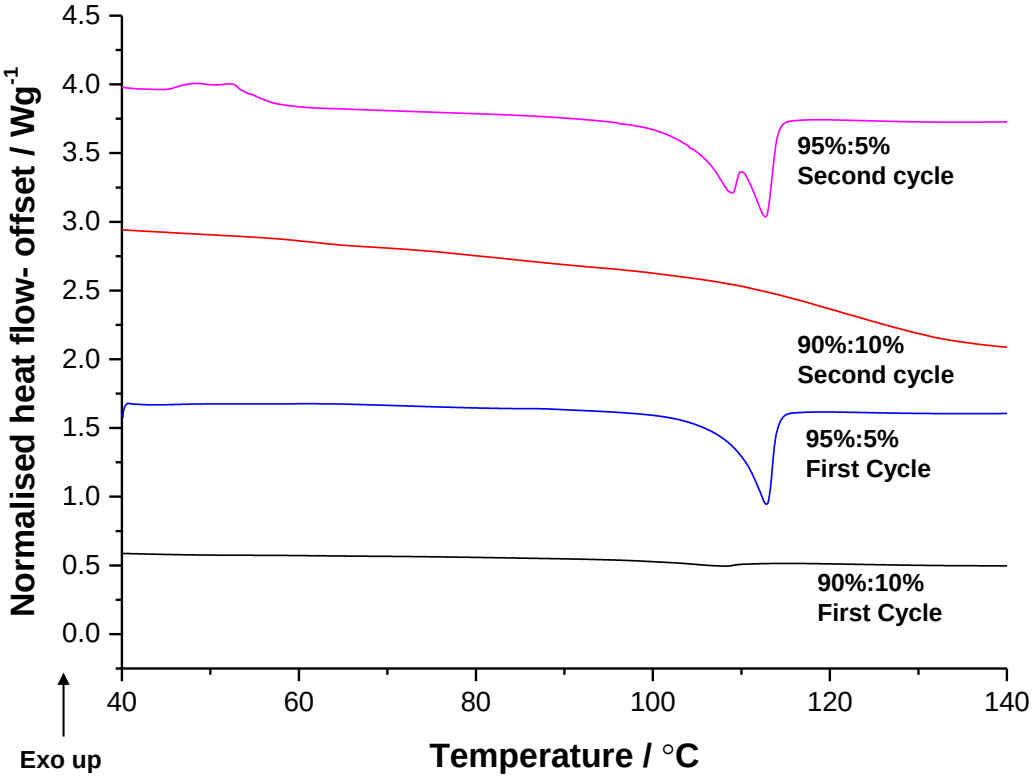

Figure 2.8 Representative DSC trace shown is 95% elemental sulfur by mass S-ENB copolymer, with a large melting transition (T_m) on both the first and second trace. The small T_m on the first cycle of the 90% elemental sulfur by mass sample can be attributed to crystallisation of long chain polysulfides.

confirmed by the observed PXRD diffraction patterns (Figure 2.7) and a strong melting transition on the first cycle by differential scanning calorimetry (DSC) (~ 118 °C)

(Figure 2.8). The second cycle in the DSC shows the 95 wt.% sulfur sample has two melting transitions which can be attributed to the melting of sulfur crystals (~ 110 °C and 119 °C). An S_8 melting transition is also visible for the 95 wt.% sample. It should be noted that on the representative DSC trace for the 90% elemental sulfur by mass sample (Figure 2.8), a slight peak at ~110 °C is observed on the first cycle only. While this could correspond to the melting transition (T_m) of elemental sulfur, such transitions have also been recently attributed to crystallisation of long chain polysulfide's present in inverse vulcanised sulfur polymers.[1,17] With the sample loading being above 90% sulfur by mass, long chain polysulfides would be expected.

To confirm the relative percentage of elemental sulfur incorporated into the S-ENB copolymers, elemental analysis was conducted (Appendix, Table A2.1). Elemental analysis corresponds well to expected values with a slight excess of sulfur likely caused by volatilisation of the crosslinker during the reaction.

Thermogravimetric analysis (TGA) of varying compositions of ENB and sulfur confirms complete reaction of sulfur and ENB (Figure 2.9). ENB was too volatile to

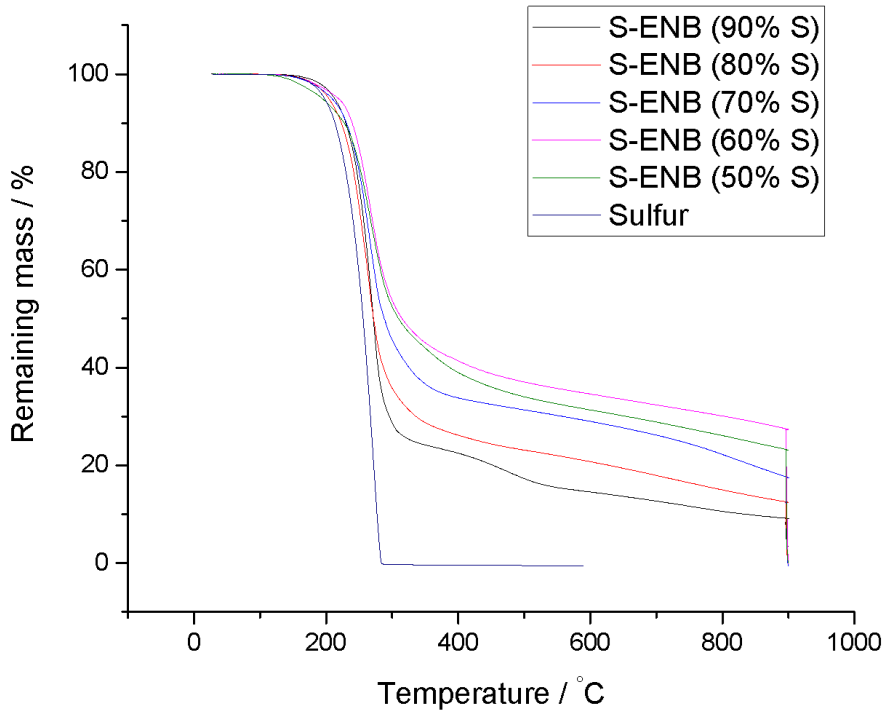

Figure 2.9 TGA thermograms of S-ENB polymers under N_2, materials with varying compositions of sulfur.

obtain TGA data, however, there is a clear decomposition for sulfur at approximately

250 °C (Figure 2.9). There is also an increasing percentage of char mass remaining as the composition of ENB increases (Figure 2.9), suggesting the polymer has successfully been synthesised.

Fourier transformation infrared (FTIR) of both 10 and 50 % ENB by mass shows either reduction or complete disappearance in the allylic =C-H and C=C stretching vibrations, 3045 cm^{-1} and 1600 cm^{-1} respectively (Figure 2.10). Overall, the characterisation suggests that the reaction between sulfur and ENB has been successful.

The glass transition temperatures (T_gs) of S-ENB copolymers were found to increase

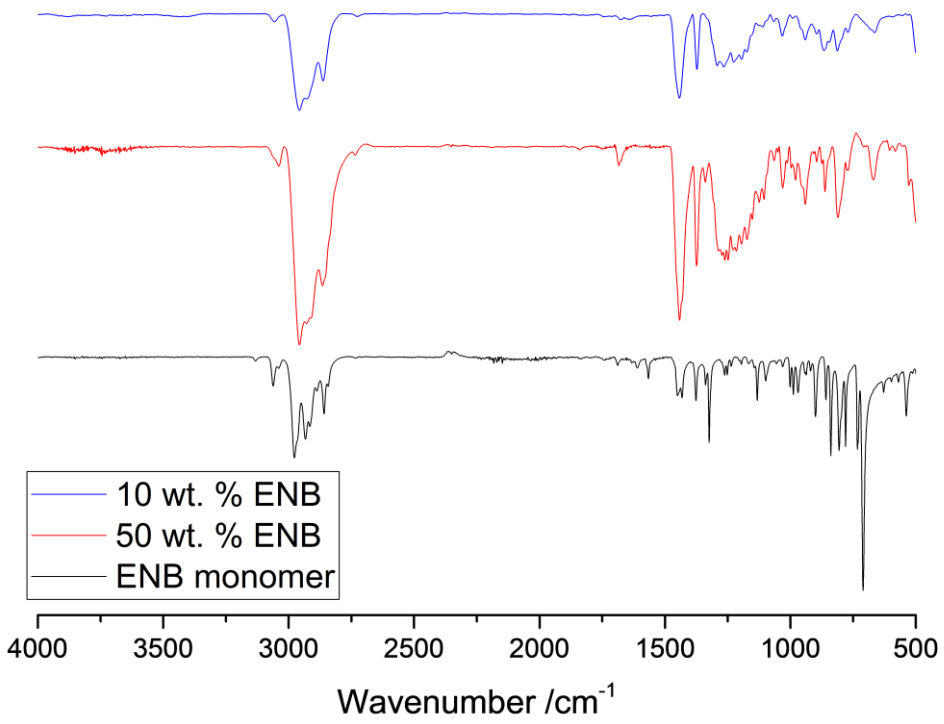

Figure 2.10 FTIR spectra of ENB and S-ENB polymers containing 10 and 50% sulfur by mass.

as a function of ENB composition (Figure 2.11), following a trend that is observed by other crosslinkers.[1,5,6] The highest observed T_g for the equal mass of sulfur and ENB, was 89 °C. This is higher than that of S-DIB (28 °C)[1] and S-limonene (-21 °C),[5] but lower than S-DCPD (115 °C).[6] When comparing crosslinkers, the relatively high T_g suggested S-ENB might have more in common with S-DCPD than S-limonene and S-DIB. It is not immediately apparent from the structures of the crosslinkers themselves why the resultant polymers have such a range of T_g. However, there is a correlation in the degree of polymerisation, crosslinking and the T_g.

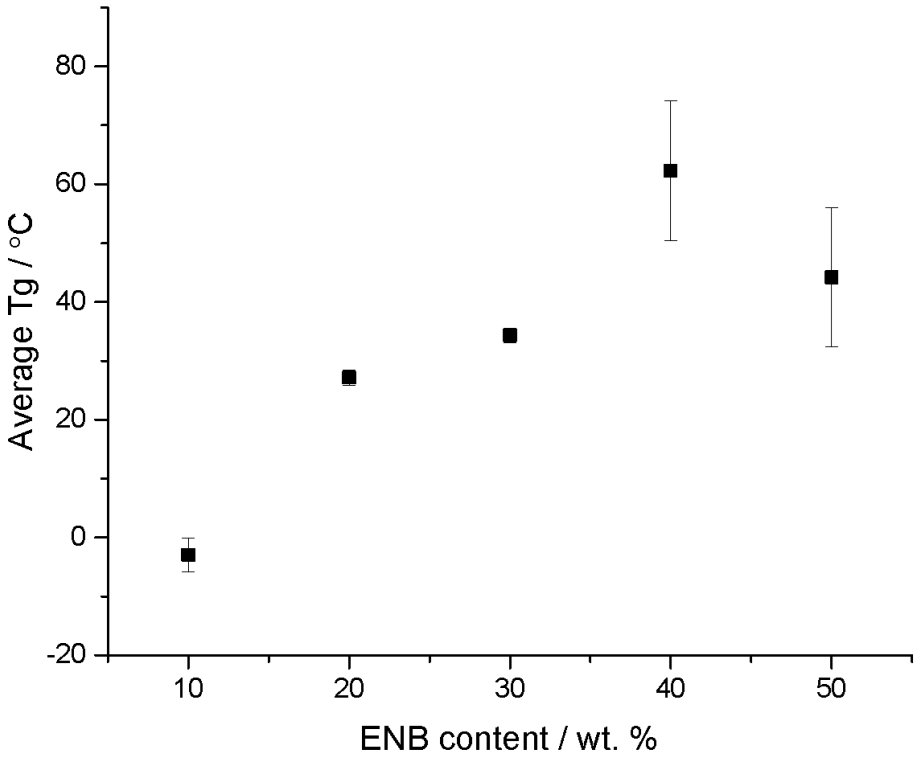

Figure 2.11 The T_g of S-ENB polymers as a function of ENB composition.

The solubility of S-ENB was compared to known polymers, with the results determined by > 100 mg solid in 10 mL solvent and stirring overnight (Appendix, Table A2.2). S-limonene and S-DIB show some solubility (Appendix, Table A2.2), with S-limonene known to be the lower molecular weight of the two. Whilst S-DCPD is fully insoluble (Table A2.2), due to what is presumably a high molecular weight, with a crosslinked structure.[6] Similar to S-DCPD, S-ENB shows a complete lack of solubility in common organic solvents. This poses the question, why do crosslinkers with similar molecular weights and the same number of double bonds, result in such differences in behaviour in the inverse vulcanisation process?

2.4.2 Understanding the reaction between sulfur and ENB

As already discussed, the inverse vulcanisation process is thought to be a bulk-free radical copolymerisation of unsaturated co-monomers in liquid sulfur; however, as with conventional vulcanisation, the mechanism is complex and not yet fully understood. At the time of this research, both radical addition across the double bonds and hydrogen abstraction had been proposed as potential mechanisms.[1,2,4] With the nature of the reaction likely to be temperature and crosslinker dependant.

Sulfur-olefin reactions are characterised as low temperature reactions up to about 140 °C, and high temperature reactions above 140 °C.[7] By this definition, the copolymerisation between sulfur and ENB is classified as a low temperature reaction. It has been previously reported that reactions between sulfur and DCPD at 140 °C were found to produce soluble linear polymers, with the norbornene double bond being the most reactive at this temperature (Figure 2.15a).[7] Since then, it has also been found

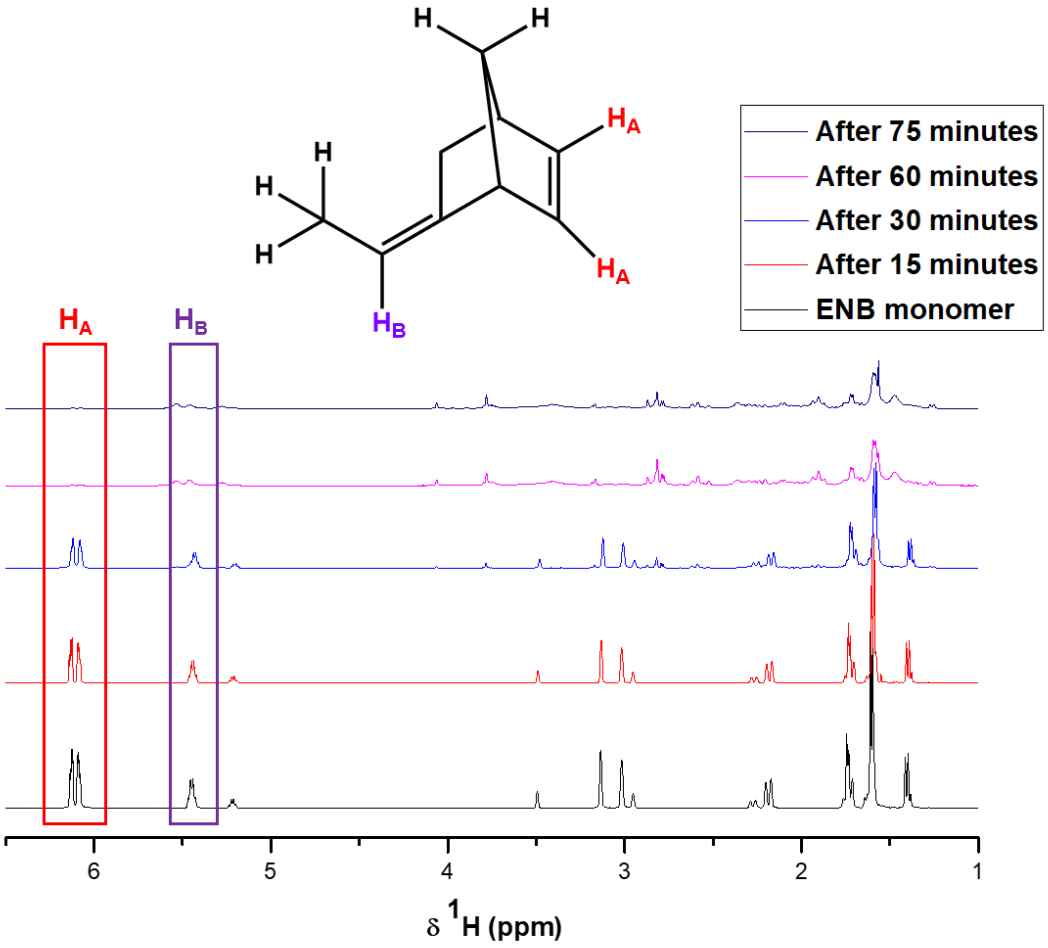

Figure 2.12 NMR kinetics experiment conducted at 135 °C. Approximately 20 mL aliquots were dissolved in $CDCl_3$ and the soluble fraction was taken at 15, 30, 60 and 75 minutes.

that in higher temperature reactions between sulfur and DCPD an insoluble product is formed, suggesting reaction at both double bonds (Figure 2.15b).[6] ENB has two double bonds, alike with DCPD, with both crosslinkers having a norbornene double bond in common. To draw comparisons, NMR kinetics experiments (experimental procedure 2.6.7) were performed at different time intervals to monitor the reactions between sulfur with ENB. NMR kinetics experiments were conducted both at low (135 °C) (Figure 2.12) and high temperatures (160 °C) (Figure 2.13) at different time intervals,

to monitor the reaction at both double bonds of the ENB monomer. At low temperature (135 °C) NMR shows a decrease in the integration of H_A resonance (the norbornene double bond) suggesting this double bond is indeed consumed preferentially at low temperature reactions, similarly to DCPD (see H_A:H_B ratios, Table 2.1). At higher temperatures (160 °C) the reaction proceeds more rapidly (Table 2.2, Figure 2.13). In both reactions, the H_B peak does not completely disappear, but shifts in position, indicative of a reaction taking place somewhere else on the molecule. Formation of peaks at ~δ 4 ppm in both spectra (Figure 2.21 & 2.22) are indicative of S-C-H protons,[18] further confirming the reaction between ENB and sulfur.

Table 2.1 Ratios of H_A:H_B at different times of the NMR kinetics experiments conducted at 135 °C.

Time (minutes)	Ratio of integrals (H_A:H_B)
15	2:1
30	0.74:1
60	0.06:1
75	0.06:1

Table 2.2 Ratios of H_A:H_B at different times of the NMR kinetics experiments conducted at 160 °C.

Time (minutes)	Ratio of integrals (H_A:H_B)
10	2.4:1
20	0.21:1
30	0.05:1
40	0:1

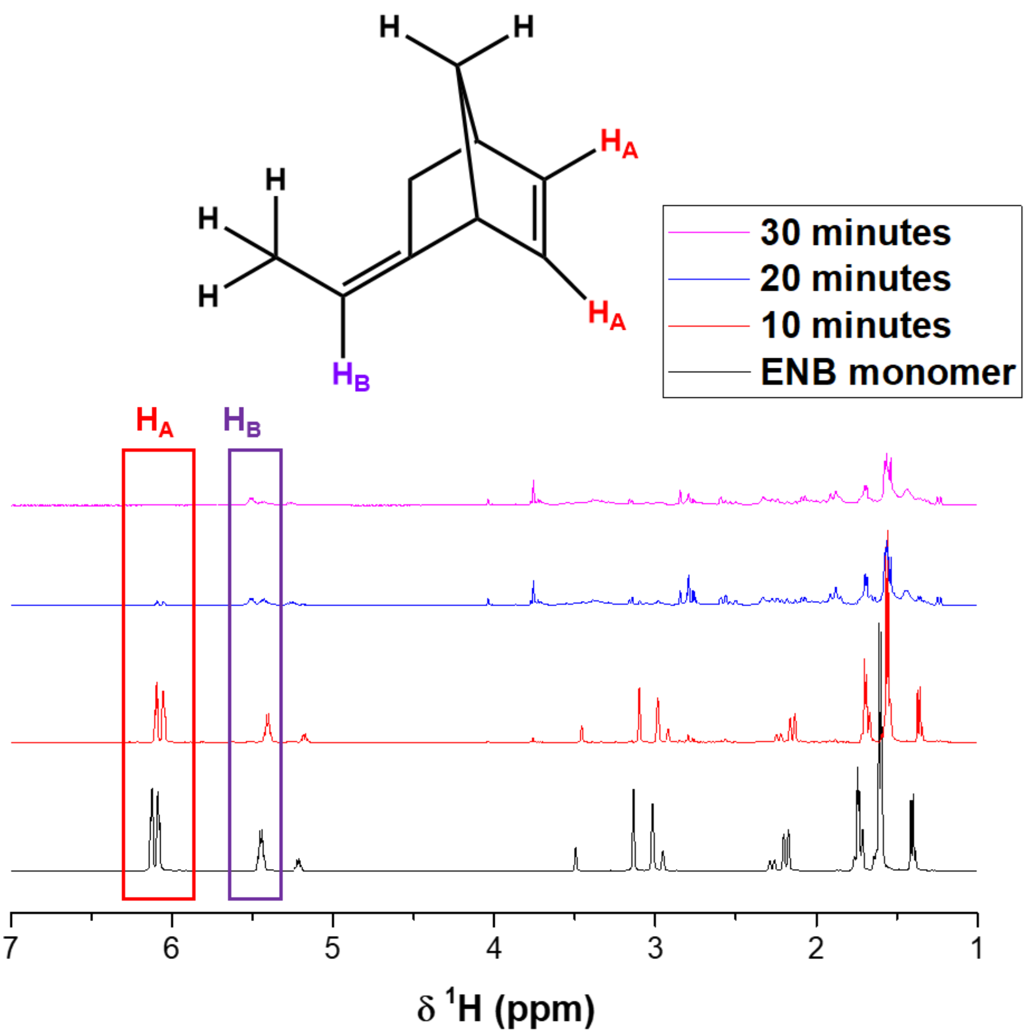

Figure 2.13 NMR kinetics experiment conducted at 160 °C. Approximately 20 mL aliquots were dissolved in $CDCl_3$ and the soluble fraction was taken at 10, 20, and 30 minutes.

However, these solution NMR results are for the soluble fraction only, and at an early reaction time. The insolubility of the material at longer reaction times suggests that reaction at the H_B position, although less favourable, does occur.

2.4.3 Calculating Fukui Indices

If the reaction mechanism is a bulk-free radical polymerisation, the susceptibility of a double bond to reaction with sulfur radicals may determine the reaction temperature, resultant molecular weight and degree of crosslinking of the material. To further elucidate how susceptible the double bonds of each crosslinker is to radical attack, computational calculations were performed to predict sites susceptible to radical attack. Condensed Fukui indices were calculated (Figure 2.14), which generates a numerical value that indicated which double bond is more likely to be attacked by a sulfur radical. The higher the numerical value the more susceptible the double bond is to radical attack.

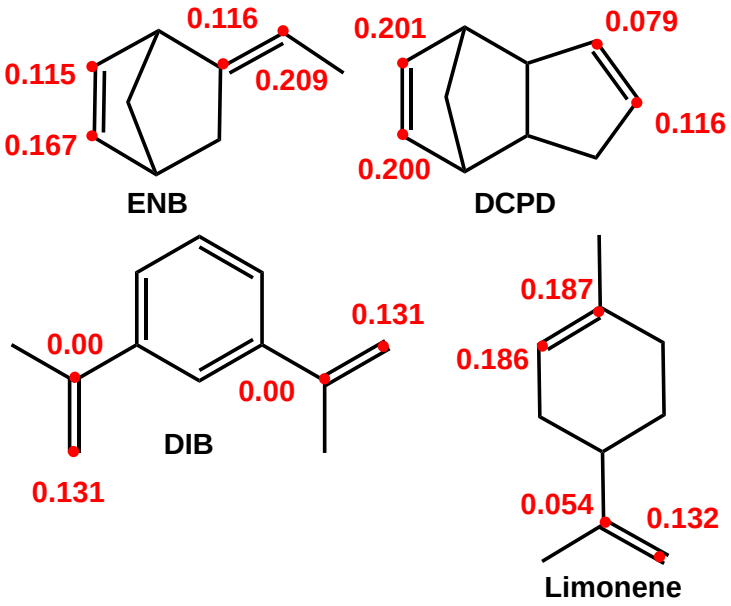

Figure 2.14 Fukui indices of carbon atoms on each double bond on the following crosslinkers; 5 ethylidene-2-norborene (ENB), dicylopentadiene (DCPD), 1,3-diisopropenylbenzene (DIB).

The Fukui index predicts the reactivity of each atom in a molecule in a nucleophilic, electrophilic or a radical sense (experimental procedure 2.6.8). These condensed Fukui values are calculated from atomic charges that are calculated from electron density population analysis. Assessing how the partial atomic charges change when an electron is added or removed from the system can indicate potential reactivity sites for attack by radicals. The computational calculations performed on the atoms in DCPD (Figure 2.14) match the NMR kinetics experiments that have been previously reported,[6] with the norbornene bond being more reactive to radicals than the cyclopentene double bond (Figure 2.14). The norbornene bond being more reactive explains why at lower

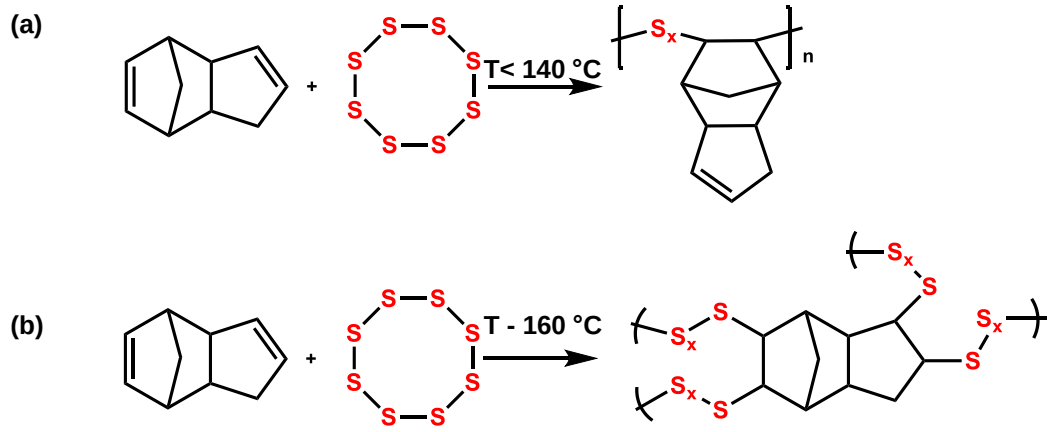

Figure 2.15 Both Fukui indices and previous NMR kinetics studies suggest that the norbornene double bond is more reactive; therefore, at lower temperatures pathway (a) is more likely. However higher temperature promotes reaction at the cyclopentene bond also with pathway (b) being more likely.

temperatures the reaction between sulfur and DCPD forms a soluble linear polymer (Figure 2.15a).[7]

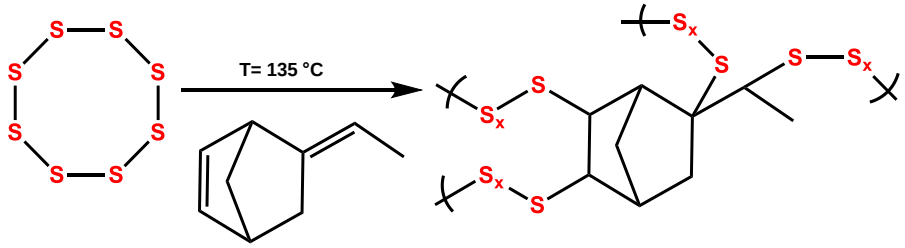

Figure 2.16 Possible pathway of reaction between sulfur and ENB, with reaction at both double bonds.

The Fukui indices calculated for ENB (Figure 2.14) show the carbon on the outer end of the exocyclic double bond to be more susceptible to radical attack than the other

carbon atoms. Despite the NMR kinetics results suggesting that the norbornene double bond is preferentially consumed during the initial reaction. In general, the Fukui indices (Figure 2.14) on both C=C atoms of the ENB monomer suggest that both double bonds are relatively reactive and susceptible to sulfur radical attack. This supports that S-ENB crosslinks at both double bonds (Figure 2.16) forming a highly cross-linked network that is impervious to common organic solvents and can stabilise a high proportion of sulfur (90% elemental sulfur by mass).

Limonene and ENB both have similar molecular masses and two double bonds, but the resultant polymers have considerably different chemical and physical properties.

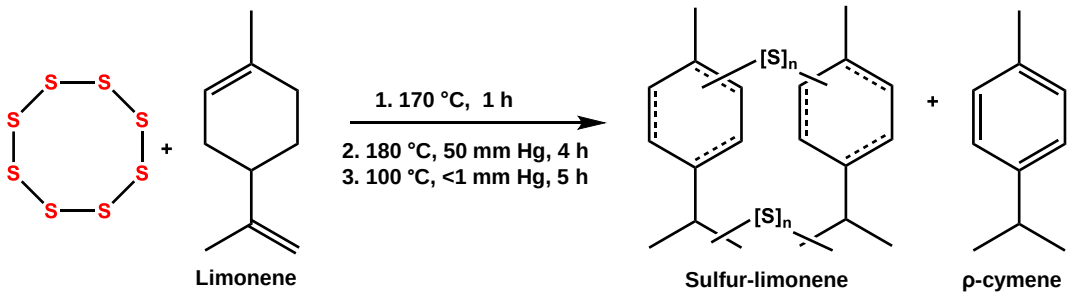

Figure 2.17 Reaction of sulfur with limonene as reported by Chalker and co-workers. ρ-cymene was detected as a by-product.

Chalker *et al.* depict the reaction of sulfur with both exocylic and endocyclic sites on limonene (Figure 2.17). This can be supported by the Fukui indices that were calculated (Figure 2.14), which indicates that each carbon atom on both double bonds shows some susceptibility to sulfur radical attack. If reaction occurred at both double bonds, we would expect a highly crosslinked and insoluble network to be formed. However, S-limonene exhibits a low T_g (-21 °C), a high degree of solubility, and lack

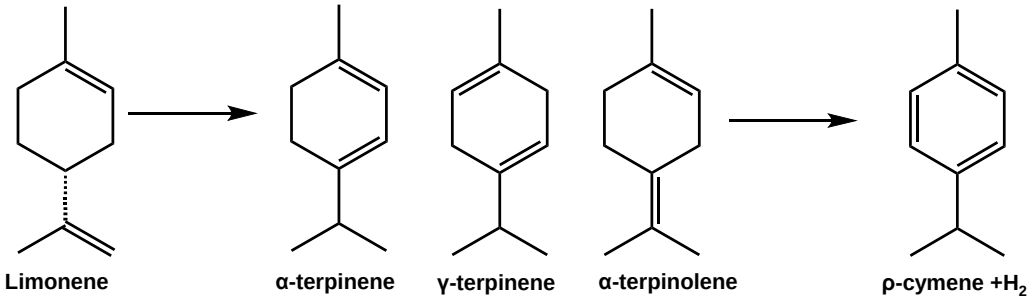

Figure 2.18 Limonene is subject to 1-3 hydrogen shifts and loss of hydrogen to form ρ-cymene, especially when reacted with sulfur at high temperatures.

of shape persistency in comparison to similar sulfur polymers.[2,5,6] A possible

explanation could be that during the reaction at high temperatures limonene is susceptible to 1,3-hydrogen shifts. Hydrogen loss forms an aromatic ring and the by-product ρ-cymene, which would result in the deactivation of the endocyclic site (Figure 2.17 and 2.18).[19,20] Loss of one of the two reactive sites will result in a more linear polymer explaining the depression of the T_g and relatively high solubility.

Loss of hydrogen from limonene is also known to produce (1-methyl-4(2-propenyl)benzene, ρ,α-dimethyl styrene (DMS) (Figure 2.19).[21] This product must proceed with loss of hydrogen. This presumably occurs in the form of H2S. Formation of DMS will lead to linear polymer subunits. The reaction of un-dehydrogenated

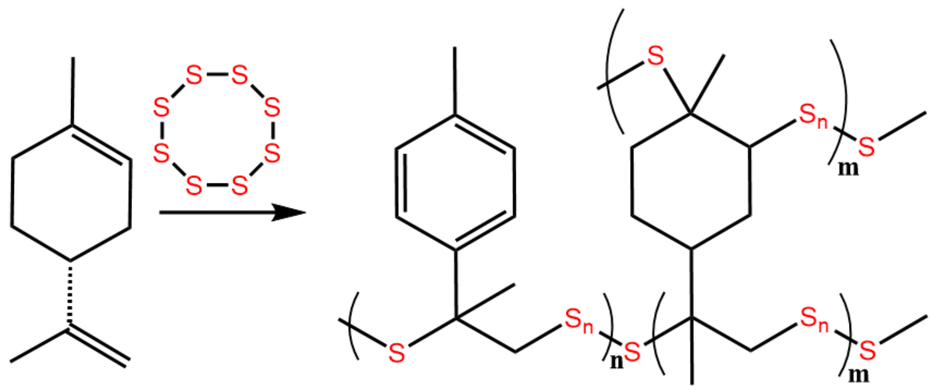

Figure 2.19 Scheme showing a representation of hypothesised structure for sulfur limonene containing both branching and linear moieties.

limonene will lead to branching units.[21] The solubility of sulfur-limonene and the low T_g suggests the linear moiety to be the major component.

2.4.4 Gas capture experiments

To test this, the gas emitted during the reaction between sulfur, limonene, DCPD and ENB was collected (Table 2.3, experimental procedure 2.6.9). Yagci *et al.* previously reported the production of H_2S during inverse vulcanisation for the reaction of sulfur with polybenzozazines.[4] The reaction between limonene and sulfur produced a larger volume of gas than the other monomers (Table 2.3) and triggered a connected H_2S detector.

Table 2.3 The volume of gas collected for the reaction between sulfur with Limonene, DCPD and ENB at different reaction temperatures.

Crosslinker	Temperature (°C)	Volume of gas collected (mL)	Maximum sulfur stabilisation reported/ (wt. %)
Limonene	180	63.0	50
DCPD	165	26.5	80
ENB	135	9.5	90

The largest volume of gas was collected for the reaction between sulfur and limonene (63 mL) (Table 2.3), the gas is thought to be mainly H_2S and did trigger a H_2S detector (alarm limit 2.4 ppm) on exposure. However, the gas produced in the reactions between sulfur and ENB did not trigger the H_2S detector. The gas released by the reaction of ENB with sulfur may mostly be ambient gasses dissolved in the monomers at room temperature, and released on heating, with H_2S release negligible at these reaction conditions.

The higher the reaction temperature the larger the volume of gas collected (Table 2.3). Each reaction was therefore conducted again at 135 °C to see the effects of reaction temperature (Table 2.4). The reaction between sulfur and ENB cannot be conducted any higher than 135 °C due to the boiling point of ENB (147.6 °C).

Table 2.4. The volume of gas collected for the reaction between sulfur with Limonene, DCPD and ENB at 135 °C for 1 hour.

Crosslinker	Temperature of reaction (°C)	Volume of gas collected (mL)
Limonene	135	<1 – no reaction
DCPD	135	~5 – only very slight reaction
ENB	135	9.5 – full reaction

However, reactions of sulfur with both limonene and DCPD at 135 °C results in an incomplete reaction with the gases collected being negligible (Table 2.4). The volume of gas collected is most likely the effects of both temperature and how susceptible the crosslinker is to hydrogen abstraction. It is important to note that there is a clear relationship between the volume of gas collected and the wt. % of sulfur that each crosslinker stabilises (Table 2.3).

The loss of hydrogen from limonene explains the aromatic signals observed in NMR and is consistent with a more soluble linear structure. Minimising the production of

poisonous H_2S would be preferable in terms of industrial scale-up and use, as previously discussed by Pyun and co-workers. In contrast, the structures of ENB and DCPD preclude hydrogen rearrangement and seem more stable against hydrogen abstraction by the sulfur, with both hetronuclear single quantum correlation (HSQC) (Appendix, Figure A2.3) and ^{1}H NMR (Figure 2.20 & 2.21) confirming the absence of aromatic by-products (~7-9 ppm).

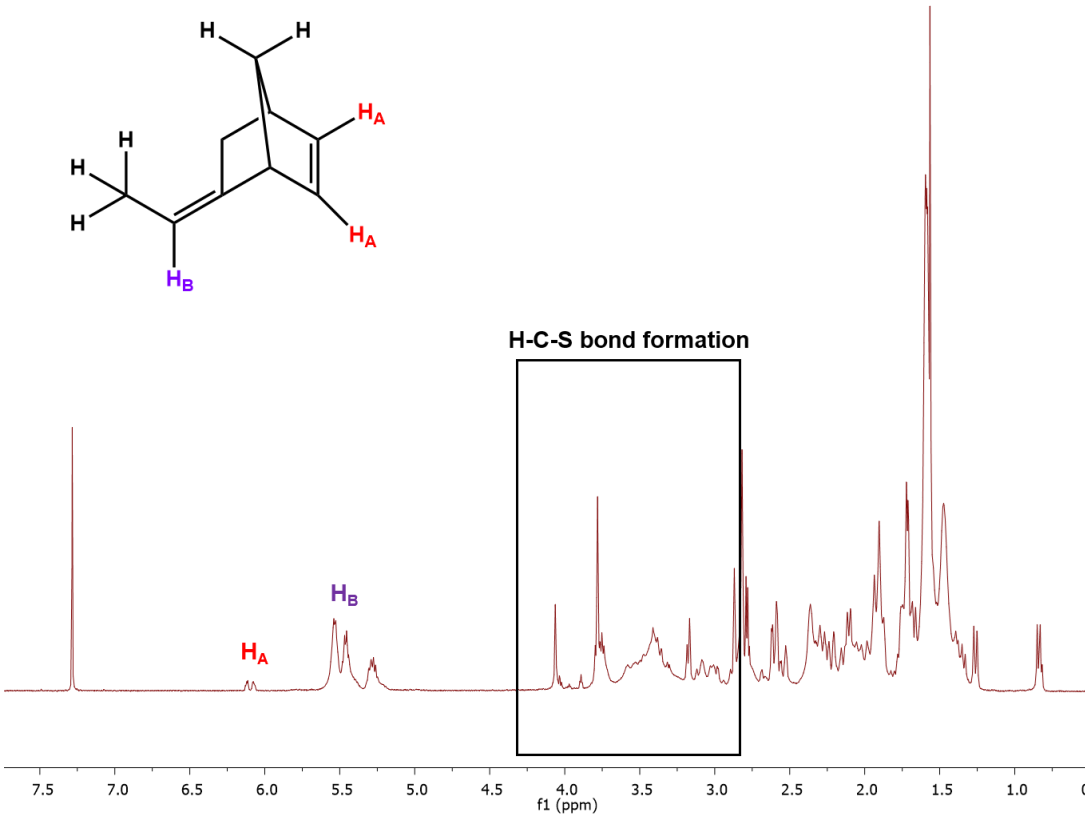

Figure 2.20 ^{1}H NMR of reaction between sulfur and ENB (50:50) after 75 minutes. ^{1}H NMR shows no evidence of aromatic protons. Reaction was conducted at 135 °C.

The loss of hydrogen as H_2S seems related to the reaction temperature required, with

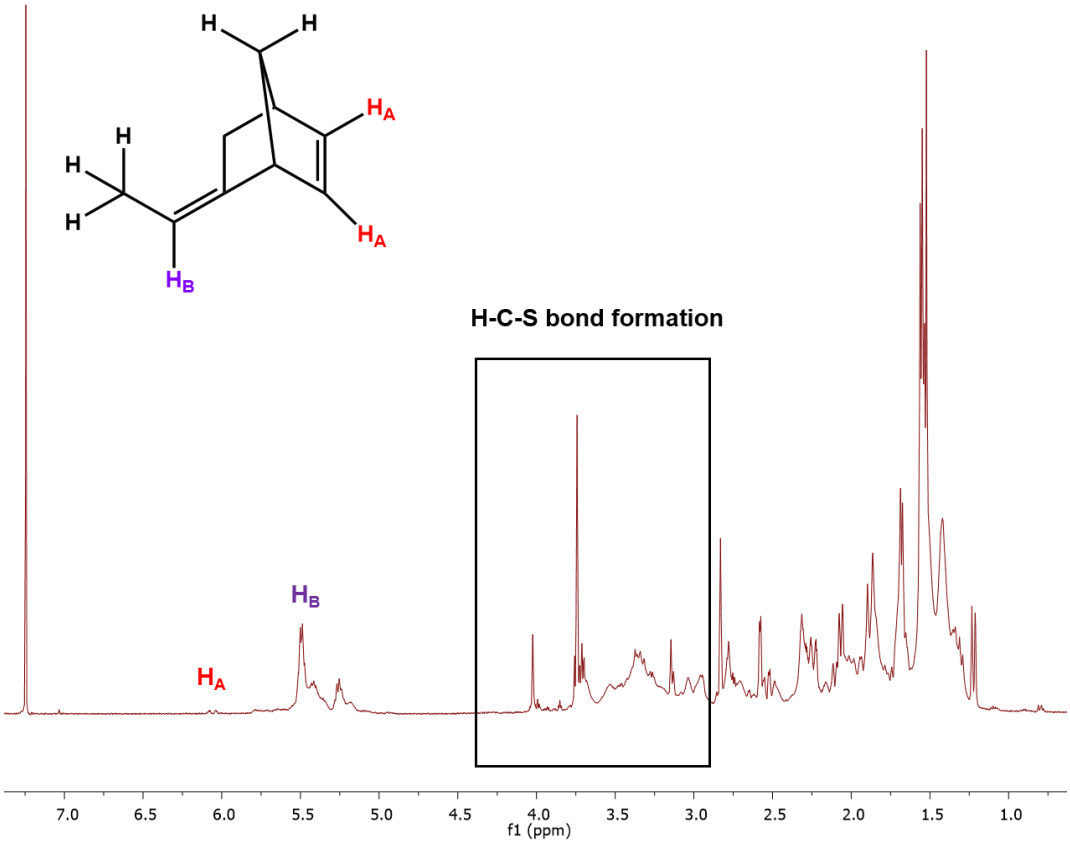

Figure 2.21 ^{1}H NMR of reaction between sulfur and ENB (50:50) after 40 minutes. ^{1}H NMR shows no evidence of aromatic protons. Reaction was conducted at 160 °C.

both following the trend S-limonene>S-DCPD>S-ENB. The highest Fukui index for each crosslinker follows the opposite trend: S-ENB>S-DCPD>S-limonene accurately predicting the relative reactivities.

2.5 Conclusions and Future work

In conclusion, this work has shown inverse vulcanisation between sulfur and ENB for the first time. The S-ENB polymers produced can stabilise a surprisingly high ratio of sulfur (up to 90 wt.%) against depolymerisation of sulfur to S_8 crystals, in comparison to S-DCPD (up to 80 wt.%) and other inverse vulcanised sulfur polymers. This is the first bulk copolymer reported to retain amorphous character at 90% elemental sulfur by mass.

The S-ENB polymers are impervious to common organic solvents, suggesting that the polymer reacts at both double bonds forming a highly crosslinked network. During the reaction between sulfur and ENB, there is no evidence of the Tromsdorff Norish effect, which is reported in other inverse vulcanisation reactions. Only a small volume of H_2S is produced compared to other crosslinkers, both of which are beneficial to industrial scale-up.

The differences in properties of high sulfur content polymers have been rationalised according to their respective crosslinkers' reactive sites, with lower reactivity requiring higher polymerisation temperature, thus causing increased hydrogen abstraction. These findings make it easier to understand the differences in the properties of other structurally diverse crosslinkers used to prepare inverse vulcanised sulfur polymers.

Potential future experiments:

- S-ENB showed no evidence of S_8 crystals by PXRD and DSC at 90% elemental sulfur by mass. Therefore, investigating S-ENB polymers as a cathode in Li-S batteries could be one future application.

2.6 Materials and methods

2.6.1 Materials

Sulfur (S_8, ≥99.5 %), dicyclopentadiene (DCPD), 5 ethylidene-2-norbornene >98.5 % purity, limonene, chloroform-d ($CDCl_3$), acetone, acetonitrile, toluene, THF, methanol, and n-hexane were purchased from Sigma Aldrich and used as received without further purification. 1,3- Diisopropenylbenzene (>97%) was purchased from Tokyo Chemical Industry UK (TCI) and used as received.

2.6.2 Synthesis of Sulfur-ENB polymer (General procedure)

Sulfur (S_8, masses shown in Table 2.5) were added to a 40 mL glass vial equipped with a magnetic stirrer bar and heated on a hot plate to 135 °C. Once sulfur was molten (transparent, yellow solution) 5 ethylidene-2-norborene (ENB masses shown in Table 2.5) was added dropwise. The mixture was heated at 135 °C for ~60 minutes yielding a very viscous orange liquid. The product was then transferred to a mould and allowed to cure for ~14 hours at 140 °C.

Table 2.5 The sample compositions for the reactions carried out according to general procedure 2.6.2.

Reaction composition (wt. % ENB)	Mass of S_8 (g)	Mass of ENB (g)	Appearance
10	9.00	1.00	Rubber-like black solid
20	8.00	2.00	Brittle black solid
30	7.00	3.00	Brittle Black solid
40	6.00	4.00	Brittle Black solid
50	5.00	5.00	Brittle black solid

2.6.3 Altering the curing temperature of sulfur-ENB polymers

Sulfur (S_8, masses shown in Table 2.5) was added to a 40 mL glass vial equipped with a magnetic stirrer bar and heated on a hot plate to 130 °C. Once sulfur was molten (transparent, yellow solution), 5 ethylidene-2-norborene (ENB masses shown in Table 2.5) was added dropwise. The mixture was heated at 135 °C for ~60 minutes until a homogenous and then the temperature was increased to 160 °C for approximately 8 minutes. The product was then transferred to a mould and allowed to cure for ~14 hours at 140 °C.

2.6.4 Adapted general procedure

Sulfur (S_8, masses shown in Table 2.5) was added to a 12 mL glass vial equipped with a magnetic stirrer bar and heated on a hot plate to 130 °C. Once sulfur was molten (transparent, yellow solution), 5 ethylidene-2-norborene (ENB masses shown in Table

2.5) was added dropwise. The mixture was heated at 135 °C to yield a bright viscous orange liquid that was not homogenous.

2.6.5 Investigating the effect of time on the glass transition temperature of S-ENB polymers

The general procedure as stated in 2.6.2 was followed except the time at which the S-ENB reaction mixture was left heating at 135 °C in a silicone vial was varied as shown in Table 2.6. This reaction was also not cured overnight as stated in procedure 3.2.

Table 2.6 Different times S-ENB mixture was heated.

Reaction composition (wt. % ENB)	Time (minutes)	Appearance
50	30	Yellow solid
50	60	Yellow/orange solid
50	90	Brown solid
50	120	Brown solid

2.6.6 Solubility studies

S-ENB (10 mg) of compositions 10-50% ENB by mass were added to a 12 mL vial. To this 10 mL of different solvents were added (acetone, acetonitrile, chloroform, n-hexane, methanol, THF, toluene, water. The solutions were left stirring for 24 hours on a tube roller.

2.6.7 NMR kinetics experiment

A reaction of 50:50 S_8: ENB was prepared as stated in procedure 2.6.2, however, was not cured overnight. Two separate experiments were carried out heating the reaction mixture at 130 °C and 160 °C. ~20 mL aliquots of the reaction mixture were taken from the vial and dissolved in ~5 mL of deuterated chloroform. An aliquot of the reaction mixture was taken at 15, 30, 60 and 75 minutes for each experiment.

2.6.8 Calculating Fukui indices

Spartan ’16 V.2.0.3 (https://www.wavefun.com/) software was used to model crosslinkers and calculate Fukui indices. Limonene, DIB, ENB and DCPD were built and initially energy minimised using a MMFF94 forcefield. Equilibrium geometry calculations at ground state in gas with density functional theory (ωB97X-D, 6-31G*, total charge = neutral, unpaired electrons = 0). Single point energy calculations were

then performed after this at ground state in gas with the same functional and basis set in both the anionic and cationic states (unpaired electron = 1). Natural atomic charges were used to calculate the condensed Fukui indices using the equation below.

Fukui function for radical attack = ($q_{N-1}^{A} - q_{N+1}^{A}$)/2

Where q_{N+1}^{A} and q_{N-1}^{A} are partial charges of atom A in the molecule with N+1 electron and N-1 electrons, respectively.

2.6.9 Gas capture

Sulfur (5 g) and crosslinker (5 g, Table 2.3) were added to a 40 mL reaction vial with a stirrer bar. The vial was sealed with a rubber septum and connected with a tube ended with a needle to a measuring cylinder (100 mL). The measuring cylinder was pre-filled with deionised water and was placed upside down in a 1 L beaker with water. The reaction mixture was heated to the normal reaction conditions for each crosslinker (Table 2.4) until each reaction produced no more gas.

2.6.10 Characterisation

Thermal gravitational analysis (TGA): TGA was carried out using platinum pans, samples were heated to 900 °C under an N_2 atmosphere and then held for 10 minutes under air to burn any remaining material.

Powder X-ray diffraction (PXRD): Powder X-Ray Diffraction (PXRD) patterns were carried out on samples using a PAN analytical X'pert powder diffractometer using CuKα radiation.

Differential Scanning calorimetry (DSC): Differential scanning calorimetry was carried out using Q2000 DSC (TA instruments). The method was a heat/cool/heat for three cycles; heating to 150 °C and cooling to – 80 °C at a heating rate of 5 °C/min with Tzero Hermetic pans.

Fourier-transform infrared spectroscopy (FT-IR) was performed using a Thermo NICOLET IR200, between 400 cm^{-1} to 4000 cm^{-1}. Samples were loaded either neat, using an attenuated total reflectance accessory, or in transmission after pressing into a KBr pellet.

2.7 Appendix

Table A2.1 Elemental analysis of S-ENB polymers for 50,60,70 and 80 % elemental sulfur by mass (S_8: ENB). Values in black are expected and values in red are the actual values obtained.

Elements present	**80:20 (%)**		**70:30 (%)**		**60:40 (%)**		**50:50 (%)**	
C	18.0	**16.4**	27.0	**24.5**	36.0	**30.8**	45.0	**39.4**
H	2.0	**1.6**	3.0	**2.6**	4.0	**2.0**	5.03	**4.2**
S	80.0	**82.2**	70.0	**72.8**	60	**65.6**	50.0	**57.0**

Table A2.2 Solubility of ENB in comparison to published crosslinkers. Solubility's are given in mg/mL. IS = insoluble, trace = colour visible in solution but <1mg/mL.

*	DIB	Limonene	Myrcene	Farnesene	Farnesol	DCPD	ENB (50 wt. %)	ENB (20 wt. %)
Acetone	1.6	trace	IS	trace	trace	**IS**	**IS**	**IS**
Acetonitrile	10.9	trace	IS	IS	IS	IS	IS	IS
Chloroform	9.7	>17.2	9.7	20.8	25.7	IS	IS	IS
Hexane	IS	trace	trace	trace	trace	IS	IS	IS
Methanol	IS	trace	IS	IS	IS	IS	IS	IS
THF	10.5	>12.4	11.7	16.8	25.1	IS	<1	IS
Toluene	13.6	>16.1	12	19.6	13	IS	IS	IS
Water	IS	IS	IS	IS	IS	IS	IS	IS

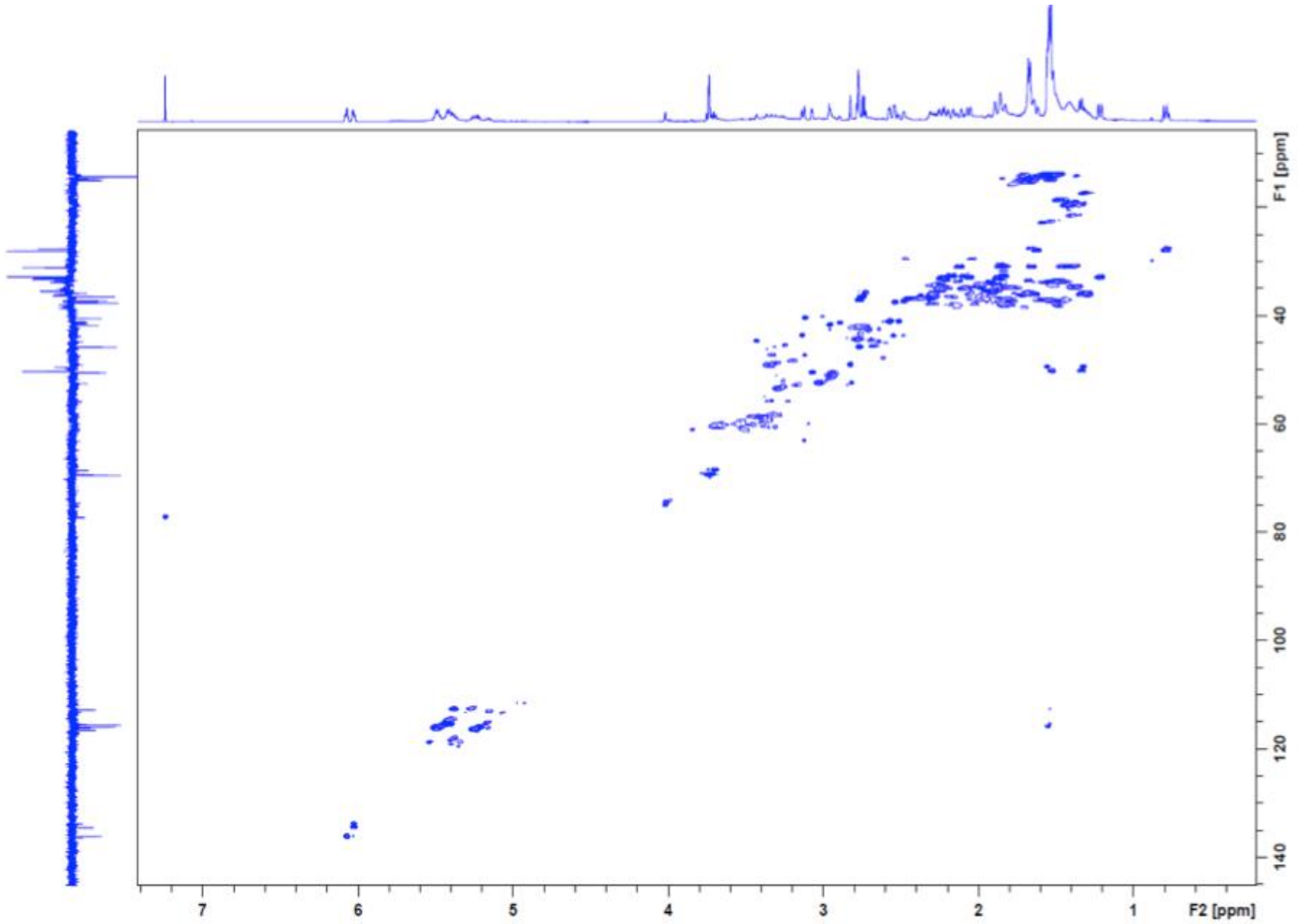

Figure A2.3 HSQC of reaction between sulfur and ENB (50:50), after 60 minutes at 135 °C. There is no evidence of any aromatic by product forming at this reaction time.

2.8 References

1 W. J. Chung, J. J. Griebel, E. T. Kim, H. Yoon, A. G. Simmonds, H. J. Ji, P. T. Dirlam, R. S. Glass, J. J. Wie, N. a Nguyen, B. W. Guralnick, J. Park, A. Somogyi, P. Theato, M. E. Mackay, Y. Sung, K. Char, J. Pyun, Á. Somogyi, P. Theato, M. E. Mackay, Y. Sung, K. Char, J. Pyun, A. Somogyi, P. Theato, M. E. Mackay, Y. Sung, K. Char, J. Pyun, Á. Somogyi, P. Theato, M. E. Mackay, Y. Sung, K. Char and J. Pyun, *Nat. Chem.*, 2013, **5**, 518–524.

2 J. M. Chalker, Kucera.L.Renata and M. J. H. Worthington, *Green Chem.*, 2017, **0**, 1–6.

3 X. Wu, J. A. Smith, J. M. Grif, T. Hasell, S. Petcher and D. J. Parker, *Nat.Comm.*, 2019, **10,** 1–9.

4 M. Arslan, B. Kiskan and Y. Yagci, *Macromolecules*, 2016, **49**, 767–773.

5 M. P. Crockett, A. M. Evans, M. J. H. Worthington, I. S. Albuquerque, A. D. Slattery, C. T. Gibson, J. A. Campbell, D. A. Lewis, G. J. L. Bernardes and J. M. Chalker, *Angew. Chemie - Int. Ed.*, 2016, **55**, 1714–1718.

6 D. J. Parker, H. A. Jones, S. Petcher, L. Cervini, J. M. Griffin, R. Akhtar and T. Hasell, *J. Mater. Chem. A*, 2017, **5**, 11682–11692.

7 L.Blight, B.R.Curell, B.J. Nash, R.A.M. Scott and C.Stillo, *Adv.Chem.Ser.*, 1978, 13-30.

8 B. K. Bordoloi and E. M. Pearce, in *New Uses of Sulfur-II, American Chemical Society*, 1978, pp. 31–53.

9 B.A.Bulgakov, M.V.Bermeshev, M.L.Gringol'ts, M.P. Filatova and E.S. Finkel'shtein, *Pet.Chem*, 2012, **52**, 119–122.

10 Y. Ma, J. Liang, D. Zhao, Y. Chen, J. Shen and B. Xiong, *RSC Adv.*, 2014, **4**, 17262.

11 Y. Zhang , R. Glass, K.Char and J.Pyun, *Polym.Chem.*, 2019,**10,** 4078–4105.

12 Y. Zhang, J. J. Griebel, P. T. Dirlam, N. A. Nguyen, R. S. Glass, M. E. Mackay, K. Char and J. Pyun, *J. Polym. Sci. Part A Polym. Chem.*, 2016, **55**, 107–116.

13 P. J. Griebel, Jared J., Nguyen.A.Ngoc, Ashtashkin.V. Andrei, Glass.S. Richard, Mackay.E. Michael, Char Kookheon, *ACS Macro Lett.*, 2014,**12**,1258–1261.

14 J. Chiefari, Y. K. B. Chong, F. Ercole, J. Krstina, J. Jeffery, T. P. T. Le, R. T.

A. Mayadunne, G. F. Meijs, C. L. Moad, G. Moad, E. Rizzardo, S. H. Thang and C. South, *Macromolecules*, 1998, **9297**, 5559–5562.

15 M. Arslan, B. Kiskan and Y. Yagci, *Macromolecules*, 2016, **49**, 767–773.

16 S. Z. Khawaja, S. V. Kumar, K. K. Jena and S. M. Alhassan, *Mater. Lett.*, 2017, **203**, 58–61.

17 A. Hoefling, Y. J. Lee and P. Theato, *Macromol. Chem. Phys.*, 2016, **218**, 18–21.

18 J. J. Griebel, R. S. Glass, K. Char and J. Pyun, *Prog. Polym. Sci.*, 2016, **58**, 90–125.

19 M. A. Martin-Luengo, M. Yates, E. S. Rojo, D. Huerta Arribas, D. Aguilar and E. Ruiz Hitzky, *Appl. Catal. A Gen.*, 2010, **387**, 141–146.

20 O. Illa, M. Arshad, A. Ros, E. M. Mcgarrigle and V. K. Aggarwal, *J. Am. Chem. So*, 2013, **135**, 11951–11966.

21 T. D. Sheppard, J. R. G. Evans and H. C. Hailes, *RSC Adv.*, 2014, **4**, 61652–61655.

22 M.Abraham, S.V.Y. Kumar and S.M.Alhassan, *Chem.Eng.J*, 2018, **332**, 1–8.

23 J. J. Griebel, G. Li, R. S. Glass, K. Char and J. Pyun, *J. Polym. Sci. Part A Polym. Chem.*, 2015, **53**, 173–177.

24 J. J. Griebel, N. A. Nguyen, S. Namnabat, L. E. Anderson, R. S. Glass, R. A. Norwood, M. E. Mackay, K. Char and J. Pyun, *ACS Macro Lett.*, 2015, **4**, 862–866.

25 J. J. Griebel, S. Namnabat, E. T. Kim, R. Himmelhuber, D. H. Moronta, W. J. Chung, A. G. Simmonds, K. J. Kim, J. Van Der Laan, N. A. Nguyen, E. L. Dereniak, M. E. MacKay, K. Char, R. S. Glass, R. A. Norwood and J. Pyun, *Adv. Mater.*, 2014, **26**, 3014–3018.

CHAPTER 3

CROSSLINKER COPOLYMERISATION FOR PROPERTY CONTROL IN INVERSE VULCANISATION

Chapter 3: Crosslinker Copolymerisation for Property Control in Inverse Vulcanisation

3.1 Context

Section 3.2 is adapted from the paper "Crosslinker Copolymerisation for Property Control in Inverse Vulcanisation", published in Chemistry-A European Journal, 2019. Chapter 2 added to the discussion of how different crosslinkers can produce materials with extremely different properties. Chapter 3 builds on this research and adds more understanding of controlling the physical properties of inverse vulcanised sulfur polymers. Due to this still being an emerging field, the physical properties are still largely underreported. As the physical properties will underpin many of the functional applications, they need to be investigated, understood, and improved in the long- term. This research sets a benchmark for other researchers to improve the physical properties of these polymers.

Four new sulfur terpolymers are discussed in this chapter, prepared from sulfur and two distinct alkene monomers. While this research was ongoing, others reported different sulfur terpolymers, which will be discussed in section 3.2. However, this is the first effort to uncover design principles and present how mechanical properties were altered, and glass transition temperatures can be tuned. The hope is this research sets a benchmark to trigger further improvements of inverse vulcanised sulfur polymers, to be used for different functions eventually.

3.1.2 Author Contributions

Jessica A Smith conducted all experiments with Mchem student Sarah. J. Green's help who focused on preparation sulfur-dcpd-terpinolene and sulfur-dcpd-limonene polymers. Samuel Petcher, Douglas J Parker, Bowen Zhang, and Dr. Xioafeng Wu, helped prepare samples for mechanical testing at Loughborough University. Dr. Helen Willcock, Thomas Baker, and Dr. Catherine Kelly performed and aided Jessica A Smith in performing flexural strength testing and tensile strength testing. Part of this research was carried out at Flinders University, South Australia, Adelaide, where Jessica A Smith was part of a Royal society exchange program. Max Worthington assisted Jessica A Smith in the laboratory, and Dr. Jonathan A Campbell trained Jessica A Smith on the TA Instruments Q800 DMA to record compression measurements. Prof.David A Lewis and Dr. Mike J Jenkins reviewed the manuscript and kindly allowed access to all of their laboratory equipment at Flinders University,

SA. Dr. Christopher T Gibson helped with recording Raman data. This part of the work was performed at the South Australian node of the Australian National Fabrication Facility at Flinders University, SA. Dr. Tom Hasell and Dr. Justin Chalker were the PIs on this project and gave much advice and guidance.

3.2. Introduction

3.2.1 Thermal/mechanical properties of inverse vulcanised sulfur polymers

Although investigations into the mechanical properties have been few, there have been preliminary investigations. Pyun and co-workers reported the first investigation of the mechanical properties of inverse vulcanised sulfur polymers.[1] There have since been reports on the mechanical properties of S-DIB all with varying results[1,2,3]

One example of this was by Pyun and co-workers.[3] A series of poly(S-r-DIB) samples with 10-50% of 1, 3-diisopropenylbenzene (DIB) by mass were melt pressed into films for tensile testing, with Young's moduli of the samples reported between 260-460 MPa.[1,3] In general, the overall properties of the poly(S-r-DIB) were found to be weak and brittle plastics. However, in other reports, it was interesting to note that the poly(S-r-DIB) samples could be either thermoplastic or thermosetting depending on the conditions to prepare and mould the materials.[3,4] Altering how the polymers were processed and moulded (PDMS mould, petri dish, and vial) had an impact on the tensile strength and the resultant Young's modulus of the samples (Figure 3.1).[3] This

allows the opportunity to enhance thermomechanical properties by modifying the organic crosslinker and the processing method.

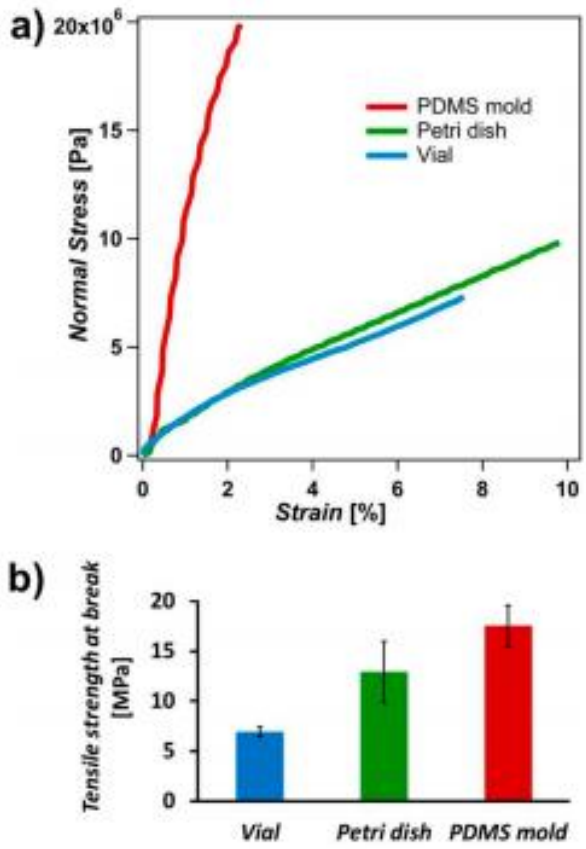

Figure 3.1 (a) Stress and strain curves for a 70 % elemental sulfur by mass sample of poly (S-r-DIB) prepared by various methods at 185 °C. (b) Plot of tensile strength of polymers in different reaction conditions. From ref 3.

As an attempt to improve the thermomechanical properties of high sulfur content polymers, Pyun and co-workers explored using 1, 3, 5-triisopropenylbenzene (TIB) for inverse vulcanisation (Figure 3.2), which formed a more highly crosslinked polymer in comparison to poly(s-r-DIB).[5] The more highly crosslinked polymer network of poly(S-r-TIB) afforded improved thermomechanical properties and an enhanced range in glass transition temperatures (T_g = 60-130 °C for 30-50 wt.% of elemental sulfur) in comparison to poly(S-r-DIB) (T_g= 43-49 °C).[5] This advancement highlighted the importance of crosslinker structure on the thermal and mechanical properties of high sulfur content polymers.[5]

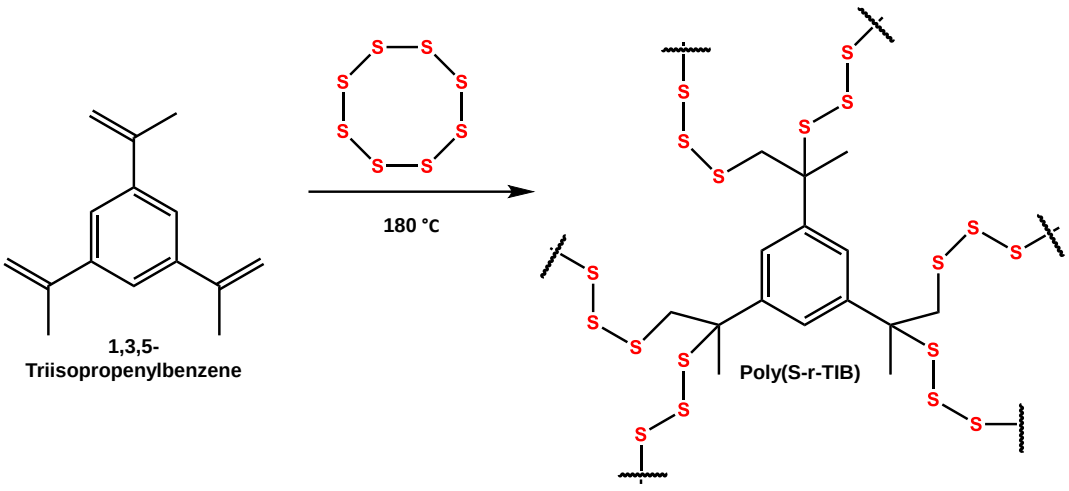

Figure 3.2. Inverse vulcanisation of poly(sulfur-random-1,3,5-Triisopropenylbenzene) (poly(S-r-TIB)) at 180 °C.

Other reports of investigating the thermal and mechanical properties of inverse vulcanised sulfur polymers include sulfur reacted with naturally occurring diallyl sulfide (DA)(Figure 3.3).[6] Flexible films of sulfur content 50-90% elemental sulfur by mass were prepared to show a low Young's modulus of 1.3 to 6.1 MPa in comparison to poly(S-r-DIB) (260-460 MPa), highlighting the increased flexibility of the sulfur-diallyl sulfide (S-DA) films (Figure 3.3).[6] Diallyl sulfide is not a rigid molecule and

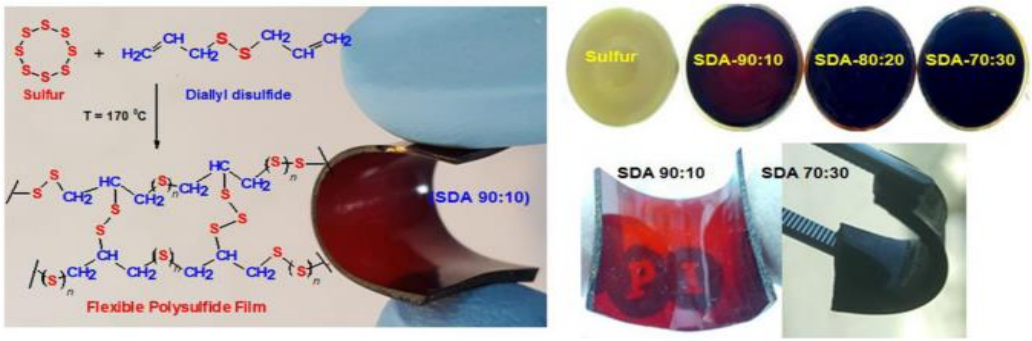

Figure 3.3 Left: Scheme showing inverse vulcanisation of sulfur with diallyl sulfide to produce a flexible polysulfide film. Right: Free standing Sulfur-diallylsulfide (S-DA) films. From ref 6.

has free rotating carbon chains, which could explain the increased flexibility and the lower Young's modulus compared to poly(S-r-DIB). This again highlights the effect of crosslinker structure on the thermomechanical properties.[6]

Similarly, the ductile and hardness properties of poly(S-r-DIB) and sulfur-divinylbenzene (S-DVB) have been compared, with poly(S-r-DIB) proven to be more ductile than S-DVB.[7] From the mechanical testing the study concluded that at monomer ratios of 15-30% by mass, poly(S-r-DIB) acted as a thermoplastic and S-DVB exhibited plastomeric behaviour.[7] Above 35 wt.% of crosslinker the behaviour of both polymers change. [7]

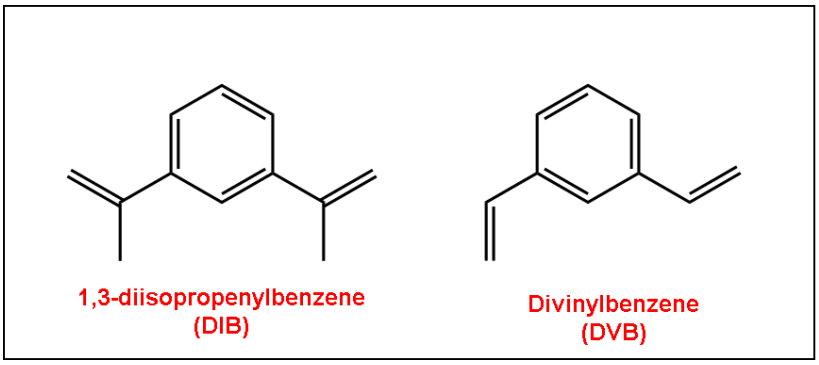

Figure 3.4 Crosslinkers/ monomers: 1,3-diisopropenylbenzene (DIB) and divinylbenzene.

In early studies, nano-indentation was used to compare the elastic modulus of sulfur polymers crosslinked with DIB, farnesol DCPD, and myrcene.[8] From this, the elastic modulus was determined that S-DCPD was more rigid than S-DIB, this was attributed to the more crosslinked structure of S-DCPD, and the higher T_g.[8] S-farnesol and S-

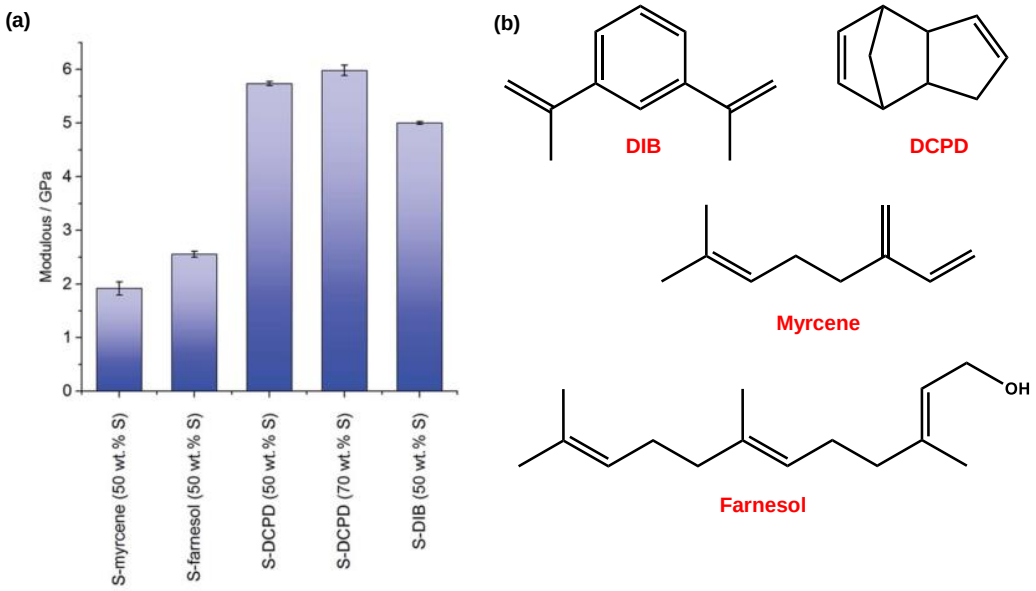

Figure 3.5 (a) Elastic modulus of sulfur polymers obtained from nanoindentation. Shows a change in mechanical properties with sulfur composition. From ref 8. (b) Crosslinkers used to prepare inverse vulcanised sulfur polymers.

myrcene showed lower rigidity which is consistent with the greater flexibility of the crosslinker molecules themselves.[8]

3.2.2 Sulfur terpolymers

Many of the previous reports of inverse vulcanised sulfur polymers consist of sulfur reacted with a single organic crosslinker. In this chapter, sulfur terpolymers are discussed, where two distinct organic crosslinkers are reacted with sulfur in an inverse vulcanisation reaction. While the research in this chapter was ongoing, there have been several different reports of sulfur terpolymers.

An initial reaction with sulfur and a styrene monomer was shown to allow the inclusion of a second vinyl crosslinker that would have not otherwise been reactive.[9] Similar to this, an initial reaction of sulfur and divinylbenzene (Figure 3.6) allows a later reaction

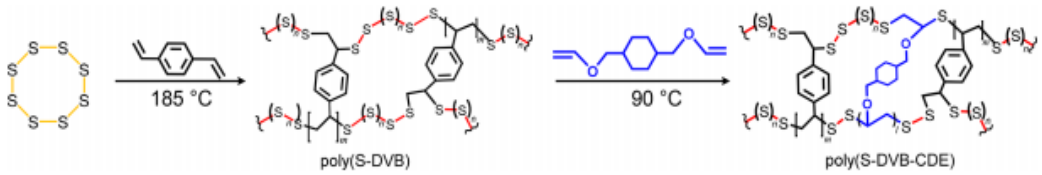

Figure 3.6 Synthesis of poly(S-DVB) followed by modification to form poly (S-DVB-CDE) at lower temperature (90 °C). From ref 10.

with 1, 4-cyclohexanedimethanol divinyl ether (Figure 3.6). If 1, 4-cyclohexanedimethanol divinyl ether had reacted with sulfur directly, the reaction temperature required would have been higher than the monomers boiling point. [10] This allowed polymerisation to occur at temperatures as low as 90 °C (Figure 3.6).[10]

Diez *et al.*, produced sulfur terpolymers of sulfur reacted with divinyl benzene with either DIB or styrene (STY) as the second organic crosslinker (Figure 3.7).[7] They show by adding a second crosslinker, the ductility could be influenced. A high DVB content led to higher strength and shape retention.[7] The addition of DIB or STY to the sulfur-

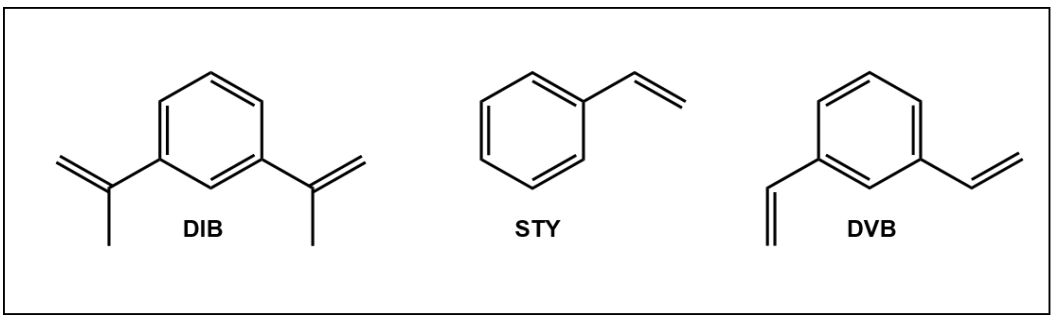

Figure 3.7 Left to right: 1, 3-diisopropenylbenzene (DIB), styrene (STY) and divinylbenzene (DVB).

DVB polymer was shown to allow control of T_g of the material, at a fixed sulfur content, over a range of almost 20 °C (-1.3 to 17 °C).[7]

Polyhedral oligomeric silsesquioxane (POSS) has been used to prepare sulfur polymers with improved thermomechanical properties due POSS' rigidity and size (Figure 3.8).[11] Sulfide linkages have been exploited to prepare healable polymeric materials due to the low bond dissociation and the reversibility of the linkages.[12] Liu *et al.* prepared a new sulfur terpolymer, S-MMA-POSS (Figure 3.8). This was prepared from a direct reaction between the methacrylated POSS monomer with molten sulfur in an inverse vulcanisation reaction. However, unlike traditional inverse vulcanisation, a co-solvent (diglyme) was used to improve the miscibility of the molten sulfur and monomer phase.[11] The healable properties of S-MMA-POSS were evaluated with tensile tests (Figure 3.8). The tensile tests provided sufficient evidence of healability of the terpolymer (Figure 3.8).[11]

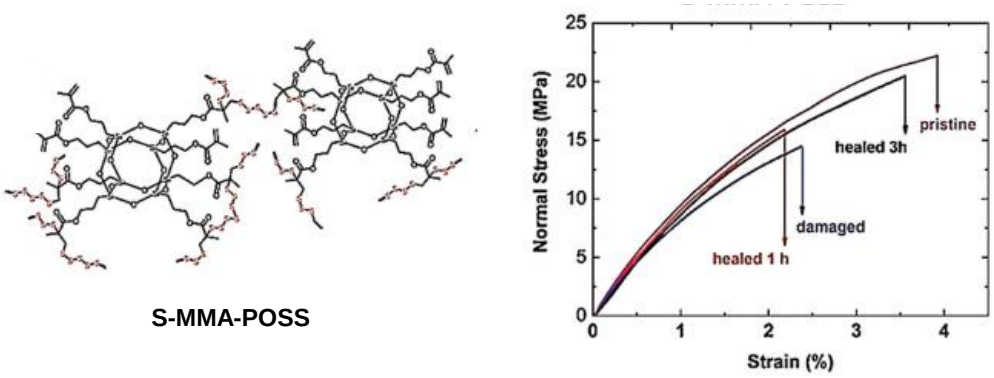

Figure 3.8 Left: inverse vulcanised sulfur-methyl methacrylate- polyhedral oligomeric silsesquixoane (S-MMA-POSS). Right: healable properties of thermally cured S-MMA-POSS. From ref 11.

As research was ongoing, these findings prompted a further investigation to see if this would be transferable to a broader range of crosslinkers, and if greater structural variety in crosslinkers could allow an even greater range of properties to be achieved.

3.2.3 Crosslinker used to prepare sulfur terpolymers

Many crosslinkers have been reported for inverse vulcanisation, both synthetic and renewable. As discussed in Chapter 2, the choice of crosslinker can give very different properties to the sulfur polymer produced, each with their advantages and disadvantages. As mentioned previously (Chapter 1 and 2), DIB as a crosslinker gives a shape persistent polymer but has a relatively high price in comparison to sulfur. Limonene is sustainable and low in cost but produces a low molecular weight polymer

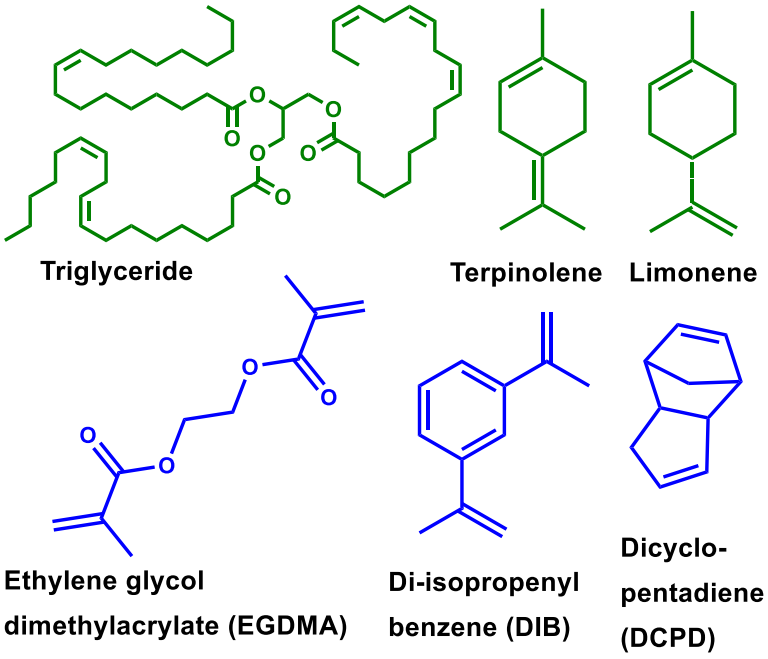

Figure 3.9 Crosslinkers that are discussed in this chapter, clockwise from top left: An example of a triglyceride structure, as found in vegetable oils, terpinolene, limonene, DCPD, DIB and EDGMA.

with a lack of shape persistency. DCPD is a low-cost industrial product that gives a hard, rigid solid but is also extremely brittle. Sustainable vegetable oils such as canola, linseed, olive, and sunflower oil can be used as a crosslinker giving a soft compressible solid and have shown potential as a sorbent for oil spills. This investigation shows how varying two distinct organic crosslinkers can be used to control and tailor these polymers' properties, focusing on the mechanical properties.

3.3 Chapter aims

1. To develop a range of new sulfur terpolymers with bespoke properties.

2. To look at the limitations of these materials by preparing them in diverse forms e.g., varying the feed ratio of monomers.
3. Investigate how the variation of organic crosslinker influences the thermal properties such as glass transition temperature (T_g).
4. Investigate how different monomer ratios can have a direct impact on mechanical properties:
    - Compression modulus
    - Flexural strength
    - Tensile strength
    - Vickers hardness

3.4 Results and Discussion

In this study, "S-crosslinker" will be used henceforth to refer to a copolymer of sulfur and the stated crosslinker (or crosslinkers).

3.4.1 Sulfur-DCPD-limonene

Sulfur-limonene and sulfur-vegetable oils have shown excellent potential in combining sulfur with low-cost renewable materials. They have both found applications in mercury absorption and improved stability as cathode materials in Li-S batteries.[13,14,15] However, S- limonene tends to form only low molecular weight polymers which are not shaped persistent.[13] Vegetable oils will also react with sulfur, but can only stabilise up to 30% elemental sulfur by mass, with any excess sulfur precipitating out as crystals of elemental sulfur (S_8).[15] Therefore, a second organic crosslinker was added to the inverse vulcanisation reaction, dicyclopentadiene (DCPD). DCPD was chosen as it is shown to produce highly stable and (no S_8 crystals precipitating and fully crosslinked) crosslinked inverse vulcanised sulfur polymers.[8] Although DCPD is not renewable itself, it is a cheap industrial by-product.[8]

The first sulfur terpolymer to be investigated was sulfur-DCPD-limonene. Pursuing the hypothesis that DCPD would increase the T_g, only a small addition of DCPD was required to improve and provide shape persistency of S-limonene copolymers (Figure 3.10).

Figure 3.10 Photographs of moulded objects produced from sulfur, DCPD and limonene (in the proportions shown). The top row shows the objects as made and below after 24 hours. Substituting only a small amount of limonene for DCPD is enough to provide shape persistency in the polymers.

As the proportion of DCPD increased, the glass transition temperature also increased linearly (Figure 3.11). The increase in T_g is likely to be the result of adding DCPD, which is thought to have increased the polymers' molecular weight by potentially forming a more branched structure. DCPD is a rigid and more conformationally constrained crosslinker, which could have produced a more rigid polymer structure.

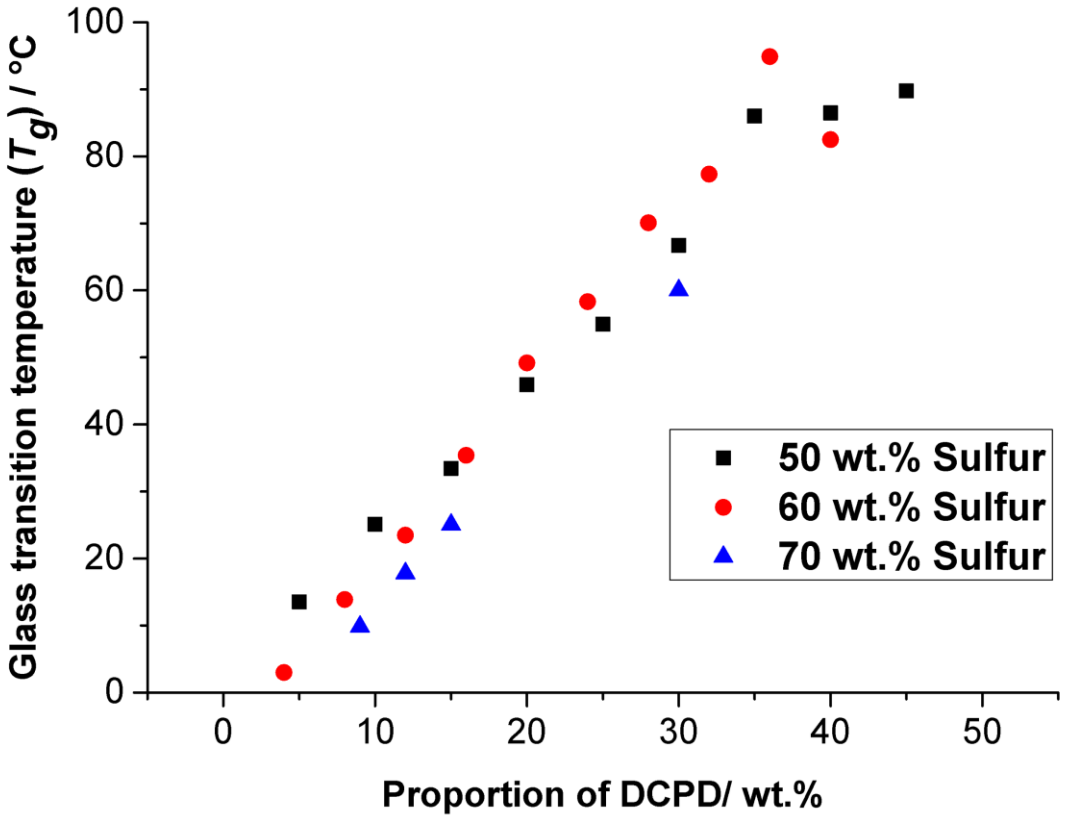

Figure 3.11 Glass transition temperatures (T_g) from DSC increasing linearly as the proportion of DCPD increases (% by mass) for a 50, 60, and 70 % elemental sulfur by mass samples. The remaining mass is from limonene, DCPD or a mixture of the two.

Gel permeation chromatography (GPC) was used to record the molecular weight of S-DCPD-limonene terpolymer ((50:40:10), Sulfur: limonene: DCPD) (Figure 3.12). GPC could not easily measure polymers that included a ratio higher than 10% DCPD

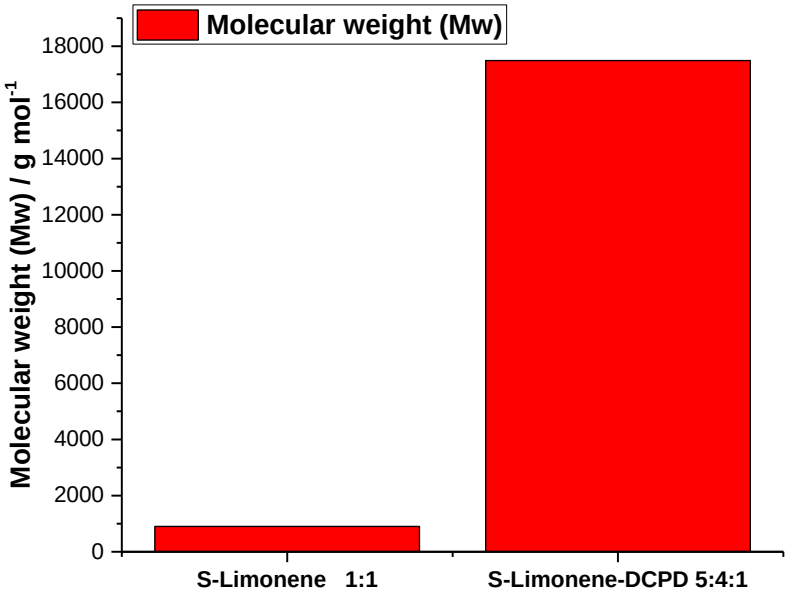

Figure 3.12 Molecular weight from GPC of polymers S-limonene (50% S_8 and 50% limonene by mass) and S-DCPD-limonene with an increase in molecular weight (50% S_8, 40% limonene, 10% DCPD by mass).

by mass. This was due to a decrease in solubility when there was a higher % of DCPD (Appendix, Figure A3.1). This is parallel to a greater degree of crosslinking. Including DCPD in the synthesis of S-limonene resulted in a higher molecular weight suggesting a higher degree of crosslinking.

3.4.2 S-DCPD-linseed oil terpolymer

DCPD was also included in the synthesis of sulfur and linseed oil to form terpolymers over a range of different sulfur: crosslinker and DCPD: linseed oil ratios. The resultant materials were stable black solids that were either rubbery or brittle, depending on the composition, with a 50% loading of elemental sulfur by mass, polymers with more than 20 wt. % or higher of DCPD was hard and brittle and under 20 wt. % of DCPD they were rubbery.

DSC showed a linear increase in T_g with the addition of DCPD as predicted (Figure 3.13). Alongside the increase in T_g, the addition of DCPD allows a higher proportion of sulfur to be stabilised without depolymerisation back to S_8. At 50 wt. % of elemental sulfur with only 10 wt. % of DCPD, DSC traces show no evidence of the melting of

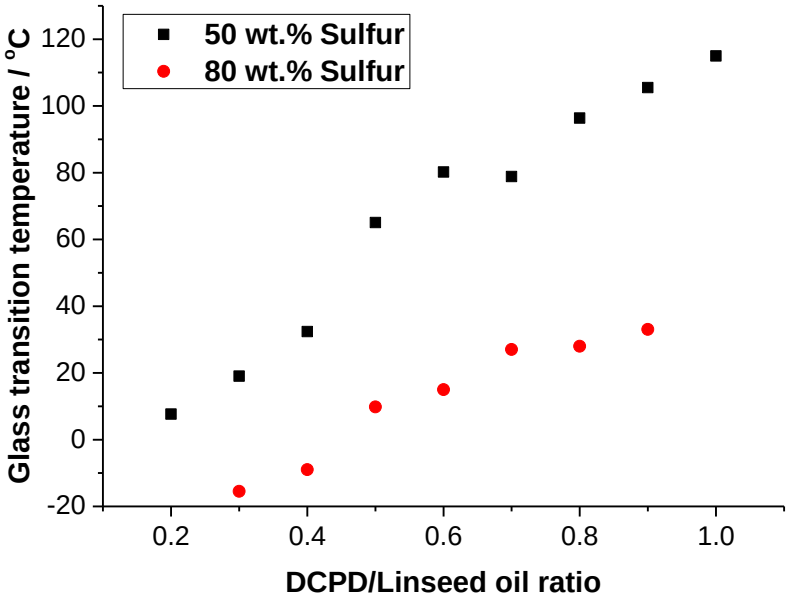

Figure 3.13 Glass transition temperatures from DSC of a range of sulfur-DCPD-linseed oil terpolymers. The DCPD/linseed oil ratio is plotted normalised between 0 (all linseed) and 1 (all DCPD).

S_8 crystals (~110 and 119.6 ºC) (Appendix, Figure A3.2). At 80 wt. % of elemental sulfur the S-DCPD-linseed oil polymers are stable against depolymerisation above 8 wt. % DCPD, but below this, there is evidence of melting of crystalline sulfur (Appendix, Figure A3.3). The peak identified by a black circle is characteristic of the melting transition (T_m) of monoclinic crystals of elemental sulfur (Appendix, Figure A3.3). This indicated the presence of 'sulfur bloom' in both samples – unstabilised sulfur that can depolymerise back to S_8 crystals. The samples where the sulfur bloom was present contained only a small portion of DCPD (2, 4, and 8 wt.%). All other samples (above 8 wt.% of DCPD) showed no T_m for elemental sulfur, indicating no crystallisation of depolymerised sulfur is taking place. The presence of only one T_g recorded by DSC suggests there has been no phase separation in the resultant material (Appendix, Figure A3.2 and A3.3).

Alongside DSC, powder X-ray diffraction (PXRD) patterns for samples of S-DCPD-linseed oil were recorded for polymers containing both 50 and 80% elemental sulfur

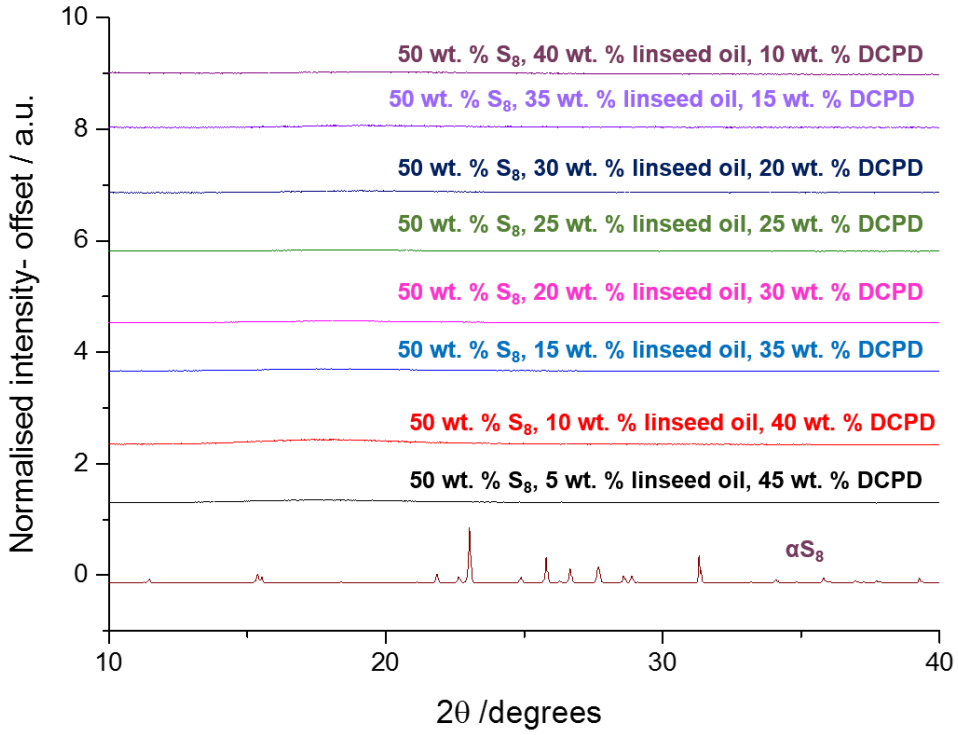

Figure 3.14 Powder X-ray Diffraction (PXRD) patterns for samples of S-DCPD-linseed oil terpolymers containing 50% elemental sulfur by mass.

by mass (Figure 3.14 & 3.15). PXRD can reveal the presence of depolymerised sulfur by the diffraction of crystals of S_8. PXRD patterns samples containing 50% elemental sulfur by mass show no evidence of crystalline sulfur to S_8 after reaction (Figure 3.14). If polymers after the reaction were not stable to depolymerisation there would be evidence of S_8 crystals, and the polymer would not retain amorphous character. No crystallinity was seen by PXRD, even for the low DCPD samples that showed a slight signal by DSC (Figure 3.15).

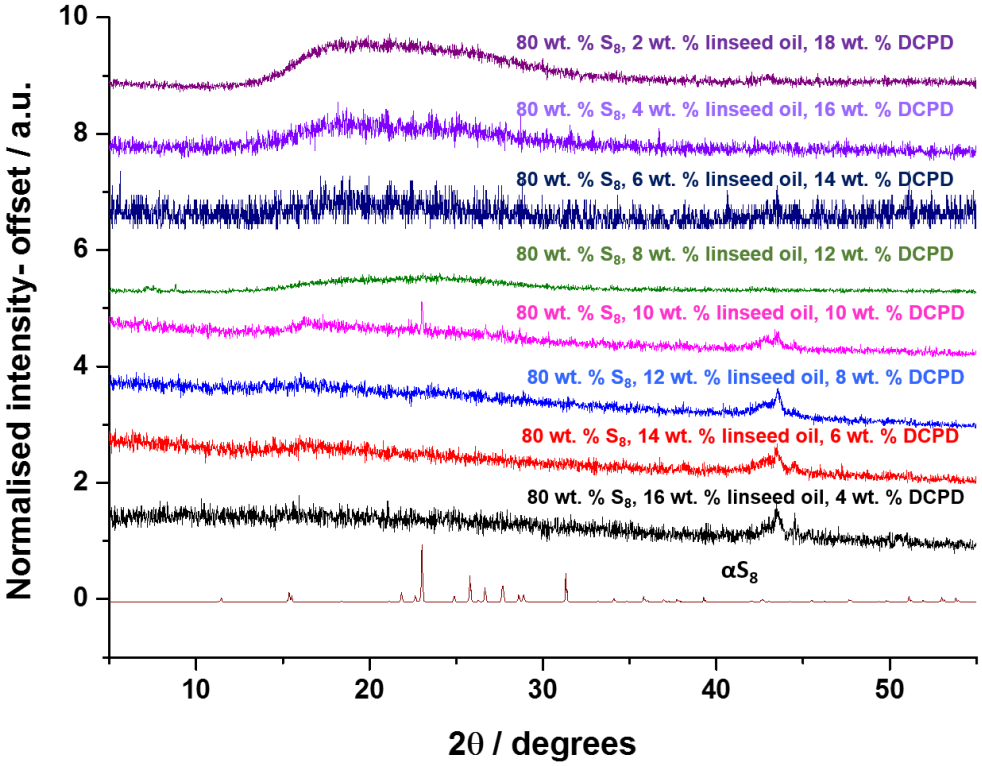

Figure 3.15 Powder X-ray Diffraction (PXRD) patterns for samples of S-DCPD-linseed oil terpolymers containing 80% elemental sulfur by mass.

Thermogravimetric analysis (TGA) thermograms of S-DCPD-linseed oil polymers were recorded of polymers that contain 50% elemental sulfur by mass and varying ratios of DCPD: linseed (Figure 3.16). Samples were recorded at a heating rate of 5 ºC min^{-1} under nitrogen. Thermograms recorded show a clear decomposition for sulfur at ~ 250 ºC (Figure 3.16). The absence of mass loss below 200 ºC indicates complete incorporation of organic monomers, which would otherwise be lost below this temperature. There is also a trend of residual char mass as a function of DCPD loading (Figure 3.16).

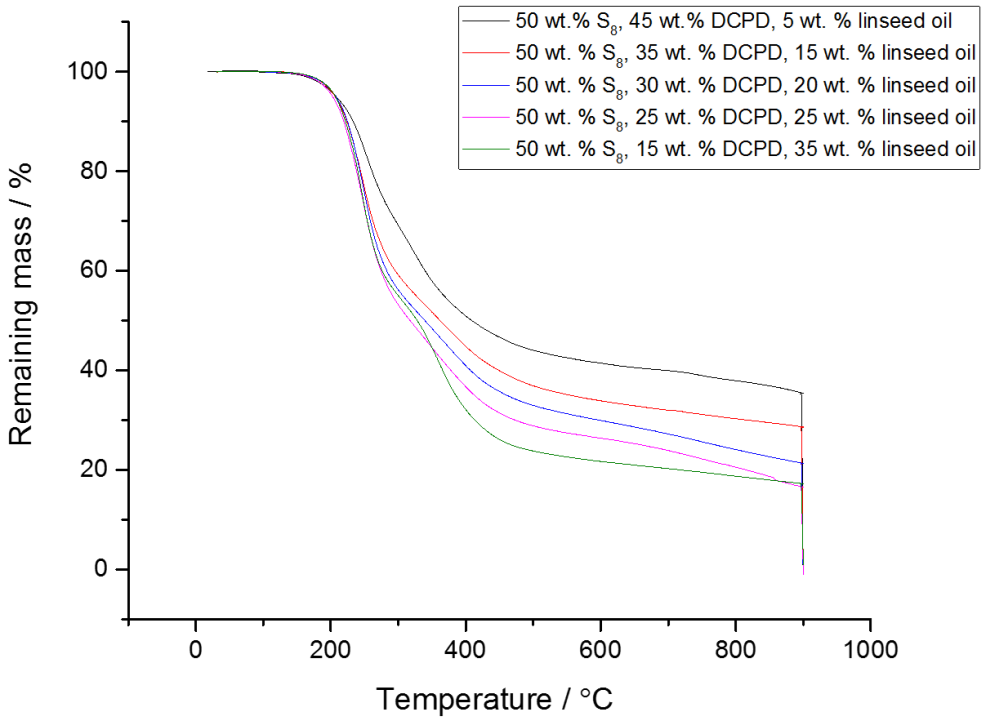

Figure 3.16 TGA thermograms of S-DCPD/linseed oil polymers with varying amounts of DCPD and linseed oil and 50 wt. % S_8 content. Recorded at a heating rate of 5 °C min^{-1} under nitrogen.

Fourier transformation infrared (FTIR) of DCPD, linseed oil, and S-DCPD-linseed oil terpolymers containing different wt.% of sulfur and monomers were recorded (Figure 3.17). The low IR absorbance of sulfur itself results in a weak signal for the sulfur polymers. By comparison to the monomer's spectra, the allylic C=H stretch at ~3100 cm^{-1} has disappeared, suggesting reaction of the C=C. The C=O stretch at 1750 cm^{-1} in the linseed oil monomer is still present in both spectra for the S-DCPD-linseed oil polymers suggesting that the linseed oil monomer has successfully formed a sulfur terpolymer.

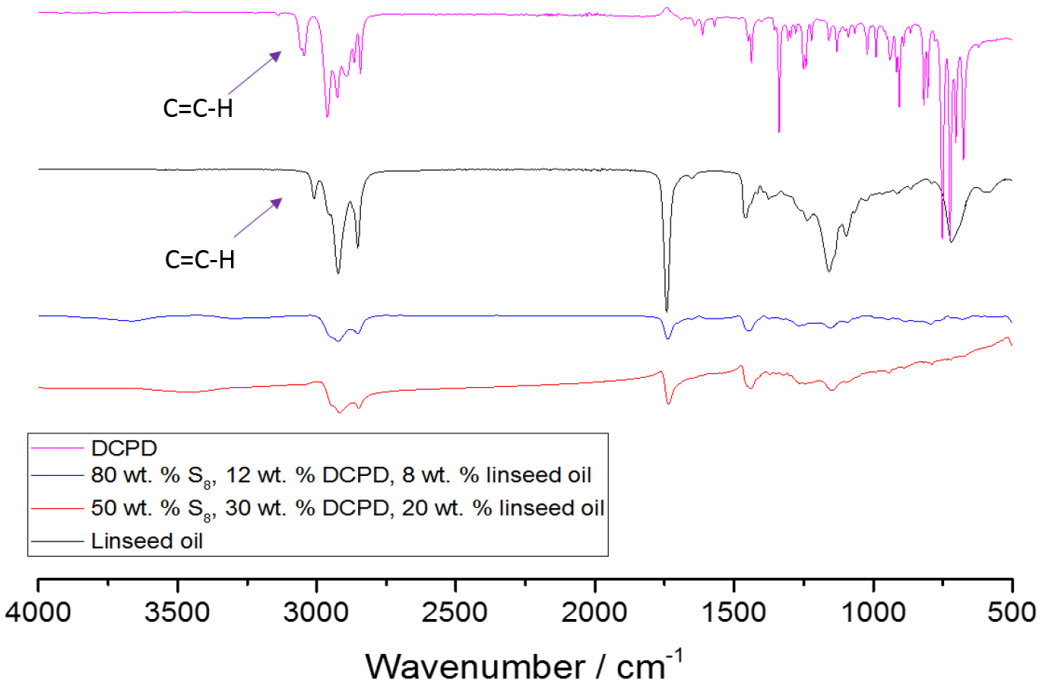

Figure 3.17 FT-IR spectra of DCPD, linseed oil and the S-DCPD/linseed oil polymers containing varying wt. % of both S_8 and monomers.

3.4.3 Sulfur- DCPD- canola oil terpolymer

DCPD was also included in the synthesis of sulfur and canola oil (rapeseed oil) to form a terpolymer, over a range of different sulfur: crosslinker and DCPD: canola oil ratios Similar to the other DCPD/vegetable oil polymers the resultant materials were black solids that exhibited different properties as a function of crosslinker ratio. The glass transition temperatures recorded by DSC increase sharply from ~25 wt. % DCPD

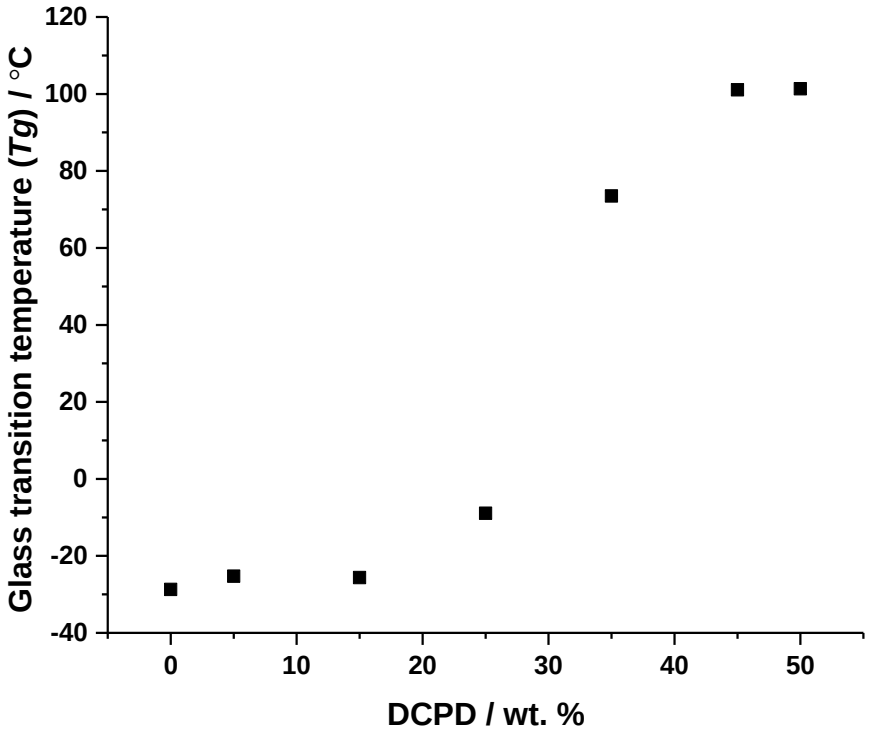

Figure 3.18 Glass transition temperature (T_g) of S-DCPD-canola oil polymers as a function of DCPD composition.

(Figure 3.18). However, there is still a similar trend to other reported polymers, with the T_g increasing as a function of DCPD.

PXRD patterns were also recorded for S-DCPD- canola oil terpolymers of 50% elemental sulfur by mass. The PXRD pattern recorded for the S-DCPD-canola oil terpolymers shows typical diffraction peaks that match the pattern for α-S_8 (Figure 3.19) for samples that contain less than 25% of DCPD by mass. The presence of S_8 was further confirmed by both DSC and Raman spectroscopy.

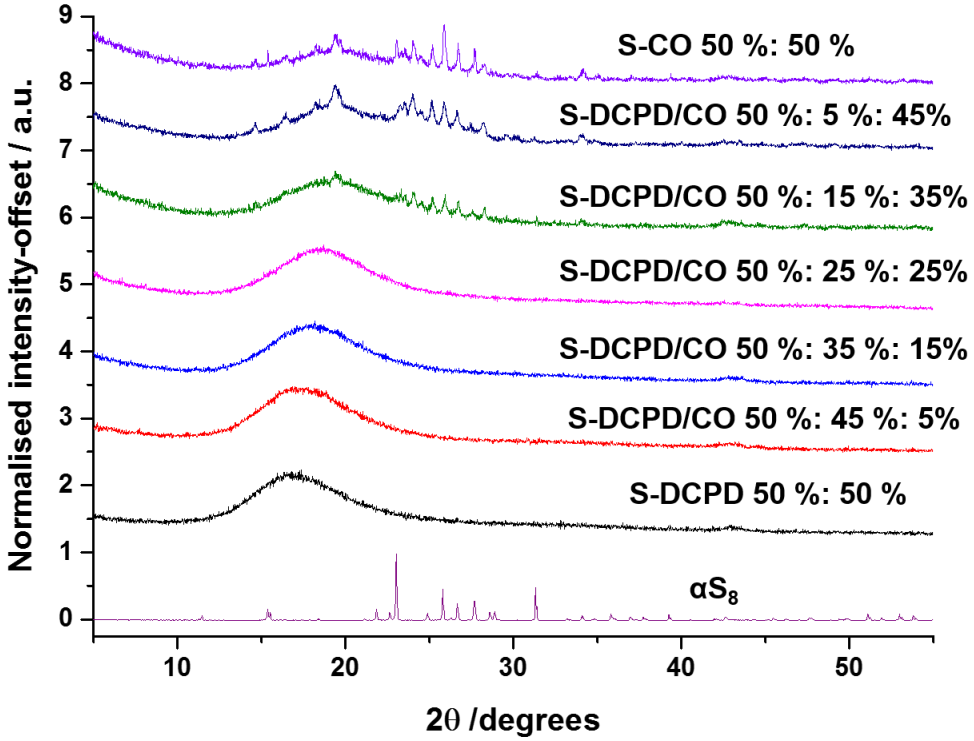

Figure 3.19 PXRD patterns of S-DCPD/CO polymers and elemental sulfur showing amorphous polymers at levels of DCPD of 25 wt.% or higher.

DSC traces of S-DCPD- canola oil terpolymers were recorded (Figure 3.20). The peak identified by the black circle is characteristic of the melting transition (T_m) of monoclinic crystals of elemental sulfur. A T_m *was* only present for samples that contained 0 and 5 wt.% DCPD. This indicates sulfur bloom in these samples which is the depolymerisation of uncrosslinked sulfur back to S_8 crystals. It should be noted

that if the T_m is on the first heating step of the DSC heat/cool/heat cycle this can be attributed to long chain polysulfides.

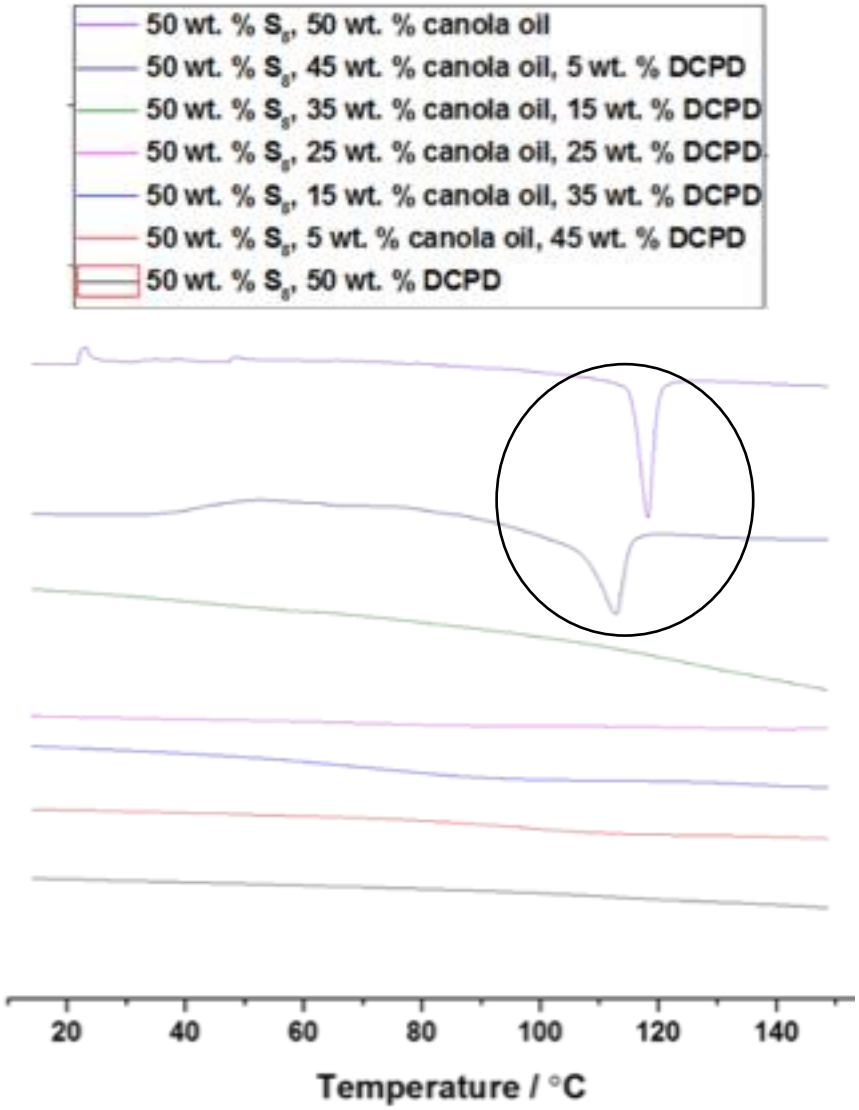

Figure 3.20 DSC traces of S-DCPD/canola oil with varying linseed oil and DCPD content at 50 wt. % S_8 content. The third heating step is shown, stacked for clarity. The peak identified by a black circle is characteristic of the melting transition (T_m) of monoclinic crystals of elemental sulfur. This indicated the presence of 'sulfur bloom' in both samples – unstabilised sulfur that is able to depolymerise back to S_8 crystals.

Raman spectra for S-DCPD-canola oil polymers were also recorded to identify the presence of elemental sulfur. Raman spectra are difficult to record for inverse vulcanised polymers due to fluorescence. Although fluorescence was recorded for both polymers, characteristic peaks for elemental sulfur (Figure 3.21) are still present for

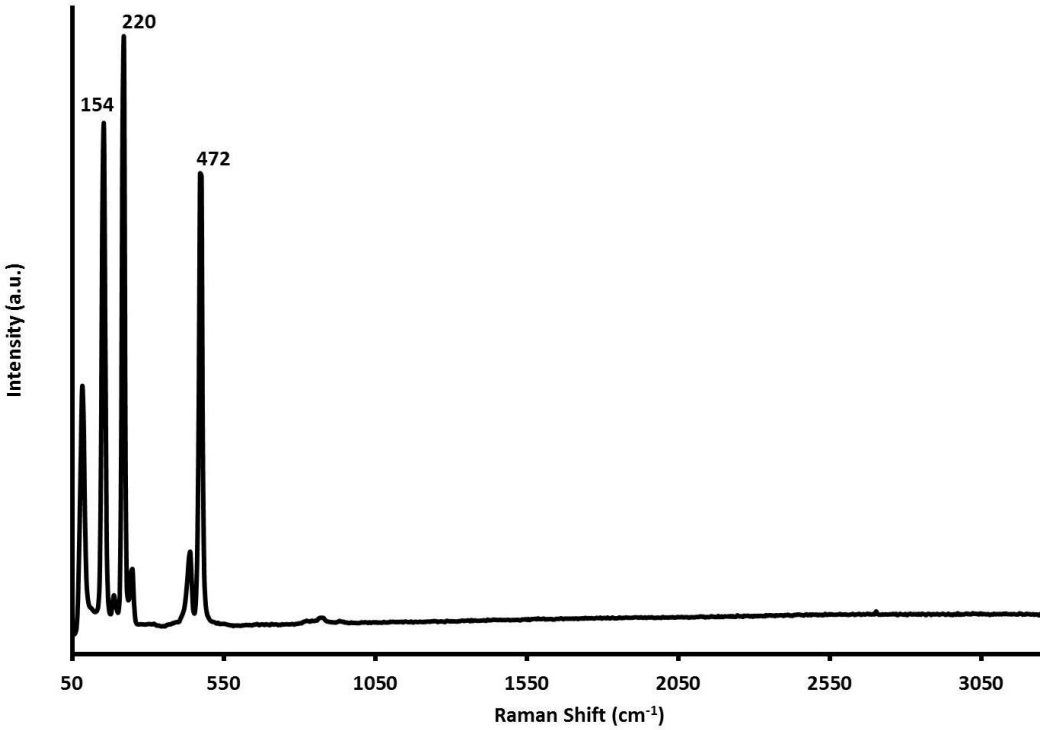

Figure 3.21 Characteristic peaks in Raman spectroscopy of a sample of pure elemental sulfur.

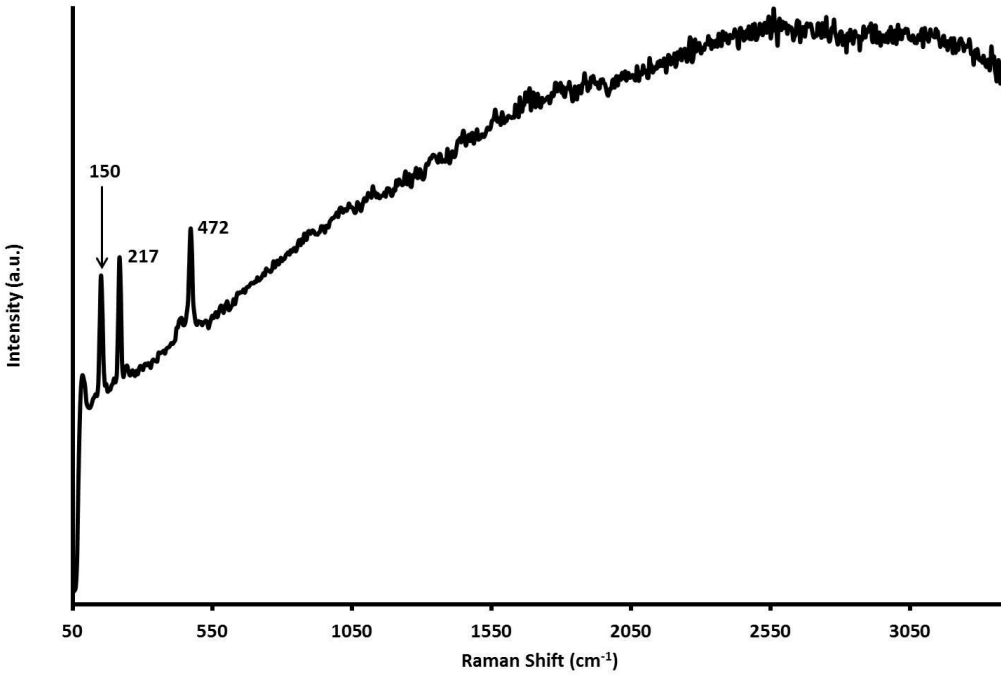

Figure 3.22 Raman spectrum for S-DCPD-canola oil terpolymer (50 wt. % sulfur, 5 wt. % DCPD, 45 wt. % canola oil) showing characteristic peaks for elemental sulfur.

the sample that contains only 5 wt.% DCPD (Figure 3.22). For the sample that contains

25 wt.% DCPD no characteristic peaks for elemental sulfur were resolved (Figure 3.23).

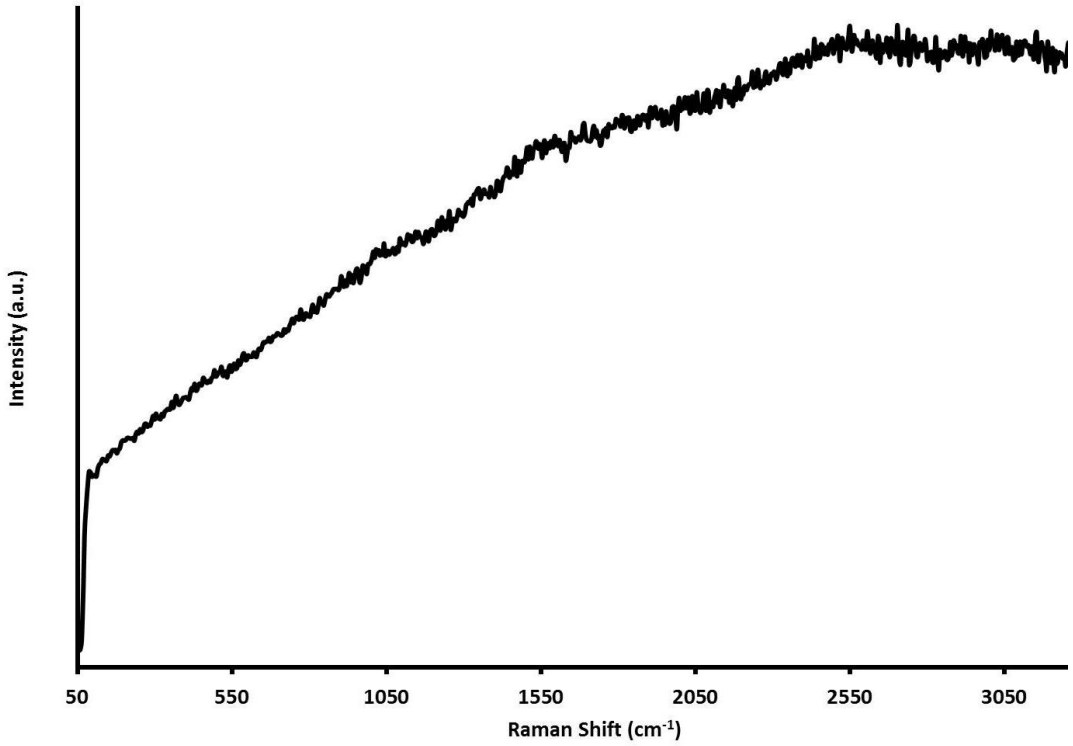

Figure 3.23 Raman spectrum for S-DCPD-canola oil (50 wt. % sulfur, 25wt. % DCPD. 25 wt. % canola oil) showing no characteristic sulfur peaks.

3.4.3.1 Compressibility of sulfur-DCPD-canola oil terpolymer

A previous investigation of S-canola oil copolymers adopted a salt templating method to induce porosity in the polymers.[15] The porosity and compressibility of this material allowed it to be used for oil absorption and reclamation, acting as a sponge.[15] To determine how DCPD affected the compressibility, a range of S-DCPD-canola oil terpolymers were produced and salt templated by the same method (Appendix, Figure A3.4).

To record compressibility, S-DCPD-canola oil (50% elemental sulfur by mass) porous polymer blocks (45,35,15, and 5% canola oil by mass) were compressed, and the instrument was used in controlled force mode (0.5 N/ min up to 10 N) to record a series of stress-strain experiments. Stress-strain curves were recorded to identify different characteristics; the compressive load (stress) and the percentage of compression (strain). From Figure 3.24 and 3.25, it can be concluded when the polymer contains a

higher wt. % of DCPD, the polymer can withstand less strain before breaking, and there is a more linear relationship between stress and strain. This is characteristic of a brittle material, with the percentage of compression being much lower for brittle materials.

For a 50:50 Sulfur-DCPD copolymer with canola oil, we see plateaus. These plateaus

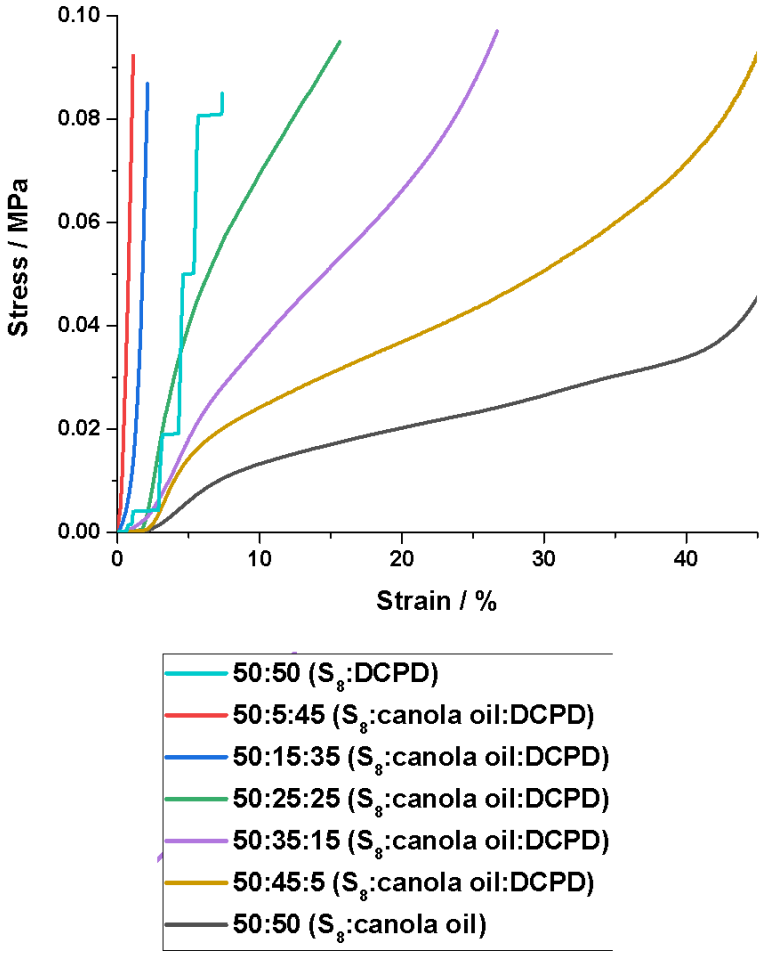

Figure 3.24 Stress-strain curves of S-DCPD-canola oil terpolymers at ratios given in the legend.

indicate when the material is breaking, providing more evidence for how brittle S-DCPD is. Figure 3.24 and 3.25 reveal how doping as little as 5 wt.% of the flexible triglyceride of canola oil can change the compressive properties of the material significantly. From Figure 3.25, it can be suggested that there is a direct relationship between the compression modulus of the sulfur and the DCPD: canola oil ratio.

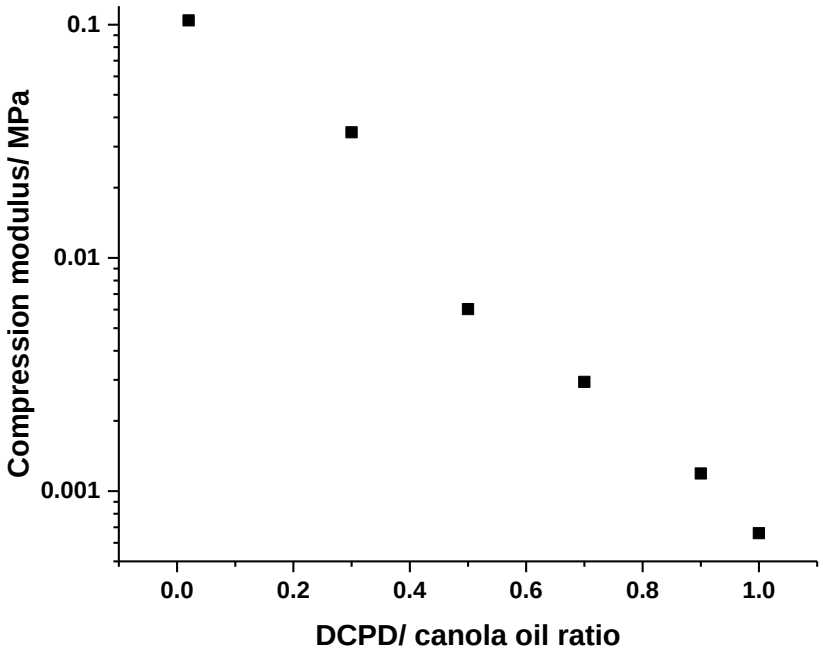

Figure 3.25 There is a direct relationship between the DCPD: canola oil ratio and the compression modulus. Normalised between 0 (all DCPD) and 1 (all canola oil).

3.4.5 Sulfur-DCPD-terpinolene

In addition to investigating how monomer ratio can affect the mechanical properties, it was found that combining crosslinkers can also modify the resultant polymers' colour. Terpinolene, until this point, had not been previously reported as a crosslinker for inverse vulcanisation. When reacted with sulfur in an inverse vulcanisation reaction, the reaction was successful; however, the resultant polymer had a low T_g (-16 °C) and lacked shape persistency. This was comparable to the reaction between sulfur and limonene, which could be due to the similarity of the crosslinker structure.

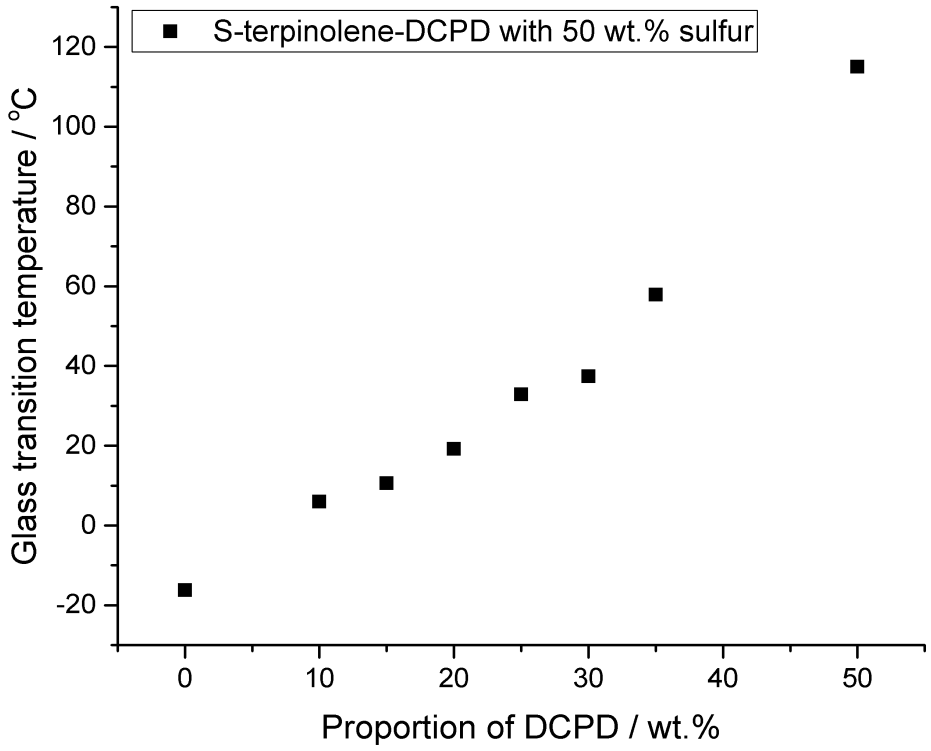

Figure 3.26 T_g, from DSC, of co-polymers consisting of 50 wt.% sulfur, with the remaining 50 wt.% from either terpinolene, DCPD, or a mixture of the two.

The glass transition temperatures recorded by DSC when DCPD was included in the synthesis increases linearly like the other inverse vulcanised sulfur polymers, with the T_g increasing as a function of DCPD (Figure 3.26).

Gel permeation chromatography (GPC) recorded the molecular weight of S-DCPD-terpinolene terpolymer ((50:40:10), Sulfur: terpinolene: DCPD) (Table 3.1). GPC could not easily measure polymers with a ratio higher than 10% DCPD by mass. This was due to a decrease in solubility when there was a higher % of DCPD. When DCPD is included in the synthesis of S-terpinolene, the molecular weight is much higher, suggesting a higher degree of crosslinking.

Table 3.1 The molecular weight recorded by GPC of S-DCPD-terpinolene terpolymer (50:40:10) and S-terpinolene (50:50).

Samples (two repeats of each)	Mn (g/mol)	Mw (g/mol)	PDI
S-terpinolene	442	793	1.8

	443	803	1.8
S-DCPD-terpinolene	582	2826	4.9
	607	3025	5.0

The resultant S-terpinolene polymer was optically transparent with an orange-yellow colour (Figure 3.27). Most of the inverse vulcanised sulfur polymers are brown/black to deep red. There is current interest in the optical properties of sulfur polymers; due to their high transmission to infrared light and high refractive index, there are investigations into thermal imaging applications. [3,16,17] DCPD was included in the synthesis of sulfur terpinolene. It was possible to improve the shape persistency by

Figure 3.27 Photographs of ~5 mm thick blocks of polymers made from 50 wt.% sulfur and 50 wt.% crosslinker, where the crosslinker was composed of copolymers of DCPD and terpinolene, going from all DCPD (left) to all terpinolene (right). Numbers written in pen under the samples can be read clearly for most samples.

doping 10 wt.% DCPD (Figure 3.27) while maintaining the transparent orange colour of the material. S-DCPD alone is opaque (Figure 3.27) and would not be seen through the visible range, and pure S-terpinolene lacks shape persistency to form a lens. Therefore, by combing the two crosslinkers to prepare an S-DCPD-terpinolene terpolymer, the material was shaped persistent and transparent. By measuring the refraction of white light through blocks of 50 wt. % sulfur, 25 wt. % DCPD, 25 wt.% terpinolene copolymers, the refractive index from Snell's law was calculated as 1.74 +/- 0.03 (Appendix, Figure A3.5). This is comparable to previously reported refractive indices of inverse vulcanised polymers at the same sulfur content, e.g., S-DIB and S-TIB have refractive indices of, 1.77[3] and 1.72[5] respectively. These indices for high sulfur polymers are significantly higher than those of many other optical materials, such as glass (1.52) or poly (methyl methacrylate) (1.49).

3.4.4 Sulfur-DCPD-EDGMA terpolymer

DCPD was also included in the synthesis of sulfur and ethylene glycol dimethacylate (EDGMA). Sulfur and EDGMA alone will not undergo an inverse vulcanisation reaction and form two immiscible phases (as mentioned in Chapter 5). However, with a small amount of DCPD, the reaction proceeded homogeneously to form inverse vulcanised sulfur-DCPD-EDGMA terpolymers alike with the other sulfur polymers.

Table 3.2 Polymer compositions of S-DCPD-EDGMA at 50% and 75% elemental sulfur by mass. DSC detects the Tm of S_8 crystals, no S8 crystals were detected in the polymer compositions displayed in the table below.

Sulfur (wt.%)	DCPD (wt.%)	EDGMA (wt.%)	T_g (°C)	Sulfur present (Y/N)
50.0	25.0	25.0	32.9	N
50.0	12.5	37.5	17.7	N
75.0	12.5	12.5	33.0	N

The three ratios of sulfur: DCPD: EDGMA is shown in Table 3.2. Similarly, to the other sulfur terpolymers prepared glass transition temperature increases with the % of DCPD. No T_m were recorded by DSC.

3.4.6 Mechanical testing

In addition to the compression tests, the flexural, tensile, and hardness properties were recorded.

3.4.6.1 Flexural testing

The sulfur terpolymers were prepared in a 150 mm x 10 mm x 10 mm silicone mould for flexural testing. The flexural tests show a clear difference in both strength and modulus, depending on the polymer compositions (Figure 3.28). The flexural strength of the sulfur terpolymers recorded is low in comparison to many commodity plastics. Polypropylene has a flexural strength of 40 MPa,[18] compared to S-DCPD with the highest flexural strength recorded of 6 MPa. The low flexural strength of these

materials could limit future applications, but these results may provide a useful benchmark to be improved by future researchers.

Conversely, the flexural modulus of S-DCPD is remarkably high (3.7 GPa) (Figure 3.29). This is much higher than polypropylene (1.5 GPa), polycarbonate (2.3 GPa) , and polystyrene (2.5 GPa).[18] The variation in flexural modulus and strength presents the potential for the properties of inverse vulcanised sulfur polymers to be tailored for

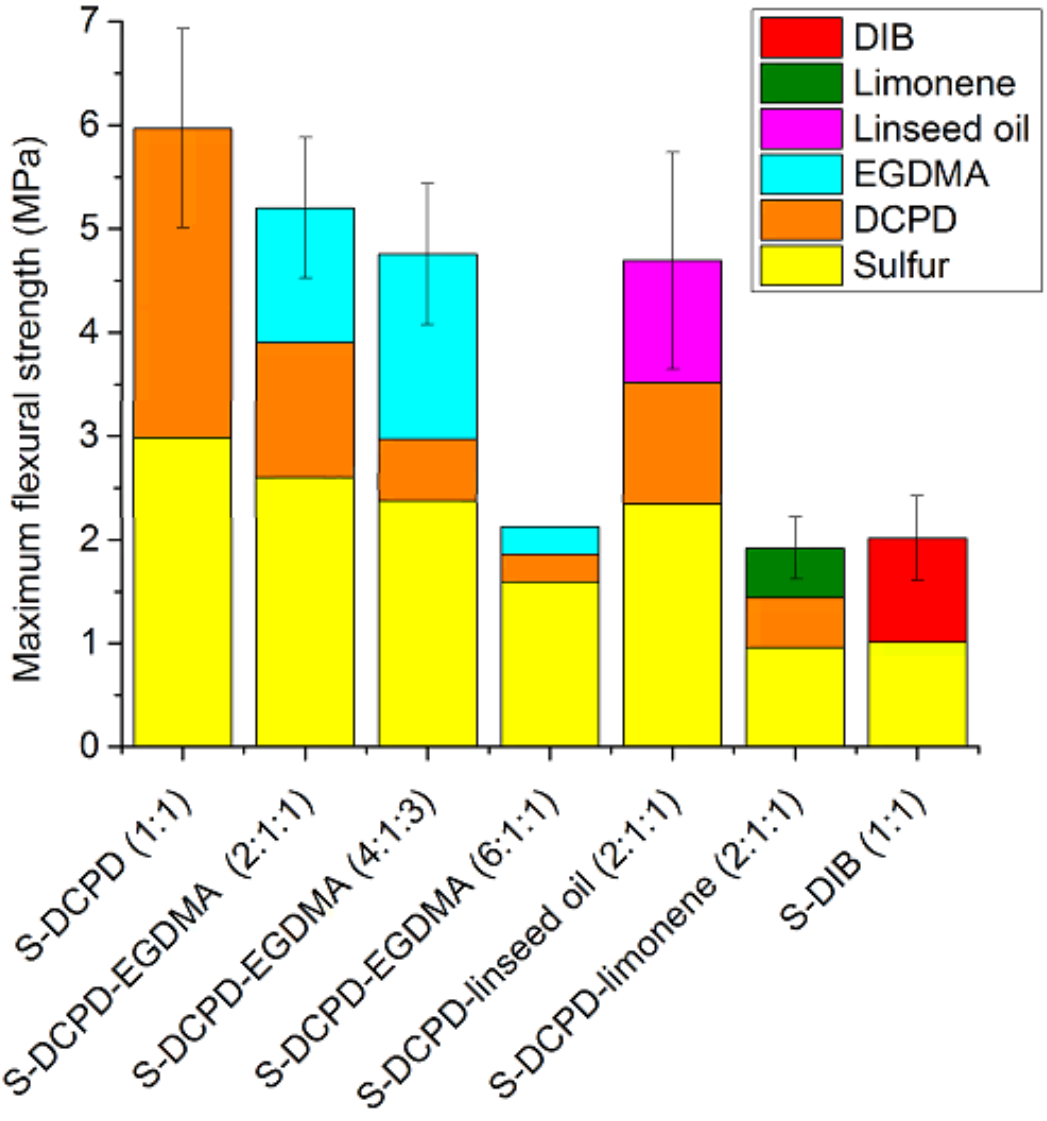

Figure 3.28 Maximum flexural strength of sulfur terpolymers with a variety of compositions. The composition of each monomer is shown by the relative height of each colour according to the legend. Weight ratios of the components of each polymer are given

applications by changing the crosslinker and ratios (Figure 3.28 and 3.29). When DCPD was replaced with EDGMA, the flexural strength and modulus were reduced by similar amounts. As the sulfur wt. % is increased in the S-DCPD-EDGMA

terpolymer; both the flexural modulus and strength are significantly reduced. However, replacing DCPD with linseed oil reduced the modulus (Figure 3.29) significantly but only had a small effect on the flexural strength compared to DCPD. Sulfur-limonene could not be measured due to the lack of shape persistency. With this said, incorporating DCPD in the reaction with sulfur and limonene increased the

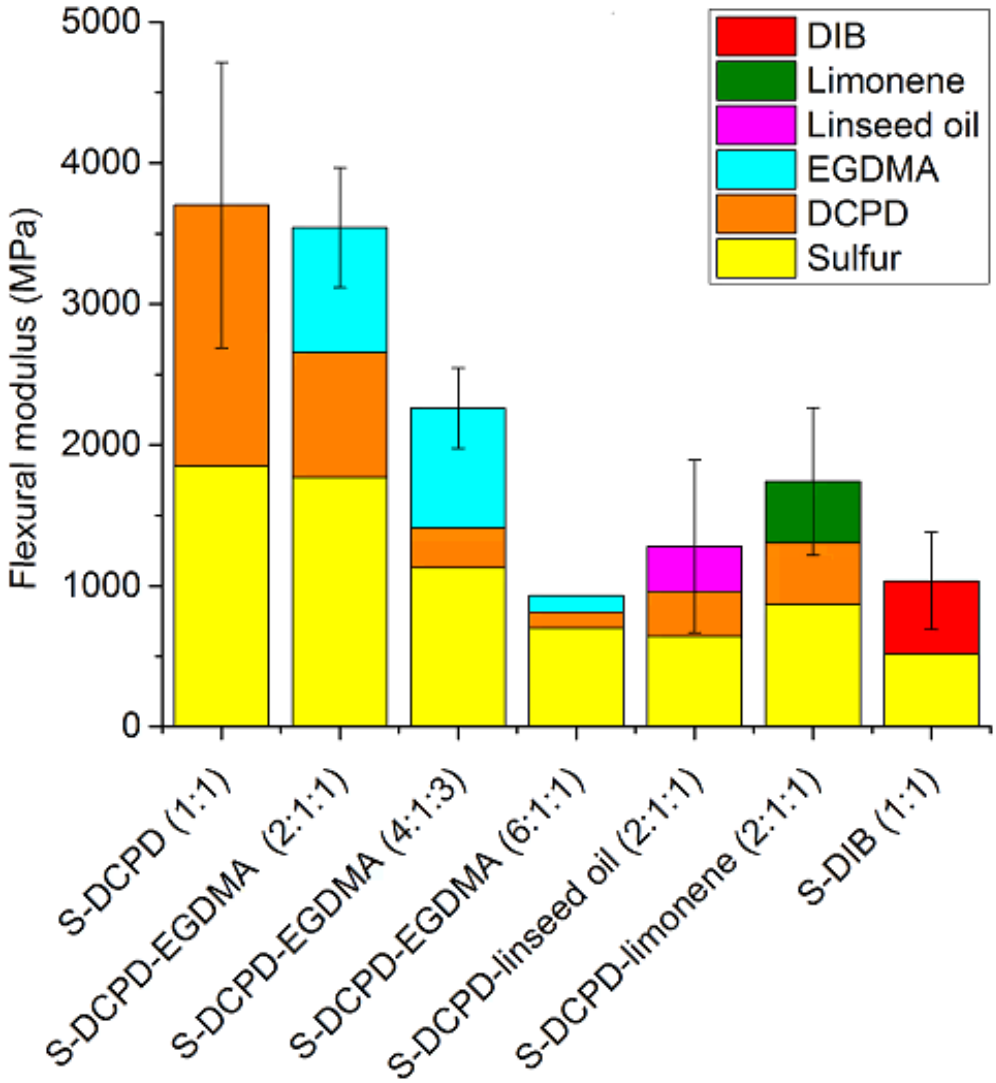

Figure 3.29 Maximum flexural modulus of sulfur terpolymers with a variety of compositions. The composition of each monomer is shown by the relative height of each colour according to the legend. Weight ratios of the components of each polymer are given.

flexural strength (Figure 3.28) and modulus (Figure 3.29) compared to S-DIB.

3.4.6.3 Vickers hardness testing

The relative hardness of the polymers was recorded by microhardness Vickers testing (Figure 3.30). All the polymers tested included sulfur reacted with crosslinkers at an equal mass ratio, and all contained DCPD in the crosslinker portion. The difference in hardness as DCPD is decreased was significantly affected. The S-DCPD-linseed oil terpolymer has a considerably lower value for hardness in comparison to the other three terpolymers (Figure 3.30). S-DCPD-EDGMA and S-DCPD-limonene show considerably higher hardness in comparison to S-DCPD-linseed oil (Figure 3.30). The highest value for hardness recorded was for S-DCPD at 34 kPa mm^{-2}. This is significantly higher than many conventional carbon-based polymers such as polystyrene, polycarbonate, poly(methyl methacrylate) at 13, 12, 21 kPa mm^{-2} , respectively.[21] The decrease in hardness of the samples in replacing a portion of DCPD with limonene, EDGMA, and linseed oil (hardness for DCPD>limonene>EGMA>linseed oil) inversely correlates with the increase in molecular flexibility across the same series.

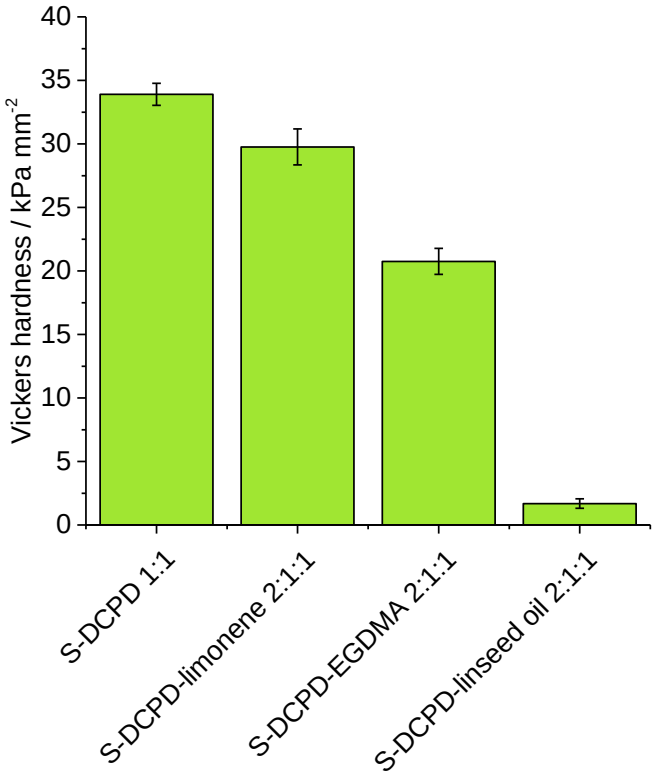

Figure 3.30 Vickers hardness of a range of S-DCPD copolymers and sulfur terpolymers. Weight ratios are given in the order of the components of the sample.

3.4.6.2. Tensile strength

The tensile properties of a set of sulfur terpolymers were recorded. However, not all samples could be tested by this method as some of the polymers (e.g., S-DCPD), were too brittle and fragile. There was a significant difference in the tensile properties of the three terpolymers produced from sulfur, DCPD, and a third crosslinker. The extension at the breaking point of the three polymers varies between 1.3 % for S-DCPD-linseed oil terpolymer and 5.5% for the S-DCPD-limonene terpolymer (Figure 3.31). These values are comparable to some commonly used polymers such as polystyrene (1.6%) epoxy resins (1.3%) and acrylonitrile-butadiene-styrene (ABS, 6%), but much lower than polycarbonate (200%) or polypropylene (80%).[19]

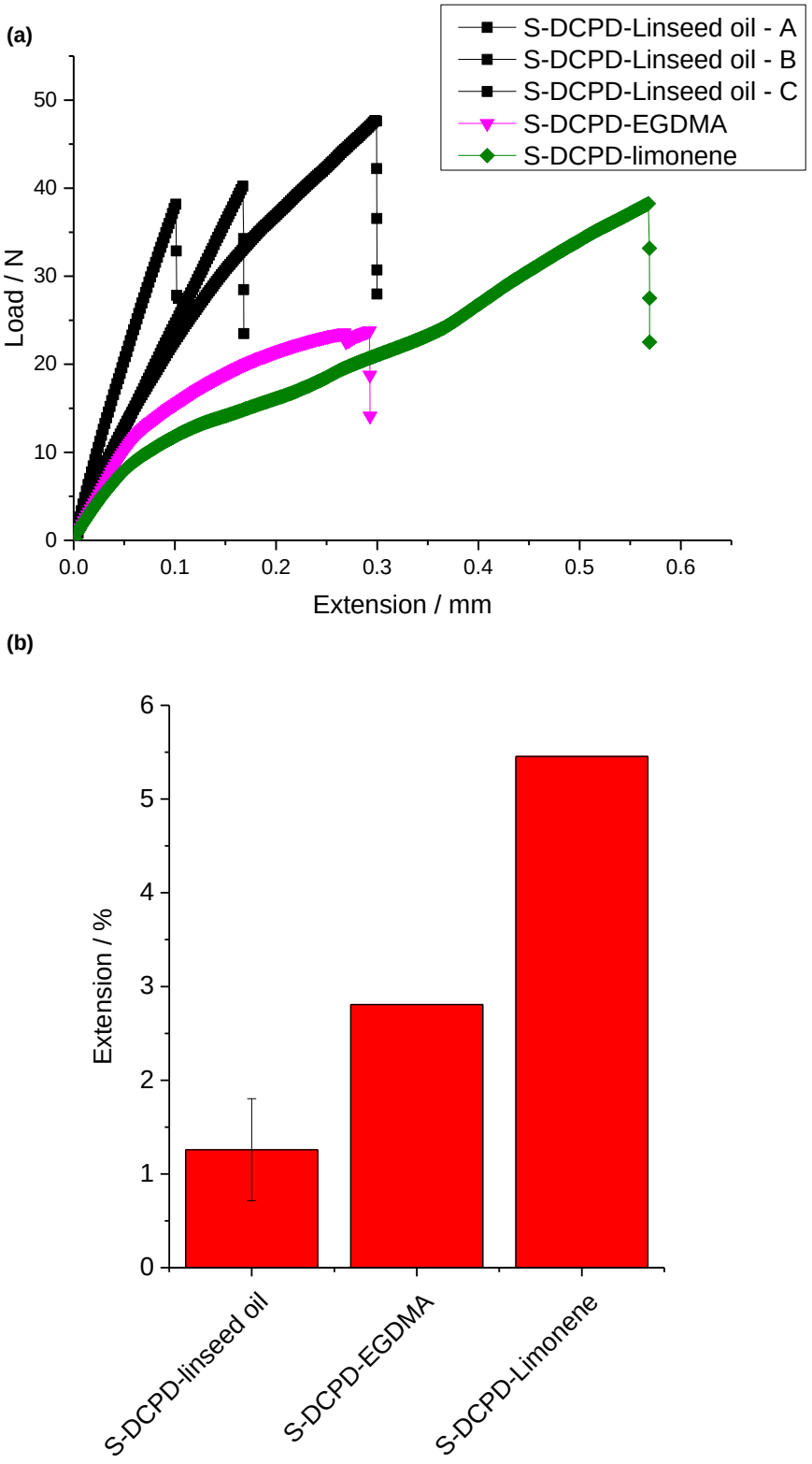

Figure 3.31 Tensile testing of sulfur polymers at 50 % elemental sulfur by mass, and 25 wt.% loading each of DCPD and another crosslinker: linseed oil, EDGMA, or limonene. Three repeat samples were measured for S-DCPD-linseed oil, and the standard deviation in the results is given. Here is the extension (%) at the break. (a) Stress-strain curves (b) Extension break.

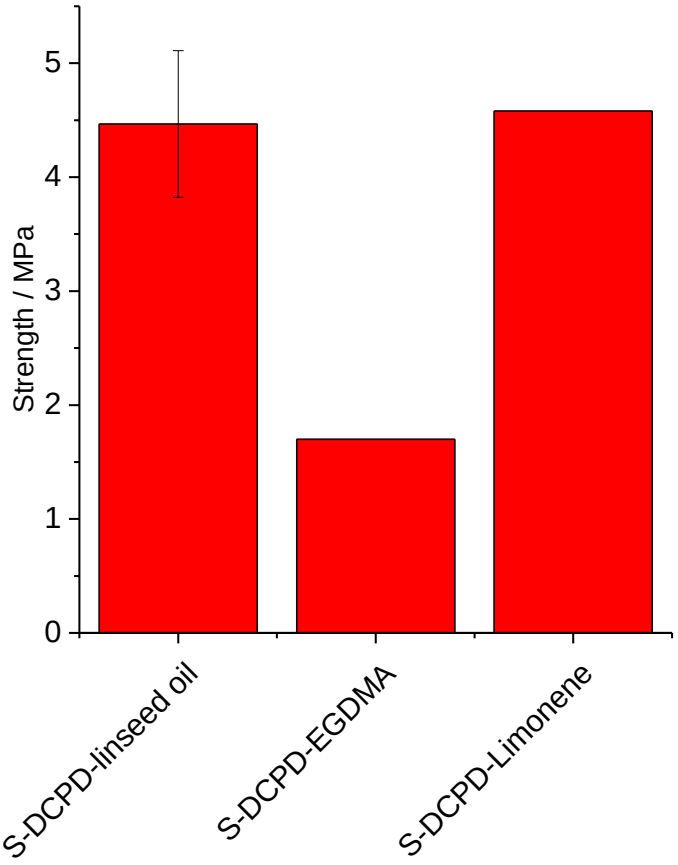

Figure 3.32 Tensile testing of sulfur polymers at 50 % elemental sulfur by mass, and 25 wt.% loading each of DCPD and another crosslinker: linseed oil, EDGMA, or limonene. Three repeat samples were measured for S-DCPD-linseed oil, and the standard deviation in the results is given. Here is the maximum breaking strength.

The tensile strength of the sulfur terpolymers recorded (~4.5 MPa) alike with the flexural strength is poor in comparison to the most common polymers (Figure 3.32). Polyethylene has a tensile strength between 10-32 MPa (dependent on the molecular weight) and polystyrene has a tensile strength of 34 MPa.[19] The tensile modulus of the three polymers (Figure 3.33) (up to ~0.5 GPa) is in a similar range to some carbon-based polymers (polyethylene 0.1 to 0.8 GPa), but lower many others (polystyrene 3.0-3.5 GPa).[20]

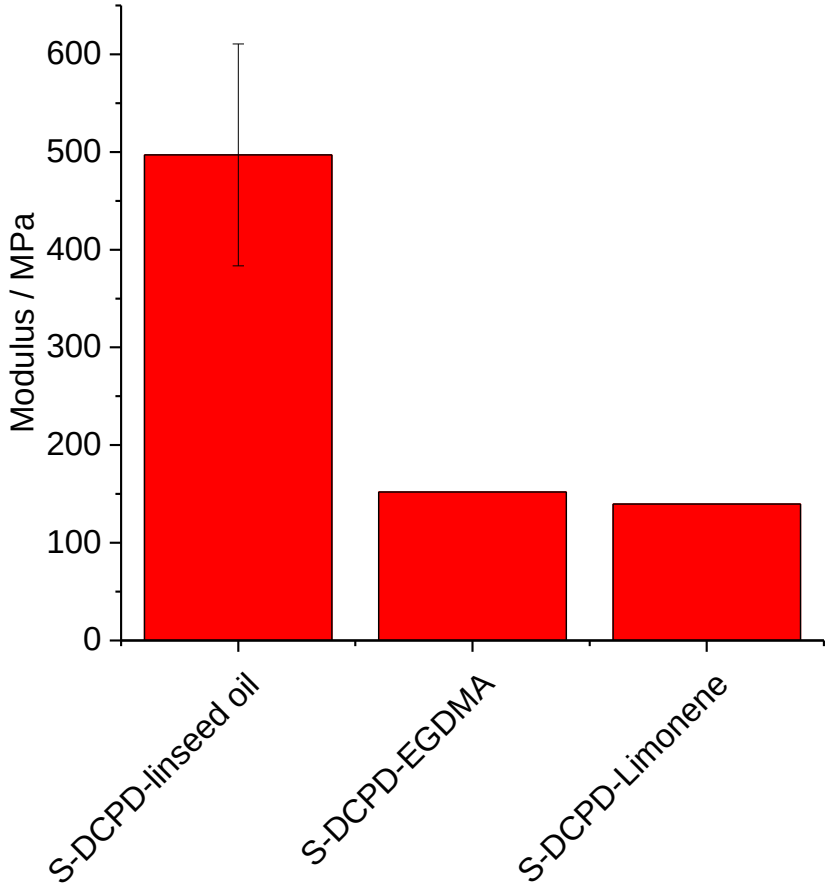

Figure 3.33 Tensile testing of sulfur polymers at 50% elemental sulfur by mass, and 25 wt.% loading each of DCPD and another crosslinker: linseed oil, EDGMA, or limonene. Three repeat samples were measured for S-DCPD-linseed oil, and the standard deviation in the results is given. Here is the tensile modulus.

3.5 Conclusions and Future Work

Inverse vulcanised sulfur polymers have very different properties to carbon-based polymers. This is still an emerging field, and the physical properties are still largely underreported. As the physical properties will underpin many of the practical applications, they must be investigated. Here four new sulfur terpolymers have been prepared. The tensile, flexural, compression, and hardness properties were tested showing that combining crosslinkers at different feed ratios can tailor the properties. For instance, the T_g can be varied controllably from -20 to 115 °C. This study is the first effort to uncover design principles so that a given mechanical or optical properties can be rationally imparted to this class of sulfur polymers. These results can set a benchmark to trigger future improvements.

Since this study, there are further improvements on this research.[22] Such as, adjusting the degree of crosslinking by introducing a two-step method which allows new control over the mechanical properties of inverse vulcanised polymers.[22] One of the main issues during this research was moulding the polymers into the correct mechanical testing dimensions. This proved challenging with air pockets forming in the materials resulting in pores. Another major issue occurred when removing the polymers from the prepared mould due to the air pockets formed the materials were extremely fragile and would easily break before testing. The new research uses a hot press to produce uniform films for mechanical testing that solves this issue.[22]

Potential future experiments:

- Recyclability of these materials should be studied to look at the deformation.
- Solid-state UV Vis spectroscopy could look at the optical properties of S-DCPD-terpinolene terpolymers.
- Additives could be introduced to the reaction, such as cellulose nanowhiskers, to see if it reinforces the materials and improves the strength.

3.6 Materials and methods

3.6.1 Materials

1,3-Diisopropenyl benzene (DIB) and dicyclopentadiene (DCPD) were purchased from Tokyo Chemicals Industry. Sulfur was purchased in 25 Kg sacks from Brenntag. Linseed oil was purchased from Sigma Aldrich. Limonene, terpinolene, ethylene glycol methacrylate (EGDMA) and all other solvents and chemicals were purchased from Sigma-Aldrich. All chemicals were used as received.

3.6.2 Characterisation

Powder X-ray diffraction (PXRD): Powder X-Ray Diffraction (PXRD) patterns were carried out on samples using a PAN analytical X'pert powder diffractometer using CuKα radiation.

Differential Scanning calorimetry (DSC): Differential scanning calorimetry was carried out using Q2000 DSC (TA instruments). The method was a heat/cool/heat for three cycles; heating to 150 °C and cooling to – 80 °C at a heating rate of 5 °C/min with Tzero Hermetic pans.

Thermogravimetric Analysis (TGA): TGA was carried out in platinum pans using a Q5000IR analyzer (TA Instruments) with an automated vertical overhead thermobalance. The samples were heated at 5 °C/min to 900 °C under nitrogen.

Fourier-transform infrared spectroscopy (FT-IR): was performed using a Thermo NICOLET IR200, between 400 cm^{-1} to 4000 cm^{-1}. Samples were loaded either neat, using an attenuated total reflectance accessory, or in transmission after pressing into a KBr pellet.

Raman Spectroscopy: Raman spectra was collected using a Witec alpha300R Raman microscope at an excitation laser wavelength of 532 nm with a 40X objective (numerical aperture 0.60). Typical integration times for Raman spectra were 20 s. Approximately 200 spectra were acquired at 5 distinct locations on each sample with each location separated by hundreds to thousands of microns.

Compression testing: S-DCPD canola oil porous polymer blocks (45, 35, 15, 5 wt. % canola oil), S-DCPD and S-Canola oil were compressed using TA Instruments Q800 DMA in compression using parallel plates. DMA was ran in controlled force mode using stress/strain experiment. The force was ramped at 0.5 N/ min up to 10 N.

Flexural testing: Based on ASTM E290. Flexural testing was carried out using an Instron 5566 in the 3-point bend mode. The force required to deflect the samples, over a 140 mm gauge length, was measured at a rate of 0.5 mm min^{-1}. Sample strips were made in a 150 mm x 10 mm x 10 mm silicone mould.

Tensile testing: Based on ASTM D638. Tensile properties were measured on an Instron 5944 system. Samples were molded into dog-bone shapes of 63.5 mm length, with a cross- sectional width of 3.18 mm, depth 3 mm and an initial gauge length of 25.4 mm (shown in Fig. S16). The crosshead speed was fixed at 10 mm/min, the capacity of the load cell was 2 kN.

Hardness testing: Microhardness Vickers testing was carried out using a diamond indenter and a 100 g load (HV 0.1) or a 50 g load for the softer materials (HV 0.05)**.**

Gel permeation chromatography (GPC): The molecular weight of the soluble fraction of the polymers was determined by gel permeation chromatography (GPC) using a Viscotek system comprising a GPCmax (degasser, eluent and sample delivery system), and a TDA302 detector array, using THF as eluent.

3.6.3 Polymer preparation

3.6.3.1 Synthesis of S-DCPD-limonene terpolymer

Sulfur (wt. % shown in Table 3.3-3.5) was added to a 40 mL glass vial equipped with a magnetic stirrer bar and heated on a hot plate to 165 °C. Molten sulfur was formed (transparent, yellow solution) and to this, DCPD (Table 3.3-3.5) was added drop-wise via a pipette. Following this, limonene was added to the mixture via a pipette (limonene wt. % shown in Table 3.3-3.5). The mixture was heated at 165 °C for ~15 minutes yielding a viscous chocolate brown mixture. The product was then transferred to a silicone mould and allowed to cure for ~14 hours at 140 °C. The resultant polymers formed a hard opaque solid. These reactions were carried out on a 10 g scale.

Table 3.3 Polymer compositions of S-DCPD-limonene at 50% elemental sulfur by mass

Reaction composition (wt. % of limonene)	Reaction composition (wt. % of DCPD)	Reaction composition (wt. % of S_8)
5	45	50
10	40	50
15	35	50
20	30	50
25	25	50
30	20	50
35	15	50
40	10	50

Table 3.4 Polymer compositions of S-DCPD limonene at 60% elemental sulfur by mass

Reaction composition (wt. % of limonene)	Reaction composition (wt. % of DCPD)	Reaction composition (wt. % of S_8)
4	36	60
8	32	60
12	28	60
16	24	60
20	20	60
24	16	60
28	12	60
32	8	60
36	4	60

Table 3.5 Polymer compositions of S-DCPD limonene at 70% elemental sulfur by mass

Reaction composition (wt. % of limonene)	Reaction composition (wt. % of DCPD)	Reaction composition (wt. % of S_8)
15	15	70
18	12	70
21	9	70

3.6.3.1 Synthesis of S-DCPD-linseed oil

Sulfur (wt. % shown in Table 3.6 and 3.7) was added to a 40 mL glass vial equipped with a magnetic stirrer bar and heated on a hot plate to 165 °C. Molten sulfur was formed (transparent, yellow solution) and to this, vegetable oils (linseed, sunflower and olive oil) (vegetable oil wt. % shown in Table 3.6 and 3.7) was added drop-wise via a pipette. Following this Dicyclopentadiene (DCPD) was added to the mixture via

a pipette (DCPD wt. % shown in Table 3.6 and 3.7). The mixture was heated at 165 °C for ~15 minutes yielding a viscous chocolate brown mixture. The product was then transferred to a silicone mould and allowed to cure for ~14 hours at 140 °C. These reactions were carried out on a 10 g scale.

Table 3.6 The sample compositions for the reactions carried out using a mixture of linseed oil and DCPD

Reaction composition (wt. % of linseed oil)	Reaction composition (wt. % of DCPD)	Reaction composition (wt. % of S_8)	Appearance
5	45	50	Black brittle solid
10	40	50	Black brittle solid
15	35	50	Black brittle solid
20	30	50	Black brittle solid
25	25	50	Black brittle solid
30	20	50	Black brittle solid
35	15	50	Black rubbery solid
40	10	50	Black rubbery solid

Table 3.7 The sample compositions for the reactions carried out using a mixture of linseed oil and DCPD

Reaction composition (wt. % of DCPD)	Reaction composition (wt. % of linseed oil)	Reaction composition (wt. % of S_8)	Appearance
18	2	80	Black brittle solid
16	4	80	Black brittle solid
14	6	80	Black brittle solid
12	8	80	Black brittle solid
10	10	80	Black brittle solid
8	12	80	Black rubbery solid
6	14	80	Black rubbery solid

4	16	80	Black rubbery solid
2	18	80	Black rubbery solid

3.6.3.3 Synthesis of S-DCPD-canola oil

Sulfur (wt. % shown in Table 3.8) was added to a 20 mL glass vial equipped with a magnetic stirrer bar and heated on a hot plate to 165 °C. Molten sulfur was formed (transparent, yellow solution) and to this canola oil (canola oil wt. % shown in Table 3.8) was added drop wise via a pipette. Following this dicyclopentadiene (DCPD) was added to the mixture via a pipette (DCPD wt. % shown in Table 3.8). The mixture was heated at 165 °C for ~15 minutes yielding a viscous chocolate brown mixture. The product was then cured on a hot plate for ~ 14 hours at 140 °C. These reactions were carried out on a 10 g scale.

Table 3.8 The sample compositions for the reactions carried out using a mixture of canola oil and DCPD

Reaction composition (wt. % of canola oil)	Reaction composition (wt. % of DCPD)	Reaction composition (wt. % S_8)	Appearance
50	0	50	Brown rubbery solid
45	5	50	Black rubbery solid
40	10	50	Black rubbery solid
35	15	50	Black rubbery solid
30	20	50	Black brittle solid
25	25	50	Black brittle solid
0	50	50	Black brittle solid
15	5	80	Brown rubbery solid

10	10	80	Brown rubbery solid

3.6.3.4 Preparing S- DCPD/ canola oil porous polymer terpolymers for compression testing

The same general synthesis procedure was followed except once a homogenous pre polymer had formed NaCl was slowly added to the reaction mixture continuing to heat at 165 °C. Once sufficient mixing had occurred between the NaCl and the homogenous pre polymer. This mixture was the removed from the 20 mL vial with a spatula and pressed into a 1 cm x 1 cm x 1 cm mould. These reactions were carried out on a 12 g scale with 70 % NaCl: 30 % polymer. This was then cured in an oven at 140 °C for ~ 16 hours. Once cooled, polymer blocks were then added to 100 mL round bottom flask and the flask was filled with distilled water. To the round bottom flask, a septum was attached, to this a needle was attached and vacuum was pulled for 48 hours to remove excess salt.

Table 3.9 The sample compositions for the reactions carried out for compression testing using a mixture of canola oil and DCPD

Reaction composition (wt. % canola oil)	Reaction composition (wt. % DCPD)	Reaction composition (wt. % S_8)
50	0	50
45	5	50
35	15	50
25	25	50
15	35	50
5	45	50
0	50	50

3.6.3.5 Synthesis of S-DCPD-terpinolene terpolymer

Sulfur (wt. % shown in Table 3.10) was added to a 20 mL glass vial equipped with a magnetic stirrer bar and heated on a hot plate to 165 °C. Molten sulfur was formed (transparent, yellow solution) and to this terpinolene (terpinolene wt. % shown in Table 3.10) was added drop wise via a pipette. Following this dicyclopentadiene (DCPD) was added to the mixture via a pipette (DCPD wt. % shown in Table 3.10). The mixture was heated and stirred at 165 °C for ~10 minutes yielding a transparent

orange colour. The product was then cured on a hot plate for ~ 14 hours at 140 °C. These reactions were carried out on a 10 g scale.

Table 3.10 Polymer composition of S-DCPD-terpinolene at 50% elemental sulfur by mass

Reaction composition (wt. % of terpinolene)	Reaction composition (wt. % of DCPD)	Reaction composition (wt. % S_8)
5	45	50
10	40	50
15	35	50
20	30	50
25	25	50
30	20	50
35	15	50
40	10	80
45	5	50

3.6.3.6 Synthesis of S-DCPD-EGDMA

Sulfur (wt. % shown in Table 3.11) was added to a 20 mL glass vial equipped with a magnetic stirrer bar and heated on a hot plate to 165 °C. Molten sulfur was formed (transparent, yellow solution) and to this (EDGMA % shown in Table 3.11) was added drop wise via a pipette. Following this Dicyclopentadiene (DCPD) was added to the mixture via a pipette (DCPD wt. % shown in Table 3.11). The mixture was heated at 165 °C for ~15 minutes yielding a viscous chocolate brown mixture. The product was then cured on a hot plate for ~ 14 hours at 140 °C. These reactions were carried out on a 10 g scale.

Table 3.11 Polymer composition of S-DCPD-EDGMA at 50 and 75 % elemental sulfur by mass

Reaction composition (wt. % of EDGMA)	Reaction composition (wt. % of DCPD)	Reaction composition (wt. % S_8)
25	25	50
37.5	12.5	50
12.5	12.5	75

3.7 Appendix

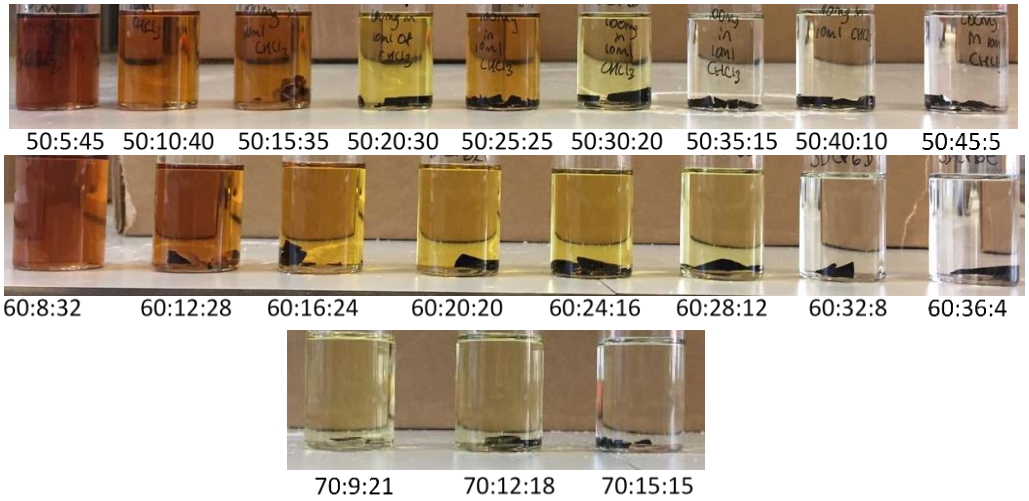

Figure A3.1 Photographs of solubility study with of S-DCPD-Limonene at 50, 60 and 70 % elemental sulfur by mass. Solubility decreased with increase sulfur % and increased DCPD. The following compositions stated are (sulfur: DCPD: Limonene, ratios are % of components by mass).

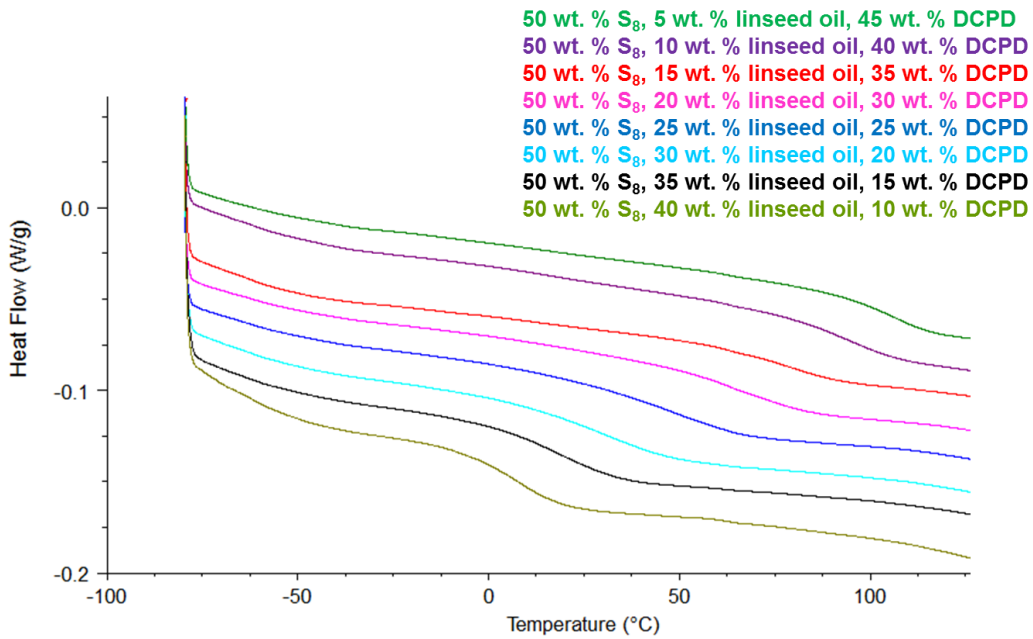

Figure A3.2 DSC traces of S-DCPD/linseed oil with varying linseed oil and DCPD content at 50 wt. % S_8 content. The second heating step is shown, stacked for clarity. The glass transition temperature moves to higher temperatures as linseed oil is replaced with DCPD.

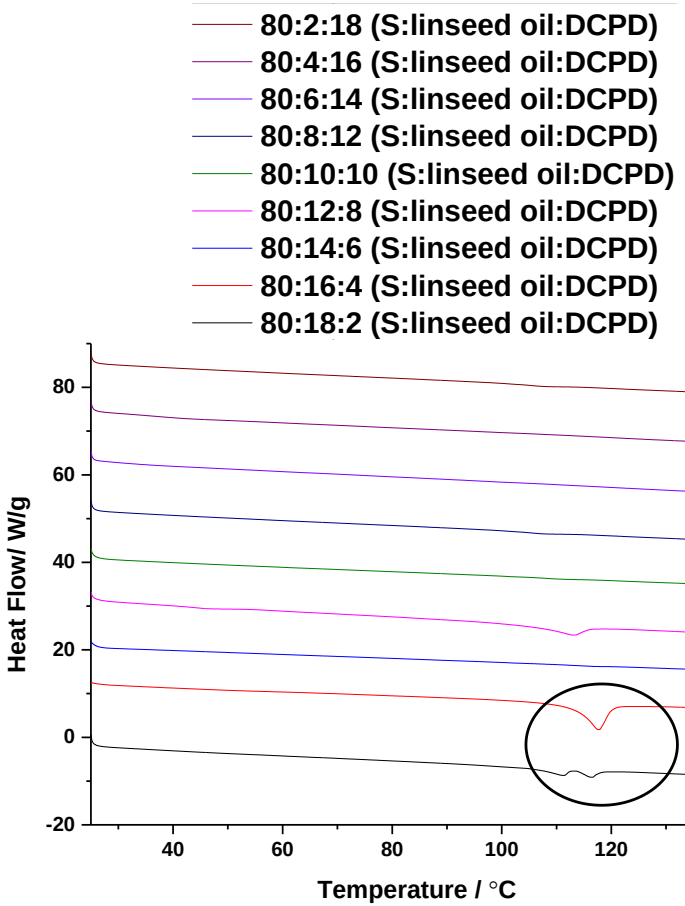

Figure A3.3 DSC traces of S-DCPD/linseed oil with varying linseed oil and DCPD content at 80 wt. % S_8 content. The second heating step is shown, stacked for clarity.

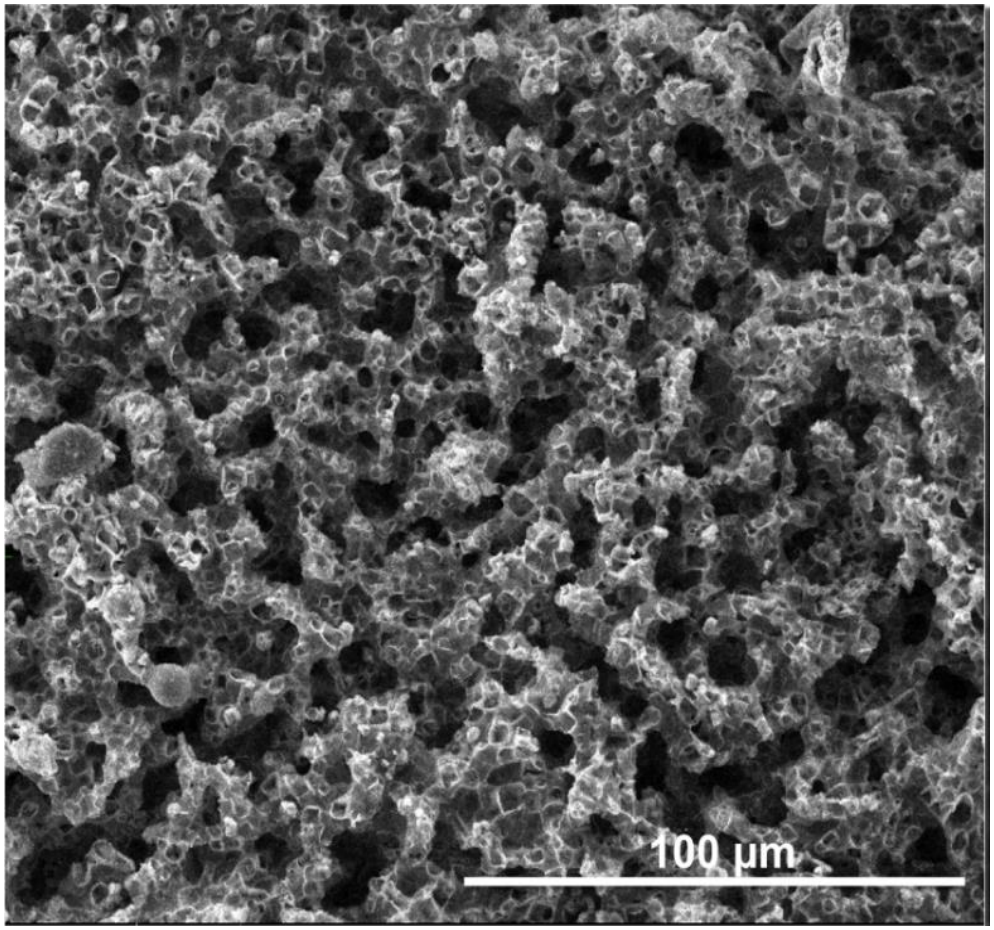

Figure A3.4 SEM image of a sample of S- canola oil (50:50), showing porosity arising from removal of the salt template.

Snells law:

$$n_1 sin\emptyset_1 = n_2 sin\emptyset_2$$

$$n_1 = indcident\ index$$

$$n_2 = refracted\ index$$

$$\emptyset_1 = incident\ angle$$

$$\emptyset_2 = refracted\ angle$$

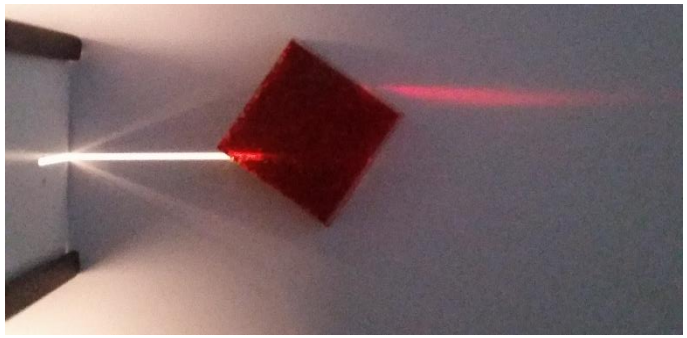

Figure A3.5 Light being passed through S-DCPD-terpinolene (50:25:25)

3.8 References

1 W. J. Chung, J. J. Griebel, E. T. Kim, H. Yoon, A. G. Simmonds, H. J. Ji, P. T. Dirlam, R. S. Glass, J. J. Wie, N. a Nguyen, B. W. Guralnick, J. Park, A. Somogyi, P. Theato, M. E. Mackay, Y. Sung, K. Char, J. Pyun, Á. Somogyi, P. Theato, M. E. Mackay, Y. Sung, K. Char, J. Pyun, A. Somogyi, P. Theato, M. E. Mackay, Y. Sung, K. Char, J. Pyun, Á. Somogyi, P. Theato, M. E. Mackay, Y. Sung, K. Char and J. Pyun, *Nat. Chem.*, 2013, **5**, 518–524.

2 Y. Xin, H. Peng, J. Xu and J. Zhang, *Adv. Funct. Mater.*, 2019, **29**, 1–7.

3 J. J. Griebel, N. A. Nguyen, S. Namnabat, L. E. Anderson, R. S. Glass, R. A. Norwood, M. E. Mackay, K. Char and J. Pyun, *ACS Macro Lett.*, 2015, **4**, 862–866.

4 J. J. Griebel, R. S. Glass, K. Char and J. Pyun, *Prog. Polym. Sci.*, 2016, **58**, 90–125.

5 T. S. Kleine, N. A. Nguyen, L. E. Anderson, S. Namnabat, E. A. LaVilla, S. A. Showghi, P. T. Dirlam, C. B. Arrington, M. S. Manchester, J. Schwiegerling, R. S. Glass, K. Char, R. A. Norwood, M. E. Mackay and J. Pyun, *ACS Macro Lett.*, 2016, **5**, 1152–1156.

6 S. Z. Khawaja, S. Vijay Kumar, K. K. Jena and S. M. Alhassan, *Mater. Lett.*, 2017, **203**, 58–61.

7 S. Diez, A. Hoefling, P. Theato and W. Pauer, *Polymers*, 2017, **9**,1–16.

8 D. J. Parker, H. A. Jones, S. Petcher, L. Cervini, J. M. Griffin, R. Akhtar and T. Hasell, *J. Mater. Chem. A*, 2017, **5**, 11682–11692.

9 Y. Zhang, K. M. Konopka, R. S. Glass and K. Char, *Polym.Chem*, 2017, **8** , 5167–5173.

10 C. R. Westerman and C. L. Jenkins, *Macromolecules*, 2018, **51**, 7233–7238.

11 H. Lin and Y. Liu, *Macromol. Rapid Commun.*, 2017, **38**, 1700051.

12 Y. Zhang, R. Glass, K.Char and J.Pyun, *Polym.Chem.*, 2019, **10**, 4078–4105.

13 M. P. Crockett, A. M. Evans, M. J. H. Worthington, I. S. Albuquerque, A. D. Slattery, C. T. Gibson, J. A. Campbell, D. A. Lewis, G. J. L. Bernardes and J. M. Chalker, *Angew. Chemie - Int. Ed.*, 2016, **55**, 1714–1718.

14 A. Hoefling, Y. J. Lee and P. Theato, *Macromol.Chem.Phys.*, 2017, **218**,1600303.

15 M. J. H. Worthington, R. L. Kucera, I. S. Albuquerque, C. T. Gibson, A. Sibley,

A. D. Slattery, J. A. Campbell, S. F. K. Alboaiji, K. A. Muller, J. Young, N. Adamson, J. R. Gascooke, D. Jampaiah, Y. M. Sabri, S. K. Bhargava, S. J. Ippolito, D. A. Lewis, J. S. Quinton, A. V. Ellis, A. Johs, G. J. L. Bernardes and J. M. Chalker, *Chem. - A Eur. J.*, 2017, **23**, 16219–16230.

16 D. A. Boyd, V. Q. Nguyen, C. C. Mcclain, F. H. Kung, C. C. Baker, J. D. Myers, M. P. Hunt, W. Kim and J. S. Sanghera, *ACS Macro Lett.*, 2019, **8**, 113–116.

17 T.S.Kleine, N.A.Nguyem, L.E.Anderson, S.Namnbat, E.A. Lavilla, S.A.Showghi, P.T.Dirlam, C.B.Arrington, M.S.Manchester, J.Schwiergerling, R.S.Glass, K.Char, R.A.Norwood, M.E.Mckay and J.Pyun, *ACS Macro Lett.*, 2016, **5**, 1152-1156.

18 L. Matweb, Matweb-material property data, http://www.matweb.com./reference/flexuralstrength.aspx (acessed 6th November 2018).

19 T. . Crompton, *Physical testing of plastics*, Smithers information limited, 2012.

20 T.E.Toolbox, Young's Modulus-Tensile and Yeild Strength for common Materials, http://www.engineeringtoolbox.com/young-modulus-d_417.html, (accessed 6th November 2018)

21 R. Buchdahl, *J.Poly.Sci.Polym.Lett.Ed.*, 1975, **13**, 120–121.

22 P. Yan, W. Zhao, B. Zhang, L. Jiang, S. Petcher, J. A. Smith, D. J. Parker, A. I. Cooper, J. Lei and T. Hasell, *Angew. Chemie - Int. Ed.*, 2020.

CHAPTER 4

INVESTIGATING THE ANTIBACTERIAL PROPERTIES OF INVERSE VULCANISED SULFUR POLYMERS

Chapter 4: Investigating the antibacterial properties of inverse vulcanised sulfur polymers

4.1 Context

Section 4.2 is adapted from the paper "Investigating the antibacterial properties of inverse vulcanised sulfur polymers", published in ACS Omega, 2020. Chapter 3 uncovered design principles and discussed how the physical properties of sulfur polymers could be controlled and altered for different functions. Chapter 4 explores the potential function of these materials and highlights how managing the properties of these polymers are essential for their functions.

As previously discussed, these polymers have potential applications covering diverse areas. However, there has been very little focus on the potential of these high sulfur content polymers for their antibacterial properties. There is an urgent need to develop solutions to combat the bacterial threats. The antibacterial activity was investigated for two polymers exhibiting different structural features, S-DIB and S-DCPD. As discussed in previous chapters, S-DIB is a shape persistent hyperbranched polymer, whereas S-DCPD is fully crosslinked. Therefore, this work compares the antibacterial activity of two different types of inverse vulcanised sulfur polymers exposed to two common hospital bacteria; *Escherichia coli* (*E. coli*) and *Staphylococcus aureus (S. aureus)*.

4.1.2 Author Contributions

Jessica A Smith wrote the manuscript and prepared all materials for antimicrobial testing. Ross Mulhall conducted bacteria testing with the help of Dr. Sean Goodman. I want thank Dr. George Fleming for his useful interpretations and biological discussions. Dr. Heather Allison and Prof. Rasmita Raval supervised Ross Mulhall. Dr. Tom Hasell was PI on the project and gave much-needed advice and direction. I would also like to thank Fiona McBride, who helped drive the collaboration; without her, this project would not have been possible.

4.2 Introduction

4.2.1 The urgent need to develop new solutions to combat bacterial threat

Since the discovery of antibiotics in 1929, they have been widely used in both human and veterinary medicine for treatment to prevent bacterial infections.[1, 2] However, the excessive use of antibiotics, whether for prevention or treatment, has significantly increased the level of bacterial resistance worldwide.[3] The overuse and misuse of antibiotics have led to the emergence of antibiotic-resistant bacteria. Some bacterial cells resist killing when antibiotics are administered (Figure 4.1). Alongside this, some beneficial bacteria that contribute to protection from infection may also be killed (Figure 4.1). The resistant bacteria are then able to grow and multiply with less competition (Figure 4.1). The issue of antibiotic resistance persists and increases with the number of deaths reaching 50 000 per year in the United States and Europe.[3] Hence, there is a pressing need for a new generation of antimicrobials to mitigate the spread of antibacterial resistance.

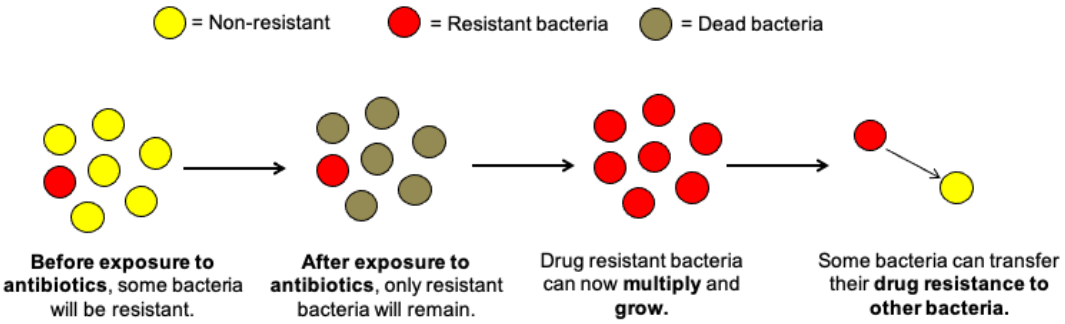

Figure 4.1 Scheme for how antibiotic resistance can occur. Before exposure to antibiotics some bacteria will be resistant. After exposure to antibiotics, only resistant bacteria will remain. The drug resistant bacteria will now multiply and grow, with some bacteria able to transfer their drug resistance to other bacteria.

As medicine is developing, there is an increasing need for implantable medical devices, such as hip prosthetics, catheters, and pacemakers.[4] These devices, along with others, have been paramount in increasing life expectancy and aiding age-related diseases. However, these devices are susceptible to bacterial adhesion and biofilm formation.[4] Gram-positive, and Gram-negative bacteria infect implant sites through biofilm formation. The main difference between Gram-positive and Gram-negative bacteria is their cell wall. The cell wall of Gram-positive bacteria consists of a thick layer of peptidoglycan. The cell wall of Gram-negative bacteria has a thinner layer of peptidoglycan protected by an outer membrane with a lipopolysaccharide component.

This additional outer membrane leads to a more impermeable cell wall and, in general Gram-negative bacteria are more resistant to antibiotics.

Due to this bacterial resistance, there is an urgency to develop new alternatives to antibiotics to improve antibacterial performance and reduce biofilm formation.[3] This chapter discusses extremely early research, which focuses on looking at the antibacterial behaviour of inverse vulcanised sulfur polymers surfaces. With more in-depth analysis and understanding of these materials' antimicrobial behaviour, they could find potential use in medical implant applications and commonly touched surfaces (door panels, light switches, traffic light buttons, etc.).

4.2.2 Biofilm formation

Biofilms can form on a range of surfaces such as living tissues, implanted medical devices, water system piping, and natural aquatic systems.[5] In biofilms, bacteria have exceptional resistance to environmental stresses, including antibiotics. Essentially a

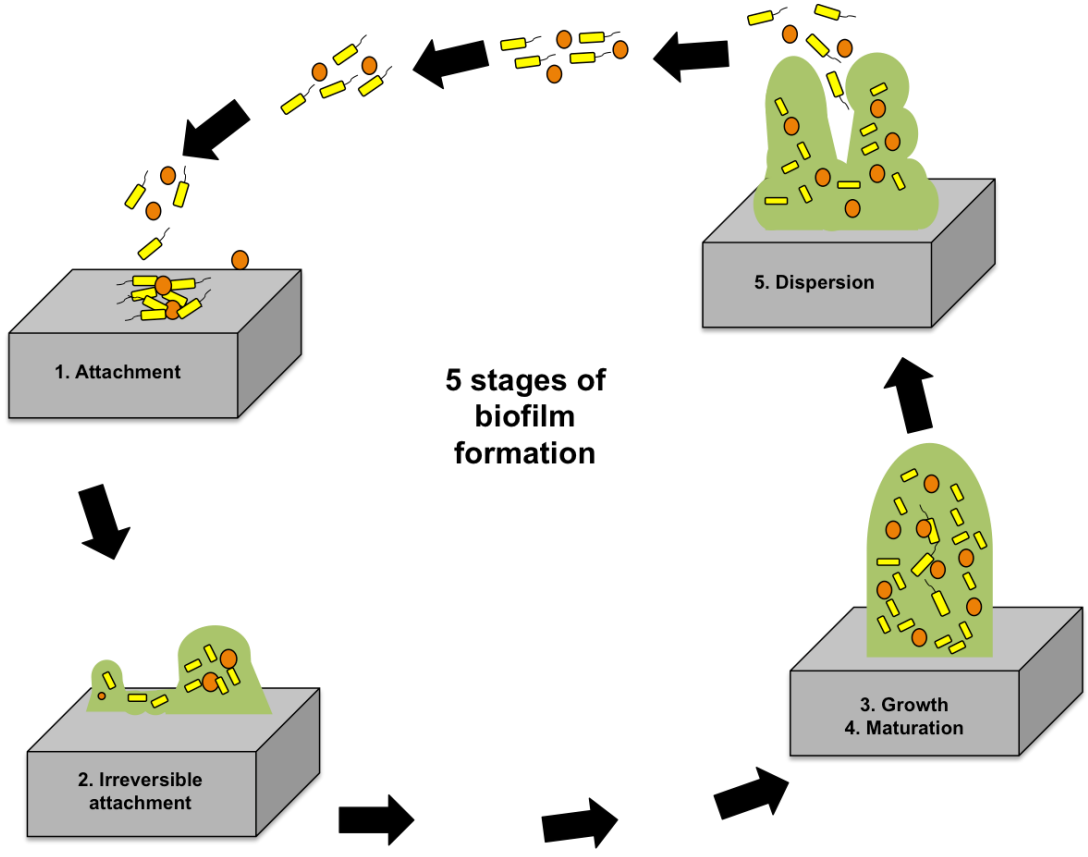

Figure 4.2 The five stages of biofilm formation: (1) Reversible attachment of planktonic bacterial cells. (2) Irreversible attachment and cell-cell adhesion occurs to the surface when ECM is secreted. (3) Proliferation occurs. (4) The biofilm then matures. (5) Cells are detached and disperse from the biofilm and the process is then repeated. Scheme adapted from Andrew Threfall [ref 9].

biofilm is an assembly of microbial cells that are irreversibly associated to a surface by secreting an extracellular matrix of polymers and polysaccharides (ECM) (Figure 4.2 (2)).[6,7] The ECM is then able to encase the cells and induce microcolony formation to form a biofilm, which can then able to grow and mature (Figure 4.2(3,4)).[7,8,9] Following this, detachment of bacteria occurs (Figure 4.2 (5)). The bacteria that are released may then colonise new areas and form another biofilm.[8]

Unlike planktonic cells, the cells within a biofilm are far less susceptible to antimicrobial agents.[8] The development of antimicrobial resistance is still not fully understood. However, recent research has proposed a variety of mechanisms to understand how and why biofilms are resistant to antimicrobial agents.

One mechanism suggested, is the failure of antimicrobials to penetrate the biofilm.[8] As discussed, one distinguishing characteristic of biofilms is the production of an exopolysaccharide matrix (ECM). One potential mechanism of resistance is that the ECM prevents the access of antibiotics and other antimicrobial substances across the biofilm membrane.[8] However, this is not always the case; alongside mathematical models, some studies have shown many antibiotics can penetrate the ECM.[8] Suci *et al.* used infrared spectroscopy to measure the rate of transport of the antibiotic ciprofloxacin to the surface of a colonised biofilm.[10] The rate of transportation of the antibiotic was reduced in comparison to the rate of diffusion to a sterile surface, and the study suggested that the ciprofloxacin was binding to the biofilm components.[10] Other research has shown that *Staphylococcus epidermidis* biofilms formed on the side of dialysis membranes and allowed diffusion of two different types of antibiotics across the biofilm membrane, rifampicin, and vancomycin.[11] These studies suggest successful and efficient penetration of this biofilm by antibiotics.[10,11] The results indicate that inhibition of diffusion of antimicrobial agents due to the production of ECM in biofilms cannot be the only mechanism of resistance.

Another suggested mechanism for the antibiotic resistance of biofilms is the presence of 'persister' cells.[8] When cells attach to a surface, they will express a general biofilm phenotype. 'Persister' cells are randomly formed phenotypic variants within the microbial population.[8] The resistant phenotype could be induced by nutrient limitation, stress, or high cell density.[8] In combination with the failure of some antimicrobials able to penetrate the biofilm, the presence of persister cells is another factor to consider.

Other mechanisms to consider, include the presence of multi-drug efflux pumps in biofilms that can extrude foreign components and toxins, like antibiotics.[8] This can result in the induction of multi-drug resistant phenotypes. One study has suggested the importance of one of these pumps in the resistance to the antibiotic, ofloxacin.[12] In addition to this, another resistance mechanism that can be induced in biofilms is the alteration of membrane-protein compositions in response to antimicrobial agents.[8] Horizontal gene transfer between conjugated cells may lead to resistant traits in biofilm populations.[8]

There is not one conclusive mechanism responsible for how bacteria growing in a biofilm develop increased resistance to antimicrobial agents. However, there is an urgent need to combat biofilm formation with cells existing in a biofilm becoming 10-1000 times more resistant to the effects of antimicrobial agents.[8] Over 65% of nosocomial infections are associated with biofilm formation.[8] Therefore, there is a pressing need to develop antimicrobial surfaces that have anti-adhesion properties that will inhibit biofilm formation.

4.2.2 Antibacterial surface design

The requirements for an antibacterial biomaterial are comprehensive and are dependent on the biomaterial application. However, through years of research, there

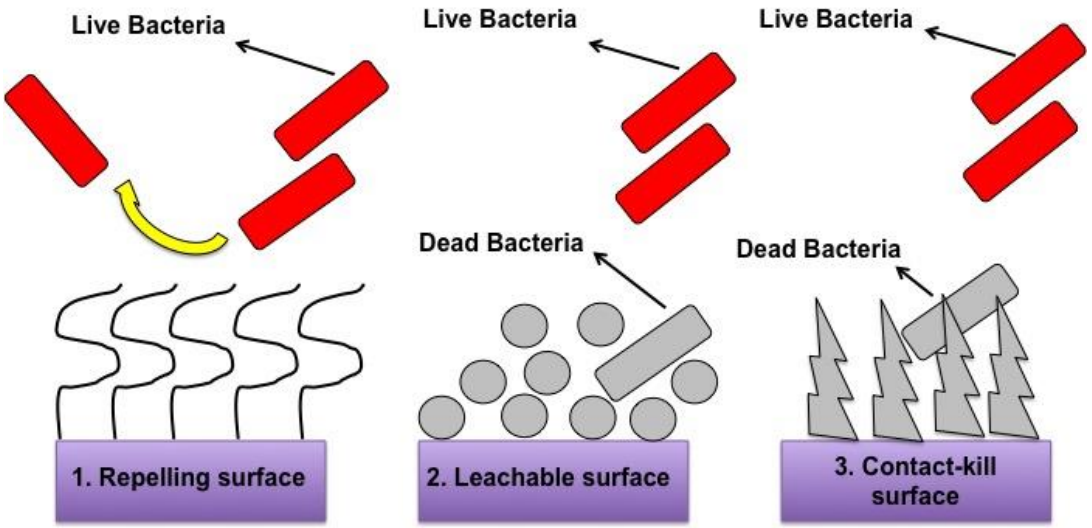

Figure 4.3 Three different classifications of an antibacterial surface (1) Antiadhesive/bacteria repelling surfaces. (2) Surfaces that incorporates leaching agents. (3) Surfaces that kill bacteria through contact. Figure is adapted from ref 13.

are three main strategies to consider when designing an antibacterial surface (Figure 4.3).

The first strategy involves the antiadhesive/bacteria-repelling surfaces (Figure 4.3).[13,14] Colonisation cannot occur if bacteria cannot adhere to a solid surface. Bacterial adhesion onto biomaterials can occur through multiple mechanisms, some are transversal to all microbial species, and others are species-specific.[14] One way to induce antiadhesive effect is by fabricating superhydrophobic surfaces; this prevents aqueous suspensions of bacteria coming into contact with the surface, as the liquid is unable to wet it, therefore less opportunity for cell-surface contact.[14] However, there are many variables to consider when controlling bacterial adhesion such as surface morphology, physico-chemical properties, environmental conditions and the type of pathogen that is being considered.[15]

The second strategy is to incorporate substrates with leaching agents such as silver and triclosan; these encapsulated biocides can leach and kill bacteria (Figure 4.3).[14] However, one known issue with this strategy is that leached biocides can accumulate in the environment making this strategy unsustainable.[14] On a smaller scale in a clinical environment, this could potentially have adverse health effects on the human body.

The final approach is to design surfaces that kill bacteria through contact. Contact-active surfaces can be developed by fixing biocides onto them through a covalent bond, which is a more sustainable alternative than using a leaching agent.[14] In this strategy, biocides are irreversibly attached to the substrate for contact kill.

4.2.2 Polysulfides as antibacterial agents

For many centuries, compounds containing sulfur have been considered natural remedies against bacterial, viral, and fungal infections. As research progresses, there is more focus on converting organosulfur compounds to inorganic polysulfides to provide an antibacterial alternative to combat infections.[16] Furthermore, polysulfides are being investigated for their antibiotic activities, cytotoxicity and potential selectivity against cancer cells.[17]

The mechanism for the antimicrobial activity of sulfur and polysulfides is unclear and research is sparse, although there are several hypothesised mechanisms in literature.[17] One proposed mechanism is thiol-polysulfide exchange reactions. In this mechanism, a polysulfide (RS_xR) can react with intercellular thiols (e.g., cysteine, R'SH) and form a mixed disulfide (RSSR') and a persulfide (RSSH) or polysulfanes/hydropolysulfides (RS_xH, $x \geq 2$).[17] In comparison to RSH, certain RSSH are strong reducing agents, which

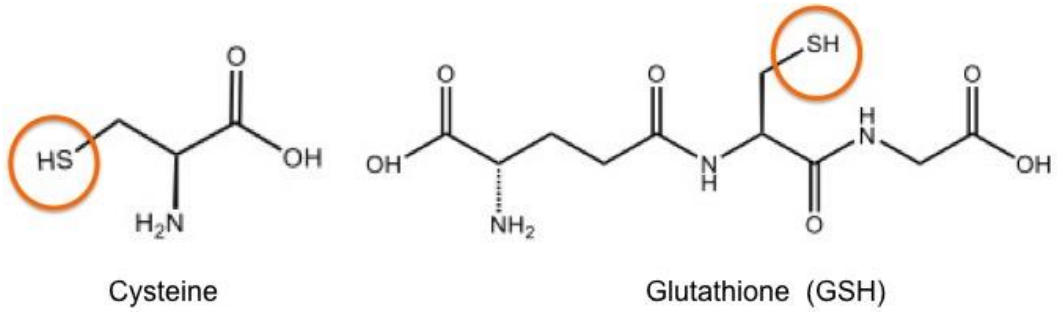

Figure 4.4 Both cysteine and gluthathione (GSH) provide a considerable source of thiols in bacteria. In particular GSH which plays a critical role in protecting cells from oxidative stress.

can react with oxidants (e.g., oxyhaemoglobin and dioxygen) to form reactive oxidative species (ROS) e.g., hydrogen peroxide.[17] The consumption of thiols and the generation of ROS can both severely damage cells by creating oxidative stress. Alongside cysteine, glutathione (GSH) (Figure 4.4) is a considerable source of thiols in bacteria. It plays a critical role in protecting cells from oxidative damage by ROS.[17] Therefore consumption of GSH by polysulfide-thiolation reactions and attack by ROS can kill bacteria.

An alternative suggested mechanism for the antimicrobial activity of polysulfides is homolytic S-S bond cleavage.[17,18,19] The bond dissociation energy for an alkyltetrasulfide (146 kJ mol^{-1}) in comparison to both trisulfide (184 kJ mol^{-1}) and disulfides (293 kJ mol^{-1}) is much lower.[17] Therefore, the longer the polysulfide chain (RS_xR), the more susceptible the central S-S bond is to nucleophilic attack. Alongside this, S-S bonds are known for their dynamic nature and reversibility. This implies that polysulfides may undergo homolytic cleavage resulting in perthiyl radicals ($RS_x^{\cdot}$, where $x \geq 2$), which can also be formed by one-electron oxidation of perthiols (RSSH).[17] As discussed in the thiolation reactions, it is the perthiols (RSSH) that can react with oxygen to form ROS that can cause oxidative stress and damage membranes, peptides ,and proteins.[17] Therefore homolytic cleavage is another potential mechanism in which polysulfides may act as an antimicrobial. Biochemical studies on

polysulfides reveal that both perthiols (RSSH) and polysulfanes (RS_xH, $x \geq 2$) are the active forms of polysulfides *in vivo.*[17]

4.2.3 Inverse vulcanised sulfur polymers as antibacterial agents

One potential application of inverse vulcanised sulfur polymers that have received very little attention is the antibacterial properties these materials may possess. While this work was on-going the only report to date other than the research discussed in this chapter is by Lienkamp *et al.*[20]

Lienkamp *et al.* studied the antibacterial properties of poly(sulfur-co-diisopropenylbenzene) (S-DIB).[20] Their findings show that the polymer covered surfaces kill up to 72% of *E.coli* for a material that contains 50 wt. % sulfur. [20]Although promising, the Lienkamp study focuses on thin polymer film coatings and only one bacterial species, applied by spraying, with the antibacterial activity assessed over a short time period (between 5 minutes and 4 hours).[20] Their findings conclude that S-DIB is not ideal for antibacterial activity.

With both *E.coli* and *S.aureus* being a severe cause of a variety of nosocomial infections,[21] the goal of this work is to expose both *E.coli* and *S.aureus* to two different types of high sulfur content polymer surfaces. By testing both gram-positive and gram-negative species on robust, homogeneous, bulk solids opposed to thin coatings. Herein, we show the anti-adhesive ability of two high sulfur content polymers (S-DIB and S-DCPD) against two species of bacteria, showing their potential for the prevention of surface biofilm formation.

4.3 Chapter aims

1. To investigate the antibacterial properties of two structurally different inverse vulcanised sulfur polymers surfaces, S-DCPD and S-DIB.
2. To expose two common hospital bacteria, *E. coli* and *S. aureus,* to the inverse vulcanised polymer surfaces.
3. Hypothesise ways in which the antibacterial killing mechanisms may be occurring for future researchers to build on.

4.4 Results and Discussion

In this study, "S-crosslinker" will be used henceforth to refer to a copolymer of sulfur and the stated crosslinker (or crosslinkers).

4.4.1 Preparation of S-DCPD and S-DIB surfaces for antibacterial testing

Inverse vulcanised S-DCPD and S-DIB polymers were successfully prepared at a ratio of 50 wt. % sulfur content, similarly to previously published inverse vulcanisation reactions (see experimental details, 4.6.3).[22,23] S-DIB and S-DCPD were chosen as polymer surfaces. At the time of this research these were two published polymers that exhibited completely different properties: As discussed in previous chapters, S-DIB is thought to be a hyperbranched polymer that is soluble to some degree.[22,23] Whereas, S-DCPD is an insoluble fully crosslinked polymer network.[24] Both polymers have very

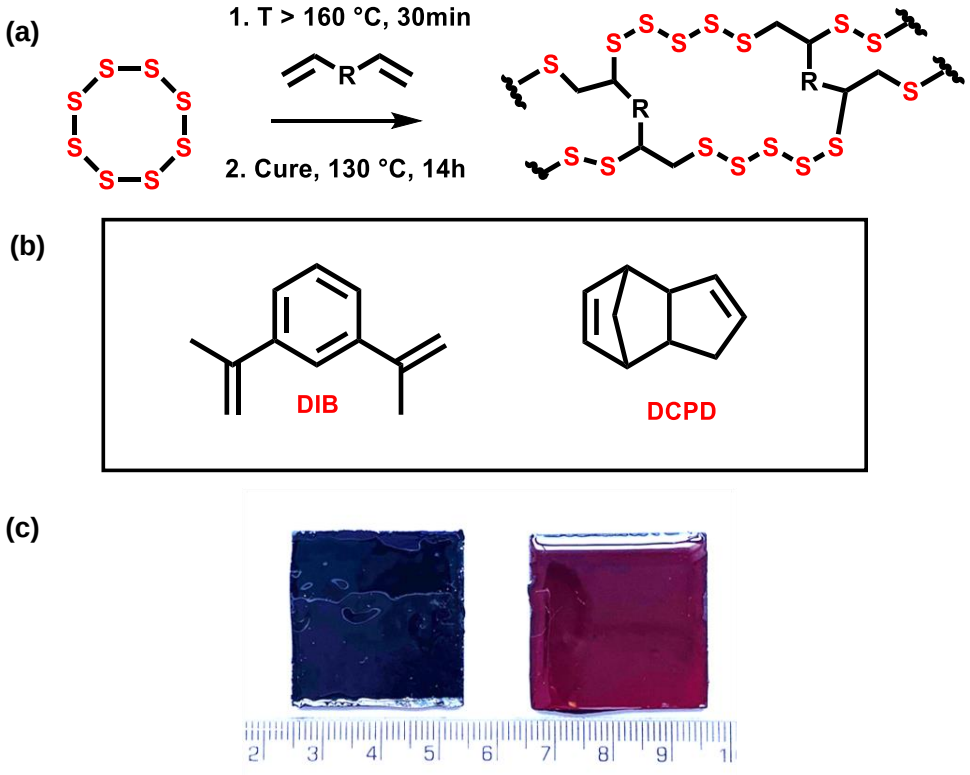

Figure 4.5 (a) Inverse vulcanisation of elemental sulfur and crosslinker. (b) Crosslinkers used to prepare polymers. Left:1,3-diisopropenyl benzene (DIB). Right: Dicyclopentadiene (DCPD) (c) Photograph showing the appearance of the polymer samples in bulk form. Left: Sulfur-DCPD copolymer (S-DCPD) Right: Sulfur-DIB copolymer (S-DIB), both prepared to dimensions 30 mm x 30 mm x 30 mm.

different glass transition temperatures (T_g) at similar S: crosslinker. At a 50:50, sulfur: crosslinker ratio S-DIB has a T_g of ~30 °C, and S-DCPD has a T_g of ~110°, highlighting the difference in physical properties. Briefly, elemental sulfur was heated

at 160 °C until molten to become a pale orange liquid. Subsequently, the crosslinker (DIB/DCPD) was directly added into molten sulfur and further heated for 20-30 minutes until a homogenous mixture was formed. The mixture was then poured into a mould with dimensions 30 mm x 30 mm x 3 mm and cured for 14 hours at 130 °C, to form a solid square suitable for further testing (Figure 4.5).

4.4.2 Fluorescent imaging to assess antibacterial effects of surfaces

To determine if the resultant polymer surfaces possessed any antibacterial effects, fluorescent microscopy using LIVE/DEAD ® BacLight™ was used to examine the response of *E.coli* to the exposure of both polymer surfaces, S-DCPD and S-DIB and polycarbonate (PC) control surfaces (Figures 4.6-4.8). *E. coli* was incubated

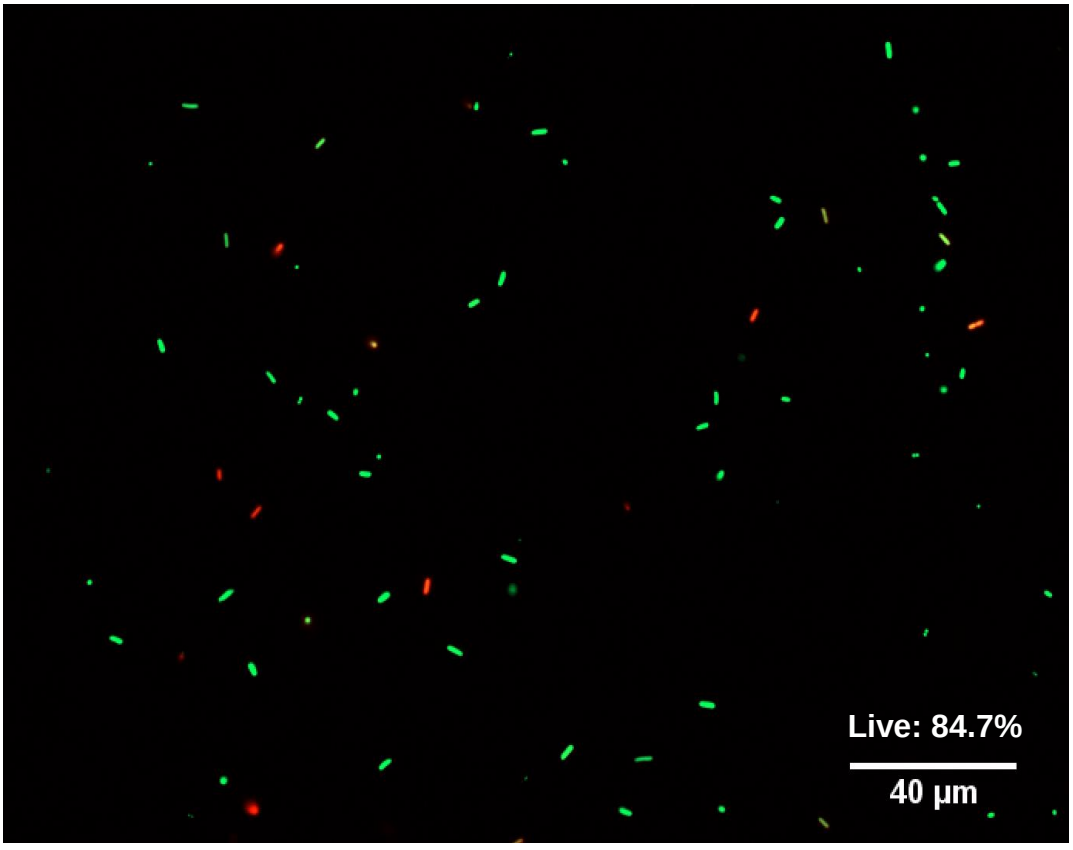

Figure 4.6 Fluorescent micrograph showing attachment of *E. coli (DSM 1576)* to polycarbonate after 24 h incubation. Cells were stained with Syto9 (green) and propidium iodide (red), detecting live and dead cells, respectively. Observation was achieved using a 100x objective lens.

independently on the three surfaces by immersing each surface in 1:500 diluted nutrient broth (see experimental details, 4.6.4). The cell density reached ~ 1 x 10^8 cells/mL after incubation for 24 hours and was confirmed by measuring optical density at 600 nm (OD_{600}). The cells were visualized on the various surfaces via fluorescent

microscopy. Micrographs (Figures 4.6- 4.8 and Appendix Figure A4.1-A4.9) indicate that S-DIB surfaces significantly reduced the percentage of live cells (green) (29.9 % ± 12.9 % survival) compared to both the control sample (84.7% ± 4.1%) and S-DCPD (49.6 % ± 9.0 % survival). Furthermore, there was no statistical difference observed for total cell numbers on the surface of the control and co-polymer surfaces after 24 h (Figure 4.9). This could potentially indicate that surfaces are killing bacterial cells with a contact-kill approach.

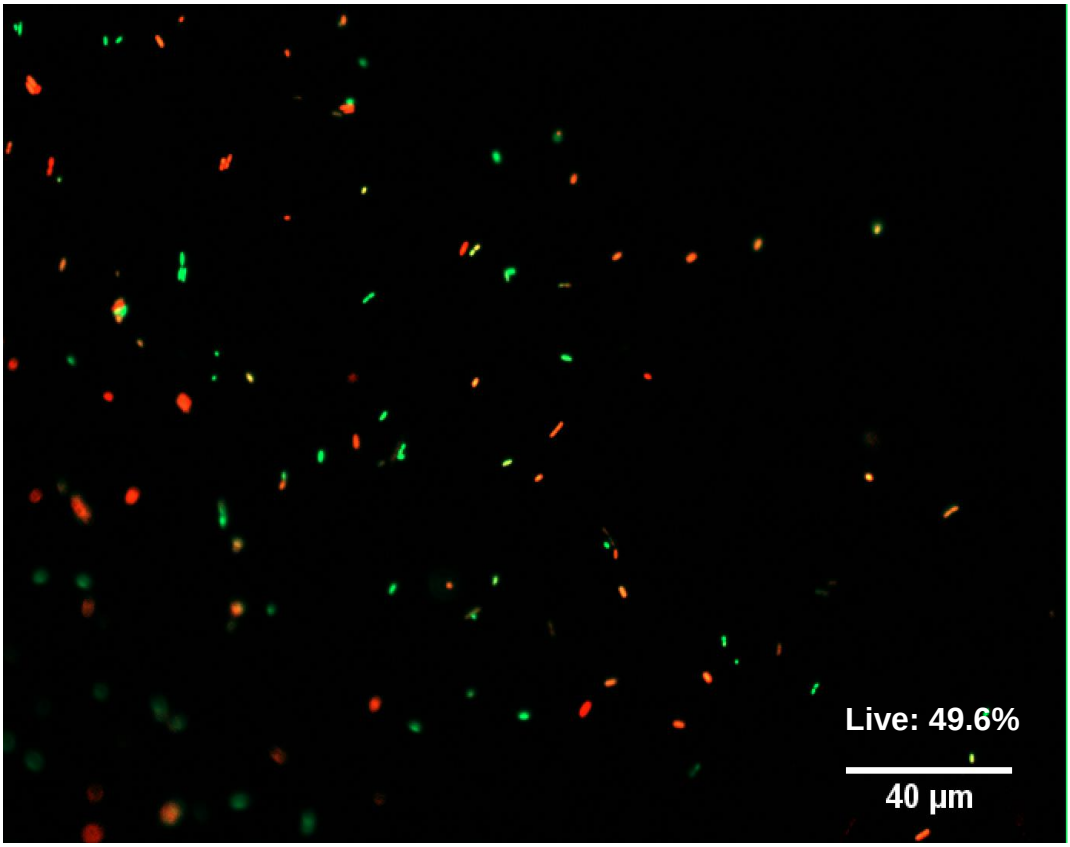

Figure 4.7 Fluorescent micrograph showing attachment of *E. coli (DSM 1576)* to S-DCPD after 24 h incubation. Cells were stained with Syto9 (green) and propidium iodide (red), detecting live and dead cells, respectively. Observation was achieved using a 100x objective lens.

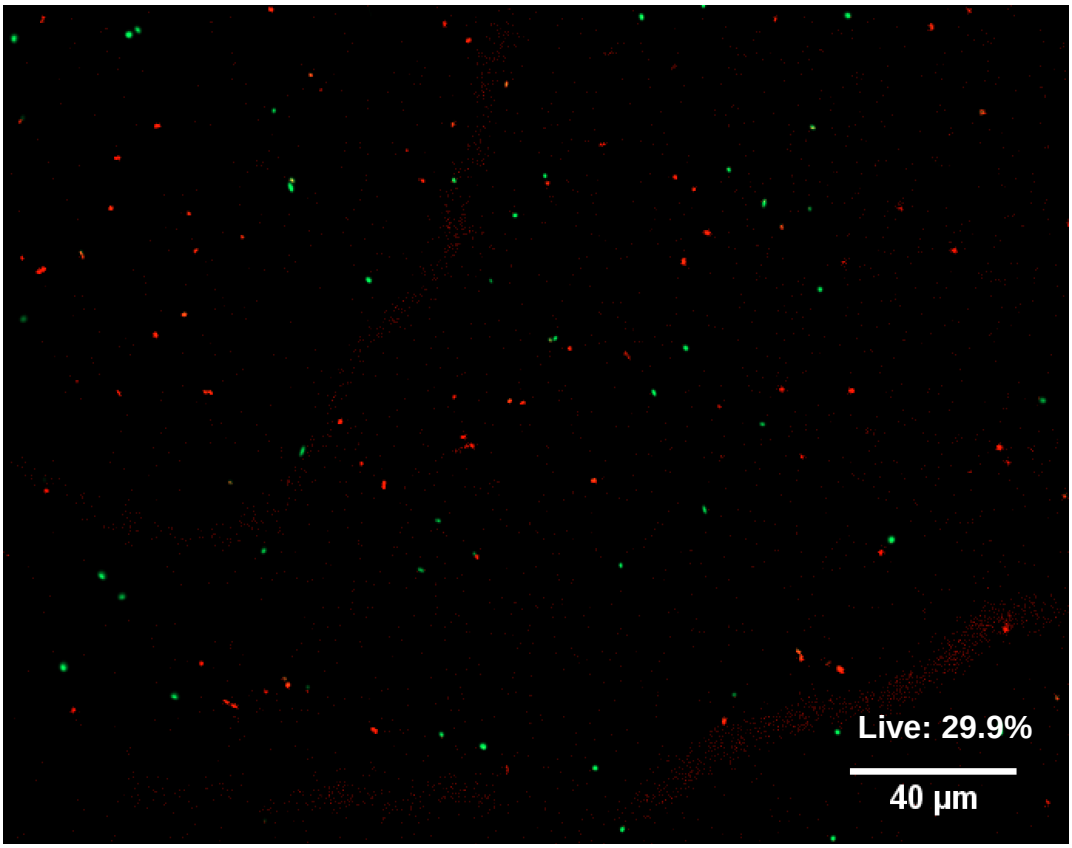

Figure 4.8 Fluorescent micrograph showing attachment of *E. coli (DSM 1576)* to S-DIB after 24 h incubation. Cells were stained with Syto9 (green) and propidium iodide (red), detecting live and dead cells, respectively. Observation was achieved using a 100x objective lens.

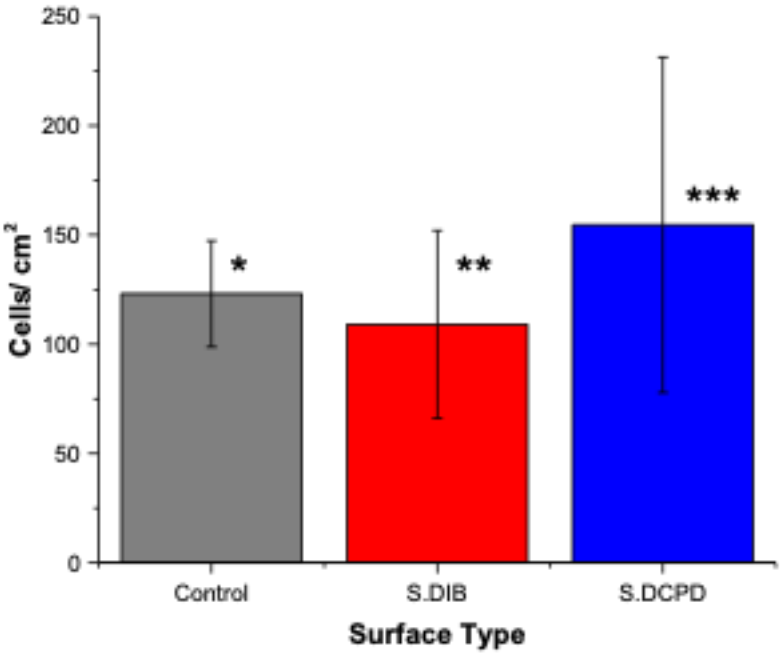

Figure 4.9 The total bacterial coverage (Live and dead cells) of *E. coli* on sulfur copolymer surfaces after 24 h, in comparison to the control, as measured by fluorescence microscopy using Baclight Live/Dead (ThermoFisher Scientific, UK) straining. Statistical analysis was carried out on the normalised data. * (p-value <0.05), ** (p-value <0.01), *** (p-value <0.001). Error bar is representative of standard deviation.

NB p is the probability and a measure of how significantly different the result is. If $p < 0.05$ is statistically significant and the null hypothesis can be rejected (i.e. there is no significant difference).

4.4.3 Scanning electron microscopy (SEM) to detect biofilm formation

Scanning electron microscopy (SEM) micrographs were recorded for both *S.aureus* and *E.coli* inoculated on the surface of polycarbonate (PC) (Appendix, Figures A4.10 and A4.11), S-DCPD and S-DIB (Figures 4.10-4.13). Results confirmed that there was no exponential growth of the *E. coli*, and no biofilm formation was observed for both S-DCPD and S-DIB surfaces. However, it should be noted that there were some cells visible when the PC surface was exposed to *S.aureus* compared to the sulfur polymer surfaces (Appendix, Figure A4.11).As discussed in the introduction to this chapter, there is an urgency to develop antimicrobial surfaces that have anti-adhesion properties, and that will inhibit biofilm formation. This is due to cells existing in a biofilm exhibiting resistance, becoming 10-1000 time more resistant to the effect of antimicrobial agents.[8] No biofilms were observed on these surfaces after a 24 h

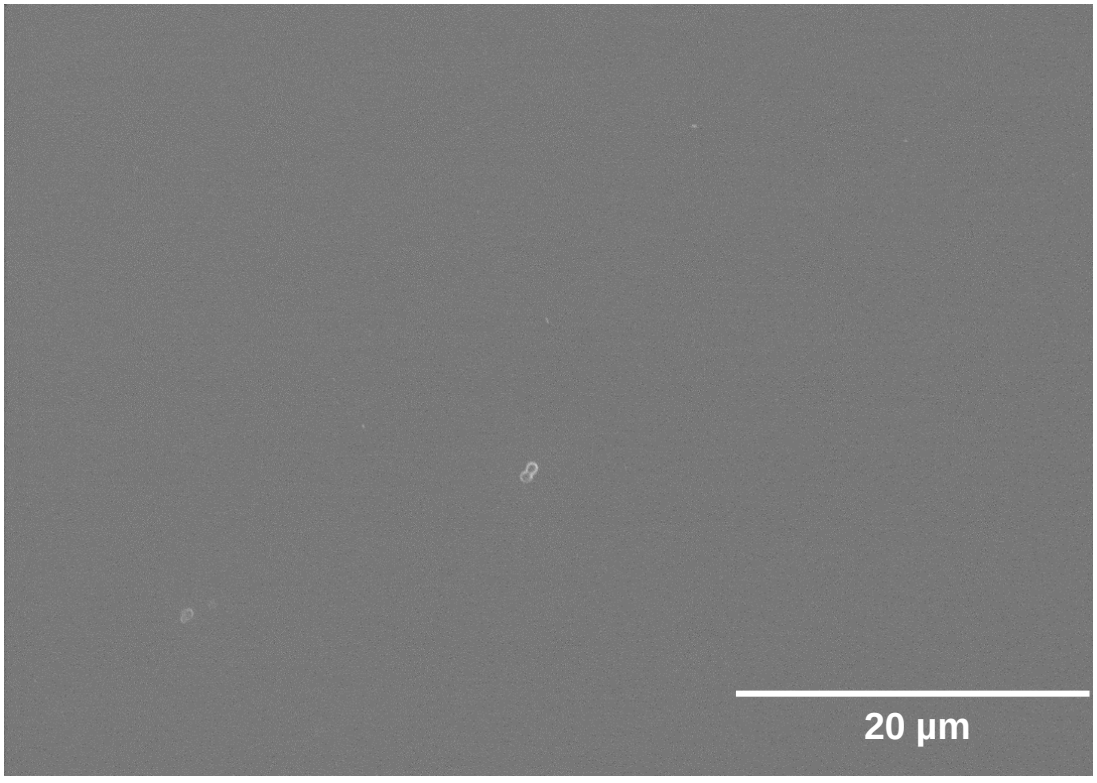

Figure 4.10 SEM micrograph showing S-DCPD surface after 24 h incubation with *S. aureus* inoculated onto the surface. Scale bar is 20 µm.

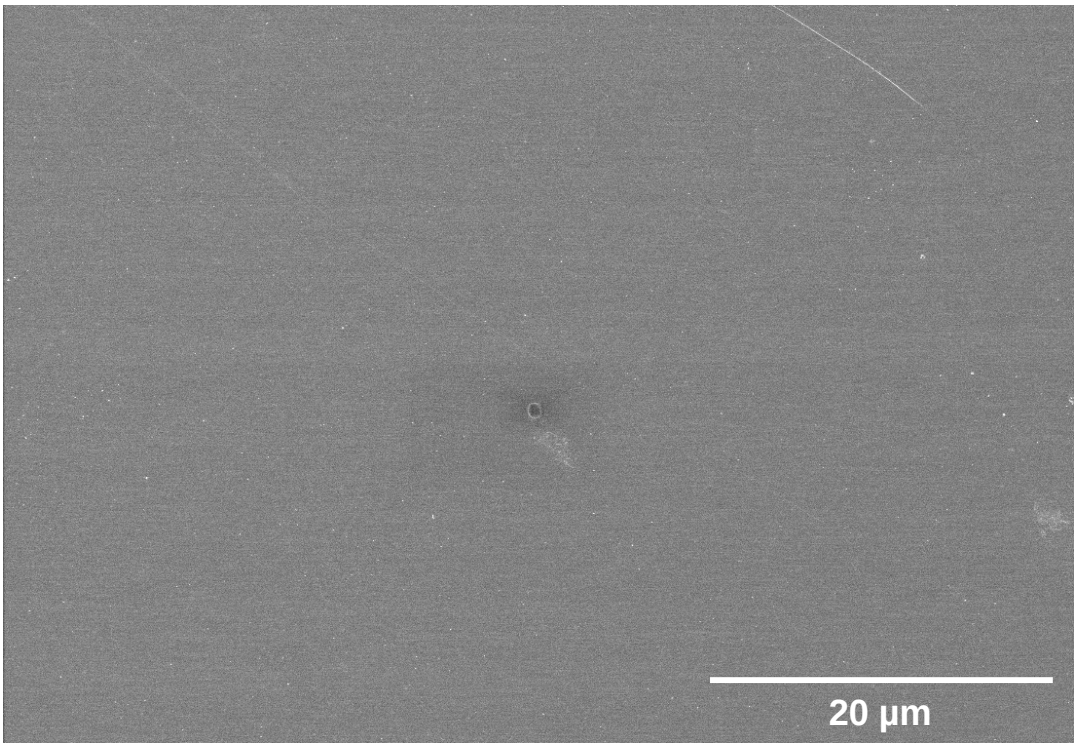

Figure 4.11 SEM micrograph showing S-DCPD surface after 24 h incubation with *E. coli* inoculated

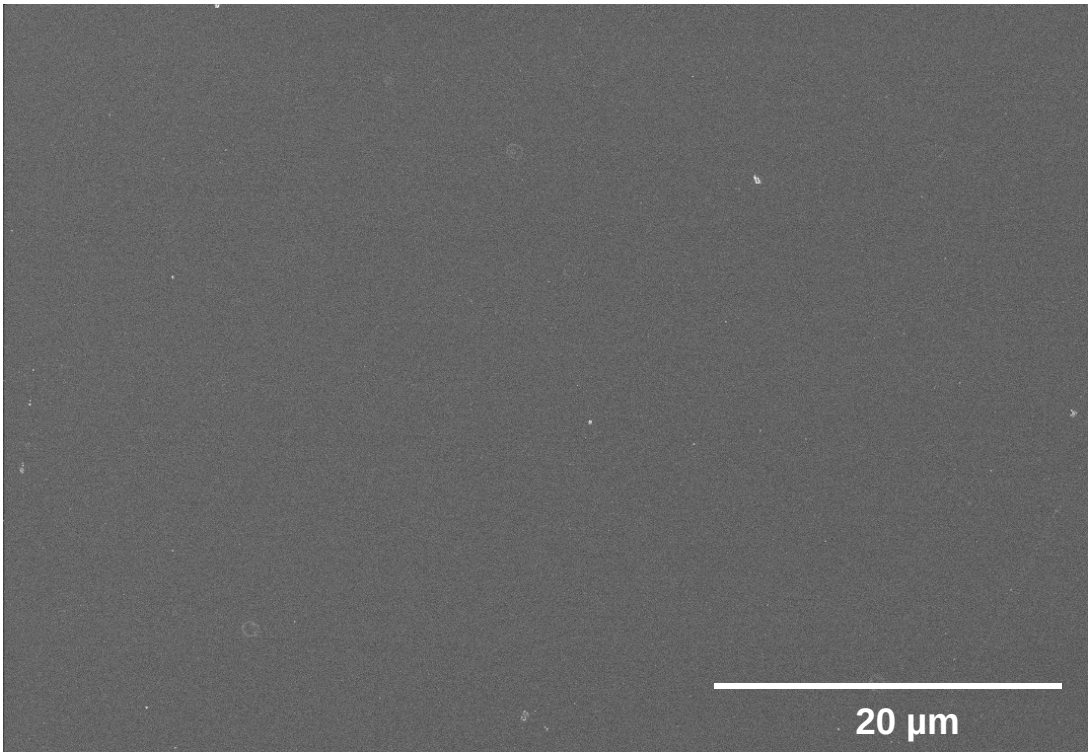

Figure 4.12 SEM micrograph showing S-DIB surface after 24 h incubation with *S. aureus* inoculated onto the surface. Scale bar is 20 µm.

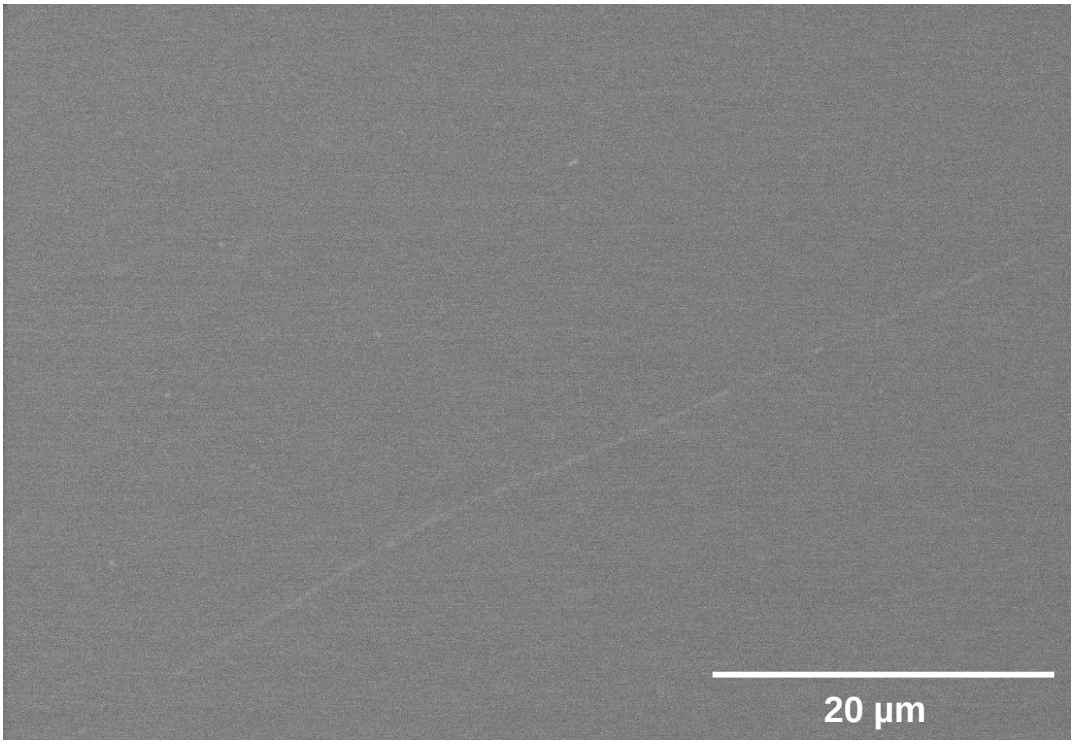

Figure 4.13 SEM micrograph showing S-DIB surface after 24 h incubation with *E. coli* inoculated onto the surface. Scale bar is 20 µm.

4.4.4 Quantifying bacterial survival

From the micrographs, it was clear that after 24 h, there was no biofilm formation. Both S-DIB and S-DCPD exhibited some antibacterial properties when *E. coli* was inoculated onto the surface. Gram -ve (*E. coli* ATCC8739) and Gram +ve (*S. aureus* DSM347) bacterial strains were exposed to both polymer surfaces and the number of viable cells recoverable from the surfaces were measured. To accurately quantify bacterial survival, a standardised methodology (see experimental details, 4.6.7 and 4.6.8) for testing the antibacterial properties of surfaces was adopted. The cells were held in a petri dish and seeded with 100 µL of bacterial cell solution (~3 x 10^6 cells/mL) in 1:100(*S. aureus*) or 1:500 (*E. coli*) nutrient broth and covered with a polyethylene film. The inoculated surfaces were encased in a humidity chamber to limit surface evaporation and incubated at 37 °C for 24 h. To recover the bacteria, the surfaces were washed with 10 mL soybean casein digest broth with lecithin and polyoxyethylene sorbitan monooleate (SCDLP).

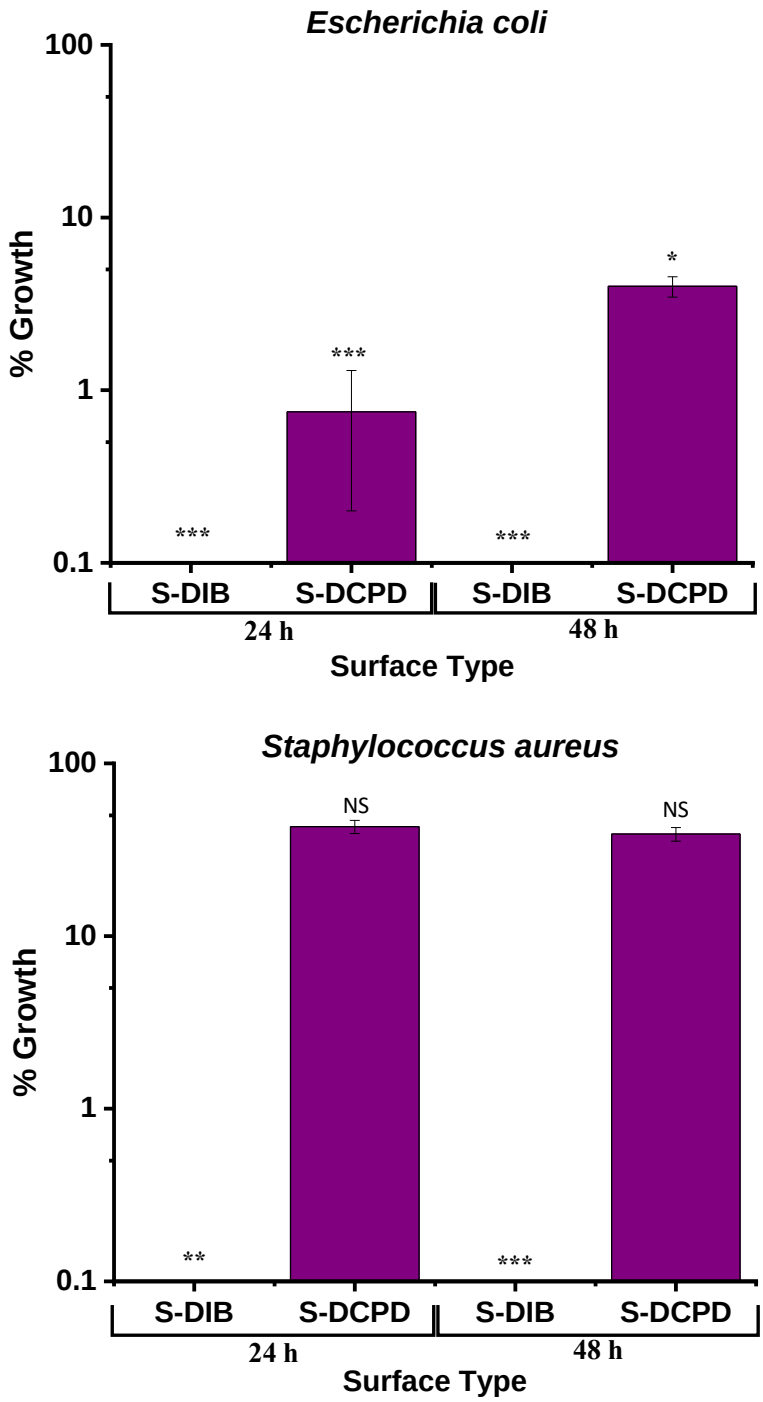

Figure 4.14 The antibacterial surface effect after 24 h and 48 h, in comparison to the control, as measured by the growth of surface adhered bacteria removed from the surface of the substrate using a neutralising solution (SCDLP). Data have been normalized. Statistical analysis was carried on the log transformed data. * (p-value <0.05), ** (p-value <0.01), *** (p-value <0.001), NS (not significant). Error bars represent standard deviation.

NB p is the probability and a measure of how significantly different the result is. If $p < 0.05$ is statistically significant and the null hypothesis can be rejected (i.e. there is no significant difference).

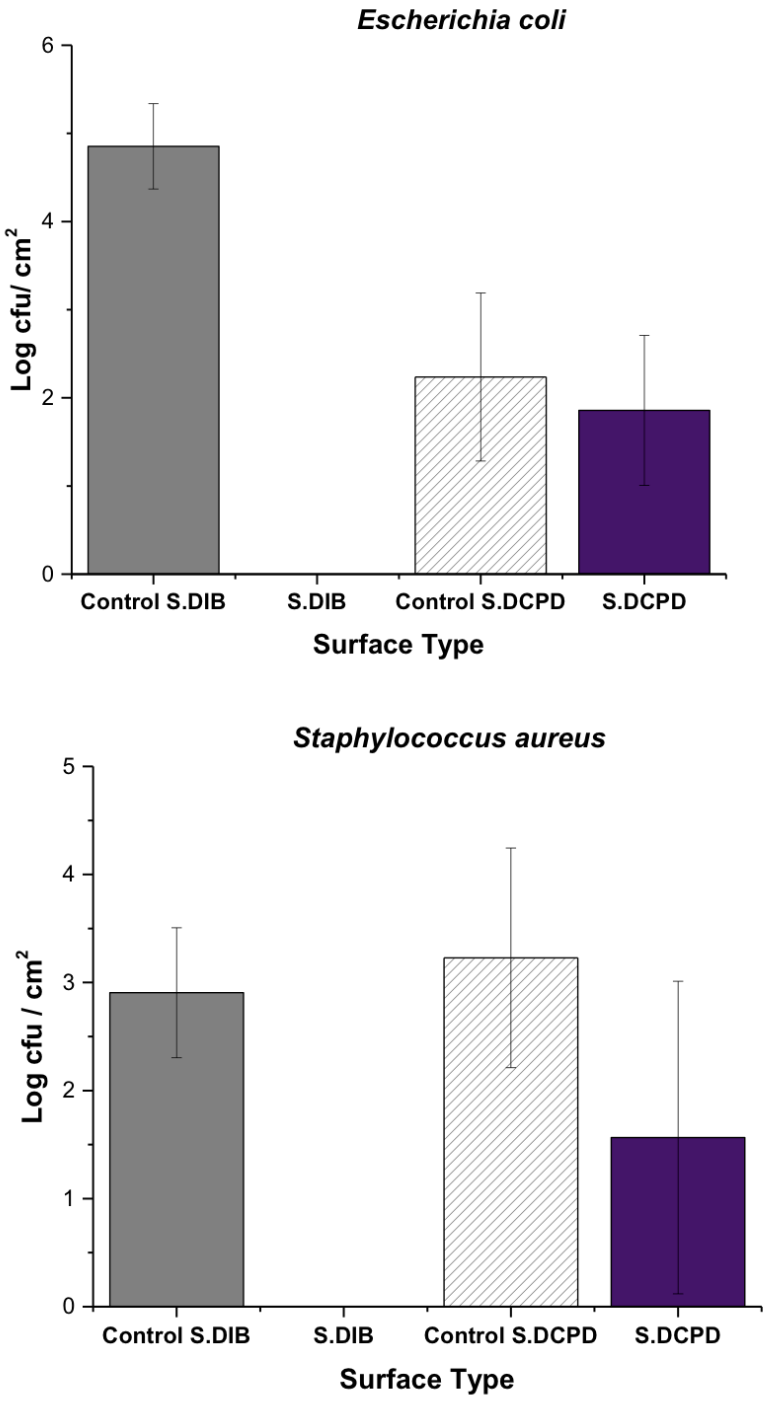

Figure 4.15 The antimicrobial surface effect after 24 h, in comparison to the control, as measured by the log growth of surface adhered bacteria removed from the surface of the substrate using a neutralising solution (SCDLP). Statistical analysis was carried on the log-transformed data. * (p-value <0.05), ** (p-value <0.01), *** (p-value <0.001).

NB P is the probability of a null hypothesis, if $p > 0.05$ the probability of the null hypothesis is true. When $p \leq 0.05$ the null hypothesis can be rejected and there is no significant difference.

From Figure 4.14 and 4.15, it is clear that S-DIB significantly reduces both *E.coli* and

S.aureus cell numbers (cfu= colony forming units), in comparison to previous investigations, which report 72% reduction for *E.coli* microorganisms on S-DIB (50 wt. % sulfur).[20] Both S-DIB and S-DCPD have less viable cells on the surface when exposed to *E.coli* microorganisms in comparison to *S. aureus,* where only S-DIB shows a reduction in viable cells on the surface. As discussed, SEM microscopy confirms that after exposure to the bacteria in equivalent conditions, there is no significant biofilm formation, which agrees with findings from confocal microscopy.

4.4.5 Assessment of sulfur leaching

As discussed in 4.2.2, there are three main ways a surface may have an antibacterial effect; antiadhesive/repelling surface, biocide leaching, and contact-kill.[14] To further

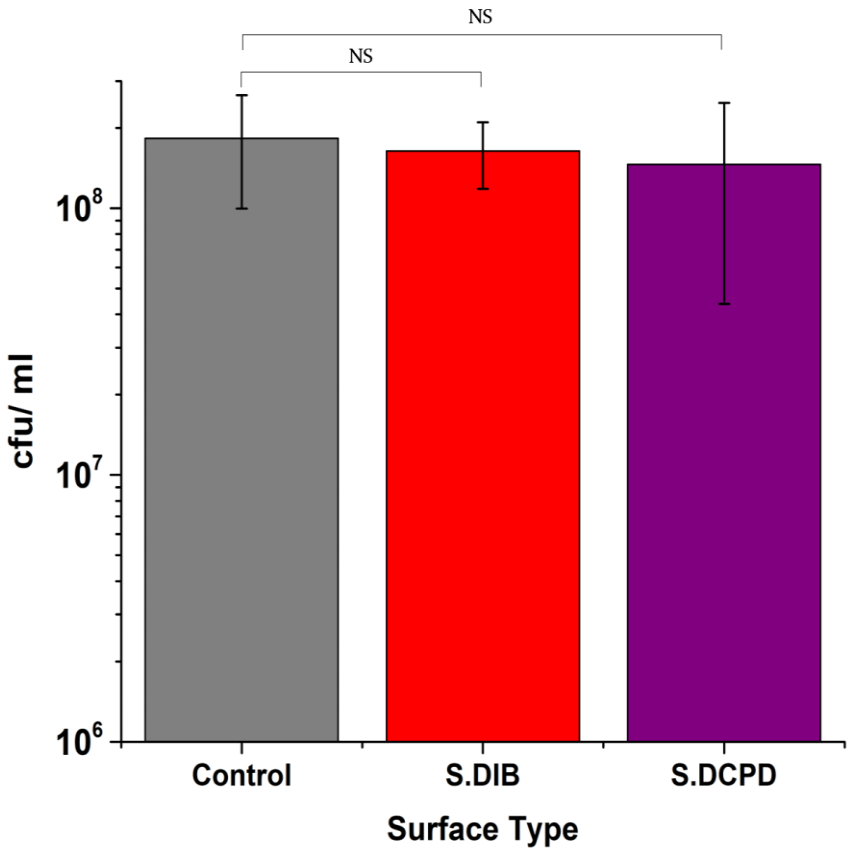

Figure 4.16 Assessment of antibacterial effects from substrate leaching, based on bulk substrate submersion in a broth culture. Cellular growth quantified by colony-forming units (cfu)/mL of broth culture after 24 h. Data has been normalised. ***NB*** *Error bars represent standard deviations from three independent replicates.* NS (not significant p- value ≥ 0.05).

understand how the polymer surfaces may be having an antibacterial effect on the

attached cells; the effect of sulfur leaching was assessed. Both bacterial strains were cultured in nutrient broth (NB)) into which one of the three surface substrates was placed, and these cultures were incubated at 37 °C.

From Figure 4.16, no significant difference in recovered c.f.u. was observed between the presence of the control ($1.8 \times 10^8 \pm 8.2 \times 10^7$, S-DIB ($1.6 \times 10^8 \pm 4.6 \times 10^7$) or S-DCPD ($1.4 \times 10^8 \pm 1.1 \times 10^8$) substrates for *E.coli* cells in the planktonic phase. The difference in cell viability between the samples is smaller than the standard deviations; this indicates that the release of any active sulfur-containing material into the liquid phase was negligible and did not affect cell viability. This is supported by the live/dead staining, as a significant surface effect is observed for *E. coli* for both copolymers. The p value is not significant (Figure 4.16), suggesting there was no significant sulfur leaching, and the bactericidal effect was at surface level.

Parallel to this, both differential scanning calorimetry (DSC) (Figure 4.17 and 4.18) and powder X-ray diffraction (PXRD) (Figure 4.19 and 4.20) were employed to

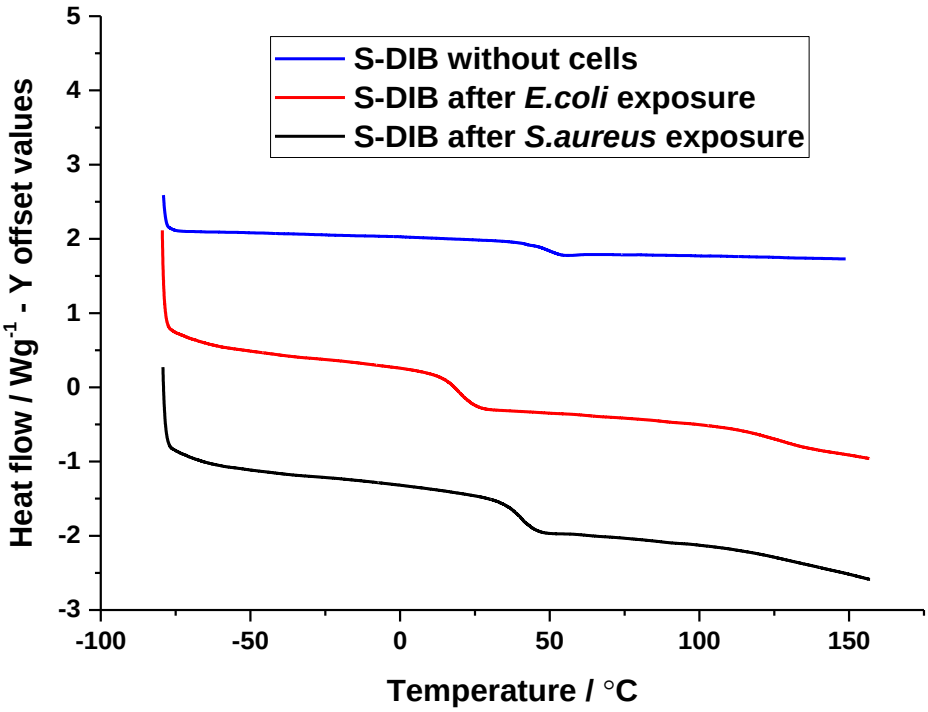

Figure 4.17 Representative DSC traces. Shown is 50 wt. % S_8, 50 wt. % DIB copolymer that has not been exposed to bacteria (blue), S-DIB after *E.coli* exposure (red) and S-DIB after *S. aureus* exposure.

confirm that when both polymer surfaces are exposed to *E. coli* and *S. aureus,* no crystalline sulfur is formed and both polymers retain an amorphous character. If the polymers were depolymerizing back to elemental sulfur (S_8), this would form crystals detectible by DSC and PXRD. Therefore, this suggests the antibacterial effect comes

from the action of the polymer itself rather than the release of S_8. However, Figure 4.15, should note that for the S-DCPD sample exposed to *E. coli,* there appears to be a second glass transition (T_g) but no sulfur melting transitions (T_m) at 110 °C and 120 °C. Therefore, this suggests that after bacteria exposure, the polymer still retains amorphous character.

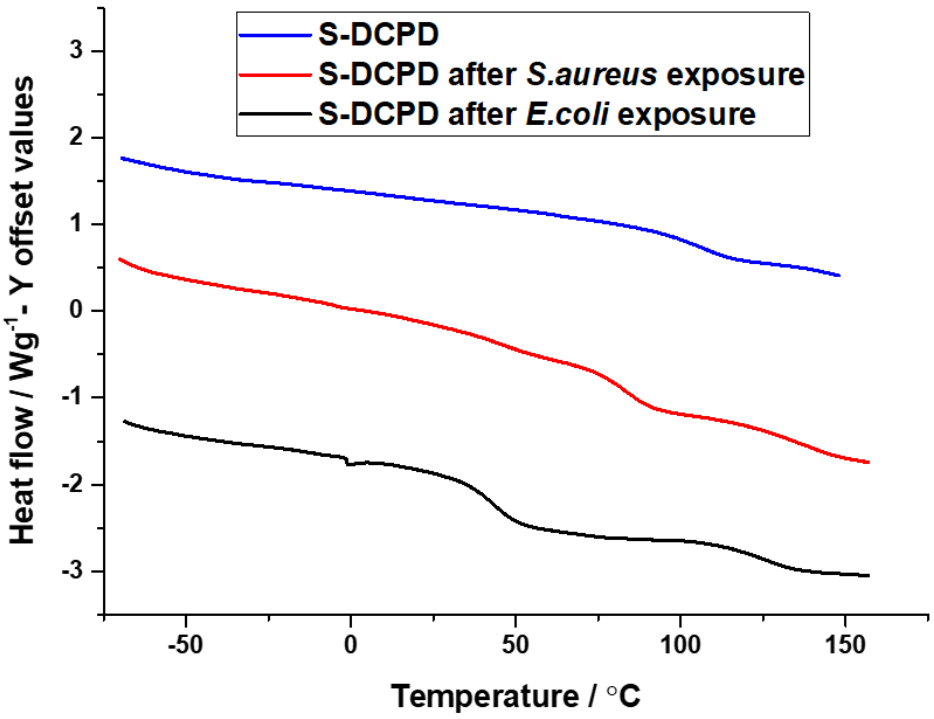

Figure 4.18 Representative DSC traces. Shown is 50 wt. % S_8, 50 wt. % DCPD copolymer that has not been exposed to bacteria (blue), S-DCPD after *E. coli* exposure (black) and S-DCPD after *S. aureus* exposure (red).

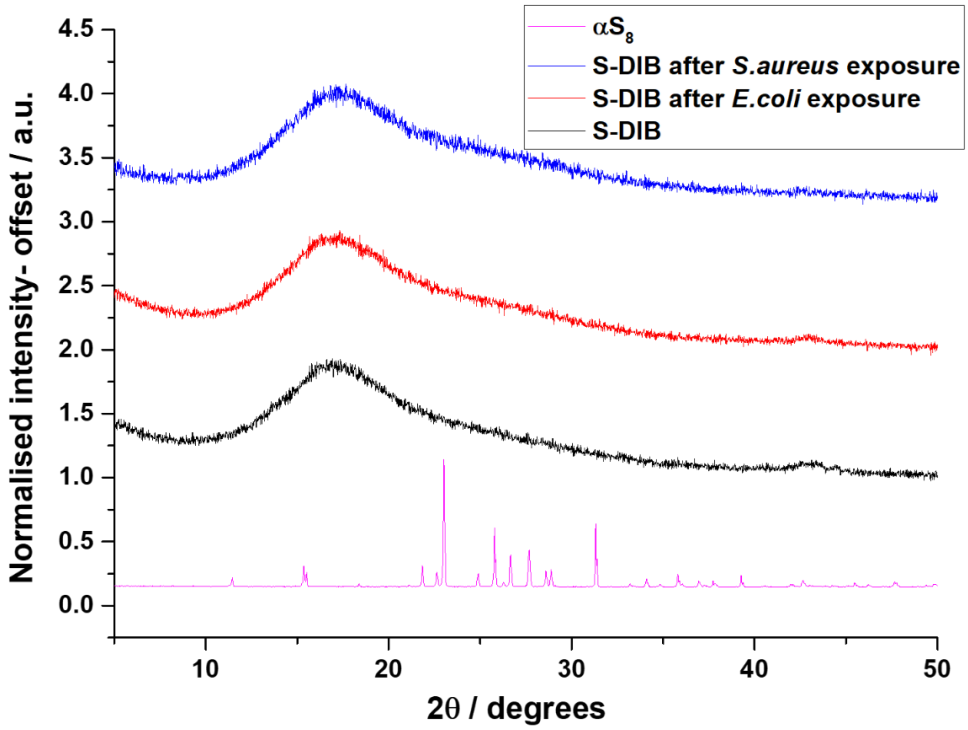

Figure 4.19 Powder X-Ray Diffraction (PXRD) pattern for samples of S-DIB polymeric materials containing 50 wt. % sulfur. The absence of diffraction peaks reveals the absence of crystalline sulfur in any of the polymers, suggesting the sulfur in these amorphous samples is stable against depolymerisation after exposure to bacteria.

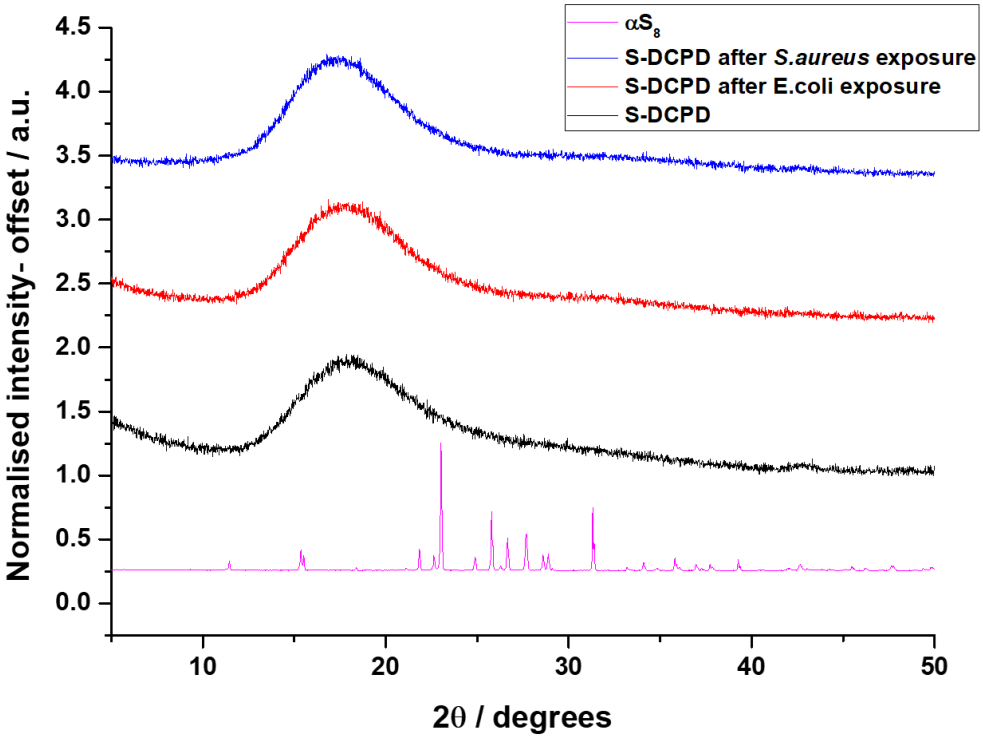

Figure 4.20 Powder X-Ray Diffraction (PXRD) pattern for samples of S-DCPD polymeric materials containing 50 wt. % sulfur. The absence of diffraction peaks reveals the absence of crystalline sulfur in any of the polymers, suggesting the sulfur in these amorphous samples is stable against depolymerisation after exposure to bacteria.

4.4.6 Potential mechanisms for antibacterial activity

The reasons why polysulfides themselves exhibit antibacterial activity are not yet definitively understood. However, there are several mechanisms suggested in the literature.[17] Comparing antibacterial activities, S-DIB shows a more significant reduction in cell numbers for both bacteria and a greater log reduction (Figure 4.14 and 4.15). Potential reasons for both polymers showing different degrees of antibacterial activity could be due to the degree of crosslinking and the molar ratio of sulfur: crosslinker. It is reported that polysulfides ($RS_xR, x \geq 3$) are toxic against bacteria, fungi, and particular types of human cells, although reasons behind this are unknown.[17] The central S-S bond in a polysulfide ($RSxR, x \geq 4$) is weak in compared to terminal S-S bonds, with bond dissociation of alkyltetrasulfides and disulfides being 146 kJ mol^{-1} and 293 kJ mol^{-1} respectively.[17] DCPD has a lower molecular mass than DIB, (132 vs. 162 $gmol^{-1}$), for the same number of reactive double bonds. Because copolymerisation is random, there will be a variable number of sulfur

atoms in between each carbon crosslinker. However, when calculating the average sulfur rank (number of sulfur atoms per crosslinker) expected for both S-DIB (5 sulfur atoms per crosslinker molecule) and S-DCPD (4 sulfur atoms per crosslinker molecule), S-DIB is expected to have longer S-S chains between each carbon crosslink. The longer the polysulfide chains, the weaker the central S-S bond, thus the more likely homolytic S-S bond cleavage is to occur. As discussed, this may lead to the formation of perthyl radicals $R\dot{S}_x$, which can undergo reduction to form perthiols (RSSH). It is then the perthiols (RSSH) that can react with oxygen species (e.g., oxyhaemoglobin and dioxygen) to form reactive oxidative species (ROS) e.g., hydrogen peroxide.[17] ROS are well known for causing oxidative stress to cell membranes and cell death, although specific reaction pathways are unknown.

From this study and others, it is apparent that polysulfides appear to have similar effects against both Gram-positive and Gram-negative bacteria.[25,26] However, the presence of low concentration sulfides has been shown to provide some microorganisms, such as *S.aureus*, with protection against oxidative stress and certain antibacterial compounds.[27] This could explain why we see subtle differences in *S.aureus* survival for S-DCPD treatment but would need to be further studied to confirm this scenario with the sulfur copolymers used here.

As the data in this study suggest, no significant amounts of material containing sulfur are leached from the materials, and the polymers retain amorphous character. This high degree of stability of sulfur within the crosslinked bulk material is a desirable feature of long-term antibacterial surfaces. Surfaces associated with leaching or product release have a fixed lifetime based on the finite amount of antibacterial compound present.[28] Furthermore, the creation of a potential concentration gradient or a local decrease in antibacterial compounds over time can lead to issues of antimicrobial resistance (AMR), and *in vivo* decreases in antibacterial drug concentrations are often associated with detrimental effects surrounding the host's immune response. However, a constitutively active antibacterial surface would benefit both financially and and reduce hospital-acquired infection or industrial contamination, particularly concerning AMR.

Bacterial infections have been considered to be one of the greatest threats to human health, and are becoming more problematic due to increasing AMR.[28] With endotracheal tubes, vascular and urinary catheters and hip prosthetics being

responsible for more than half of nosocomial infections in the USA; it is essential to research different materials that may exhibit antibacterial properties for future development, particularly with the increasing prevalence of AMR. This study demonstrated the ability of inverse vulcanised sulfur polymers as bulk substrates to act as antibacterial surfaces against *E. coli* and *S. Aureus,* the causes of common persistent bacterial infections. This study reports the highest log reduction (>log 4.3) of both bacteria on different inverse vulcanised polymers to date. To fully translate this to a biological setting, complete knowledge of how the surfaces kill bacteria, and comparison of different high sulfur content polymers is essential. This investigation compares two structurally different polymers and highlights key experiments which can help us identify potential mechanisms of how these surfaces exhibit an antibacterial effect. It is interesting to note that while the mechanism of action is not yet known with certainty, it is not inhibited by the thick peptidoglycan layer of Gram-positive bacteria.

4.5 Conclusions and Future Work

This work shows the activity of two high sulfur content polymers, as bulk solids against both Gram-negative and positive bacteria. S-DIB was found to have more significant antibacterial activity than S-DCPD; this could be attributed to S-DIB having a higher sulfur rank (the number of sulfur atoms in between each carbon crosslink CS_x), therefore having a weaker central S-S bond promoting homolysis.

The low-cost availability of sulfur on a vast scale provides the potential for use as antibacterial materials and surfaces in bulk applications that would not be possible for more expensive complex materials. The promising results found already, and the difference in efficacy between these crosslinkers against two bacterial strains suggests that the broader antibacterial effect of sulfur polymers may be further improved in the future and warrants further investigation and development.

Potential future experiments:

- Cytotoxicity experiments to assess the safety of the materials.
- Screening crosslinkers with different sulfur ranks to see if this has an impact on antimicrobial activity.
- Carry out antimicrobial testing on polymers with a range of different glass transition temperatures (T_gs), that are both below and above the temperature of the test.
- Exposing materials to different bacteria, e.g. *Pseudomonas Aeruginosa* a pathogen that is in urgent need of new antibacterial agents.
- Examine the antibacterial resistance of the polymer surfaces to super -resistant pathogens such as MRSA.
- Expose the materials to other microbes such as fungi, mold, and viruses.

4.6 Materials and methods

4.6.1 Materials

1, 3- diisopropenylbenzene (DIB) and dicyclopentadiene (DCPD) were purchased from Tokyo Chemicals Industry. Sulfur was purchased 25 Kg sacks from Brenntag. *Escherichia coli* (*E. coli*) DMS 1576 and *Staphylococcus aureus* (*S. aureus*) DSM 346 strains provided by the University of Liverpool were used for the antimicrobial surface tests.

4.6.2 Characterisation

X-ray diffraction (PXRD): Powder X-Ray Diffraction (PXRD) patterns were carried out on samples using a PAN analytical X'pert powder diffractometer using CuKα radiation.

Differential Scanning calorimetry (DSC): Differential scanning calorimetry was carried out using Q2000 DSC (TA instruments). The method was a heat/cool/heat for three cycles; heating to 150 °C and cooling to – 80 °C at a heating rate of 5 °C/min with Tzero Hermetic pans.

Scanning Electron Microscopy (SEM): Scanning electron microscopy (SEM) was achieved using a Hitachi S-4800 cold field emission scanning electron microscope (FE-SEM). Samples were prepared by sticking them to the SEM stub using conductive silver adhesive paint. The sample was then coated with chrome using a current of 120 mA for 15 s to give approximately 15 nm chrome coatings, using a Quorum S150T ES sputter coater. Imaging was conducted at a working distance of between 7.9 and 8.5 mm at an accelerating voltage of 1.5 kV.

4.6.3 Synthesis of S-DIB and S-DCPD polymer surfaces

Sulfur (10 g) was added to a 40 mL glass vial equipped with a magnetic stirrer bar and heated on a hot plated to 165 °C. Molten sulfur was formed (transparent, yellow solution) and to this 1, 3-diisopropylenebenzene (DIB)/ dicylcopentadiene (DCPD) (10 10 g) was added to the mixture via a pipette. The reaction mixture was heated at 165 °C until homogenous (15-20 minutes). The product was then immediately transferred from the glass vial into a silicone mould of dimensions of 30 mm x 30 mm x 3 mm. This was then cured at 130 °C for 14-16 hours.

4.6.4 Bacteria preparation

Bacterial strains were stored on nutrient agar containing: 10 g L^{-1} peptone, 5 g L^{-1} NaCl, 2 g L^{-1} yeast extract, 5 g L^{-1} meat extract, 15 g L^{-1} agar at pH 7.1 ± 0.1. A scrape of bacteria was transferred to fresh nutrient agar and incubated for 37 °C for 18 h, this was then subsequently repeated. A loopful of agar-grown bacteria was transferred to nutrient broth (1:500 dilution for *Escherichia coli* and 1:100 dilution for *Staphylococcus aureus*.) containing: 5 g L^{-1} meat extract, 10 g L^{-1} peptone (enzymatic digest of casein), 5 g L^{-1} sodium chloride and 15 g L^{-1} agar at pH 7 ± 0.2. The bacterial cells were homogeneously suspended by vortexing 10 sec and water bath sonication 10 sec 50kHz (Grant Ultrasonic XB3). Bacterial enumeration was conducted using a calibration curve from spectrophotometer value. The bacterial suspension was then adjusted to the desired optical density to achieve a target concentration of 3 x 10^6 cells mL^{-1}.

4.6.5 Fluorescent imaging

Testing was conducted on the control (polycarbonate), SDIB50:50 and SDCPD50:50 surfaces (30 mm x 30 mm) and sterilized by submersion in 70% ethanol for 5 min, then ABS ethanol 10 sec. *E. coli* was grown overnight in LB Broth (15 mL), then subculture into fresh LB and grown until an OD_{600} 0.4 was achieved. 10 mL of this subculture was centrifuged at 5,000 rpm for 5 min. The supernatant was discarded, and the pellet resuspended in 30 mL 1:500 diluted LB Broth at a concentration of approximately 10^7 cells mL^{-1}. The surface was submerged in the cell suspension for 24 h. After incubation, the cell suspension was removed, and the surface gently washed with 0.85% sodium chloride (25 mL) three times. Live/Dead Baclight Bacterial Viability Kit L7007 was prepared by placing 1.5 µL of SYTO 9 and 1.5 µL of propidium iodide in 1 mL 0.85% sodium chloride. From this prepared stain, 1 mL was placed directly onto the surface and incubated in darkness for 15 min. The surface was washed with 25 mL 0.85% sodium chloride and then imaged using a Ziess Plan Apochromat 40x/1.0 DIC VIS-IR objective (Zeiss Axio Imager 2 microscope).

4.6.6 Assessment of sulfur leaching

Both bacterial strains were inoculated in nutrient broth (NB) at a concentration of 10^5 cell/mL and a final volume of 30 mL. Substrates were added to the broth and incubated at 37 °C for 24 h . The growth was monitored by taking absorbance at 600 nm and an aliquot of 200 µl was serially diluted and plated on NA using Miles and Misra method

for enumeration of colony forming units (CFU). Data shown in Figure 4 of main paper after normalization to set the control as 100 %.

4.6.7 Surface preparation and ISO standard testing

Testing was conducted on the control (polycarbonate), SDIB50:50 and SDCPD50:50 surfaces (30 mm x 30 mm) and sterilized by submersion in 70% ethanol for 5 minutes, then ABS ethanol for 10 seconds. The surfaces were subsequently dried in the sterile environment using aseptic technique. The test surface was placed in a petri dish, with an autoclaved sponge (20 mm x 20 mm) containing 3 mL sterilized H_2O. 100 µL of the bacterial suspension (3×10^6 cell mL^{-1}) was then placed on the test surface and covered with a polyethylene film (20 mm x 20 mm). The petri dish was placed in a humidity chamber for 24 h. The surface was washed using a serological pipette up taking and releasing Soybean casein digest broth with lecithin and polyoxyethylene sorbitan monooleate (SCDLP broth) 10 mL (10x). The resulting wash was the ten-fold serially diluted to 10^{-6} using sterile phosphate buffer solution. 1 mL of the dilutions was added to 15 mL plate count agar containing: 2.5 g L^{-1} yeast extract, 5 g tryptone L^{-1} , 1 g glucose L^{-1} , 15 g agar L^{-1} at pH 7.1 ± 0.1 and incubated at (35 ± 1) °C for 40 h to 48 h (any modifications to the ISO 22196 were stated in the methods, however the protocol was followed as close as possible). Data shown in Figure 3 of main paper after normalization to set the control as 100 %.

4.6.8 Bacteria enumeration and statistical analysis

For each dilution series, colony number was recorded and converted to recovered bacteria using the formula CFU/mL = (colony number x dilution factor) x 10. The antibacterial activity was calculated using the following formula:

$$\mathbf{R = [\log(B/A) - \log(C/A)] = [\log(B/C)],}$$

where R represents antibacterial activity, A is the average number of viable bacteria immediately after inoculation on the control specimen, B is the average number of viable bacteria on the control specimen after 24 h, and C is the average number of viable bacteria on the antibacterial specimen after 24 h.

Fixation of Bacterial Cells for SEM Analysis

Surfaces were prepared as in '**Surface preparation and ISO standard testing**', and then washed with PBS 3 times. The bacteria on the surface were then fixed with 2.5%

glutaraldehyde solution in sterile PBS for 4 hrs. The bacteria were then dehydrated in increasing concentrations of ethanol (30, 50, 75,90, 95 and 100 v/v %) by soaking for 5 min in each ethanol concentration. The samples were dried in air and stored at 4 $^{\circ}$C before SEM imaging

4.7 Appendix

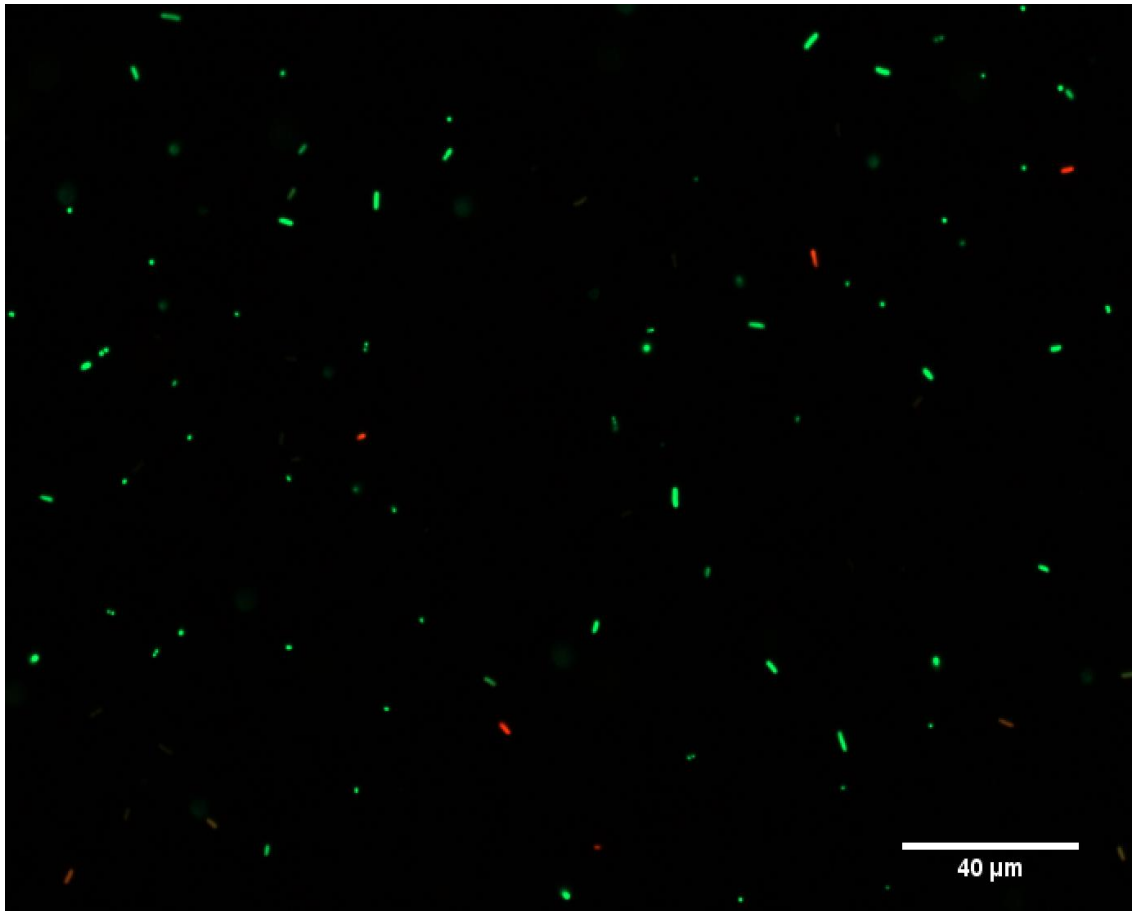

Figure A4.1 Fluorescent micrograph showing attachment of E. coli (DSM 1576) to polycarbonate after 24 h incubation (Micrograph 1). Cells were stained with Syto9 (green) and propidium iodide (red), to detect live and dead cells, respectively. Observation was achieved using a 100x objective lens.

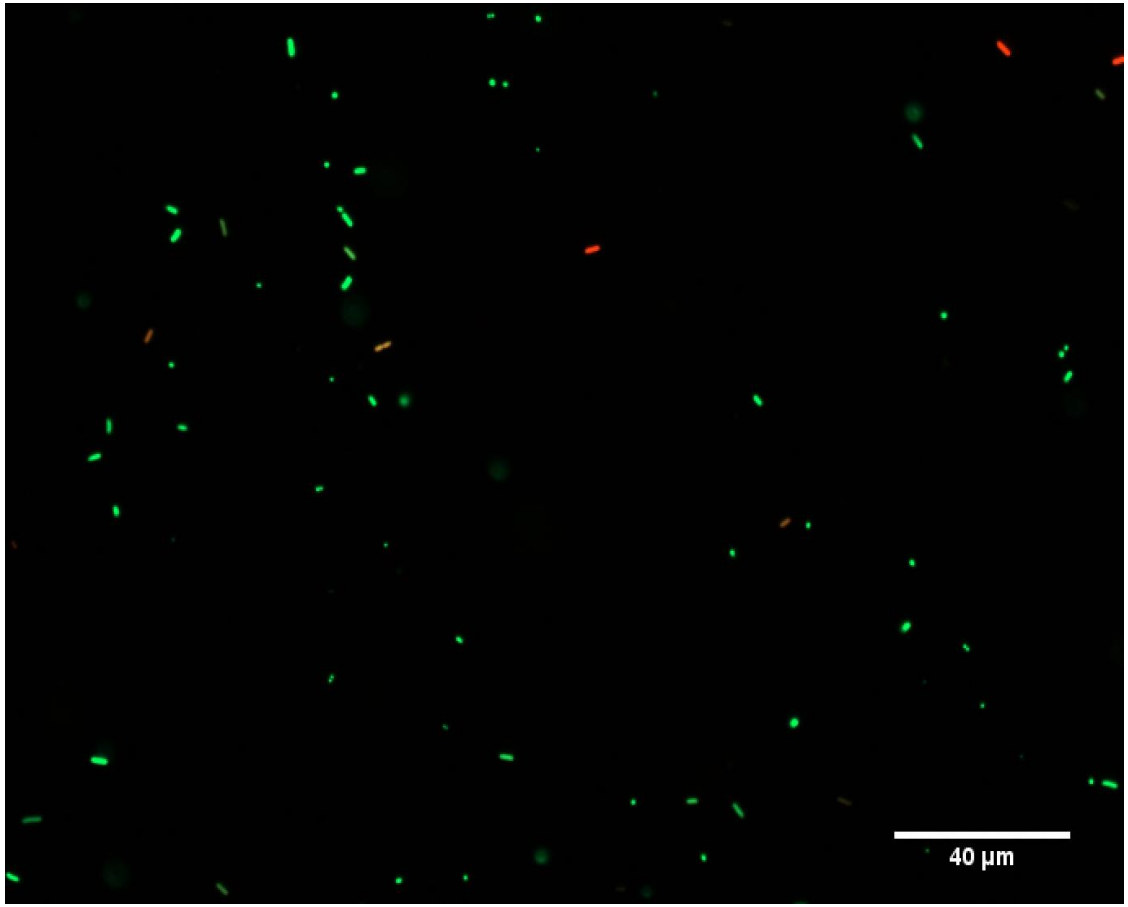

Figure A4.2 Fluorescent micrograph showing attachment of E. coli (DSM 1576) to polycarbonate after 24 h incubation (Micrograph 2). Cells were stained with Syto9 (green) and propidium iodide (red), to detect live and dead cells, respectively. Observation was achieved using a 100x objective lens.

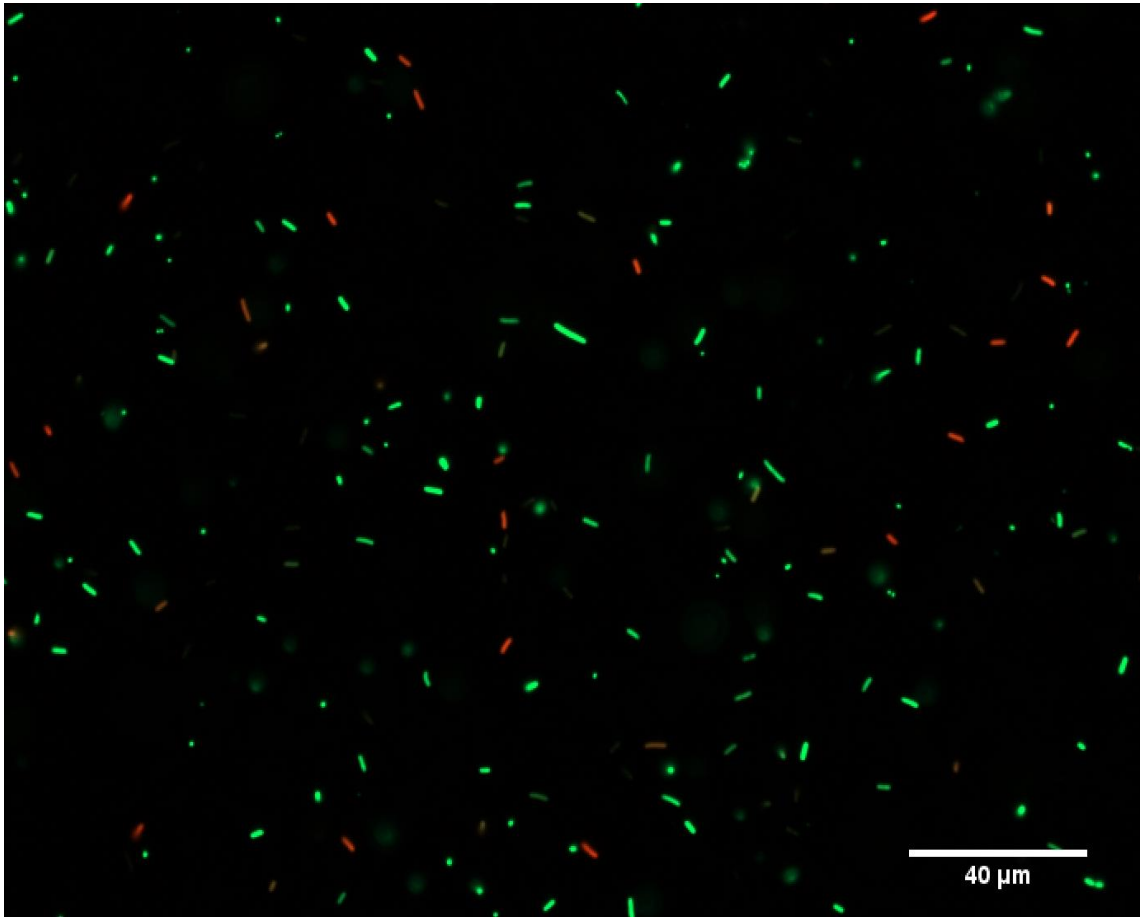

Figure A4.3 Fluorescent micrograph showing attachment of *E. coli* (DSM 1576) to polycarbonate after 24 h incubation (Micrograph 3). Cells were stained with Syto9 (green) and propidium iodide (red), to detect live and dead cells, respectively. Observation was achieved using a 100x objective lens.

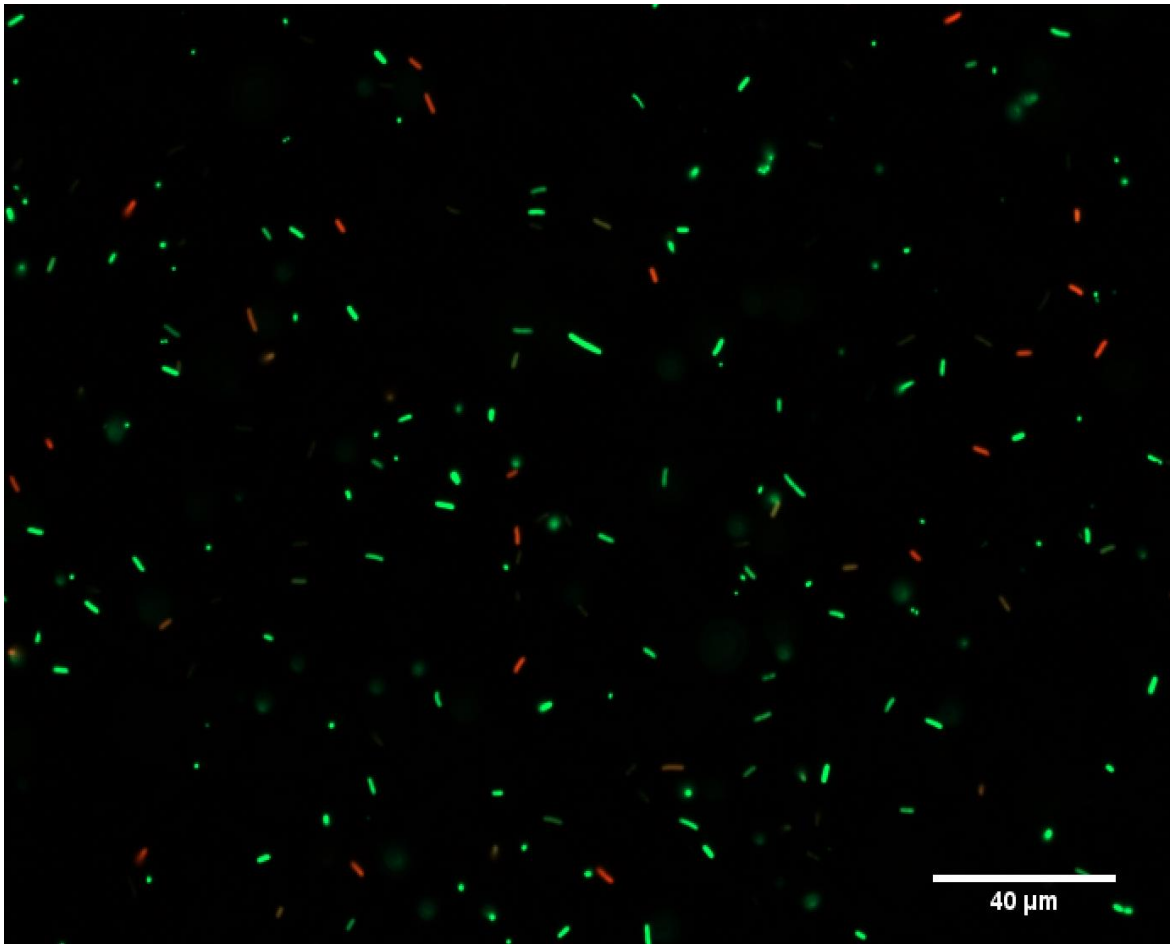

Figure A4.4 Fluorescent micrograph showing attachment of E. coli (DSM 1576) to S-DCPD after 24 h incubation (Micrograph 1). Cells were stained with Syto9 (green) and propidium iodide (red), to detect live and dead cells, respectively. Observation was achieved using a 100x objective lens.

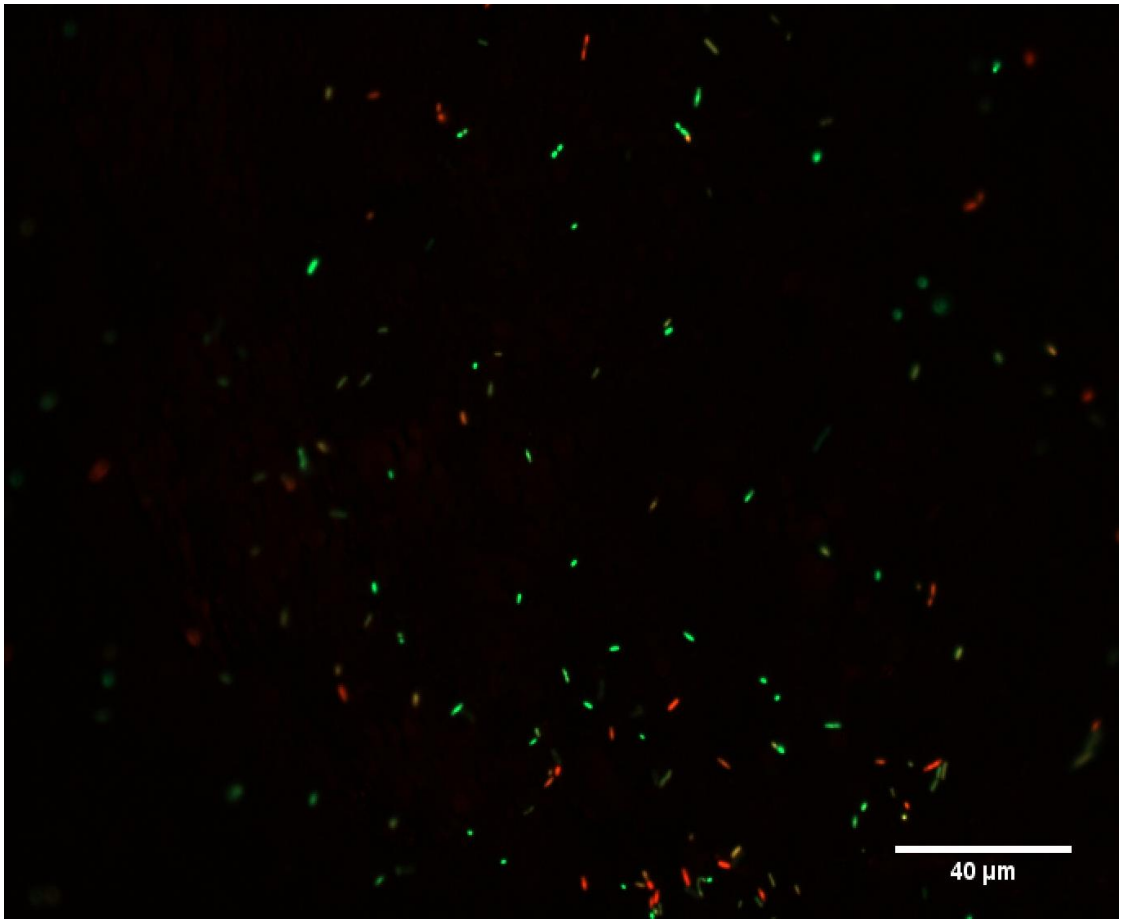

Figure A4.5 Fluorescent micrograph showing attachment of E. coli (DSM 1576) to S-DCPD after 24 h incubation (Micrograph 2). Cells were stained with Syto9 (green) and propidium iodide (red), to detect live and dead cells, respectively. Observation was achieved using a 100x objective lens.

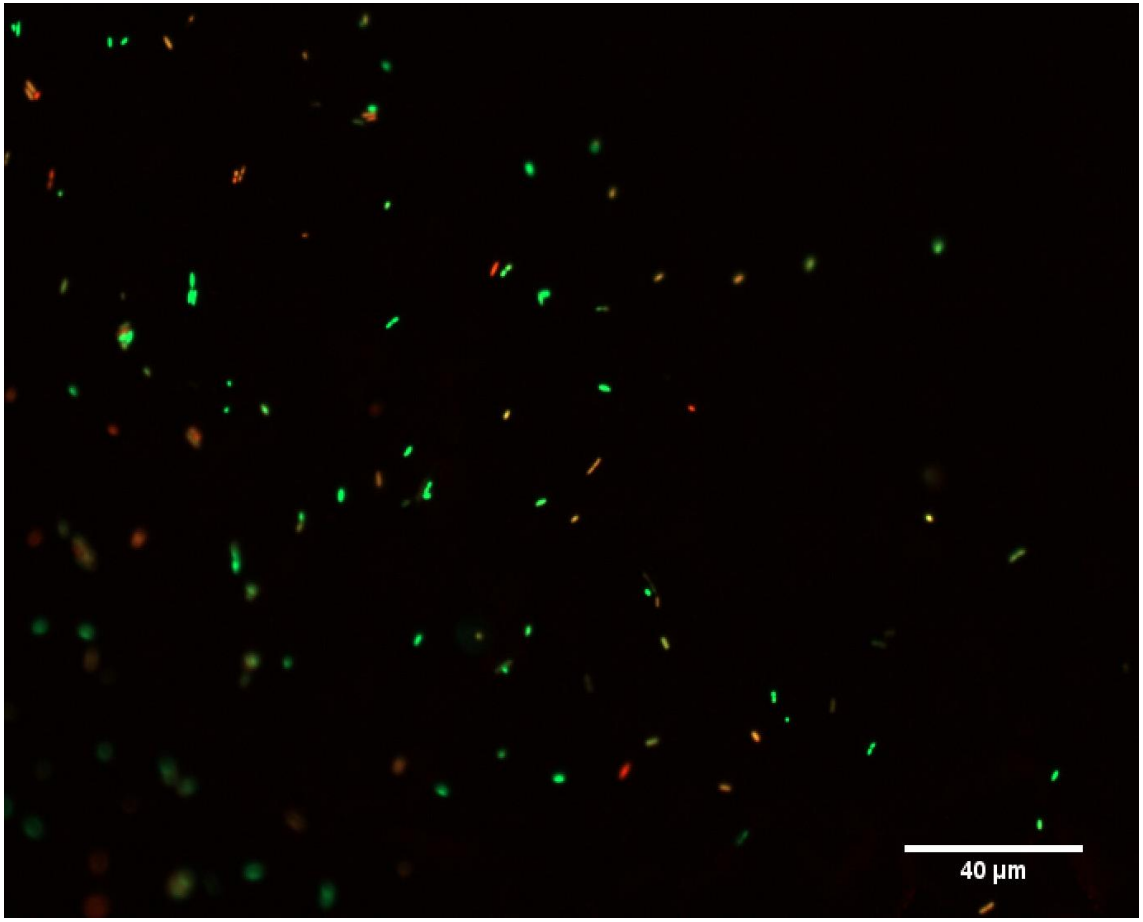

Figure A4.6 Fluorescent micrograph showing attachment of E. coli (DSM 1576) to S-DCPD after 24 h incubation (Micrograph 3). Cells were stained with Syto9 (green) and propidium iodide (red), to detect live and dead cells, respectively. Observation was achieved using a 100x objective lens.

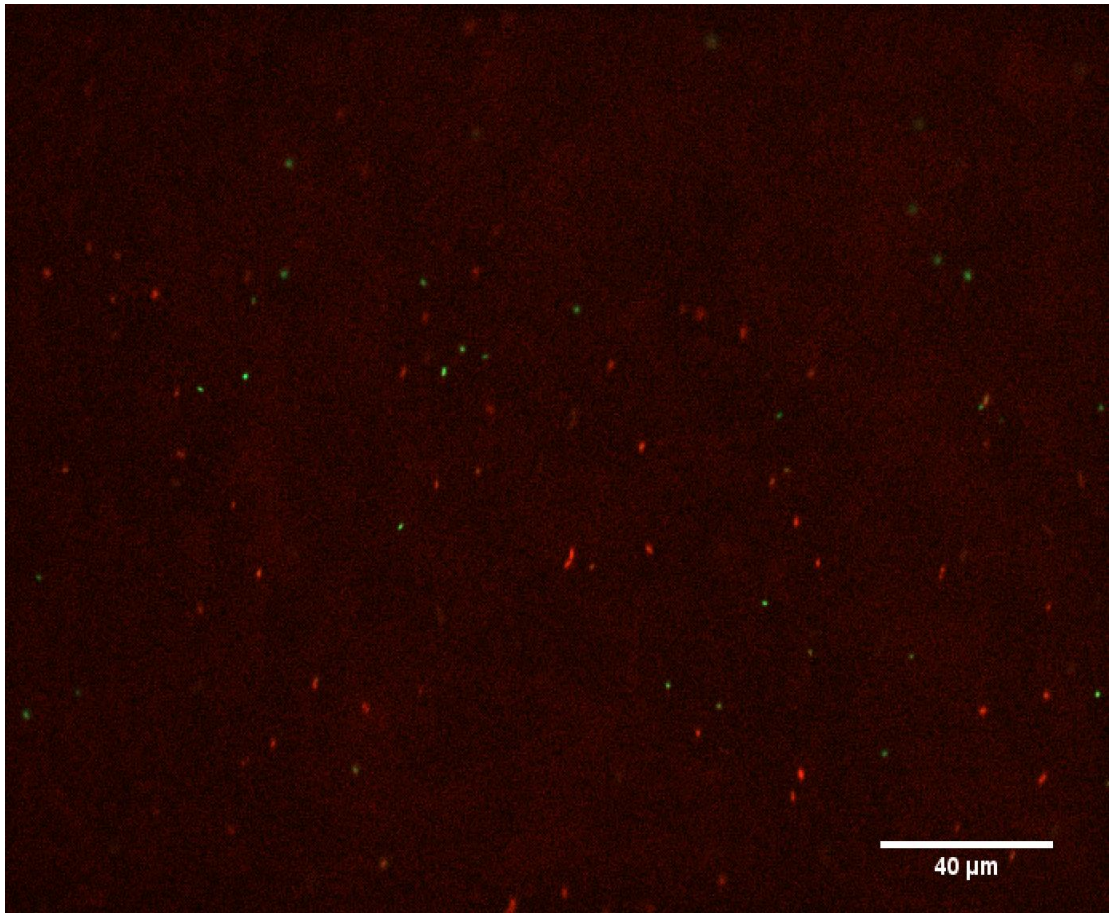

Figure A4.7 Fluorescent micrograph showing attachment of E. coli (DSM 1576) to S-DIB after 24 h incubation (Micrograph 1). Cells were stained with Syto9 (green) and propidium iodide (red), to detect live and dead cells, respectively. Observation was achieved using a 100x objective lens.

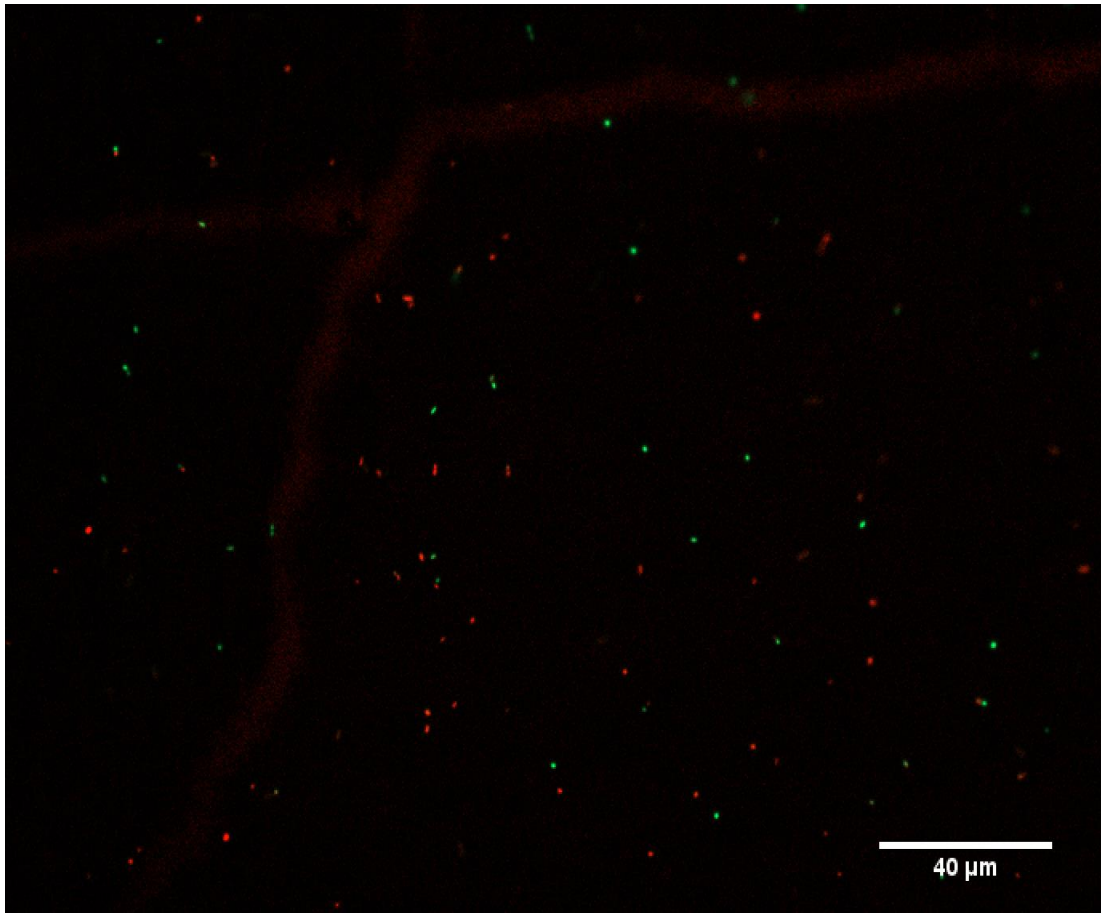

Figure A4.8 Fluorescent micrograph showing attachment of E. coli (DSM 1576) to S-DIB after 24 h incubation (Micrograph 2). Cells were stained with Syto9 (green) and propidium iodide (red), to detect live and dead cells, respectively. Observation was achieved using a 100x objective lens.

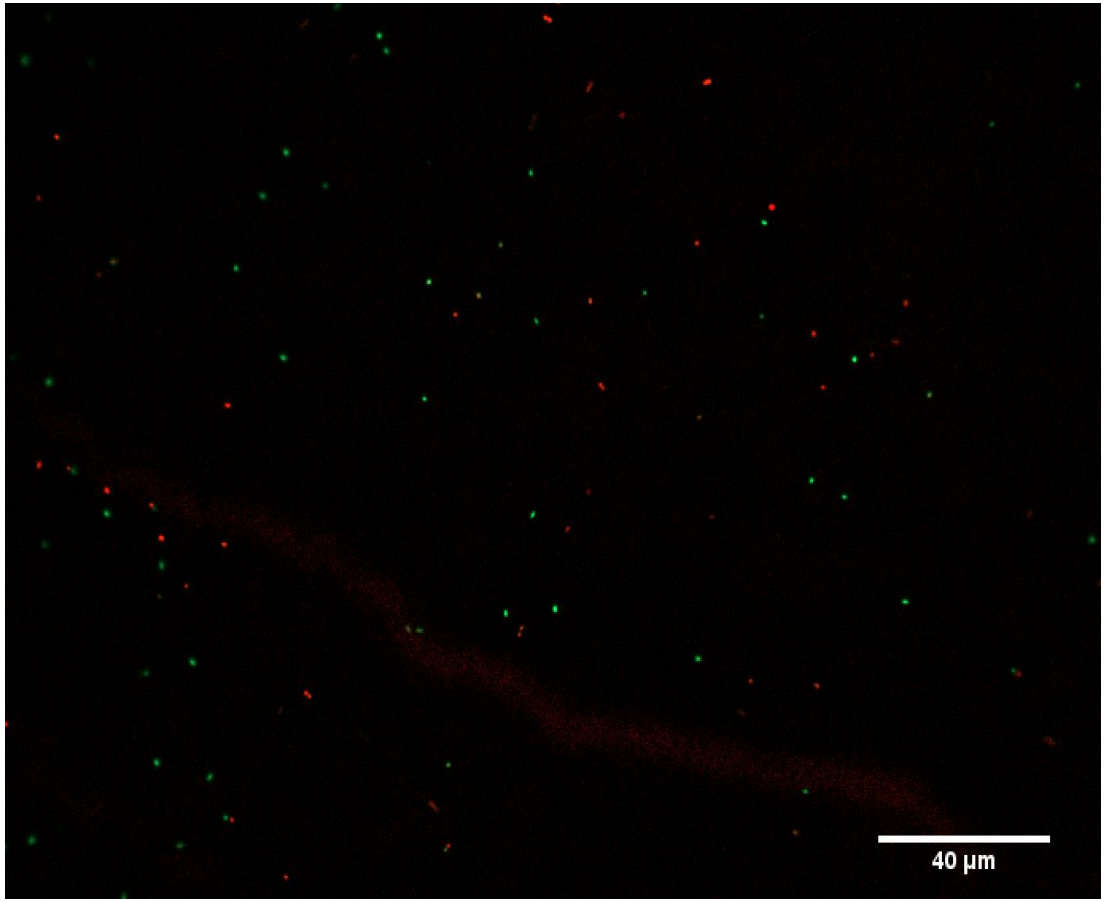

Figure A4.9 Fluorescent micrograph showing attachment of E. coli (DSM 1576) to S-DIB after 24 h incubation (Micrograph 3). Cells were stained with Syto9 (green) and propidium iodide (red), to detect live and dead cells, respectively. Observation was achieved using a 100x objective lens.

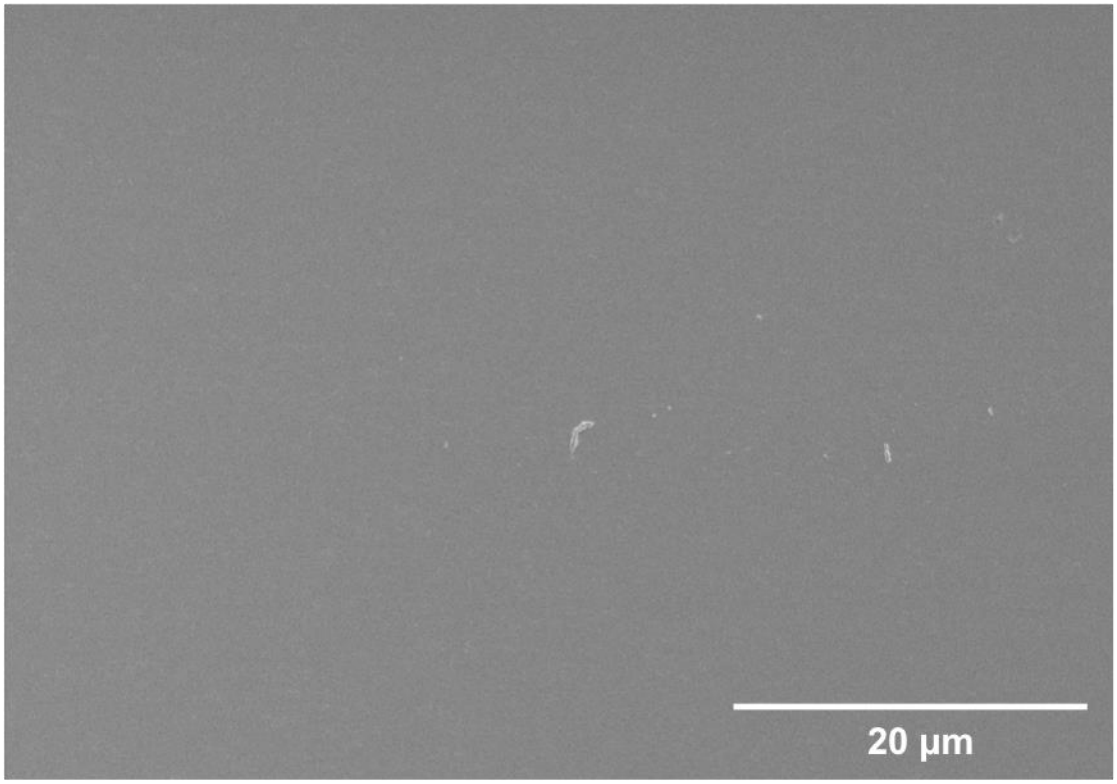

Figure A4.10 SEM micrograph showing polycarbonate surface after 24 h incubation with *E. coli* inoculated onto the surface. Scale bar is 20 µm.

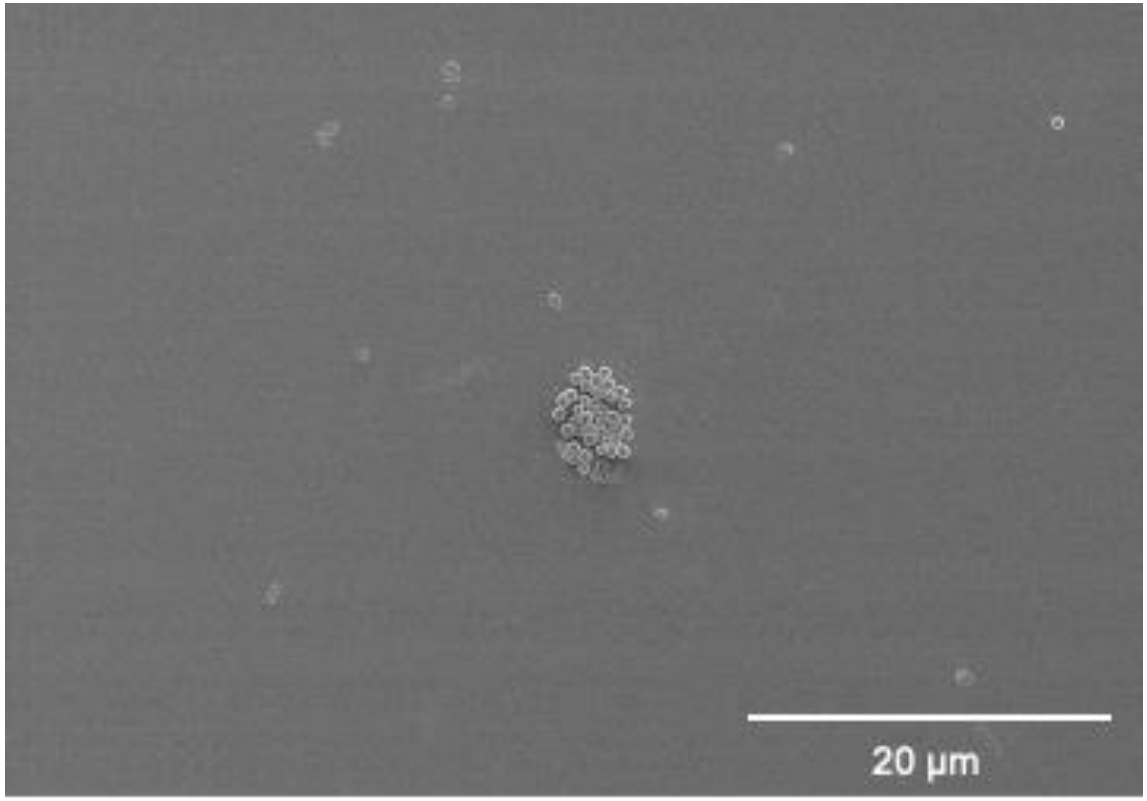

Figure A4.11 SEM micrograph showing polycarbonate surface after 24 h incubation with *S. Aureus* inoculated onto the surface. Scale bar is 20 µm.

4.8 References

1 A. Fleming, *Br. Med. Bull.*, 1944, **2**, 4–5.

2 G. Moulin, P. Cavalié, I. Pellanne, A. Chevance, A. Laval, Y. Millemann, P. Colin and C. Chauvin, *J. Antimicrob. Chemother.*, 2008, **62**, 617–625.

3 N. Mobarki, B. Almerabi and A. Hattan, *Int. J. Med. Dev. Ctries.*, 2019, **40**, 561–564.

4 Z. Khatoon, C. D. McTiernan, E. J. Suuronen, T. F. Mah and E. I. Alarcon, *Heliyon*, 2018, **4**, e01067.

5 S. Aiola, G. Amico, P. Battaglia and E. Battistelli, *Clin. Microbiol. Rev.*, 2002, **15**, 167–193.

6 D. J. W. Dominique H. Limoli, and Christopher J. Jones, *microbiol spectr.*, 2015, 1191–1200.

7 R. M. Donlan, *Clin. Infect. Dis.*, 2001, **33**, 1387–1392.

8 G. A. C Mah, Thien-Fah , O'Toole, *Trends Microbiol.*, 2001, **9**, 34–39.

9 A. Threefall, Perfectus Biomed Group, http://perfectusbiomed.com/cbe-meeting-anti-biofilm-technologies/biofilm-formation-slide-technologies/biofilm-formation-slide-copy/. (accessed 1st May 2020).

10 P. A. Suci, M. W. Mittelman, F. P. Yu and G. G. Geesey, *Antimicrob. Agents Chemother.*, 1994, **38**, 2125–2133.

11 W. M. Dunne, E. O. Mason and S. L. Kaplan, *Antimicrob. Agents Chemother.*, 1993, **37**, 2522–2526.

12 A. Brooun, S. Liu and K. Lewis, *Antimicrob. Agents Chemother.*, 2000, **44**, 640–646.

13 C. Adlhart, J. Verran, N. F. Azevedo, H. Olmez, M. M. Keinänen-Toivola, I. Gouveia, L. F. Melo and F. Crijns, *J. Hosp. Infect.*, 2018, **99**, 239–249.

14 R. Kaur and S. Liu, *Prog. Surf. Sci.*, 2016, **91**, 136–153.

15 R. M. Donlan, *Emerg Infect Dis*, 2002, **9**, 881–890.

16 Z. Xu, Z. Qiu, Q. Liu, Y. Huang, D. Li, X. Shen, K. Fan, J. Xi, Y. Gu, Y. Tang, J. Jiang, J. Xu, J. He, X. Gao, Y. Liu, H. Koo, X. Yan and L. Gao, *Nat. Commun.*, 2018, **9**, 1–13.

17 U. Münchberg, A. Anwar, S. Mecklenburg and C. Jacob, *Org. Biomol. Chem.*, 2007, **5**, 1505–1518.

18 T. L. Pickering, K. J. Saunders and A. V. Tobolsky, *J. Am. Chem. Soc.*, 1967, **89**, 2364–2367.

19 A. S. Mozaffari Nejad, S. Shabani, M. Bayat and S. E. Hosseini, *Jundishapur J. Microbiol.*, 2014, **7**, 1–5.

20 Z. Deng, A. Hoefling, P. Théato and K. Lienkamp, *Macromol. Chem. Phys.*, 2018, **219**, 1–6.

21 K. Ejrnæs, *Dan.Med.Bull*, 2011, **58**, 1no B4187.

22 D. J. Parker, H. A. Jones, S. Petcher, L. Cervini, J. M. Griffin, R. Akhtar and T. Hasell, *J. Mater. Chem. A*, 2017, **5**, 11682–11692.

23 W. J. Chung, J. J. Griebel, E. T. Kim, H. Yoon, A. G. Simmonds, H. J. Ji, P. T. Dirlam, R. S. Glass, J. J. Wie, N. a Nguyen, B. W. Guralnick, J. Park, A. Somogyi, P. Theato, M. E. Mackay, Y. Sung, K. Char, J. Pyun, Á. Somogyi, P. Theato, M. E. Mackay, Y. Sung, K. Char, J. Pyun, A. Somogyi, P. Theato, M. E. Mackay, Y. Sung, K. Char, J. Pyun, Á. Somogyi, P. Theato, M. E. Mackay, Y. Sung, K. Char and J. Pyun, *Nat. Chem.*, 2013, **5**, 518–524.

24 D. J. Parker, H. A. Jones, S. Petcher, L. Cervini, J. M. Griffin, R. Akhtar and T. Hasell, *J. Mater. Chem. A*, 2017, **5**, 11682–11692.

25 H. Lim, K. Kubota, A. Kobayashi and F. Sugawara, *Phytochemistry*, 1998, **48**, 787–790.

26 Z. Xu, Z. Qiu, Q. Liu, Y. Huang, D. Li, X. Shen, K. Fan, J. Xi, Y. Gu, Y. Tang, J. Jiang, J. Xu, J. He, X. Gao, Y. Liu, H. Koo, X. Yan and L. Gao, *Nat. Commun.*, 2018, **9**, 3713.

27 K. Shatalin, E. Shatalina, A. Mironov and E. Nudler, *Science (80-.).*, 2011, **334**, 986–990.

28 H. Murata, R. R. Koepsel, K. Matyjaszewski and A. J. Russell, *Biomaterials*, 2007, **28**, 4870–4879.

CHAPTER 5

CATALYTIC INVERSE VULCANISATION

Chapter 5: Catalytic inverse vulcanisation

5.1 Context

Section 5.2 is adapted from the paper "Catalytic inverse vulcanisation", published in Nature Communications, 2019. Chapter 3 uncovered design principles, discussing how the physical properties of sulfur polymers may be controlled and altered for different functions. Chapter 4 explores the potential of these materials as antibacterial surfaces and highlights how controlling these polymers' properties is of vital importance for their potential functions.

In this chapter, catalytic inverse vulcanisation is demonstrated for the first time. In comparison to un-catalysed inverse vulcanisation the reaction temperature can be reduced; the properties of the polymers are improved, and the production of toxic H_2S gas is significantly reduced. Finding new ways to control these reactions is vital for scale-up. Alongside this, catalytic inverse vulcanisation allowed reaction with new crosslinkers that wouldn't otherwise undergo polymerisation with sulfur. It is still not clear whether the catalysts discussed in this chapter are acting as accelerators (see discussion below). However, for the remainder of this chapter, the substances will be referred to as catalysts. A series of metal diethyldithiocarbamate complexes are explored as potential phase transfer catalysts for inverse vulcanisation reactions.

5.1.2 Author Contributions

In this chapter, Dr. Xiaofeng Wu carried out all catalyst screening experiments, and Jessica A Smith carried out characterisation. Jessica A Smith carried out reactions in the chapter of this thesis. Samuel Petcher carried out alternative catalytic reactions with different crosslinkers.[1] This work was a collaborative process with much help and discussions between both Jessica A Smith and Samuel Petcher. Bowen Zhang carried out NMR studies, which can be found in the full article.[1] Douglas J Parker and Samuel Petcher also looked at the improved properties of these materials (e.g.,mercury uptake).[1] John M Griffin carried out all Solid-State NMR experiments. Dr. Tom Hasell was the PI on this project and gave much guidance and advice.

5.2 Introduction

5.2.1 Controlling inverse vulcanisation reactions

In general, most inverse vulcanisation reactions require heating to or over 159 °C to generate a high enough concentration of reactive sulfur radicals for polymerisation. However, there are exceptions reported, such as styrene[2] and 2-ethylidene-5-norbornene (ENB),[3] where reaction temperatures around 130 °C were observed to form both oligomeric and polymeric materials. With this said, there are both opportunities and challenges to developing improved methods to lower reaction temperatures and to explore other functional monomers with lower boiling points than sulfur.

In addition to this, avoiding high reaction temperatures could be crucial in reducing/preventing the production of H_2S in these reactions, which would be beneficial to industrial scale-.[4] Finding a catalytic pathway that lowers reaction

Figure 5.1 An inverse vulcanisation reaction between sulfur and DCPD that has undergone auto acceleration. The liquid reaction was filled less than 100 mL of the 500 mL round bottom flask. After a few seconds the reaction mixture 'boiled' violently to overflow the container, venting both gas and volatalised monomer.

temperatures for inverse vulcanisation, avoids H_2S generation and auto-acceleration via the Trommsdorff-Norrish effect (Figure 5.1), alongside the ability to introduce

other functional monomers with lower boiling points/lack of reactivity is highly desired.

5.2.2 What are accelerators?

In the rubber industry, an accelerator is known as a chemical that speeds up the vulcanisation of rubber at a lower temperature.[5] Metal salts, oxides, and complexes have been successfully applied as accelerators in conventional vulcanisation. During vulcanisation, an accelerator is thought to convert the sulfur into a compound that reacts more with rubber than sulfur.[5] Accelerators are consumed in the process; therefore are not referred to as catalysts in the industry. However, the exact mechanism of their action is unknown. In this thesis, the chemical compounds used to speed up the inverse vulcanisation reactions will be referred to as 'catalysts'; however, it should be noted whether they are acting as accelerators or catalysts is still under discussion.

5.2.3 Accelerators in inverse vulcanisation reactions

Pyun and co-workers have reported two types of organic accelerators that were found to increase the rate of inverse vulcanisation (Figure 5.2).[6] They demonstrated this by using both activated vinyl monomers such as, 4-vinylaniline (4VA) to significantly increase the rate of inverse vulcanisation, which they attributed to polarity reversal effects and the introduction of nucleophilic activators such as, N-methylimidazole (NMI) which was used to initiate ring-opening of S_8 to enhance rate and reactivity.[6] The group observed that when 1 mol% of 4VA or NMI was added to the inverse

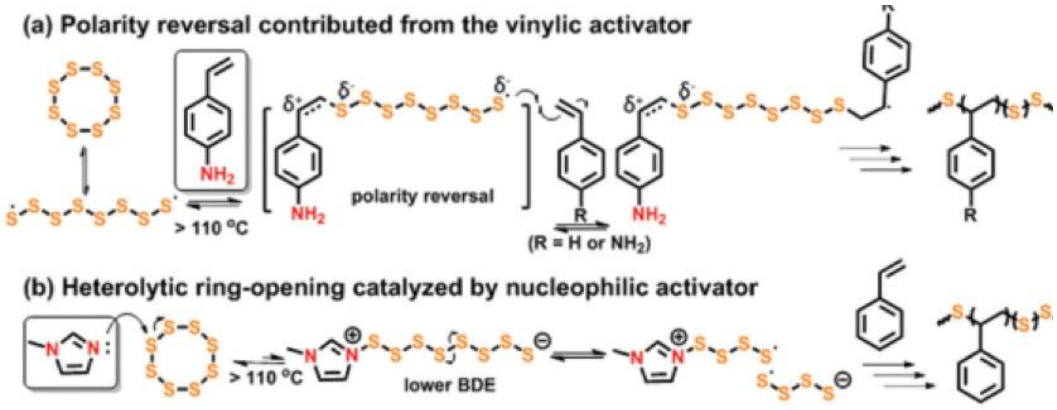

Figure 5.2 (a) Polarity reversal effects when using vinyl activators e.g. 4VA (b) nucleophillic ring opening of S_8 using an added activator e.g. NMI. From ref 4.

vulcanisation reaction of sulfur-styrene, the rate was increased by a factor of 2.[6]

Alongside this, it was found that with the addition of 4VA, polymerisation could be conducted at a lower temperature.

5.2.3 Crosslinkers discussed in this chapter

Crosslinkers discussed in this chapter will be split into three different categories (Figure 5.3); crosslinkers unreactive without catalysis, crosslinkers newly reported in this work, and previously reported crosslinkers. Other crosslinkers used in catalytic inverse vulcanisation can be found in the literature as part of the more comprehensive study.[6] Figure 5.3 highlights the crosslinkers that where investigated for inverse

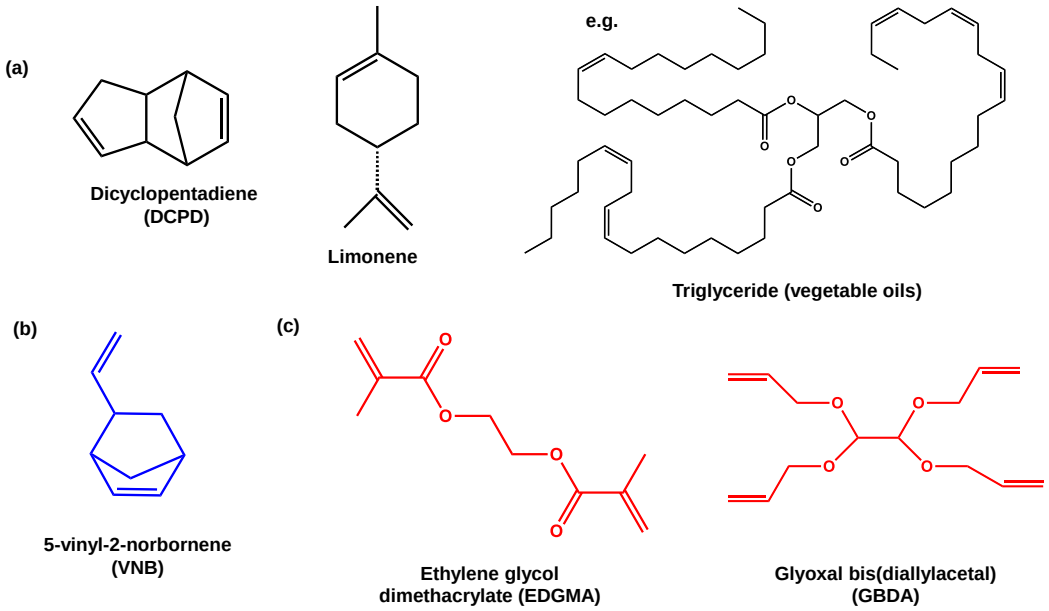

Figure 5.3 (a) Previously reported crosslinkers in inverse vulcanization reactions (black). (b) Crosslinkers newly reported in this work (blue). (c) Crosslinkers that are unreactive without catalysis (red).

vulcanisation in this work. Dicyclopentadiene (DCPD) has previously been reported in inverse vulcanisation and is a compound that comes from industrial feedstocks.[7] Both limonene and vegetable oils have also been employed in inverse vulcanisation reactions to form sustainable polymers.[7,8,9] These reactions require heating over 160 °C, and in the reaction between sulfur and limonene significant volumes of H_2S are reported.[3,10,11] Therefore, using a catalytic pathway to avoid these high temperatures (over 140 °C) and prevent/reduce the formation of H_2S is crucial.

In addition to this, many crosslinkers do not undergo polymerisation with sulfur due to their lack of reactivity/ low boiling point (Figure 5.2). Therefore, a series of metal diethyldithiocarbamate complexes are investigated with a series of crosslinkers (Figure 5.3) to study the effects on the reactions.

5.3 Chapter aims

1. Screen a variety of catalyst/accelerators for inverse vulcanisation reactions
2. Screen different crosslinkers with chosen catalyst/accelerator to see if new crosslinkers can be unlocked and the effect on the reaction (e.g., rate, temperature etc.)
3. Investigate how catalysis effects the production of harmful H_2S gas and yield.
4. Propose a potential mechanism for how the catalyst/accelerator could be acting.

5.4 Results and Discussion

5.4.1 Catalyst screening

As previously discussed in Chapter 3, some crosslinkers are found to be unreactive with sulfur unless there is second crosslinker, thereby forming a sulfur terpolymer. Therefore, finding a pathway to allow sulfur to react with a range of different crosslinkers is essential in producing materials that can be applied to various applications. The introduction of catalysts/accelerators (Figure 5.4) into these inverse vulcanisation reactions was trialed. The reaction of crosslinker ethylene glycol dimethacrylate (EDGMA) with sulfur was used as a model reaction, as it was found to be un-reactive without catalysis (Table 5.1, experimental 5.6.3).

Table 5.1 Screening of catalysts for inverse vulcanisation of sulfur with EGDMA

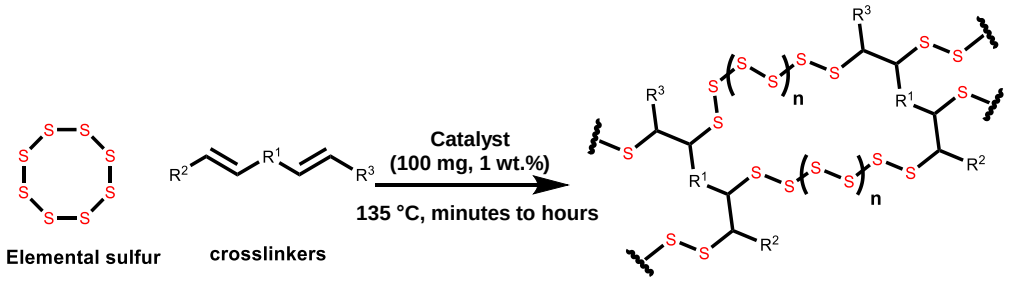

Catalyst:	Observation:	Results
ZnO	Yellow cloudy solution	No reaction
Zn	Yellow cloudy solution	No reaction
$ZnCl_2$	Yellow cloudy solution	No reaction
$FeCl_2$	Yellow-green cloudy solution	No reaction
CuO	Brown-yellow cloudy solution	No reaction
$CuCl_2$	Brown-yellow cloudy solution	No reaction

Zn-stearate	Orange-brown solution	Partially reacted
Zn-diethyldithiocarbamate	Dark-red solid	Fully reacted
Fe-diethyldithiocarbamate	Black-green solid	Fully reacted
Co-diethyldithiocarbamate	Dark-brown solid	Fully reacted
Cu-diethyldithiocarbamate	Dark-red solid	Fully reacted
Ni-diethyldithiocarbamate	Dark-brown solid	Fully reacted
Na-diethyldithiocarbamate	Dark-red solid	Fully reacted
Thiram	Yellow-orange-red inhomogeneous solid	Partially reacted
2-Cyano-2-propyl benzodithioate	Yellow cloudy solution	No reaction

The reaction was heated at 135 °C for 10 hours, with stirring. Weight ratio of cross-linker (EGDMA, 5 g) and sulfur (5 g) of 1:1 and 1 wt.% catalyst loading. b: partly reacted = some polymer formed, but unreacted S_8 remains; fully reacted = no remaining S_8 detected by DSC or PXRD.

Sulfur itself is known to be a slow vulcanisation agent, which requires high temperatures and long heating periods.[12] As discussed, metal oxides, complexes, and salts have been successfully implemented as accelerators for conventional vulcanisation in industry.[12] One of the most common accelerators used in industry is Zinc Oxide (ZnO).[12] When ZnO was incorporated into the inverse vulcanisation reactions, it did not show catalytic activity, nor did copper, zinc , or iron chloride (Table 5.1). However, zinc stearate[13] did show some catalytic activity for the inverse

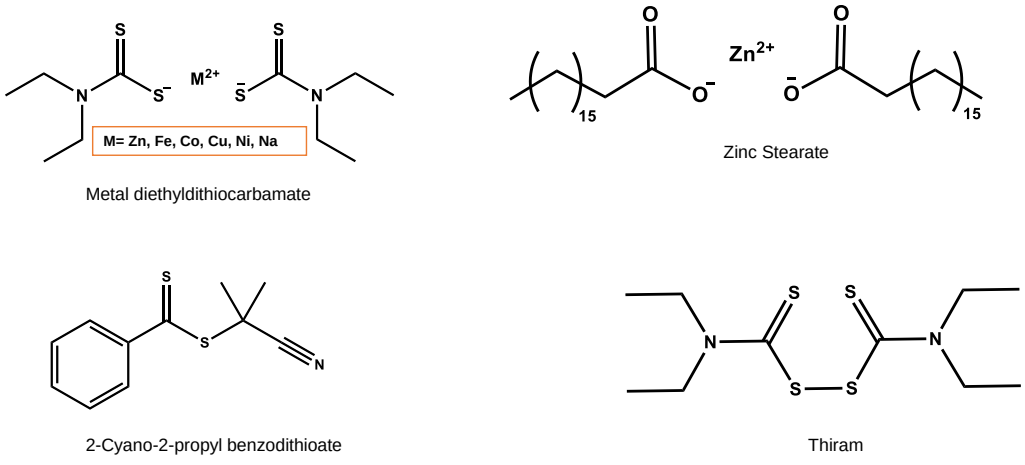

Figure 5.4 Catalysts that were trialled in inverse vulcanisation reactions.

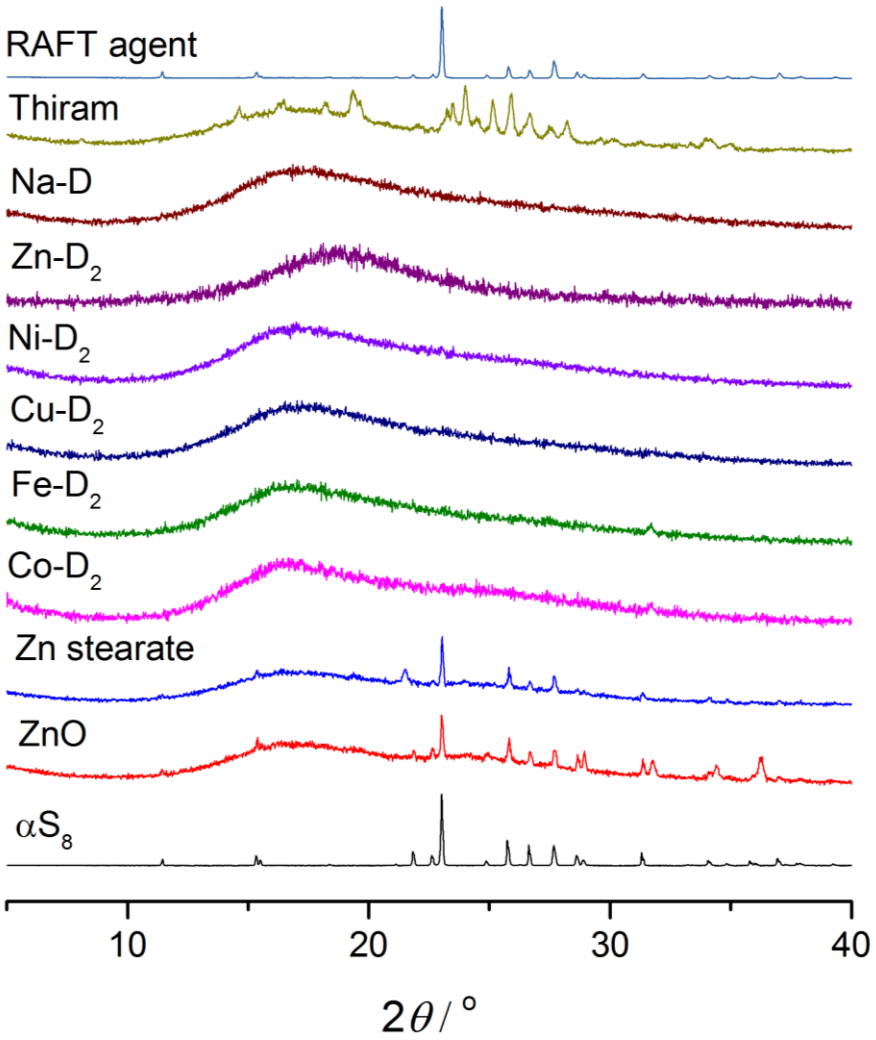

Figure 5.5 PXRD diffraction patterns of the products of sulfur reacted with EDGMA (1:1 mass ratio) for catalyst loading of 1 wt. %

vulcanisation reaction between sulfur and EDGMA (Table 5.1). Although, when using Zinc stearate even after curing the polymer for 10 hours, there were unreacted or depolymerised S_8 crystals recorded by PXRD (Figure 5.5). When the stearate ligand was replaced with the diethyldithiocarbamate (D), the reaction rate was noticeably quicker with the colour of the reaction changing from molten yellow sulfur to orange/red within minutes of adding EDGMA. The reaction progressed to form a homogenous red, clear solution, and finally, a deep-red viscous gel, seizing the stirrer bar. When the same reaction between sulfur and EDGMA is conducted without the catalyst, the reaction is not homogeneous with two noticeable separate layers, even at a temperature of 200 °C.

The diethyldithiocarbamate ligand appears to be more significant than the metal, as the other metals such as Fe and Cu were found to work effectively with this ligand (Table 5.1). Sodium diethyldithiocarbamate (NaD) reacted the quickest with EDGMA, forming a gel within minutes. However, the short mixing time led to an inhomogeneous product, and NaD was not compatible with all crosslinkers tested. With several metal complexes showing viability, it seemed possible the catalytic effect could be arising from the diethyldithiocarbamate ligand, opposed to the metal by a process that is similar to reversible addition-fragmentation chain-transfer polymerisation (RAFT).[14] To test this thiram and a common raft agent (2-Cyano-2-propyl benzodithioate) were also trialed, but showed very little or no activity (Table 5.1).

PXRD diffraction patterns (Figure 5.5) of the products of sulfur reacted with EDGMA (1:1 mass ratio) was recorded for a catalyst loading of 1 wt. %. Both Zinc oxide and Zinc stearate catalysts showed residual S_8 crystals present. All of the diethyldithiocarbamate catalysts resulted in amorphous materials, indicating the absence of depolymerised S_8 crystals. Although polymerisation of EGDMA occurred with thiram, there was poor mixing and an incomplete reaction. The RAFT agent used was 2-Cyano-2-propyl benzodithioate but showed no reaction with sulfur. ZnD_2 is an effective accelerator in conventional vulcanisation and accelerated the reactions for a broad range of crosslinkers in inverse vulcanisation. Therefore, going forward, ZnD_2 was selected for further optimisation.

5.4.2 Effect of catalysis- Characterisation

Both reported and unreported crosslinkers were tested with Zinc diethyldithiocarbamate (ZnD_2) (Figure 5.3). Examining a broad range of crosslinkers is of importance, as different crosslinkers will result in materials with entirely different properties. Therefore, it is essential to find ways to accelerate these reactions successfully for potential future functions.

5.4.2.1 Crosslinkers that are unreactive without catalysis

In this work, three crosslinkers were found to be unreactive without catalysis; EDGMA, glyoxal bis(diallylacetal) (GBDA), and 1,3,5,7-tetravinyltetramethylcyclotetrasiloxane (TVTCSi). Both EDGMA and GBDA will be discussed in this section. GBDA is chosen due to the similarities with EDGMA. This is to see if the addition of ZnD_2 both may accelerate and result in a successful reaction between sulfur and GBDA. Both polymers in this section will be referred to as S-EDGMA (sulfur-EDGMA) and S-GBDA (sulfur-GBDA). Reactions were carried out at 135 °C with equal masses of sulfur: crosslinker (1:1).

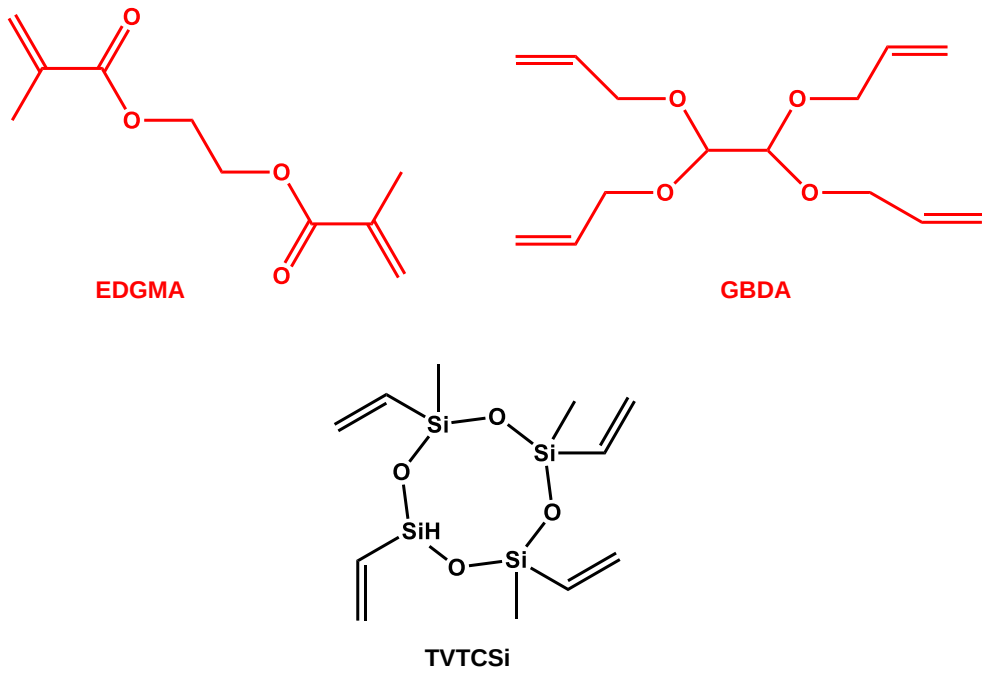

Figure 5.6 Unreported crosslinkers: Ethylene glycol dimethacrylate (EDGMA), glyoxal bis(diallylacetal) (GBDA), 1,3,5,7-tetravinyltetramethylcyclotetrasiloxane. EDGMA and GBDA highlighted in red will be discussed in this section.

S-EDGMA

As discussed, the reaction between sulfur and EDGMA was used as a model reaction when screening crosslinkers, as without ZnD_2, the reaction was unsuccessful. When 1 wt. % of ZnD_2 was added to the reaction; the resultant product was a deep-red solid that was insoluble even in strong organic solvents such as tetrahydrofuran (THF) and Chloroform ($CHCl_3$), indicating that a highly crosslinked network was formed. When

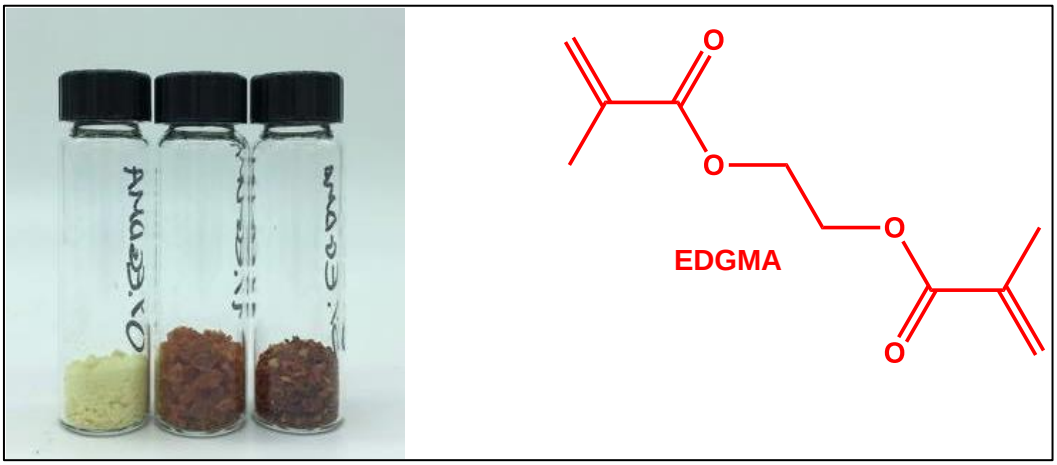

Figure 5.5 Left to right: 0%, 1% and 5 % by mass of ZnD_2 added to the inverse vulcanisation reaction between sulfur and EDGMA. With 0% of ZnD_2 there is no colour change and the appearance is similar to elemental sulfur.

sulfur is reacted with EDGMA without ZnD_2, there is no colour change, and the appearance is similar to elemental sulfur (Figure 5.5.)

To further confirm polymerisation, solid-state ^{13}C nuclear magnetic resonance spectroscopy (NMR) was recorded (Figure 5.6). Equal masses of both crosslinkers

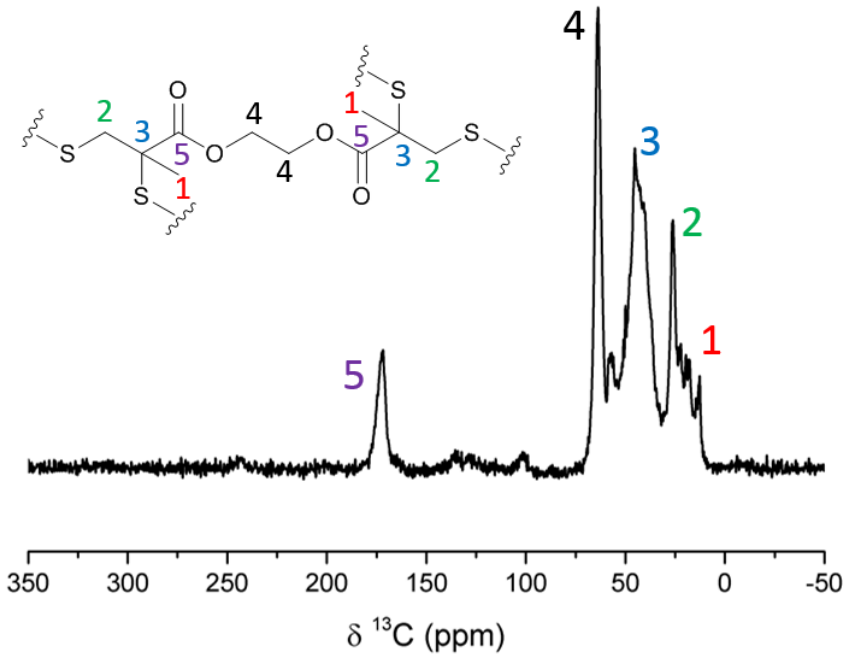

Figure 5.6 . Solid state ^{13}C NMR spectra of ethylene glycol dimethyl acrylate (EGDMA) after polymerisation with sulfur. Conditions: equal mass of sulfur and crosslinker, 1 wt.% ZnD_2 catalyst, 135 °C. The spectrum shows the formation of C-S bonds, and near complete loss of C=C signal.

were reacted (1:1) with the addition of 1 wt.% ZnD_2. This spectrum shows the formation of C-S bonds **(3)**, and the significant loss of C=C signal.

FT-IR spectra (Figure 5.7) were recorded of EDGMA monomer, and after polymerisation with sulfur and the addition of the catalyst (5% ZnD_2 by mass). After polymerisation there is a reduction in the signal at ~1650 cm^{-1} of the C=C stretching vibrations, suggesting some of the C=C has been consumed.

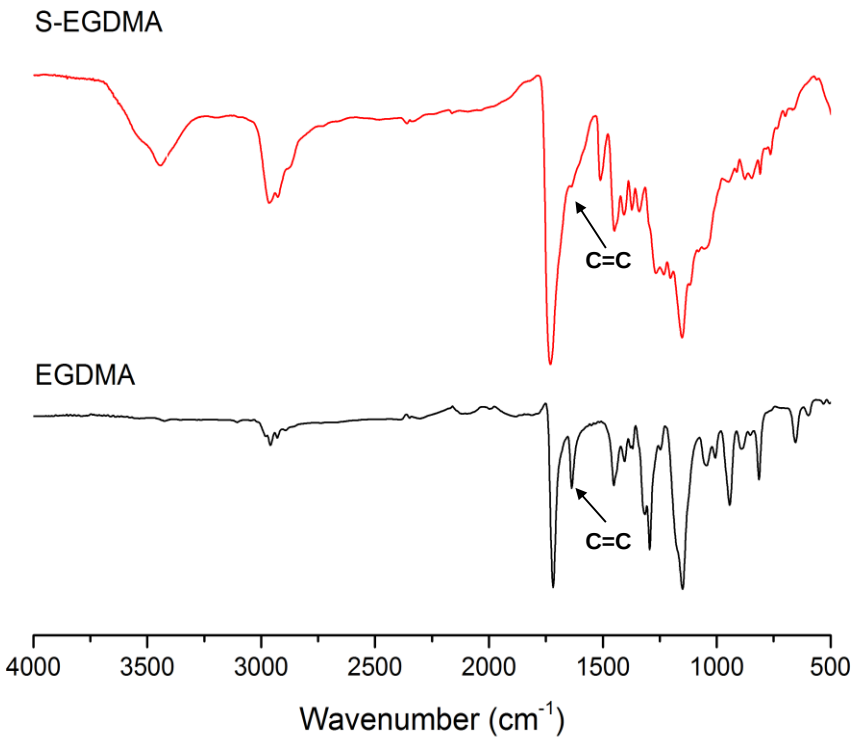

Figure 5.7 FT-IR spectra of EGDMA monomer, bottom, and after polymerization with sulfur, top. The reaction was carried out at a 1:1 mass ratio of sulfur to crosslinker, 5 wt.% ZnD_2 catalyst loading, at 135 °C. After polymerization there is a reduction in the signal at ~1650 cm^{-1} of the C=C stretching vibrations.

Differential scanning calorimetry (DSC) traces were recorded for when 0, 1 , and 5 % of ZnD_2 by mass was incorporated into the reaction (Figure 5.8). In the absence of ZnD_2, there is a melting transition for S_8 crystals at approximately 110 °C, which indicates the reaction without a catalyst is not complete. PXRD patterns (Figure 5.9) were also recorded to confirm the reaction between sulfur and EDGMA in the presence of ZnD_2. In parallel to the DSC traces, it is clear that with no ZnD_2, there are S_8 crystals

present indicating without ZnD_2 the resultant material is not amorphous, and the

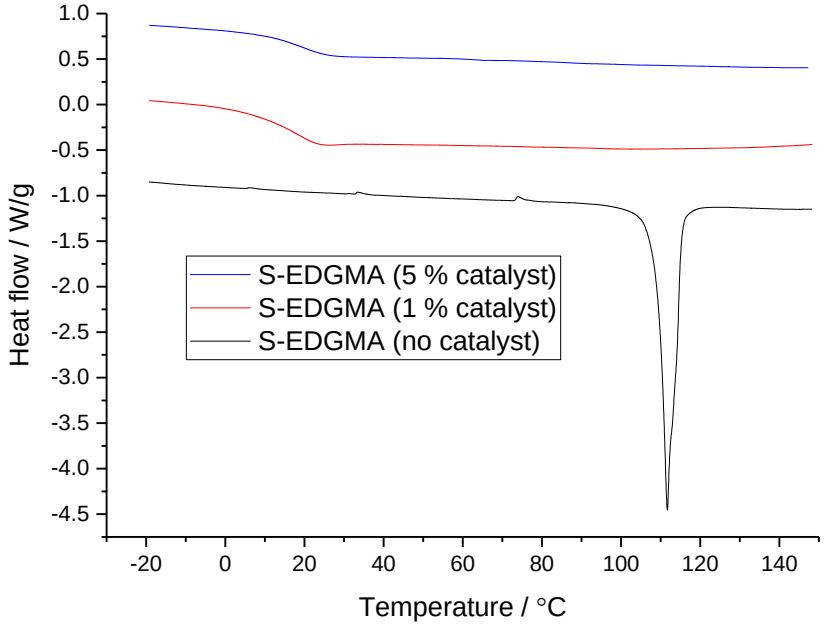

Figure 5.8 Offset DSC traces of sulfur reacted with EDGMA with 0, 1 and 5 % of ZnD_2 by mass. In the absence of ZnD_2 there is a melting transition for S_8 crystals at approx. 120 °C.

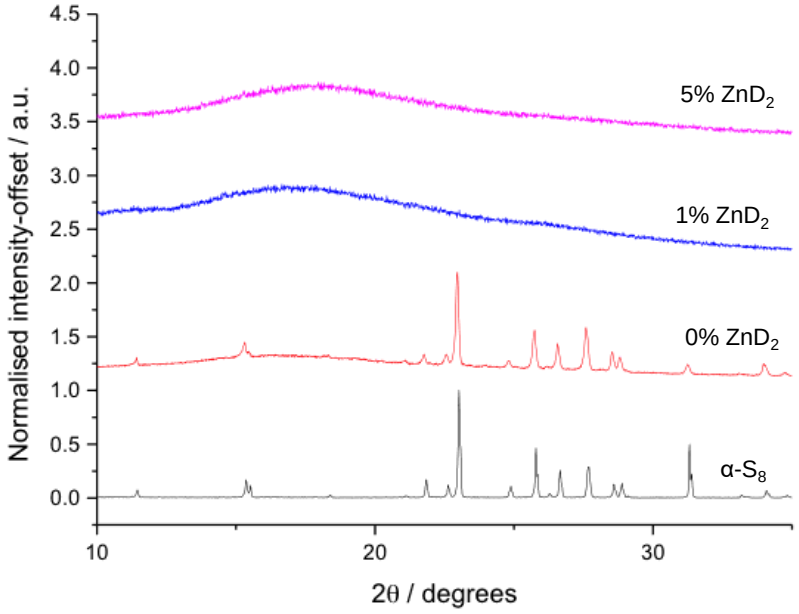

Figure 5.9 Offset PXRD patterns of sulfur reacted with EDGMA. In the absence of ZnD_2 S_8 crystals are present.

reaction has not gone to completion.

Figure 5.10 confirms by thermogravimetric analysis (TGA) that when S-EDGMA has

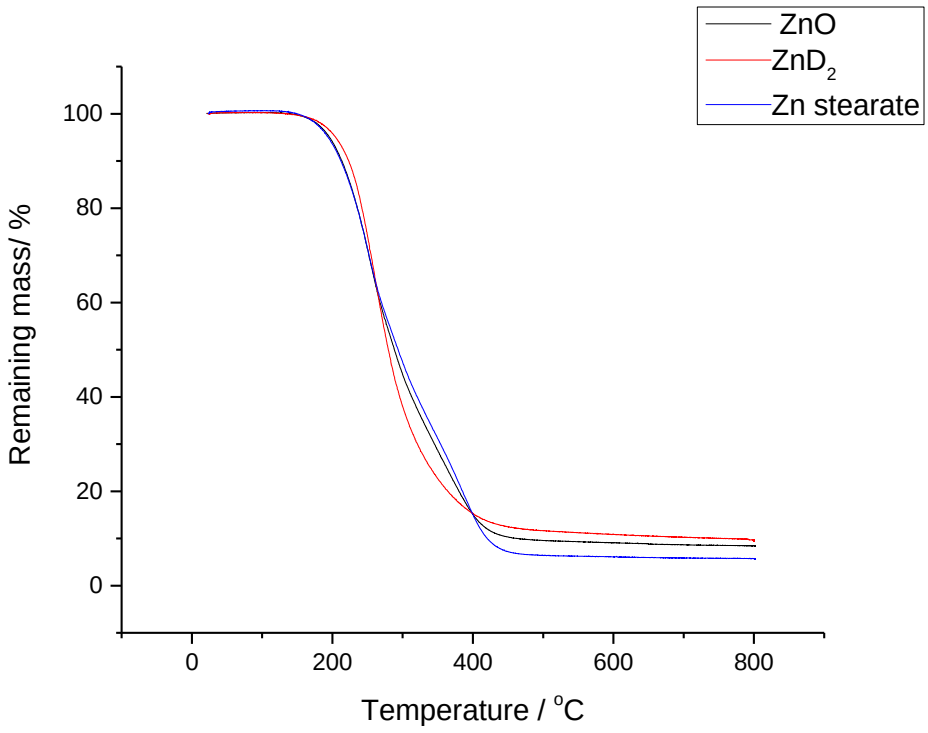

Figure 5.10 Thermogravimetric analysis, under nitrogen, of S-EGDMA copolymers (equal mass ratio of sulfur to crosslinker) with a range of potential catalysts, all at 1 wt.% loading.

reacted with a range of catalysts, all at 1 wt.% loading that they were thermally stable to 200 °C. This is similar thermal stability to other previous reported uncatalysted inverse vulcanisation reactions.

S-GBDA

Similar to EDGMA, when sulfur was reacted with GBDA, the reaction formed an inhomogeneous viscous liquid that never solidified even after curing for 10-14 hours. Therefore 1 and 5% ZnD_2 by mass was added to the reaction between sulfur and GBDA to see if polymerisation would proceed.

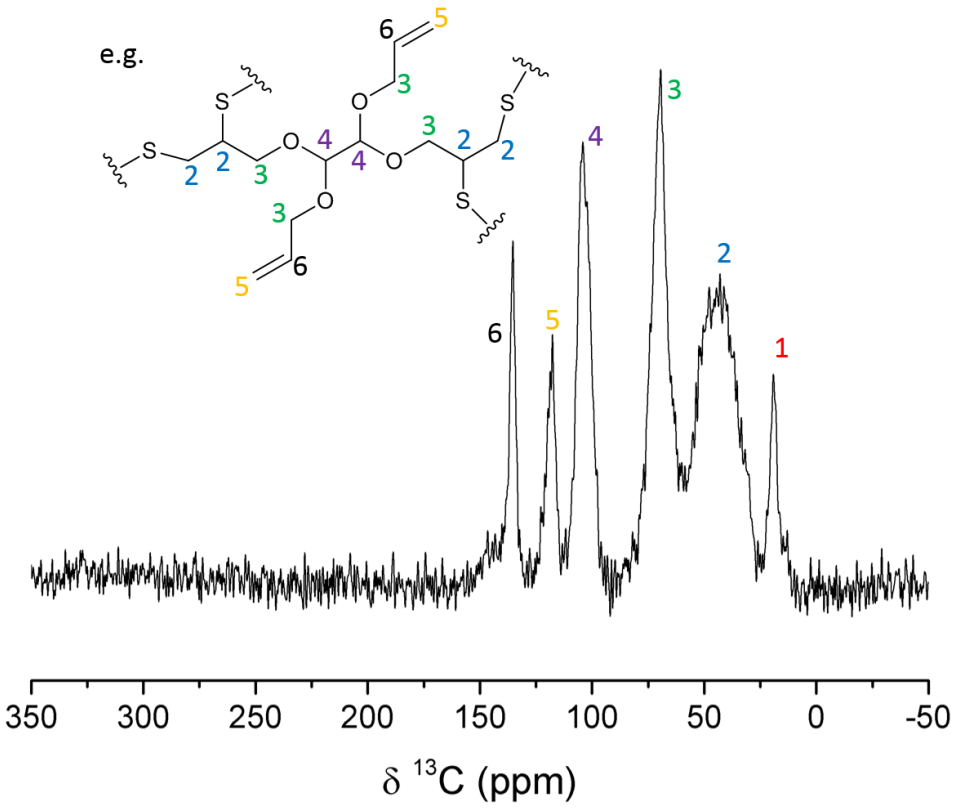

Figure 5.11 Solid state ^{13}C NMR spectra of GBDA after polymerisation with sulfur. Conditions: equal mass of sulfur and crosslinker, 1 wt.% ZnD_2 catalyst.

To confirm whether the reaction between sulfur and GBDA had been successful solid-state ^{13}C nuclear magnetic resonance spectroscopy (NMR) was recorded (Figure 5.11). Equal masses of both crosslinkers were reacted (1:1) with the addition of 1 wt.% ZnD_2. The spectrum shows the formation of a C-S bond **(2)**. However, there is still some significant C=C present **(5),** this indicates that this crosslinker has a relatively low reactivity compared to the other crosslinkers investigated. The signal at position **(1)** is unknown as no functional group is present in the structure of the crosslinker that would account for this signal. One hypothesis for this could be that some degree of

isomerisation has occurred, such as shifting the double bond position or proton migration, which may generate a primary alkyl group.

FT-IR spectra (Figure 5.12) recorded the GBDA monomer, S-GBDA with no ZnD_2 present and S-GBDA with 5% ZnD_2 by mass. However, there does not seem to be much reduction in the signal at ~1650 cm^{-1} which corresponds to C=C stretching. When examining the fingerprint region, there is a slight reduction in the alkene C-H bending modes ~550,900,100 cm^{-1}. The significant remaining C=C signals indicate that there has not been a complete reaction even when ZnD_2 is incorporated into the reaction, which supports the evidence recorded by solid-state ^{13}C NMR.

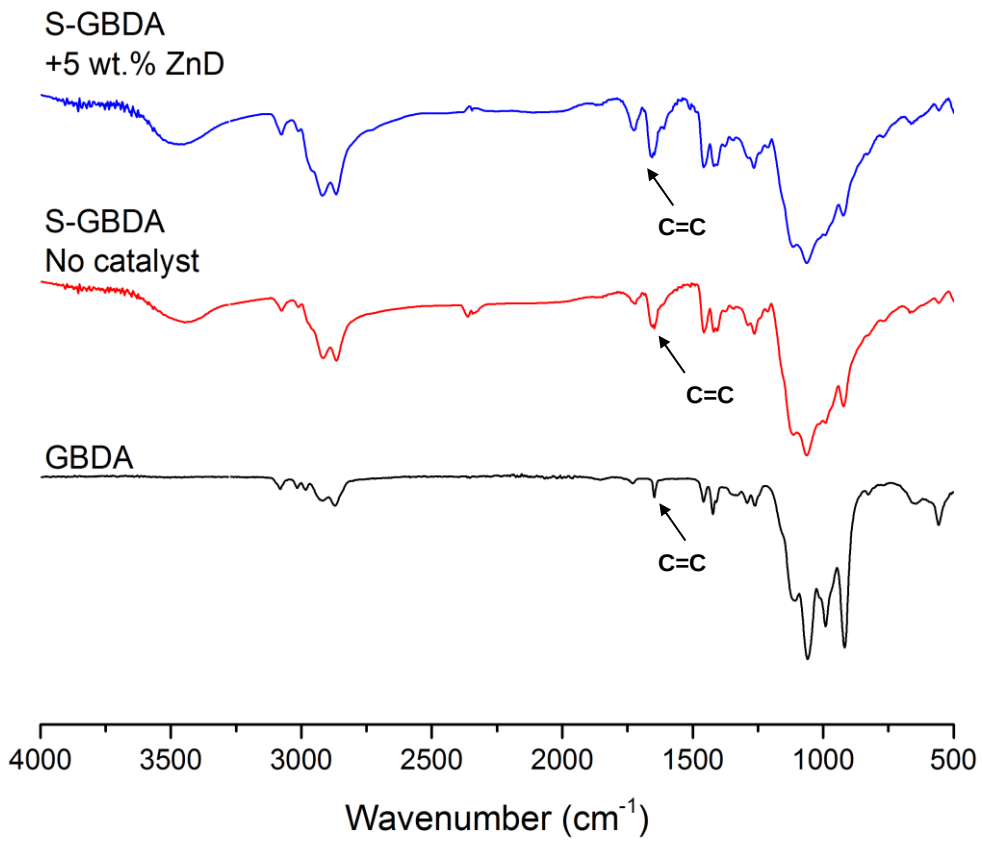

Figure 5.12 FT-IR spectra of GBDA monomer, bottom, and after polymerization with sulfur, top. The reaction was carried out at a 1:1 mass ratio of sulfur to crosslinker, at 135 °C.

Glass transition temperatures (Figure 5.13) were recorded as a function of catalyst loading for the polymerisation of sulfur with GBDA. Only very faint glass transition temperatures were detected; this made it difficult to record the glass transition temperatures, which is likely to cause the poor accuracy of the measurement. There is a slight decrease in glass transition temperature moving from 0% ZnD_2 loading to the 1% loaded sample. Then an increase in the 5% loaded sample, however, due to the poor reproducibility, this may not be significant. It should be noted that no S_8 melting transitions were detected for the reaction between sulfur and GBDA at 0, 1, and 5% of

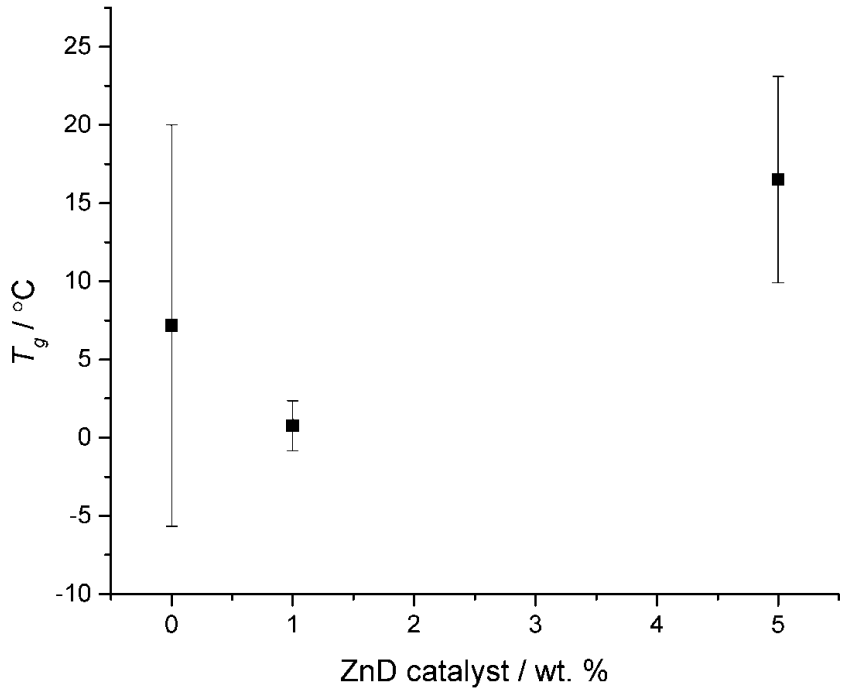

Figure 5.13 Glass transition temperatures recorded by differential scanning calorimetry (DSC) as a function of catalyst loading for the reaction of sulfur with GBDA. The reaction was carried out in a 1:1 mass ratio of sulfur to crosslinker, without catalyst, at 135 °C. Standard deviation is given for an average of three parallel reactions.

ZnD_2. However, for the reaction between sulfur and GBDA without the presence of ZnD_2, the reaction time was >36 hours; this led to noticeable sublimation of sulfur in the reaction vessel.

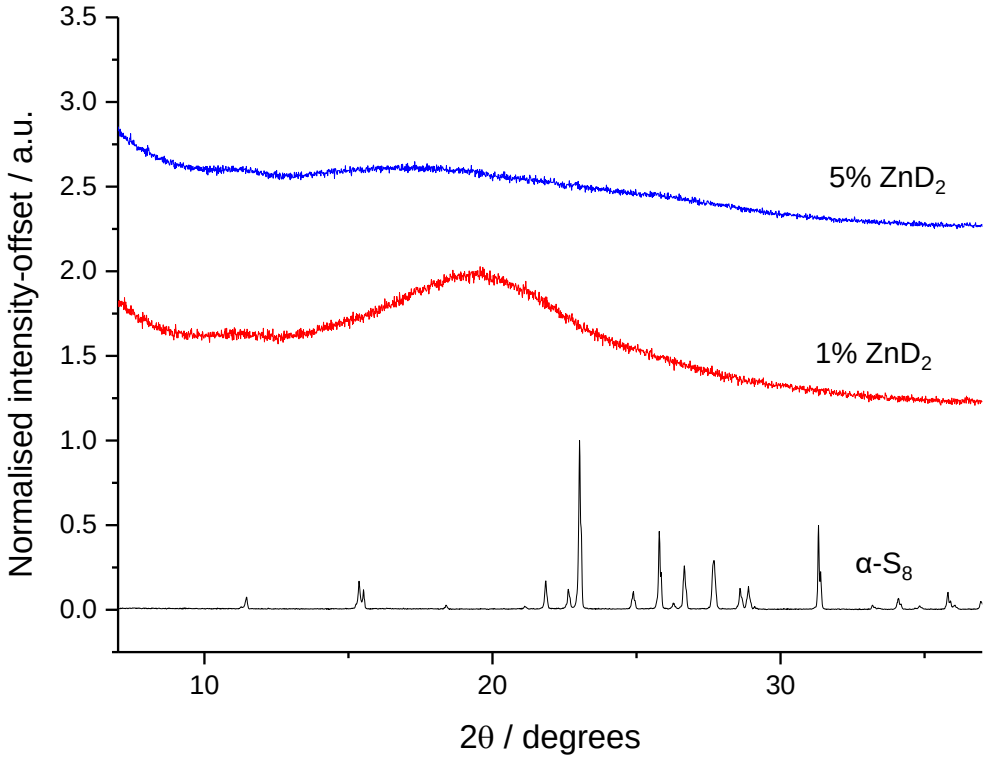

Figure 5.14 Offset PXRD patterns of sulfur reacted with GBDA with 1 and 5 % ZnD_2 by mass.

PXRD diffraction patterns (Figure 5.14) confirm that after the reaction between sulfur and GBDA there were no S_8 crystals present.

Like with other inverse vulcanised sulfur polymers, TGA (Figure 5.15) confirms that when 1 wt.% of ZnD_2 was added to the reaction between sulfur and GBDA, the resultant S-GBDA polymer was thermally stable up to 200°C.

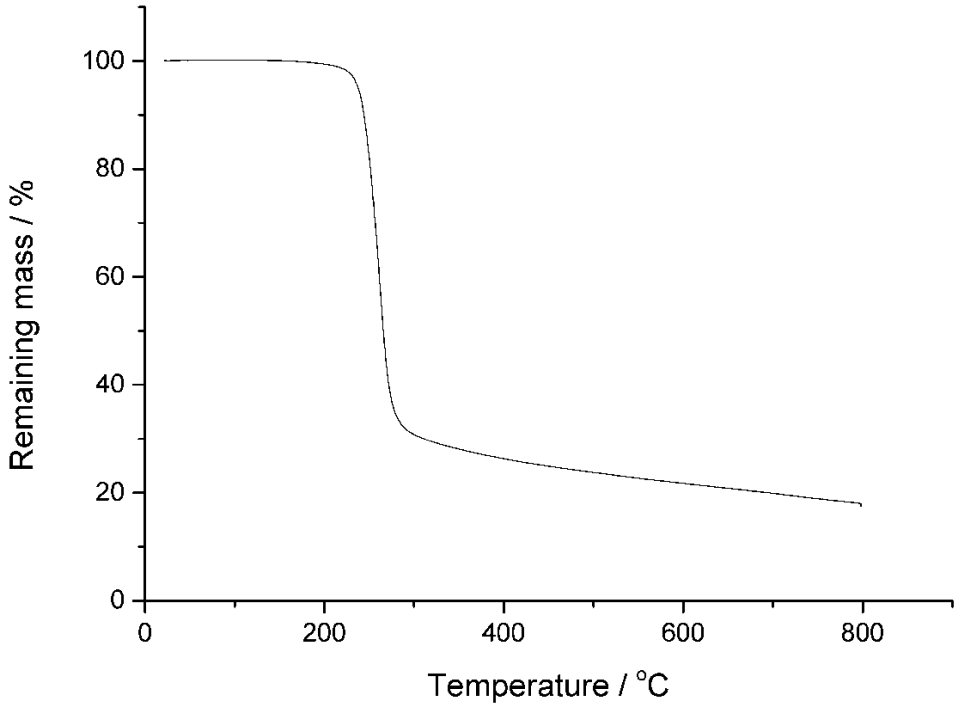

Figure 5.15 Thermogravimetric analysis, under nitrogen, of sulfur reacted with GBDA (equal mass ratio of sulfur to crosslinker) with 1 % ZnD_2.

One of the critical benefits of catalytic inverse vulcanisation has been the ability to bring crosslinkers that are unreactive to use, expanding the range of sulfur polymers for different functions. EDGMA, GBDA, and TVTCSi crosslinkers only reacted with sulfur in the presence of a catalyst. If the polymerisation is not complete, depolymerisation can occur, both DSC and PXRD can detect the presence of S_8. It was interesting to note that the crosslinkers that contained heteroatoms all had residual S_8 crystals present in the DSC and PXRD, but complete reaction occurred with the catalyst. One reason for this could be that the heteroatoms of these crosslinkers deactivate the vinylic positions. Using a catalyst could unlock the reactivity of acrylates, which don't react with sulfur on their own, opening up many new potential crosslinkers. Unlocking the reactivity of new crosslinkers allows more property control.

5.4.2.2 Crosslinkers newly reported in this work

S-VNB

The reaction between sulfur and 5-vinyldene-2-norbornene (VNB) had never been reported before. VNB was chosen as a potential crosslinker due to its similarities to previously reported 5-ethylidene-2-norbornene (ENB) (Chapter 2), to see if some parallels can be drawn between both of the resultant polymers.

Solid-state ^{13}C NMR spectra (Figure 5.16) was recorded of 5-vinylidene-2-norbornene (VNB) after polymerisation with sulfur. Equal masses of both crosslinkers were reacted (50:50) with the addition of 1 wt.% ZnD_2. This spectrum shows the formation of C-S bonds **(3)**, and the significant loss of C=C signal **(4)**. It should be noted that signal **(1)** arises from a small portion of VNB isomerising to 5-ethylidene-2 norbornene (ENB). The formation of C-S bonds and loss of C=C suggests

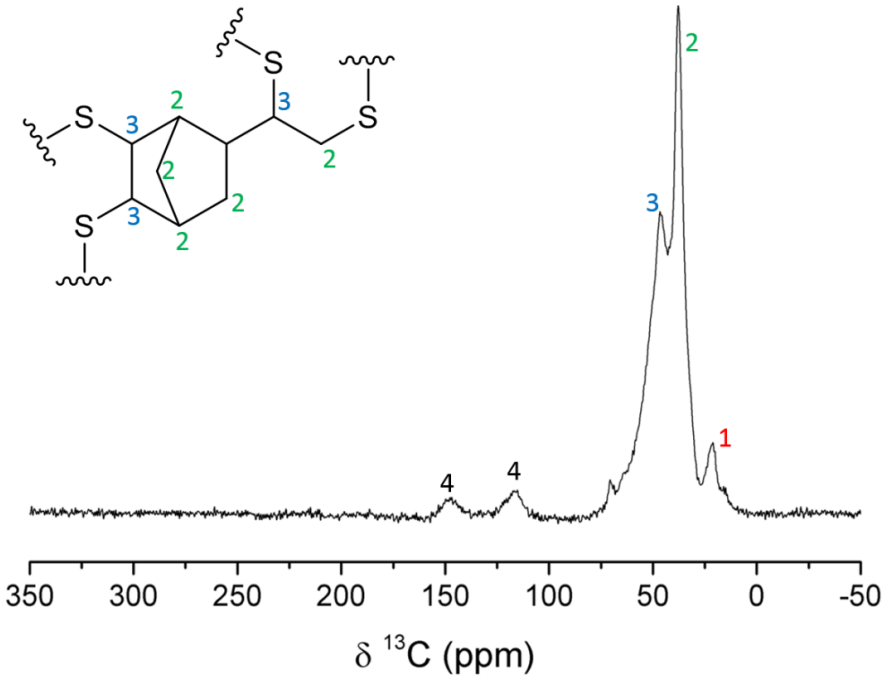

Figure 5.16 Solid state ^{13}C NMR spectra of 5-vinylidene-2-norbornen (VNB) after polymerisation with sulfur. Conditions: equal mass of sulfur and crosslinker, 1 wt.% ZnD_2 catalyst.

polymerisation has been successful.

FT-IR spectra (Figure 5.17) of VNB monomer, after polymerisation with sulfur and with the addition of catalyst, was recorded. Without ZnD_2, there is a reduction in signals at ~3100 cm^{-1} (C=C-H vibrations), as well as at ~1750 and 1650 cm^{-1}, of the two inequivalent C=C stretching positions. After the reaction between sulfur and VNB from the FT-IR spectra, there is still some remaining double bond character, and the C=C position at ~1750 cm^{-1} appears to react more readily than the C=C position at 1650 cm^{-1}. When the fingerprint region was examined, there is reduction of the alkene C-H bending modes at ~750, 900, 1000 cm^{-1}. When ZnD_2 is incorporated into the reaction there is almost complete conversion of both double bonds.

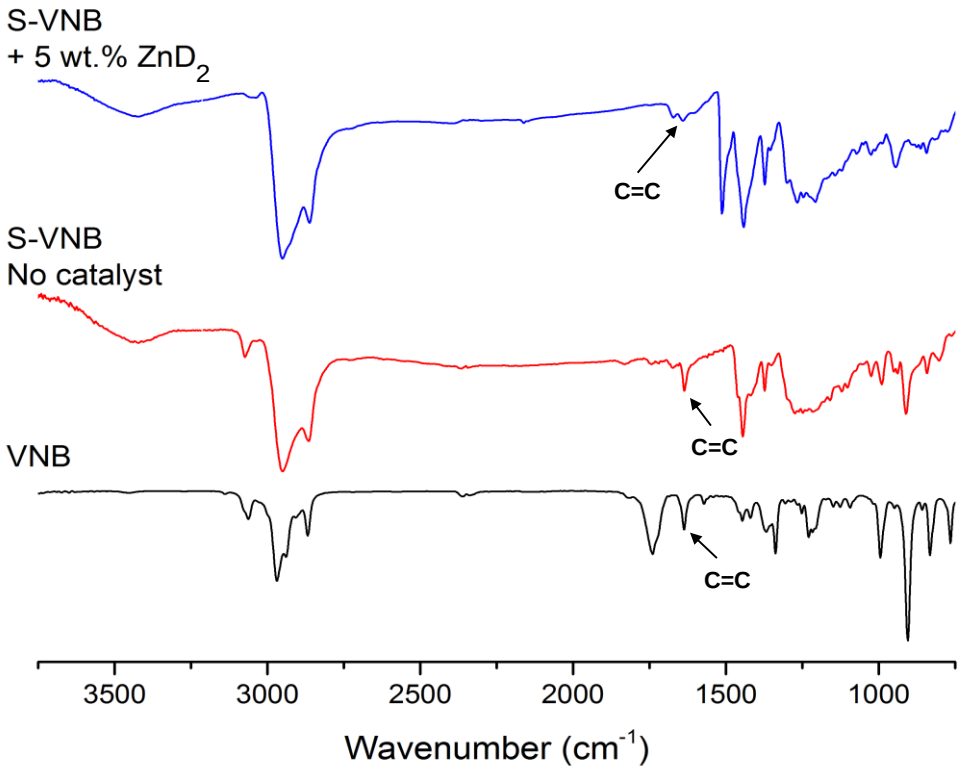

Figure 5.17 FT-IR spectra of VNB monomer (bottom), after polymerisation with sulfur with no catalyst (middle) and after polymerisation with sulfur and the addition of 5 wt. % of ZnD_2.

DSC recorded glass transition temperatures (Figure 5.18) as a function of catalyst loading for the polymerisation of sulfur with VNB. Figure 5.18 shows that there is a slight increase in glass transition temperature for the 1 wt.% ZnD_2 sample, compared to the sample without ZnD_2 incorporated into the reaction. When the mass of ZnD_2 is increased to 5%, there is a significant reduction in glass transition temperature. This may be due to excess loading of catalyst where the catalyst is not providing additional benefit to the reaction and is potentially plastising the material, as a small molecule additive. The glass transition temperatures recorded for the reaction between sulfur and VNB with no ZnD_2 present were faint, which may explain the large standard deviation. However, for a 1 and 5% loading of ZnD_2 by mass, the glass transition temperatures were more pronounced and easier to record. No melting transition for S_8 crystals was recorded in the DSC traces for the reaction of sulfur with VNB, and no S_8

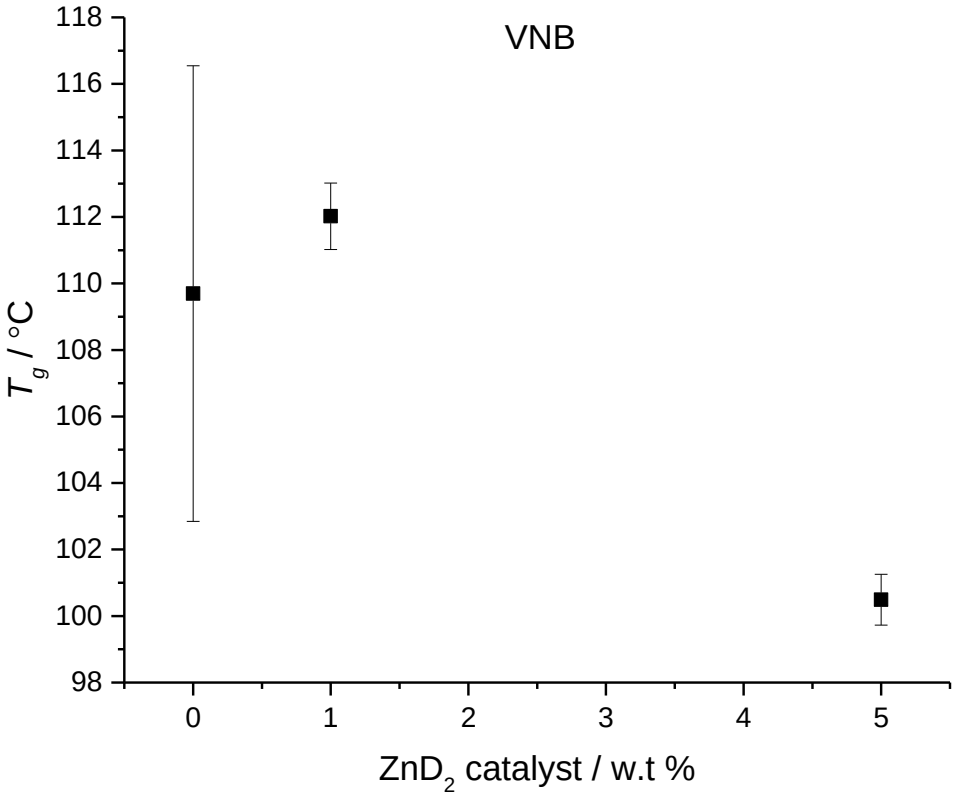

Figure 5.18 Glass transition temperatures recorded by DSC as a function of catalyst loading for the polymerisation of sulfur with VNB. Standard deviations are given for the average of three parallel reactions.

crystals were recorded by PXRD (Figure 5.19) for 0,1 ,and 5 % loading of ZnD_2, suggesting the resultant material is amorphous.

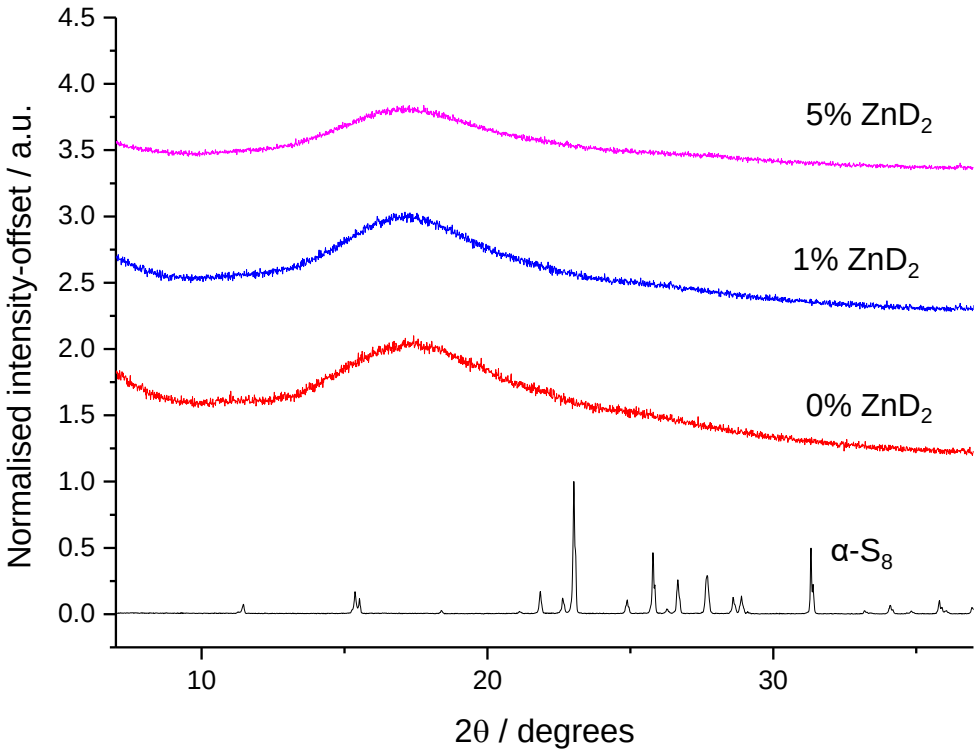

Figure 5.19 Offset PXRD patterns of sulfur reacted with VNB with 1 and 5 % ZnD_2 by mass.

TGA (Figure 5.20) also confirms that like with other inverse vulcanised sulfur polymers, when ZnD_2 is incorporated into the reaction they were thermally stable to 200 °C.

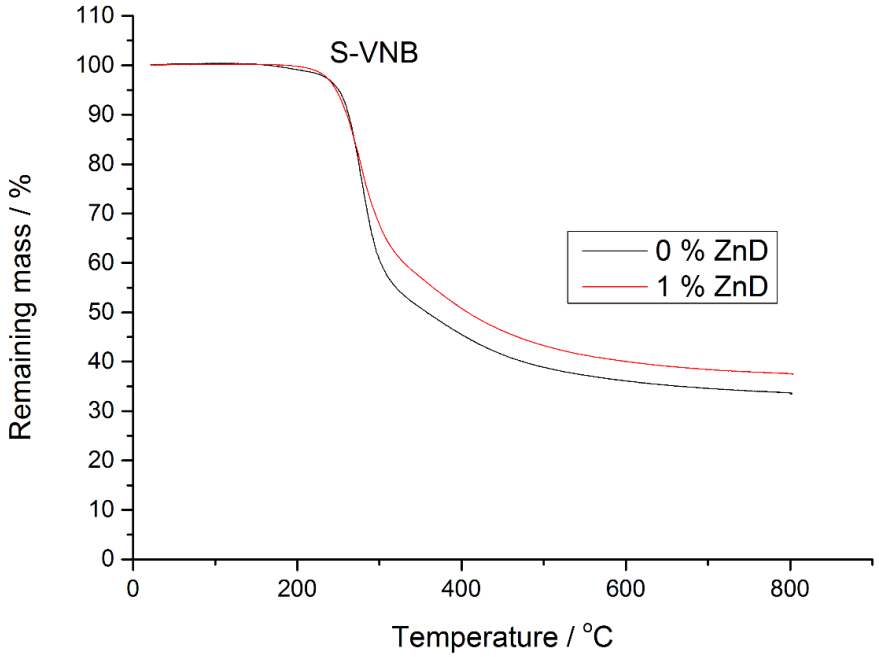

Figure 5.20 Thermogravimetric analysis, under nitrogen, of S-VNB copolymers (equal mass ratio of sulfur to crosslinker) with and without catalysis by Zn diethyldithiocarbamate.

5.4.2.3 Previously reported crosslinkers that benefit from catalytic inverse vulcanisation

S-DCPD

S-DCPD was previously reported by Hasell *et.al* in 2017 and is a polymer that has been under investigation throughout this thesis.[15] Reports show that when sulfur reacts with DCPD, the resultant material is an amorphous, highly crosslinked network that is impervious to most common organic solvents.[15] Therefore, ZnD_2 was added to the reaction to see if this could lower the temperature of the reaction, improve the physical properties further and increase reaction time.

Glass transition temperatures (Figure 5.21) were recorded from DSC as a function of catalyst loading for the polymerisation of sulfur with DCPD. S-DCPD can be reacted without ZnD_2 at two different temperatures to form a linear polymer were reaction

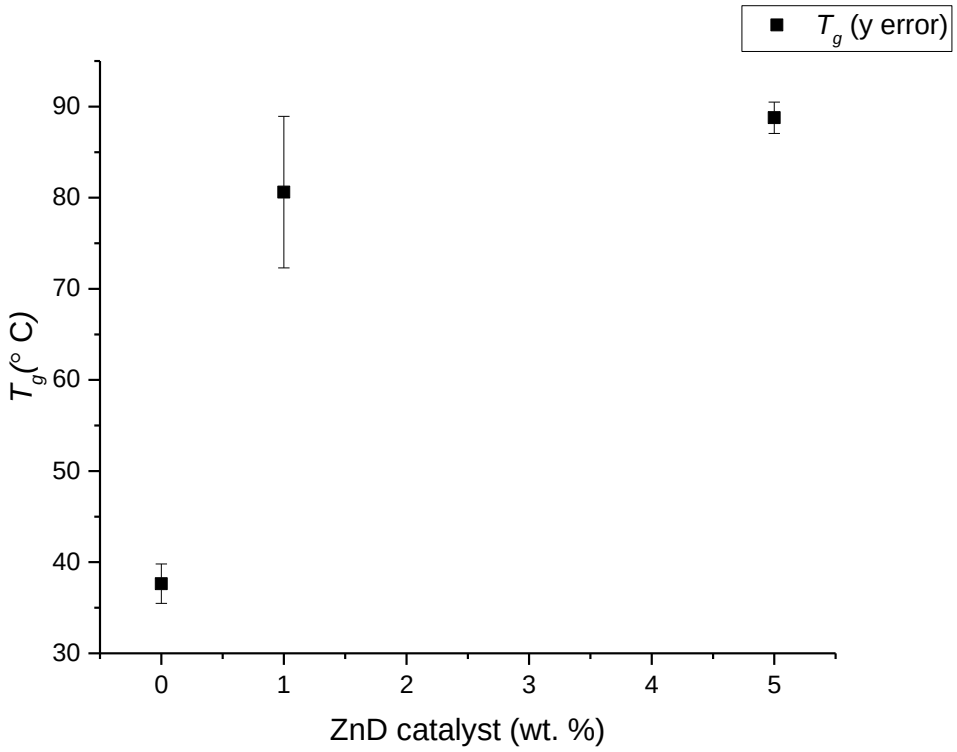

Figure 5.21 Glass transition temperatures (from DSC) as a function of catalyst loading for the polymerization of sulfur with DCPD. The reaction was carried out at a 1:1 mass ratio of sulfur to crosslinker, without catalyst, at 135 °C, and in triplicate. Standard deviation is given for the average of three parallel reactions.

only occurs at one double bond (~140°C) and a highly crosslinked network (~165°C) were both double bonds react.[15] Thus, at the temperature these reactions are conducted at (135°C); without catalyst, we would expect a linear polymer. When just 1 wt.% of ZnD_2 is added to the reaction, there is a significant increase in glass transition temperature for the 1% catalyzed sample. There is then a slight increase when the catalyst loading is increased to 5% by mass. This suggests that when the catalyst is added to the reaction, the physical properties of the polymer are significantly altered, and potentially reaction at both double bonds may have occurred.

PXRD patterns (Figure 5.22) recorded to confirm that there were no S_8 crystals present after the reaction between sulfur and DCPD.

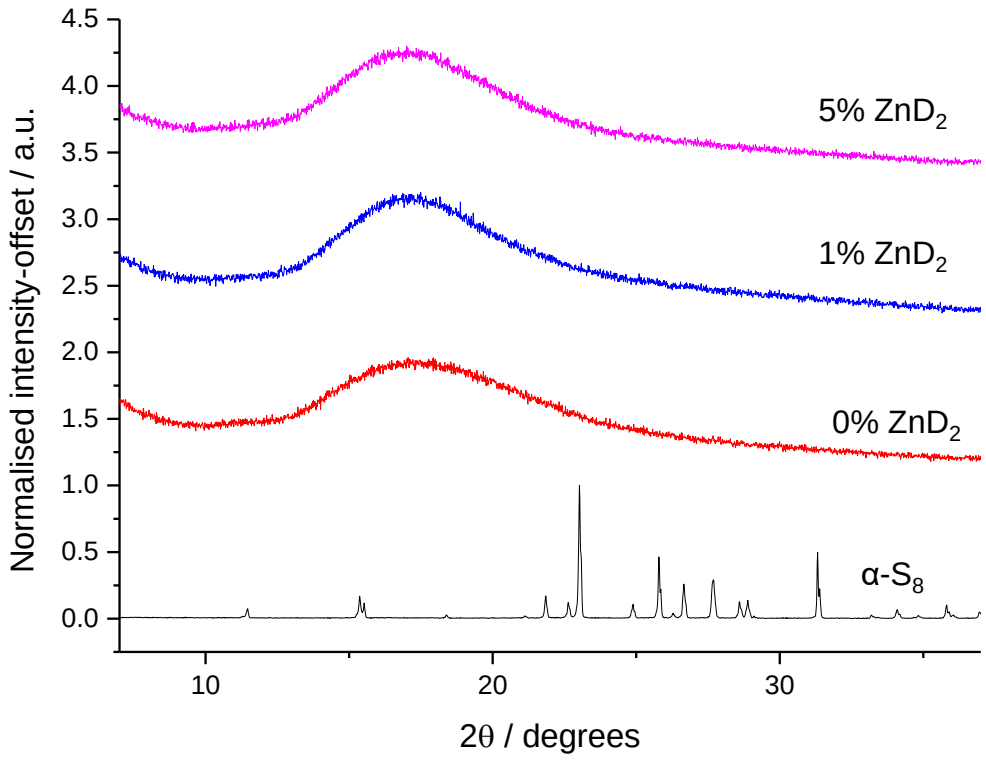

Figure 5.22 Offset PXRD patterns of sulfur reacted with DCPD with 0,1 and 5 % ZnD_2.

S-limonene

Chalker *et al.* first reported sulfur-limonene and the material was promising due to it being bioderived and cheap.[16] However, as mentioned previously, it lacked shape persistency. Equal masses of both sulfur and limonene (1:1) were reacted with 0,1, and 5% ZnD_2.

Glass transition temperatures (Figure 5.23) were recorded by DSC as a function of catalyst. There is a slight decrease in the glass transition temperature moving from 0%

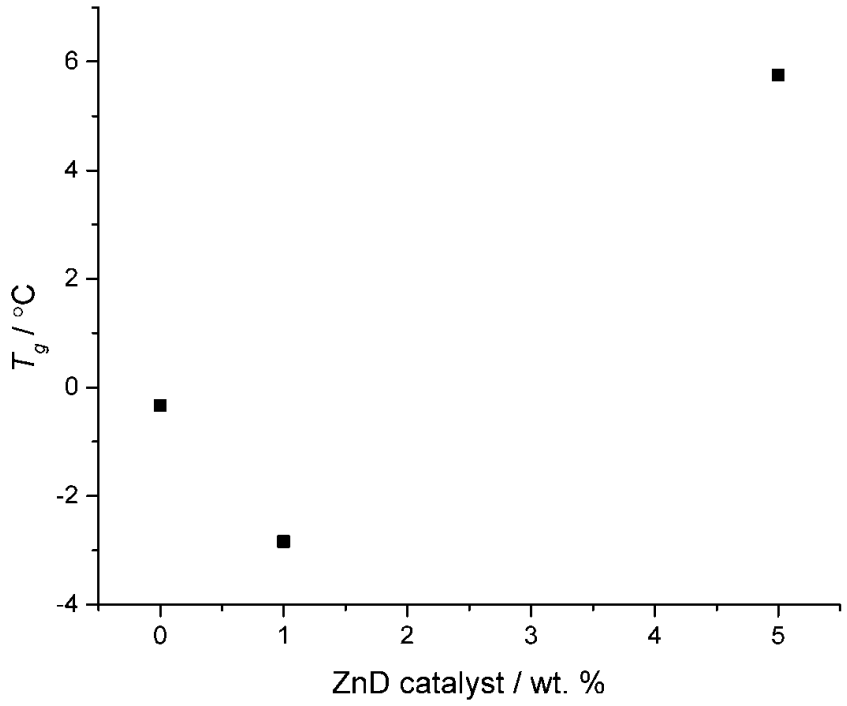

Figure 5.23 Glass transition temperature (from DSC) as a function of catalyst loading for the polymerization of sulfur with limonene. The reaction was carried out at a 1:1 mass ratio of sulfur to crosslinker.

to 1% ZnD_2 and then an increase in the 5% loaded sample. The reasons for this are unknown.

One of the main issues with S-limonene that stops it being useful as a functional material is the lack of shape persistency. S-limonene was loaded with 0, 1, and 5% catalyst and moulded into shape to investigate if shape persistency improved (Figure 5.24). Limonene is known to undergo hydrogen abstraction, form by-products (cymene), and produce only low molecular weight polysulfides rather than high molecular weight shape persistent polymers.[10,11,16] As can be concluded from the photographs, after 24 hours shape persistency was lost in all samples (Figure 5.24). However, the sample with 5% catalyst loading was less ‘tacky’ to touch and deformed

less, therefore adding catalyst did show some improvement to the overall shape persistency.

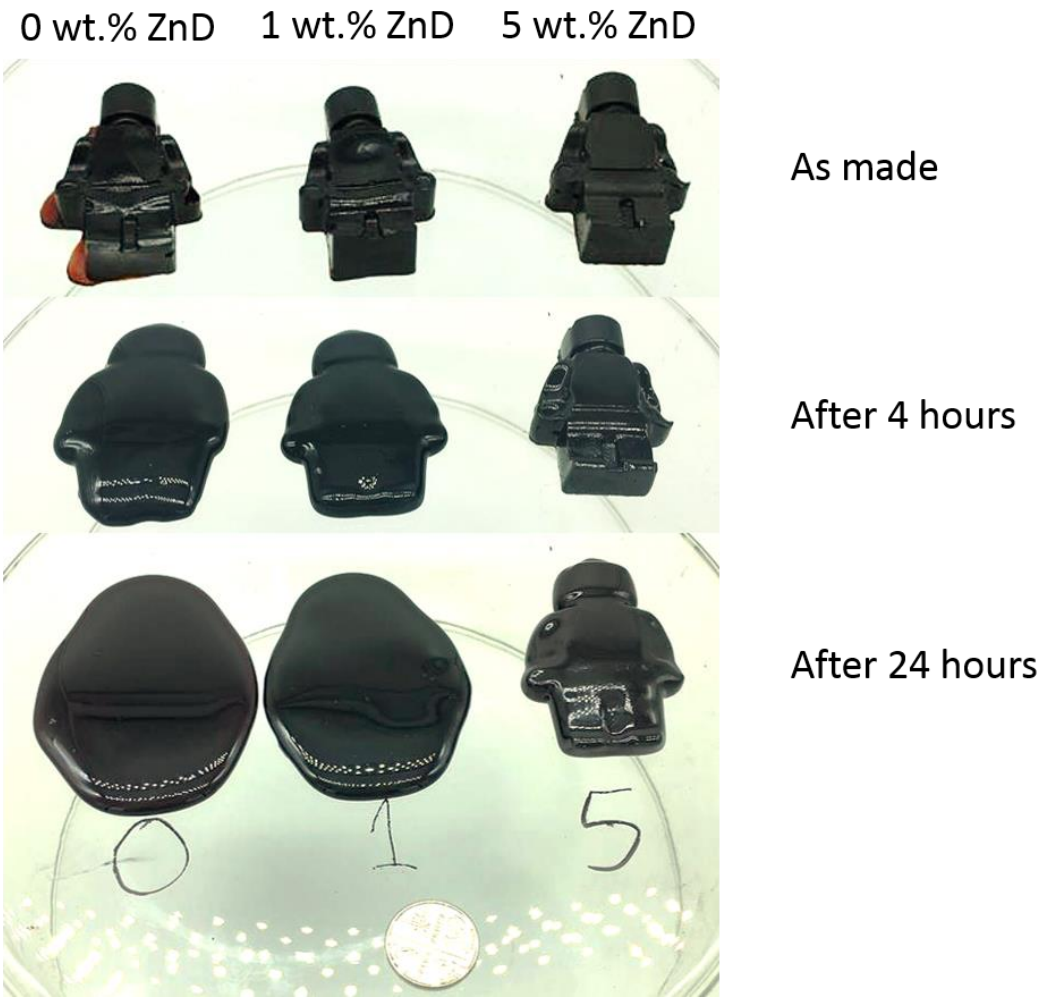

Figure 5.24 S-Limonene polymers made by reacting an equal mass of sulfur with limonene, with and without catalyst (Zn Diethyldithiocarbamate).

S-limonene with 5% ZnD_2 was able to undergo compression with a 200 g weight with no noticeable effects after 5 minutes (Figure 5.25). However, when left under compression for 24 hours, the sample is noticeably deformed. Un catalysed samples are fully deformed within 5 minutes under compression (Figure 5.25). Again, with the addition of ZnD_2, there is some improvement to shape persistency.

Figure 5.25 S-Limonene polymer catalysed by Zn Diethyldithiocarbamate undergoing compression with a 200 g weight.

S-linseed oil

Glass transition temperatures (Figure 5.26) were recorded by DSC as a function of catalyst. There is a slight decrease in glass transition temperature moving from 0% to 1% ZnD_2 and then an increase in the 5% loaded sample. The reasons for this are

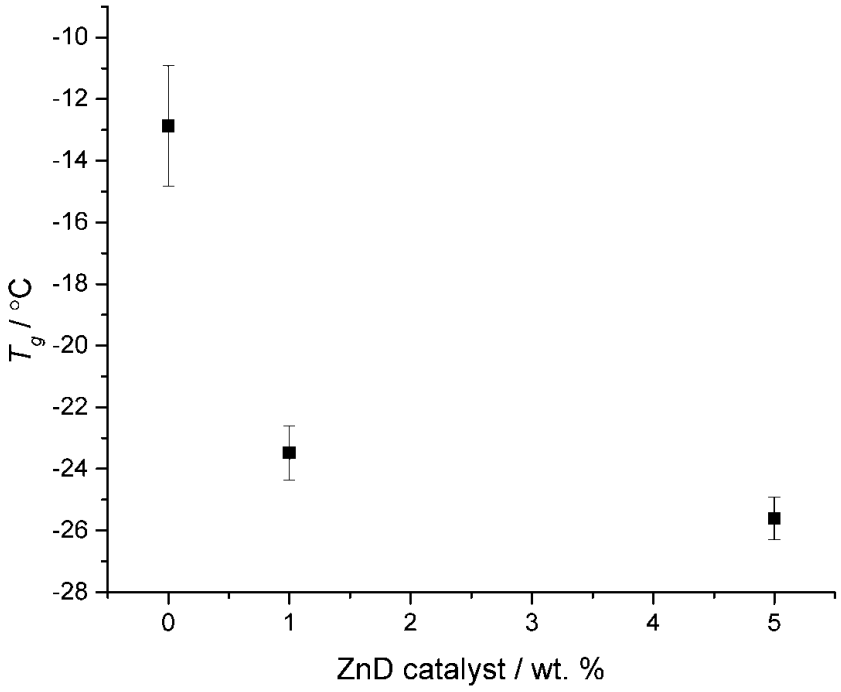

Figure 5.26 Glass transition temperature (from DSC) as a function of catalyst loading for the polymerisation of sulfur with linseed oil. The reaction was carried out at a 1:1 mass ratio of sulfur to crosslinker.

unknown. A melting transition for S_8 crystals was detected for the reaction between sulfur and linseed oil with no ZnD_2, however, no melting transitions were detected when 1% and 5% were added to the reaction.

PXRD patterns (Figure 5.27) record the diffraction of S_8 crystals in both the 0% and 5% ZnD_2 samples for the reaction between sulfur and linseed oil.

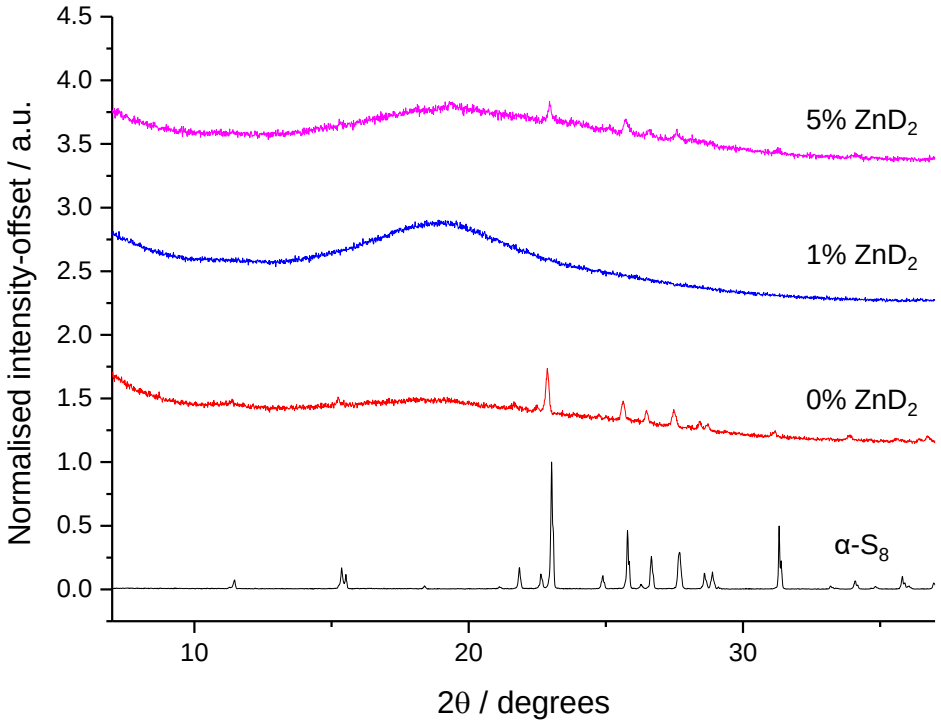

Figure 5.27 Offset PXRD patterns of sulfur reacted with linseed oil with 0,1 and 5 % ZnD_2.

5.4.2.4 Summary of S_8 crystals detected by PXRD and DSC

DSC is used to determine the melting transition of S_8 crystals present after the reaction between sulfur and a crosslinker. If no S_8 crystals can be detected, this suggests that the reaction has gone to completion. Table A5.1 (Appendix) summarises the polymers discussed in this chapter and the whether S_8 melting transitions were detected by DSC.

Alongside DSC, PXRD is another method to confirm whether S_8 crystals are present in the resultant materials by detecting the diffraction pattern of crystalline S_8. Table A5.2 (Appendix) summarises the polymers discussed in this chapter and whether the S_8 melting transitions were detected by PXRD.

5.4.3 Increased rate of reaction

Overall, the catalysed reactions required significantly less time to reach completion at a lower temperature (Appendix, Figure A5.3) than most previous reported inverse vulcanisation reactions.[15,16,17] Reducing both the reaction times and temperatures of these polymers is significant if the reactions are ever scaled up for bulk applications.[4] The time is taken from the start of the reaction, until solidification of the reaction mixture causes the stirrer bar to cease is recorded for all crosslinkers (Appendix, Figure

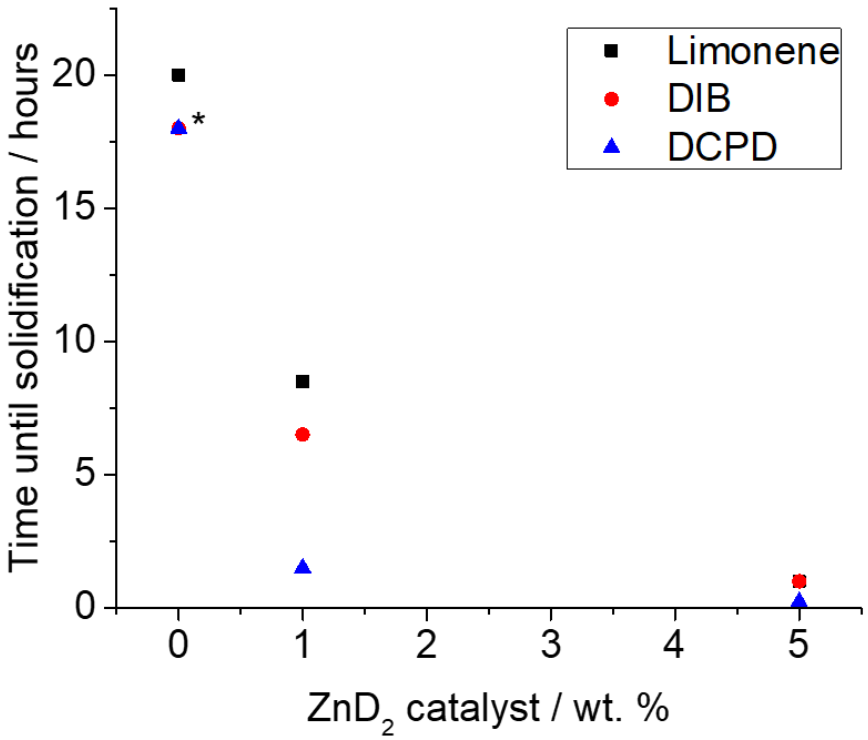

Figure 5.28 Reaction time plotted against catalyst loading at 135°C *Uncatalysed DCPD and DIB took between 12 to 14 hours, plotted as 18 hours (unobserved).

A5.3). When recording the times, the reactions were monitored for the first hour and then in half-hour intervals for the first 12 hours, then checked again after 24 hours;

therefore, some reaction times are listed between 12 and 24 hours. The general trend is, as the % of ZnD_2 is increased, the time it took for the solidification of the reaction decreased (Appendix A5.3 and Figure 5.28).

Figure 5.29 shows the yield of S-DIB, S-DCPD, and S-VNB when the reaction vessel was open to make a direct comparison to when no catalyst is added to the reaction. As the catalyst is added, the yield of the reaction also increases; the increased reaction rate

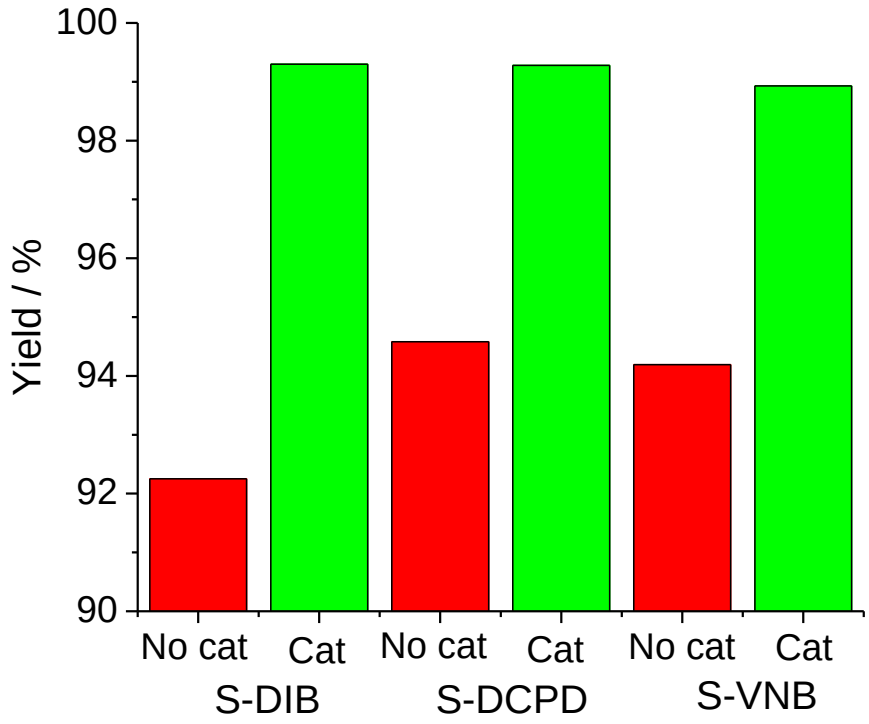

Figure 5.29 Yield of open reaction performed at 135°C, without ZnD_2 (red) and with ZnD_2 (green).

corresponds to a higher yield. It is important to note in an open reaction vessel, there will also be a gradual loss of mass by evaporation of the monomers. Figure 5.30 shows the investigation of the effect of the catalyst on reaction yield at a higher temperature in comparison. Here, sulfur and DCPD was reacted at a temperature of 160 °C with stirring in a 40 mL open glass vial for 12 hours. This shows that even at reactions that are carried out at a higher temperature, the catalysis provides a benefit to the yields.

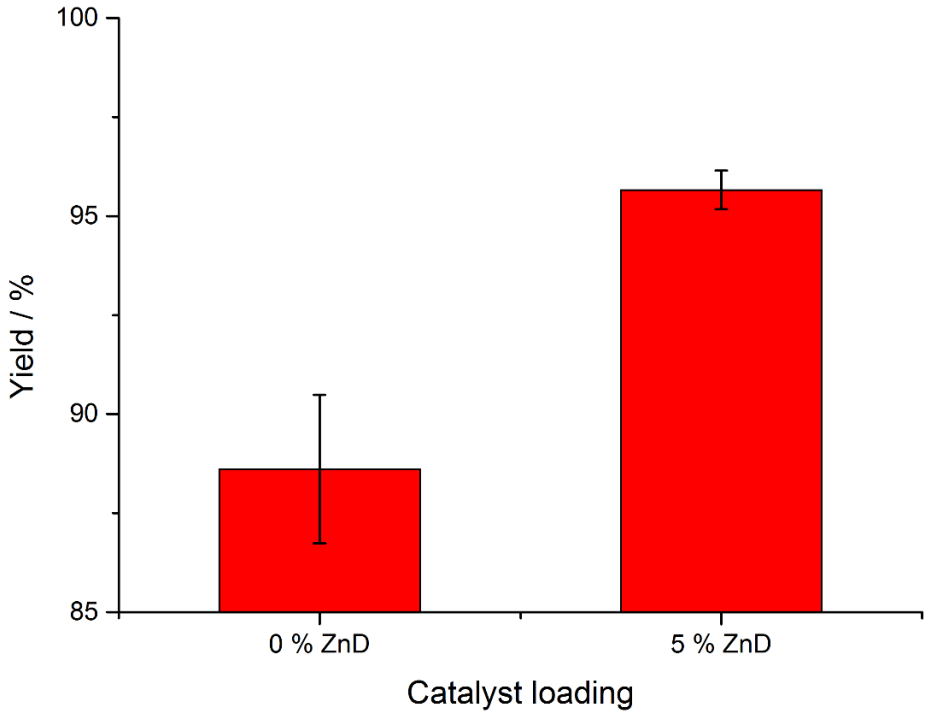

Figure 5.30 Investigation of the effect of catalyst on reaction yield at higher temperatures. The crosslinker used was DCPD, and the crosslinker to sulfur mass ratio was 1:1 (5 g each), reacted at 160 °C with stirring in a 40 mL open glass vial, for 12 hours.

5.4.4 Prevention of H_2S production during polymerisation

As discussed in Chapter 2, the production of toxic H_2S gas as a by-product for inverse vulcanisation reactions has been reported.[3,18] Therefore, to test this, a series of reactions were performed both with and without catalyst at the reaction temperatures of 135 °C for comparison (Figure 5.31). The catalysed reactions were found to produce up to 7 times less H_2S (Figure 5.31). However, the small amount of H_2S produced is likely due to the lower reaction temperatures, as high reaction temperatures are known to produce H_2S and thiols in conventional vulcanisation.

The reaction between sulfur and limonene without a catalyst is ran at a temperature of 180 °C. Therefore, both catalysed and non-catalysed reactions were performed at 180 °C for comparison. Even when both reactions were performed at the same temperature significantly less H_2S is produced.

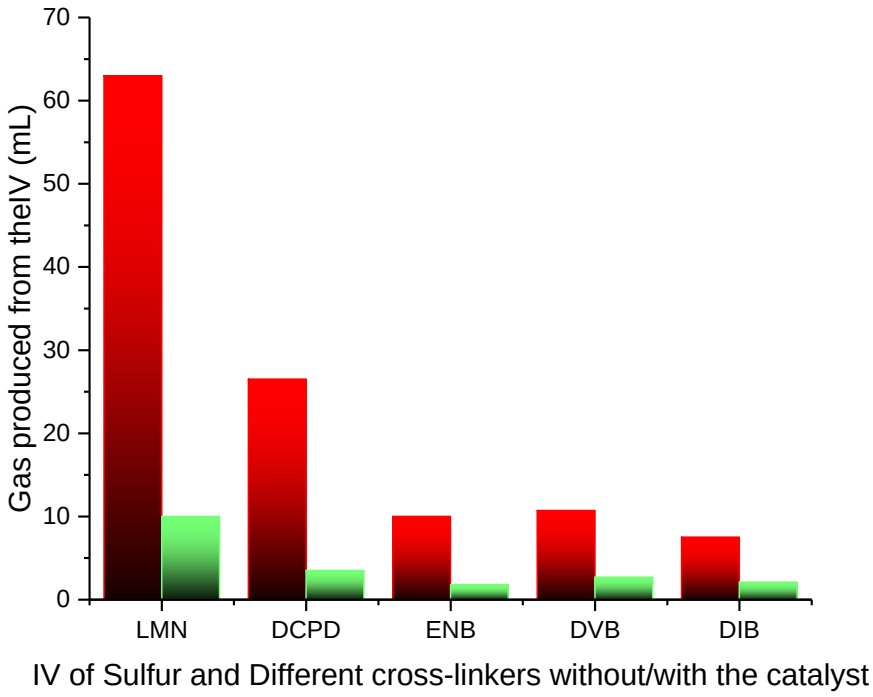

Figure 5.31 Investigation of the effect of catalyst on reaction yield at higher temperatures. The crosslinker used was DCPD, and the crosslinker to sulfur mass ratio was 1:1 (5 g each), reacted at 160 °C with stirring in a 40 mL open glass vial, for 12 hours.

The reaction between sulfur and limonene with a catalyst generate 63 mL of H_2S gas, similar to other reported values.[3] When 1 wt.% of the catalyst is added to the reaction, only 10 mL of gas is produced in comparison. However, the former reaction was

carried out at 180 °C 15 minutes, and the latter were carried out at 135 °C for 50 minutes. Similarly, the reaction between sulfur and DCPD was carried out at 165 °C for 27 minutes, and the reaction produced 26.3 mL of gas. When 1 wt.% of catalyst was added to this reaction at 135 °C for 45 minutes, the amount of gas produced was reduced to 3.5 mL. The generation of H_2S gas is dependent on the presence of α-proton of allyl groups and related to the reaction temperature. Therefore, with those crosslinkers without α-proton of allyl groups (e.g. DVB, DIB), lower amounts of gas were released, and only at the beginning of the reaction, were there not any gas generated after the first 3-5 min, especially for the reactions with catalysts. ENB is more reactive than DCPD, and as a result, requires lower temperatures, producing less H_2S. In the cases only small amounts of gas were produced (few mL from 10 g reactions), the recorded volume may be partly the result of the desorption of gases and moisture dissolved in the reactants, because of heating. In the samples, more significant amounts of gas were produced (DCPD and limonene without catalyst), the production of H_2S was confirmed by exposing a H_2S detector to the gas produced.

To compare the volume of gas produced at higher reaction temperatures, the volume of gas produced during the reaction between sulfur and limonene, with and without catalyst was monitored (Figure 5.32). Even at a higher reaction temperature of 180 °C, there is significantly less H_2S produced.

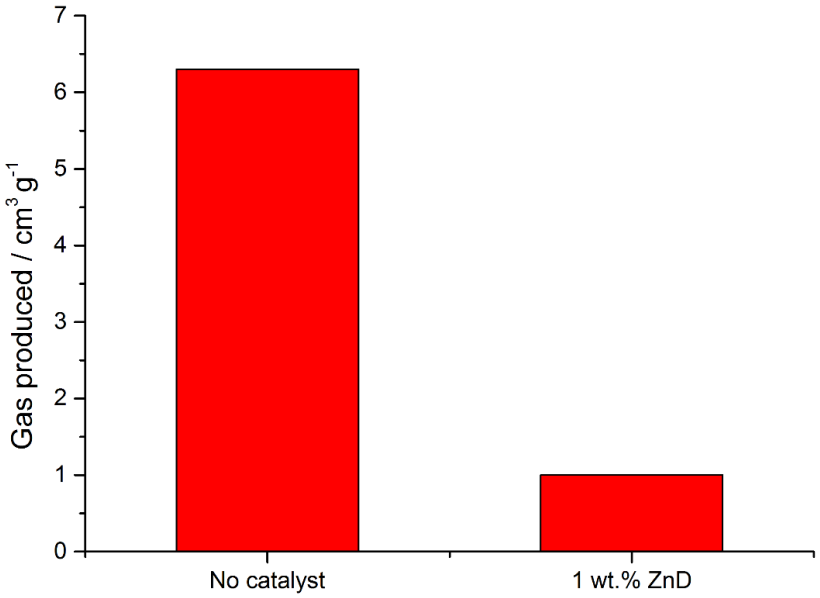

Figure 5.32 Volume of gas produced during reactions of sulfur with limonene, with and without catalyst. Both reactions were at an equal mass ratio of sulfur to crosslinker, at 180 °C.

5.4.6 Mechanism

The mechanism of uncatalysed conventional vulcanisation remains complex and challenging to understand. Despite being implemented in the industry for many years, the mechanism is still hard to characterise and remains complex. As discussed in Chapter 1, the most agreed pathway in literature for conventional vulcanisation is hydrogen abstraction of the α hydrogen adjacent to the C=C, which leads to crosslinking by proton substitution with sulfur atoms (Figure 5.33).

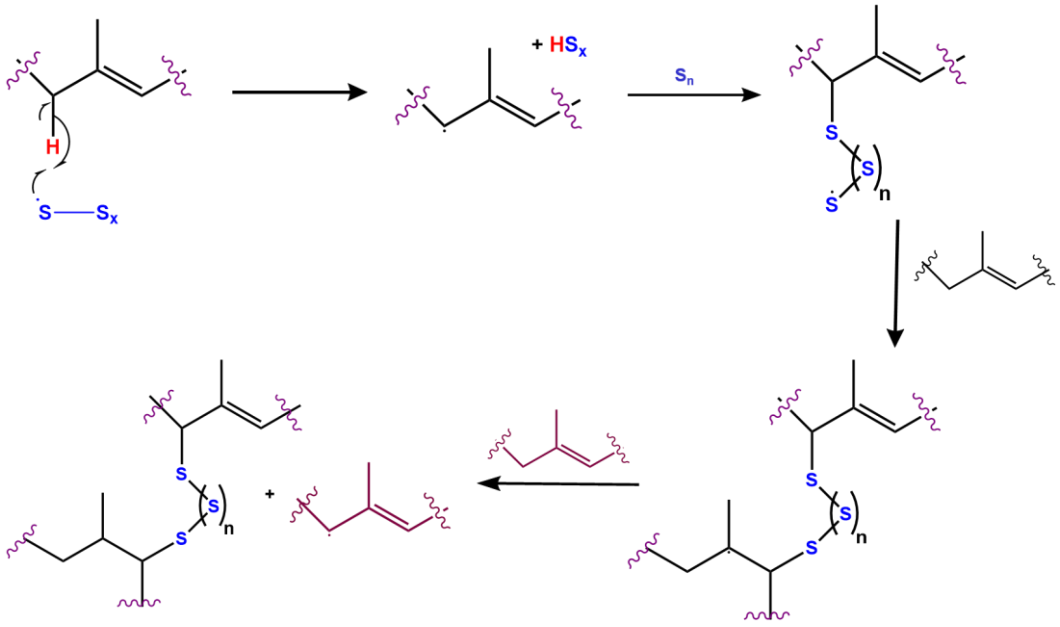

Figure 5.33 Reaction scheme of conventional vulcanisation. Crosslinking by proton substitution via hydrogen abstraction.

It is still not agreed whether inverse vulcanisation proceeds by a radical or an ionic pathway; this depends on whether the S_8 ring undergoes homolytic or heterolytic fission. The temperature at which homolytic fission occurs has been reported between 140 °C to 181 °C, with some polymerisations reported at lower temperatures. Pyun and co-workers first reported that the polymerisation of molten sulfur is above the floor temperature, 159°C.[17] This may be why most inverse vulcanisation reactions are reported to be performed over 160 °C.[15,16,17] Alike in conventional vulcanisation the α proton of the allyl group is very reactive and it has already been reported that thiyl radicals can abstract this α-proton during vulcanisation.

Therefore, uncatalysed inverse vulcanisation is likely to undergo a mechanism that is initially triggered by hydrogen abstraction. The thiyl radicals may abstract a proton to

generate carbon radicals on the C=C double bond and then further initiate polymerisation (Figure 5.34).

For catalytical inverse vulcanisation, a stepwise mechanism is suggested (Figure 5.35).

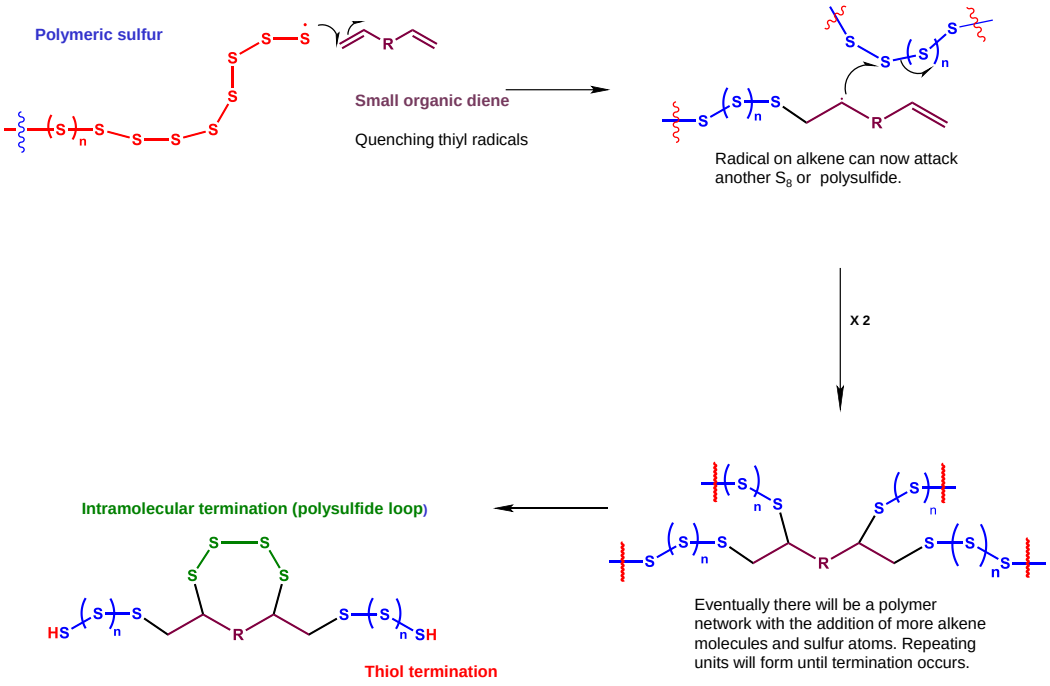

Figure 5.34 Reaction scheme for uncatalysed inverse vulcanisation, highlighting both intramolecular and thiol termination.

The metal-sulfur bond may allow the opening of the S_8 ring at lower temperatures; this then could lead to the insertion of sulfur between the metal and diethyldithiocarbamate ligand to generate the active pre-catalyst (Figure 5.35). The catalyst may then lower the energy barrier to bond formation between the crosslinker and the sulfur. As discussed, it cannot be concluded whether this step is radical or iconic. The lack of activity shown by conventional RAFT agent, 2-Cyano-2-propyl benzodithioate, could be attributed to the lack of S-S or the absence of metal-S bonds. The S-S bonds and the metal-S bonds may be crucial for the insertion of sulfur from the S_8 phase to the organic crosslinker phase to allow reaction. Thriam showed some efficiency when screening different catalysts/accelerators. This could be due to the reversible S-S bond, allowing the insertion of sulfur from the S_8 phase. However, efficiency was lower than for catalysts with a metal present, which could suggest that the metal-sulfur bond is crucial for lowering the energy barrier to bond formation between the organic crosslinker and sulfur. Many of the inverse vulcanisation reactions that were screened

had poor miscibility between the organic crosslinker and the molten sulfur phase. The oleophilic and sulfurphillic properties ZnD_2 possess may allow it to be the perfect candidate to act as a phase transfer catalyst to shuttle sulfur to the organic phase (crosslinker) in inverse vulcanisation reactions.

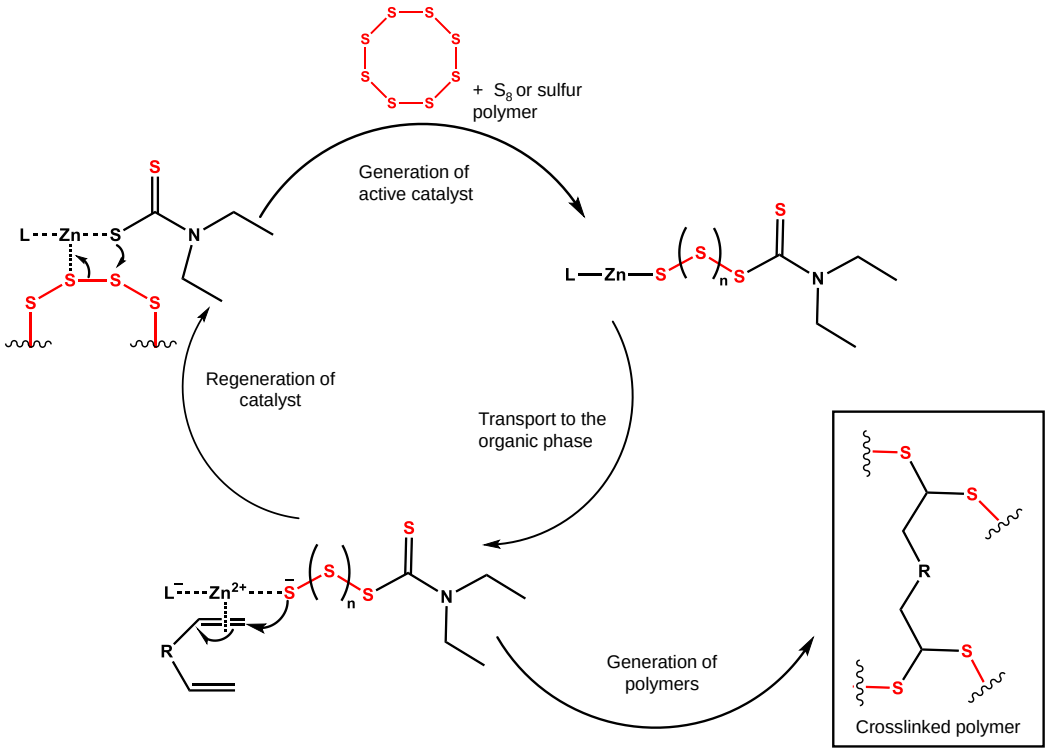

Figure 5.35 Suggested stepwise mechanism for catalytic inverse vulcanisation. ZnD_2 is represented as a phase transfer agent.

5.5 Conclusions and Future work

Catalytic inverse vulcanisation is demonstrated for the first time. A range of catalysts were screened that include low cost and non-toxic metals. In comparison to un-catalysed inverse vulcanisation the reaction temperature and time was reduced, the properties of the polymers were improved, and the production of toxic H_2S gas was minimised. Catalytic inverse vulcanisation has many benefits that is likely to enable scale-up of these materials for different applications. This work has reported new materials that include crosslinkers that are unreactive without catalysis.

The hope is that the functions of inverse vulcanised sulfur polymers can be broadened by the catalytic method in this chapter, by exploring many new crosslinkers that will result in functional materials.

Potential future experiments:

- Trial alternative catalysts and crosslinkers and investigate the mechanism further.
- Trial a free radical scavenger in the reaction to differentiate whether the mechanism may be free radical or ionic. However, the mechanism could still be a combination of both free radical and ionic.
- Selenium (Se) could potentially replace sulfur in an inverse vulcanisation reaction. ^{77}Se is NMR active; therefore, reactions could be monitored by NMR to gain a detailed insight into specific reaction pathways.

5.6 Materials and methods

5.6.1 Materials

Sulfur (S_8, sublimed powder, reagent grade, ≥99.5 %, Brenntag UK & Ireland. Purchased in 25 Kg bags), ethylene glycol dimethylacrylate (EGDMA, 98%, Alfa Aesar), glyoxal bis(diallyl acetal) (GBDA, Aldrich), *trans,trans,cis*-1,5,9-cyclododecatriene (CDDT, 98%, Alfa Aesar), dicyclopentadiene (DCPD, >95%, TCI), 1,3-diisopropenylbenzene (DIB, 97%, Aldrich), divinylbenzene (DVB, 80%, Merck), (*R*)-(+)-limonene (97%, Aldrich), squalene (≥98 %, Alfa Aesar), linseed oil (Aldrich), sodium diethyldithiocarbamate trihydrate (Alfa Aesar), copper diethyldithiocarbamate (TCI), nickel diethyldithiocarbamate (TCI), ZnO (Aldrich), zinc (Aldrich), $ZnCl_2$ (Aldrich), $FeCl_2$ (Aldrich), CuO (Aldrich), $CuCl_2$ (Aldrich), zinc stearate (Aldrich), 2-Cyano-2-propyl benzodithioate (>97%, Aldrich), thiram (Aldrich), chloroform (Aldrich), and chloroform-d (CDCl3,Cambridge Isotope Laboratories Inc.) were commercially available and used as received without any further purification. Iron diethyldithiocarbamate and cobalt diethyldithiocarbamate were both synthesized from sodium diethyldithiocarbamate following a method reported in the literature.

5.6.2 Characterisation

Powder X-ray Diffraction (PXRD): Data was measured using a PANalytical X'Pert PRO diffractometer with Cu-$K_{\alpha 1+2}$ radiation, operating in transmission geometry.

Differential Scanning Calorimetry (DSC) were performed on a TA Instruments Q200 DSC, under nitrogen flow, and with heating and cooling rates of 5 °C/min.

Thermogravimetric analysis (TGA) samples were heated under nitrogen to 800 °C at a heating rate of 20 °C min^{-1} using a TA Instruments Q500.

Fourier-transform infrared spectroscopy (FT-IR) was performed using a Thermo NICOLET IR200, between 400 cm^{-1} to 4000 cm^{-1}. Samples were loaded either neat, using an attenuated total reflectance accessory, or in transmission after pressing into a KBr pellet.

Solid-State NMR: ^1H magic-angle spinning (MAS) NMR spectra ws performed on a Bruker Avance III operating at a ^1H Larmor frequency of 700 MHz, using a Bruker 4mm HX probe. Chemical shifts were referenced using the CH_3 resonance of solid alanine at 1.1 ppm (^1H). The ^1H heteronuclear decoupling using two-pulse phase modulation and a radiofrequency field strength of 100 kHz was applied during acquisition. The ^1H MAS NMR spectrum was recorded at a MAS frequency of 9881

Hz with DUMBO homonuclear decoupling applied to achieve high resolution. An empirically determined scaling factor of 0.44 was applied to the ^{1}H chemical shifts.

5.6.3 General procedure for the catalyst screening: preparation of poly (sulfur-*random*-(ethylene glycol dimethacrylate)) (Poly(S-*r*-EGDMA))

To a 40 mL glass reaction vial equipped with a magnetic stir bar 5 g (19.5 mmol) of elemental sulfur was added, catalysts (masses detailed below) and heated until molten by placing the vial in a metal heating block set to 135 °C. The reactions were stirred at 200 RPM using cross-shaped magnetic stirrer bars. When the sulfur was molten, 5 g of Ethylene glycol methacrylate (EGDMA) cross-linker was added. The stirring rate was then increased to 900 RPM, and the reaction continued for up to 10 hours. Samples that were observed to react to form a homogeneous molten state (does not separate if removed on a spatula and cooled to room temperature), were then removed from stirring and cured in an oven at 140 °C for 10 hours further. Samples that showed no sign of reaction, and that were still two phases after 10 hours were aborted.

a. **Preparation of Poly(S-*r*-EGDMA) with 1 wt.% of ZnO as catalyst:** The copolymerisation was carried out by the following the general method mentioned above with ZnO (100 mg, 1 wt.% loading, 1.22 mmol) to afford two layers of mixture with yellow solid at bottom and a clear liquid on the top (yield: 9.7 g). Elemental Analysis for $(C_{10}H_{14}O_4+S_8)_n$ (50 w% S), Calcul. (%): C, 32.95; H, 3.56; S, 50; Found: C, 29.52; H, 3.30; S, 49.58. PXRD and DSC confirmed the presence of unreacted sulfur.
b. **Preparation of Poly(S-*r*-EGDMA) with 1 wt.% of Zinc as catalyst:** The copolymerisation was carried out by the following the general method mentioned above with Zinc (100 mg, 1 wt.% loading, 1.53 mmol) to afford two layers of mixture with yellow solid at bottom and a clear liquid on the top (yield: 9.3 g). PXRD and DSC confirmed the presence of unreacted sulfur.
c. **Preparation of Poly(S-*r*-EGDMA) with 1 wt.% of Zinc Chloride as catalyst:** The copolymerisation was carried out by the following the general method mentioned above with $ZnCl_2$ (100 mg, 1 wt.% loading, 0.736 mmol) to afford two layers with gray-brown solid at the bottom and a clear liquid above (yield: 9.5 g). PXRD and DSC confirmed the presence of unreacted sulfur.

d. **Preparation of Poly(S-*r*-EGDMA) with 1 w% of Iron Chloride as catalyst:** The copolymerisation was carried out by the following the general method mentioned above with $FeCl_2$ (100 mg, 1 wt.% loading, 0.787 mmol) to afford two layers with brown-red solid at the bottom and clear liquid on above (yield: 9.3 g). PXRD and DSC confirmed the presence of unreacted sulfur.

e. **Preparation of Poly(S-*r*-EGDMA) with 1 wt. % of Copper oxide as catalyst:** The copolymerization was carried out by the following the general method mentioned above with CuO (100 mg, 1w% loading, 1.26 mmol) to afford two layers of mixture with brown solid at bottom and liquid on the top (yield: 9.1 g). PXRD and DSC confirmed the presence of unreacted sulfur.

f. **Preparation of Poly(S-*r*-EGDMA) with 1 wt.% of Copper Chloride as catalyst:** The copolymerisation was carried out by the following the general method mentioned above with $CuCl_2$ (100 mg, 1w% loading, 0.743 mmol) to afford two layers with a brown-green solid at the bottom and a clear liquid above (yield: 9.3 g). PXRD and DSC confirmed the presence of unreacted sulfur.

g. **Preparation of Poly(S-*r*-EGDMA) with 1 wt.% of Zinc Stearate (Zn-STR) as catalyst:** The copolymerization was carried out by the following the general method mentioned above with Zn-STR (100 mg, 1w% loading, 0.743 mmol) to afford an orange -red solution that cooled to a solid (yield: 9.3 g). Elemental Analysis for $(C_{10}H_{14}O_4+S_8)_n$ (50 w% S), Calcul. (%): C, 32.95; H, 3.56; S, 50; Found: C, 31.75; H, 3.64; S, 47.33. PXRD and DSC confirmed the presence of unreacted sulfur.

h. **Preparation of Poly(S-*r*-EGDMA) with 1 wt.% of Zinc diethyldithiocarbamate (ZnD_2) as catalyst:** The copolymerisation was carried out by the following the general method mentioned above with ZnD_2 (100 mg, 1w% loading, 0.276 mmol) to afford a dark-red homogeneous gel and then black-red solid (yield: 9.9 g). Elemental Analysis for $(C_{10}H_{14}O_4+S_8)_n$ (50 w% S), Calcul. (%): C, 32.95; H, 3.56; S, 50; Found: C, 28.72; H, 3.25; S, 51.48. DSC and PXRD confirm the absence of crystalline S_8. The T_g was 20 °C.

i. **Preparation of Poly(S-*r*-EGDMA) with 1 wt.% of Iron diethyldithiocarbamate (Fe-D) as catalyst:** The copolymerization was carried out by the following the general method mentioned above with Fe-D (100 mg, 1w% loading, 0.284 mmol) to afford a black-green homogeneous gel and then a black solid (yield: 9.8 g). Elemental Analysis for $(C_{10}H_{14}O_4+S_8)_n$ (50 w% S), Calcul. (%): C, 32.95; H, 3.56; S, 50; Found: C, 29.73; H, 3.29; S, 49.99. DSC and PXRD confirm the absence of crystalline S_8. The T_g was 22 °C.

j. **Preparation of Poly(S-*r*-EGDMA) with 1 wt.% of Cobalt diethyldithiocarbamate (Co-D) as catalyst:** The copolymerization was carried out by the following the general method mentioned above with Co-D (100 mg, 1w% loading, 0.281 mmol) to afford a dark-brown homogeneous gel and then a black solid (yield: 9.6 g). Elemental Analysis for $(C_{10}H_{14}O_4+S_8)_n$ (50 w% S), Calcul. (%): C, 32.95; H, 3.56; S, 50; Found: C, 28.89; H, 3.29; S, 51.10. DSC and PXRD confirm the absence of crystalline S_8. The T_g was 18 °C.

k. **Preparation of Poly(S-*r*-EGDMA) with 1 wt.% of Copper diethyldithiocarbamate (Cu-D) as catalyst:** The copolymerization was carried out by the following the general method mentioned above with Cu-D (100 mg, 1w% loading, 0.278 mmol) to afford a dark-red homogeneous gel and then a black-red solid (yield: 9.8 g). Elemental Analysis for $(C_{10}H_{14}O_4+S_8)_n$ (50 w% S), Calcul. (%): C, 32.95; H, 3.56; S, 50; Found: C, 30.07; H, 3.39; S, 49.49. A slight melting transition was detected for unreacted S_8 by DSC, but no crystallinity was detected by PXRD. The T_g was 24 °C.

l. **Preparation of Poly(S-*r*-EGDMA) with 1 wt.% of Nickel diethyldithiocarbamate (Ni-D) as catalyst:** The copolymerization was carried out by the following the general method mentioned above with Ni-D (100 mg, 1w% loading, 0.282 mmol) to afford a dark-brown homogeneous gel and then a black solid (yield: 9.7 g). Elemental Analysis for $(C_{10}H_{14}O_4+S_8)_n$ (50 w% S), Calcul. (%): C, 32.95; H, 3.56; S, 50; Found: C, 29.63; H, 3.38; S, 50.13. DSC and PXRD confirm the absence of crystalline S_8. The T_g was 18 °C.

5.6.4 Synthesis of sulfur polymers with a range of crosslinkers with and without ZnD_2 catalyst

To a 40 mL glass reaction vial equipped with a cross shaped magnetic stir bar 5 g of elemental sulfur was added, 5 g of crosslinker, and Zn-Diethyldithiocarbamate catalyst (0 mg, 100 mg, or 500 mg) and heated until molten by placing the vial in a metal heating block set to 135 °C. The melting point of sulfur is ~120 °C. A rubber septum was placed over the top of the vial and pierced with a needle to allow outgassing during heating. After the first 10 minutes, by which time the sample was completely molten, the needle was removed, and the stirring increased to 900 RPM. The use of a rubber septum reduces loss of monomers by evaporation. The high stirring rate aids heat transfer to the sides of the reaction to prevent increases in temperature due to the exothermic reaction. The end-point of the reaction was taken as the point at which solidification of the reaction mixture caused the stirrer bar to cease motion. However, all reactions were left in the heating blocks for at least 24 hours before being removed and allowed to cool. The reactions were monitored for the first hour, and then in half hour intervals for the first 12 hours, then checked again after 24 hours, therefore this is why some of the reaction times are stated to be between 12-24 hours. After cooling samples were recovered by breaking the vials. All of these reactions were performed in triplicate to ensure the timings were consistent and allow DSC to be performed on three separate reactions. All crosslinkers were prepared according to the above method, except for limonene, which is known to produce low molecular weight by-products including cymene, where the reaction was performed under vacuum distillation as reported by Chalker *et al.*

5.6.5 H_2S gas determination

General procedure for catalytic inverse vulcanization: In a glove box, Sulfur (5 g,), cross-linkers (5 g), and ZnD_2 catalyst (100 mg) were added to a 40 mL reaction vial equipped with a stirrer bar under N_2 atmosphere. The vial was sealed with a rubber septum and the reaction was setup in a fume hood. The vial was then connected with an N_2-degassed tube ended with a needle to a measuring cylinder (100 mL). The measuring cylinder was filled with deionised water and was placed upside down in a 1 L beaker with water. The reaction mixture was heated until molten by placing the vial in a metal heating block set to 135 °C. The reactions were stirred vigorously using

magnetic stirrer bars for each crosslinkers until each reaction produced no more gas, typically under an hour.

General procedure for non-catalytic inverse vulcanization: In a glove box, Sulfur (5 g) and cross-linkers (5 g) were added to a 40 mL reaction vial equipped with a stirrer bar under N_2 atmosphere. The vial was sealed with a rubber septum and the reaction was setup in the normal fume hood. The vial was then connected with a N_2-degassed tube ended with a needle to a measuring cylinder (100 mL). The measuring cylinder was filled with deionised water and was placed upside down in a 1 L beaker with water. The reaction mixture was heated until molten by placing the vial in a metal heating block set to normally higher temperatures that the equivalent reactions without catalysts, to induce similar degrees of reaction over the same timescale. Temperatures were therefore chosen according to the relative reactivities of the crosslinkers and were as follows: Limonene 180 °C, DCPD 170 °C, ENB 135 °C, DVB and DIB 160 °C. The reactions were stirred vigorously using magnetic stirrer bars for each crosslinkers until each reaction produced no more gas, typically under an hour. Another experiment was performed in the same manner with limonene, at 1 wt.% ZnD_2 loading, but at 180 °C, the same temperature as the uncatalysed reactio

5.7 Appendix

Table A5.1 Summary of S_8 detection by DSC. Reaction temperatures are 135 °C unless stated otherwise. * No S_8 crystals were detected in the lower phase of the uncatalysed GBDA reaction, but the extremely long reaction time required for gelation (over 36 hours) led to significant sublimation of crystalline sulfur above this.

Crosslinker	S_8 melting detected by DSC?		
	0 wt. % ZnD_2	1 wt. % ZnD_2	5 wt. % ZnD_2
Limonene	No	No	No
DCPD	No	No	No
Linseed oil	Yes	No	No
VNB	No	No	No
EDGMA	Yes	No	No
GBDA	No*	No	No

Table A5.2 Summary of S_8 detection. Reaction temperatures are 135 °C unless stated otherwise. * No S_8 crystals were detected in the lower phase of the uncatalysed GBDA reaction, but the extremely long reaction time required for gelation (over 36 hours) led to significant sublimation of crystalline sulfur above this.

Crosslinker	S_8 crystals detected by PXRD?		
	0 wt. % ZnD_2	1 wt. % ZnD_2	5 wt. % ZnD_2
Limonene	No	No	No
DCPD	No	No	No
linseed	Yes αS_8	No	Yes – slight αS_8
VNB	No	No	No
EDGMA	Yes	No	No
GBDA	No*	No	No

Table A5.3 Time taken from the start of the reaction, until solidification causes the stirrer bar to cease. All reactions were conducted at 135 °C with equal crosslinker to sulfur mass (1:1) on a 10g scale in triplicate. Reactions were monitored for the first hour and then in 30-minute intervals for the first 12 hours, then checked after 24 hours.

Crosslinker	Time until solidification, hours			
	0 wt. % ZnD_2	**1 wt. % ZnD_2**	**5 wt. % ZnD_2**	**Comments**
DIB	>12, <24	6.5	1	
Limonene	20	8.5	1	
DVB	3.5	1.5	0.85	
DCPD	>12, <24	1.6	0.4	
Squalene	>12, <24	>12 (<24)	1.5	
Sunflower oil	>24	>12 (<24)	<2	S8 detected in all, 0% catalyst reaction still liquid after 24 hr
linseed	>24	4	2.5	S8 detected at 0%, and trace S8 at 5% catalyst, 0% catalyst reaction still liquid after 24 hr
VNB	>12, <24	>4, <6	2	
CDDT	>12, <24	6	3	

TVCH	>12, <24	6	2	Both CDDT and TVCH, at O% catalyst loading, did react to form polymeric material, but with significant evaporation of the crosslinker, low yields, and unreacted sulfur sublimed on the sides of the vessel.
TVTCSi	No reaction	3.5	1.75	Reacted at 160 °C (No reaction at any catalyst loading at 135 °C
EDGMA	No reaction	>12, <24	>12, <24	0 % looks like sulfur
GBDA	>36, <48	>12, <24	2.5	0% catalyst loading reaction is prohibitively slow, taking over 36 hours to form a solid

5.8 References

1 X. Wu, J. A. Smith, S. Petcher, B. Zhang, D. J. Parker, J. M. Griffin and T. Hasell, *Nat. Commun.*, 2019, **10**, 1–9.

2 Y. Zhang, J. J. Griebel, P. T. Dirlam, N. A. Nguyen, R. S. Glass, M. E. Mackay, K. Char and J. Pyun, *J.Polym.Sci.Part A Polym.Chem.*, 2017, **55**, 107–116.

3 J. A. Smith, X. Wu, N. G. Berry and T. Hasell, *J. Polym. Sci. Part A Polym. Chem.*, 2018, **56**, 1777–1781.

4 J. J. Griebel, G. Li, R. S. Glass, K. Char and J. Pyun, *J. Polym. Sci. Part A Polym. Chem.*, 2015, **53**, 173–177.

5 E. of E. Britannica, Accelarator- Rubber manafacturing, http://britannica.com/technology/accelerator (accessed 5th May 2020)

6 Y. Zhang, R. S. Glass, K. Char and J. Pyun, *Polym. Chem.*, 2019, **10**, 4078–4105.

7 D. J. Parker, H. A. Jones, S. Petcher, L. Cervini, J. M. Griffin, R. Akhtar and T. Hasell, *J. Mater. Chem. A*, 2017, **5**, 11682–11692.

8 A. Hoefling, Y. J. Lee and P. Theato, *Macromol.Chem.Phys.*, 2016, **218,** 18-21.

9 N. A. Lundquist, M. J. H. Worthington, N. Adamson, C. T. Gibson, M. R. Johnston, A. V. Ellis and J. M. Chalker, *RSC Adv.*, 2018, **8**, 1232–1236.

10 M. A. Martin-Luengo, M. Yates, E. S. Rojo, D. Huerta Arribas, D. Aguilar and E. Ruiz Hitzky, *Appl. Catal. A Gen.*, 2010, **387**, 141–146.

11 S. A. Sanchez-Vazquez, T. D. Sheppard, J. R. G. Evans and H. C. Hailes, *RSC Adv.*, 2014, **4**, 61652–61655.

12 W. Martin, JM, Smith, *Handbook of Rubber Technology, Vol.1.Satish Kumar Jain for CBS Publishers & Distributors: New Dehli.*, 2007.

13 Y. Ikeda, Y. Yasuda, T. Ohashi, H. Yokohama, S. Minoda, H. Kobayashi and T. Honma, *Macromolecules*, 2015, **48**, 462–475.

14 G. Moad, E. Rizzardo and S. H. Thang, *Polymer (Guildf).*, 2008, **49**, 1079–1131.

15 D. J. Parker, H. A. Jones, S. Petcher, L. Cervini, J. M. Griffin, R. Akhtar and T. Hasell, *J. Mater. Chem. A*, 2017, **5**, 11682–11692.

16 M. P. Crockett, A. M. Evans, M. J. H. Worthington, I. S. Albuquerque, A. D. Slattery, C. T. Gibson, J. A. Campbell, D. A. Lewis, G. J. L. Bernardes and J.

M. Chalker, *Angew. Chemie - Int. Ed.*, 2016, **55**, 1714–1718.

17 W. J. Chung, J. J. Griebel, E. T. Kim, H. Yoon, A. G. Simmonds, H. J. Ji, P. T. Dirlam, R. S. Glass, J. J. Wie, N. a Nguyen, B. W. Guralnick, J. Park, A. Somogyi, P. Theato, M. E. Mackay, Y. Sung, K. Char, J. Pyun, Á. Somogyi, P. Theato, M. E. Mackay, Y. Sung, K. Char, J. Pyun, A. Somogyi, P. Theato, M. E. Mackay, Y. Sung, K. Char, J. Pyun, Á. Somogyi, P. Theato, M. E. Mackay, Y. Sung, K. Char and J. Pyun, *Nat. Chem.*, 2013, **5**, 518–524.

18 M. Arslan, B. Kiskan and Y. Yagci, *Macromolecules*, 2016, **49**, 767–773.

CHAPTER 6

CONCLUSIONS

6.1 Conclusions

The main aim of the research in this thesis was to investigate inverse vulcanised sulfur polymers for functional materials. Inverse vulcanisation is still a new field of research that was first reported by Pyun and co-workers in 2013. This thesis explores new research ideas that have triggered future developments in this field.

Chapter 2 was the first publication highlighting that crosslinkers with the same number of double bonds and similar molecular masses can result in materials with significantly different properties. At the time of this research, there were no ideas which crosslinkers to trial experimentally in an inverse vulcanisation reaction. The computational calculations in this chapter allowed ways to screen crosslinkers before the reaction with sulfur. The inverse vulcanisation reaction between sulfur and ENB is the first bulk copolymer to see no remaining sulfur crystals by PXRD and DSC at 90% elemental sulfur.

This chapter rationalises the differences in properties of high sulfur content polymers according to their respective crosslinkers' reactive sites, with lower reactivity requiring higher polymerisation temperature, causing increased hydrogen abstraction. These findings make it easier to understand the differences in the properties of other structurally diverse crosslinkers used to prepare inverse vulcanised sulfur polymers.

Potential future experiments:

- S-ENB showed no evidence of S_8 crystals by PXRD and DSC at 90% elemental sulfur by mass. Therefore, investigating S-ENB polymers as a cathode in Li-S batteries could be one future application.

Chapter 3 reports four new sulfur terpolymers and studies the mechanical properties of these materials (tensile, flexural, compression, and hardness properties). To develop materials for functional applications, the mechanical properties must be improved. When the study in this chapter was conducted, there were very few publications on this topic. Since this study, there have been many advancements and developments that have shown both strength and process improvements. The hope was the research in this chapter would trigger future developments.

The tensile, flexural, compression, and hardness properties were tested showing that combining crosslinkers at different feed ratios can tailor the properties. For instance, the T_g can be varied controllably from -20 to 115 °C. This study is the first effort to

uncover design principles so that a given mechanical or optical properties can be rationally imparted to this class of sulfur polymers.

Since this study, there are further improvements on this research. Such as, adjusting the degree of crosslinking by introducing a two-step method which allows new control over the mechanical properties of inverse vulcanised polymers. One of the main issues during this research was moulding the polymers into the correct mechanical testing dimensions. This proved challenging with air pockets forming in the materials resulting in pores. Another major issue occurred when removing the polymers from the prepared mould due to the air pockets formed the materials were extremely fragile and would easily break before testing. New research uses a hot press to produce uniform films for mechanical testing that solves this issue.

Potential future experiments:

- Recyclability of these materials should be studied to look at the deformation.
- Solid-state UV Vis spectroscopy could look at the optical properties of S-DCPD-terpinolene terpolymers.
- Additives could be introduced to the reaction, such as cellulose nanowhiskers, to see if it reinforces the materials and improves the strength.

Chapter 4 is the second example in literature that investigates the antibacterial properties of inverse vulcanised sulfur polymers. This work shows the activity of two high sulfur content polymers, as bulk solids against both Gram-negative and positive bacteria. S-DIB was found to have more significant antibacterial activity than S-DCPD; this could be attributed to S-DIB having a higher sulfur rank (the number of sulfur atoms in between each carbon crosslink CS_x), therefore having a weaker central S-S bond promoting homolysis.

The low-cost availability of sulfur on a vast scale provides the potential for use as antibacterial materials and surfaces in bulk applications that would not be possible for more expensive complex materials. The promising results found already, and the difference in efficacy between these crosslinkers against two bacterial strains suggests that the broader antibacterial effect of sulfur polymers may be further improved in the future and warrants further investigation and development.

Potential future experiments:

- Cytotoxicity experiments to assess the safety of the materials.

- Screening crosslinkers with different sulfur ranks to see if this has an impact on antimicrobial activity.
- Carry out antimicrobial testing on polymers with a range of different glass transition temperatures (T_gs), that are both below and above the temperature of the test.
- Exposing materials to different bacteria, e.g. *Pseudomonas Aeruginosa* a pathogen that is in urgent need of new antibacterial agents.
- Examine the antibacterial resistance of the polymer surfaces to super -resistant pathogens such as MRSA.
- Expose the materials to other microbes such as fungi, mold, and viruses.

In **Chapter 5**, catalytic inverse vulcanisation is demonstrated for the first time. This study shows reactions with a range of different catalysts that include low cost and non-toxic metals. In comparison to un-catalysed inverse vulcanisation, the reaction temperature and time are reduced, the properties of the polymers are improved, and the production of toxic H_2S gas was significantly reduced. Catalytic inverse vulcanisation has many benefits that are likely to enable scale-up. This work has reported new materials that include crosslinkers that are unreactive without catalysis.

Potential future experiments:

- Trial alternative catalysts and crosslinkers and investigate the mechanism further.
- Trial a free radical scavenger in the reaction to differentiate whether the mechanism may be free radical or ionic. However, the mechanism could still be a combination of both free radical and ionic.
- Selenium (Se) could potentially replace sulfur in an inverse vulcanisation reaction. ^{77}Se is NMR active; therefore, reactions could be monitored by NMR to gain a detailed insight into specific reaction pathways.

Overall, each chapter explores either a functional application of inverse vulcanised sulfur polymers or ways in which these materials can be improved to unlock new functions. The hope is that the research conducted in this thesis aids and triggers future developments in this rapidly growing field.